CHEMOTHERAPEUTIC EFFECT OF EVEROLIMUS AND ABT-737 COMBINATION ON RENAL CELL CARCINOMA

by
Ayşe Hande Nayman

Submitted to Graduate School of Natural and Applied Sciences
in Partial Fulfillment of the Requirements
for the Degree of Doctor of Philosophy in
Biotechnology

Yeditepe University
2018

CHEMOTHERAPEUTIC EFFECT OF EVEROLIMUS AND ABT-737 COMBINATION ON RENAL CELL CARCINOMA

APPROVED BY:

Prof. Dr. Dilek Telci ……
(Thesis Supervisor)

Prof. Dr. Faruk Yencilek ……
(Thesis Co-supervisor)

Prof. Dr. Asıf Yıldırım ……

Prof. Dr. Fikrettin Şahin ……

Assoc. Prof. Dr. Elif Damla Arısan ……

Assist. Prof. Dr. Hüseyin Çimen ……

DATE OF APPROVAL: ..../..../2018

This thesis is dedicated to Şeyda,
Hikmet, and Atakan Nayman…

ACKNOWLEDGEMENT

I would like to thank to my supervisor Prof. Dilek Telci for her support, supervision of my thesis as well as scientific and personal suggestions during the difficult PhD period. I am also thankful to Prof. Fikrettin Şahin who helped me right at the beginning of my academic career where I almost lost the enthusiasm for science. Additionally, I would like to thank to Prof. Asıf Yıldırım, who always made me to fell comfortable during presentations, my co-advisor Prof. Faruk Yencilek, and my Jury member Prof. Gamze Köse for their support and advices. It is important for me to mention Assoc. Prof. Ebru Zemheri for her contribution with pathological examinations and Assist. Prof. Emrah Nikerel, who always answered my questions when I was stuck with statistics. Of course, I appreciate the help of Engin Sümer during animal studies and of Burçin Asutay during flow cytometry analysis. I would like to thank to The Scientific and Technological Research Council of Turkey (TUBITAK) for the support of my Ph.D. thesis with a grant entitled as "Anti-tumor effects ABT-737 and RAD-001(Everolimus) combination chemotherapy on Renal Cell Carcinoma in a murine RenCA model" (114S332). I would like to also thank to Halime Sığınç for her help with numerous western blot and *in vivo* experiments, to İnci Kurt Celep for her support and friendship, and to other present and former lab members, Polen Koçak, Bürge Ulukan and Meltem Önal for chit chat at the coffee breaks and the music they play. I am also thankful to Sevda Deniz Mert and Ebru Yılmaz for our precious talks and discussions about spirituality and psychology and to my friends, who never gave up to ask me when I am going to finish studying. My specials thanks go to my dearest friends Bahar Özdemir, Ayça Ece Nezir and Gözde Korkmaz who always support me with their wisdom, maturity, love, and fun. Without their existence in my life, it would be really hard to stand up at each time when doing PhD exceeded my limits. Last of all and always, I will be thankful and grateful to my great, humorous, and unique mother, Şeyda Nayman, who always supported my decisions no matter what and made my whole life easier, and to my lovely and precious brother, Atakan Nayman, who always tolerated my psychological and radical up and downs. Finally, I pay my gratitude to my late father, Ahmet Hikmet Nayman, for changing the direction of my life by providing me with an European mentality.

ABSTRACT

CHEMOTHERAPEUTIC EFFECT OF EVEROLIMUS AND ABT-737 COMBINATION ON RENAL CELL CARCINOMA

2-3 per cent of all malignant tumors are characterized as renal cell carcinoma (RCC) that shows a high mortality rate. Among a number of histopathological subtypes, clear cell RCC (ccRCC) comprises the majority and 20-30 per cent of patients diagnosed with ccRCC are already at locally advanced or metastatic stage. As the elevated activity of mTOR pathway is associated with RCC tumorigenesis, the mTOR kinase inhibitor, everolimus, is used in clinic for the cure of patients with metastatic RCC (mRCC). However, the low rate of progression free survival and the development of everolimus resistance are the main clinical limitations observed with everolimus therapy. Given the possible contribution of anti-apoptotic Bcl-2 protein in RCC development, everolimus was combined with a Bcl-2 protein inhibitor ABT-737 to overcome the everolimus resistance. The effect of everolimus combination with ABT-737 was studied in Bcl-2 overexpressing RCC cell lines, A-498 and Caki-1, and in RCC xenograft mouse model. The *in vitro* results indicated that the everolimus-ABT-737 combination led to a significant decrease in the both RCC cell lines' viability, which is associated with the attenuated cell cycle as a result of completely suppressed mTOR pathway as well as with the induction of apoptosis. Diminished level of anti-apoptotic Bcl-2 protein was also detected in A-498 and Caki-1 as a response to ABT-737 monotherapy and its combination with everolimus. In support of *in vitro* findings, the synergistic anti-tumor effect of everolimus-ABT-737 combination was validated in RCC xenograft Balb/c mouse model generated with the $RenCa^{res}$ cell line. Taken together, the findings from this thesis suggest that the everolimus-ABT-737 combination as a novel therapy strategy can provide therapeutic benefit for the patients suffering from the advanced RCC. This study was supported by TUBITAK (114S332).

ÖZET

EVEROLİMUS VE ABT-737' NİN RENAL HÜCRELİ KARSİNOM ÜZERİNDEKİ KEMOTERAPÖTİK ETKİSİ

Böbrek hücreli karsinom (BHK) yüksek ölüm oranıyla tüm habis tümörlerin yüzde 2 ila 3'ünü oluşturur. Histopatolojik alt tipler arasında çoğunluğu berrak hücreli BHK alır ve berrak hücreli BHK tanısı konmuş hastaların yüzde 20 ila 30'u lokal ileri veya metastatik evredelerdir. mTOR yolağının yüksek aktivitesi, BHK tümörijeneziyle ilişkilendirildiği için mTOR inhibitörü olan everolimus klinikte metastatik BHK hastalarının tedavisi için kullanılmaktadır. Buna karşın, tedavi sonucunda progresyonsuz sağkalım oranının düşük olması ve tümörlerin ilaca karşı direnç geliştirmesi everolimus tedavisini klinik olarak sınırlamaktadır. Bahsi geçen ilaç direncinde antiapoptotik Bcl-2 protein ifadesinin olası rolünü araştırmak için everolimus, Bcl-2 inhibitörü olan ABT-737 ile kombine edilmiş ve bu kombinasyonun etkinliği Bcl-2'yi yüksek miktarda ihtiva eden A-498 ve Caki-1 BHK hücre hatları ile BHK ksenogreft fare modeli üzerinde araştırılmıştır. *İn vitro* sonuçlar, everolimus ve ABT-737 kombinasyonunun, hücre canlılığında istatistiksel olarak anlamlı bir düşüşe yol açtığını göstermişlerdir. Kombinasyon tedavisi ayrıca apoptoz mekanizmasını tetiklemiş ve mTOR yolağının aktivitesini tamamen susturarak hücre döngüsünü duraklatmıştır. ABT-737 mono terapisi ve onun everolimus ile ona kombinasyonuna cevap olarak iki hücre hattında da düşük antiapoptotik Bcl-2 protein ifadesine rastlanmıştır. Bu sonuç ABT-737'nin başarılı bir şekilde Bcl-2 proteininin hücre ölümü üzerindeki inhibitör etkisinin üstesinden geldiğine işaret etmektedir. *İn vitro* sonuçları destekler şekilde, everolimus ve ABT-737 kombinasyonunun anti tümör etkisi, everolimus'a dirençli $RenCa^{res}$ hücre hattı kullanılarak oluşturulan BHK ksenogreft Balb/c fare modelinde doğrulanmıştır. Tüm bu sonuçlar özgün bir terapi stratejisi olarak everolimus ve ABT-737 kombinasyon tedavisinin, ileri evre BHK'dan mustarip hastalar için terapötik yarar sağlayabileceğini önermektedirler. Bahsi geçen bu çalışmalar Türkiye Bilimsel ve Teknolojik Araştırma Kurumu (TÜBİTAK) tarafından desteklenmiştir.

TABLE OF CONTENTS

LIST OF FIGURES

LIST OF TABLES

LIST OF SYMBOLS/ABBREVIATIONS

µl	Microliter
µM	Micromolar
4E-BP1	Eukaryotic translation initiation factor 4E binding protein 1
ACD	Acquired cystic disease
AKT	Protein kinase B
AML	Acute myeloid leukemia
APAF-1	Apoptotic protease activating factor-1
APS	Ammonium persulfate
ARNT	Aryl hydrocarbon receptor nuclear translocator
ASK1	Apoptosis signal-regulating kinase 1
ATP	Adenosine triphosphate
Bcl-2	B-cell lymphoma 2
Bcl-xL	B-cell lymphoma extra-large
BH3	Bcl-2 homology 3
BHD	Birt-Hogg-Dubé
CBD	Calmodulin binding domain
CDC	Collecting duct carcinoma
CDKI	Cyclin-dependent kinase inhibitor
chRCC	Chromophobe renal cell carcinoma
CLL	Chronic lymphocytic leukemia
CLS	Capillary leak syndrome
CO_2	Carbon dioxide
Deptor	DEP-domain-containing mTOR-interacting protein
DMSO	Dimethyl sulfoxide
DNA	Deoxyribonucleic acid
DPBS	Dulbecco's Phosphate-Buffered Saline
ECL	Enhanced Chemo-Luminescence
eEF2K	Eukaryotic translation elongation factor 2 kinase

EGF	Epidermal growth factor
eIF4B	Eukaryotic translation initiation factor 4B
eIF4E	Eukaryotic translation initiation factor 4E
EMT	Epithelial mesenchymal transition
ERK	Extracellular signal-related kinase
FBS	Fetal bovine serum
FDA	U.S. Food and Drug Administration
FH	Fumarate hydratase
FKB	FKBP-rapamycin binding
FKBD	FK506 binding domain
FKBP12	FK506-binding protein 12
FKBP38	FKBP12 homologue FKBP38
FoxO1/3a	Forkhead box O1/3a
FRB	FKBP12-rapamycin binding
GAP	GTPase-activating protein
GDP	Guanosine diphosphate
GLUT	Glucose transporter
Grb10	Growth factor receptor–bound protein 10
GSK-3	Glycogen synthase kinase-3
GTP	Guanosine triphosphate
GTPase	Guanosine triphosphate hydrolase
HIF	Hypoxia-inducible factor
HLRCC	Hereditary leiomyomatosis and renal cell cancer
HPRC	Hereditary papillary renal carcinoma
HRE	Hypoxia response element
IFN-α	Interferon α
IGF	Insulin-like growth factor
IgH	Immunoglobulin heavy chain
IL-2	Interleukin-2
IRS1	Insulin receptor substrate 1
JNK	Jun N terminal kinase
kDA	kilo Dalton

Mcl-1	Myeloid cell leukemia 1 protein
mA	Milliamper
ml	Milliliter
mLST8	mammalian Lethal with Sec13 protein 8
mm	Millimeter
mM	Milli Molar
MOI	Multiplicity of infection
MOM	Mitochondrial outer membrane
MOMP	Mitochondrial outer membrane permeabilization
mRCC	Metastatic renal cell carcinoma
VEGF	Vascular endothelial growth factor
mSin1	Mammalian stress activated protein kinase interacting protein
mTOR	Mammalian target of rapamycin
mTORC	Mammalian target of rapamycin complex
MTS	Mitochondria targeting sequences
Na_3VO_4	Sodium Orthovanadate
NF-κB	Nuclear factor κB
ng	Nano gram
NMR	Nuclear magnetic resonance
Noxa	BH3 (Bcl-2 homology 3)-only Bcl-2 protein
NSCLC	Non small cell lung carcinoma
OS	Overall survival
PARP	Poly-ADP-ribose polymerase
PDCD4	Programmed cell death 4
PDGF	Platelet-derived growth factor
PDGFR-β	platelet-derived growth factor receptor, beta polypeptide
PDK1	Phosphoinositide-dependent protein kinase-1
PFS	Progression free survival
PHD	Prolylyl hydroxylase
PHLPP	PH domain leucine rich repeat phosphatase
PI3K	Phosphoinisitide 3-kinase
PIKK	Phosphatidylinositol kinase-related kinase

PIP2	Phosphatidylinositol-3,4-bisphosphate
PIP3	Phosphatidylinositol-3,4,5-trisphosphate
PKCα	Protein kinase C alpha
PLD	Phospholipase D
PH	Plecktrin homology
PPIase	Peptidylprolyl cis/trans isomerase
PRAS40	Proline-rich AKT substrate 40kDa
pRCC	Papillary renal cell carcinoma
Protor-1	Protein observed with Rictor-1
PP2	Protein phosphatase 2
PTEN	Phosphatase and tensin homolog deleted on chromosome 10
PTM	Posttranslational modification
PUMA	p53 upregulated modulator of apoptosis
Raptor	Regulator-associated protein of mTOR
RCC	Renal cell carcinoma
ccRCC	Clear cell renal cell carcinoma
$RenCa^{res}$	Everolimus-resistant RenCa
Rheb	Ras homolog enriched in brain
Rictor	Rapamycin insensitive companion of mTOR
RIPA	Radio immunoprecipitation assay
RTK	Receptor tyrosine kinase
S6K1	70kDa ribosomal protein S6 kinase 1
SDH	Succinate dehydrogenase
SDS	Sodium Dodecyl-sulfate
SDS-PAGE	Sodium Dodecyl-sulfate Polyacrylamide Gel Electrophoresis
Ser	Serine
SGK1	Serum/glucocorticoid regulated kinase 1
TEMED	Tetramethylethylenediamine
TCA	Tricarboxylic acid
Thr	Threonine
TPR	Tetratricopeptide repeats
TSC1	Hamartin

TSC2	Tuberin
TSC1/2	Tuberous sclerosis complex ½
V	Volt
VEGFR	Vascular endothelial growth factor receptor
VHL	von Hippel-Lindau

1. INTRODUCTION

1.1. KIDNEY CANCER

Kidneys are a pair of organs of the urinary system. They regulate the blood pressure and maintain the homeostasis of acid-base and electrolyte. Additionally, kidneys secrete erythropoietin as a response to hypoxia to trigger the production of red blood cells from bone marrow [1]. Kidneys are located at the retroperitoneal region in the abdominal cavity of human body. Anatomy of a kidney comprises of renal cortex and renal medulla that forms the functional unit of the organ, called parenchyma. Renal pelvis, collecting and papillary ducts to where the nephrons drain the filtrated metabolic wastes as urine in, belong to the collection system of the kidney.

Kidney cancer is the twelfth most widely seen cancer diagnosed in worldwide and has an incidence of 2.4 per cent of all cancers [2]. 2-3 per cent of kidney malignancies are familial/hereditary renal cancers observed in earlier age and 90 per cent are characterized as renal cell carcinoma (RCC) [3]. RCC accounts for two to three per cent of all adult tumors and is the seventh and ninth most widely seen cancer seen in men and women, respectively [4]. The mortality rate of RCC is about 1.4 in 100.000 and its incidence showed 2 per cent increase in last 20 years [5]. Among the risk factors for RCC development, smoking is placed on the top, followed by obesity and hypertension [6-8]. The highly vascularized structure of RCC tumors is associated with the disease's metastatic potential where metastasis is mostly observed in lung, followed by soft tissue, bone, liver, and brain [9]. In most of the cases, RCC is diagnosed at locally advanced stage where 20-30 per cent of patients already developed metastasis [10].

RCC originates from epithelium of renal tubes and is divided into four main subtypes according to the histopathological features [11]. Clear cell renal cell carcinoma (ccRCC) comprises 80-90 per cent of all histological subtypes followed by papillary (10 per cent), chromophobe (5 per cent), and collecting duct carcinoma (less than 1 per cent) (Figure 1.1). Besides these major RCC variants, a number of other RCC subtypes is still being discovered [12]. All the subtypes of RCC can be either sporadic or have a hereditary background. The hereditary/familial RCC is mostly associated with the syndromes that

predispose the individuals to the malignant tumor development. Syndromes classified for familial RCCs are tuberous sclerosis syndrome, Birt-Hogg-Dubé (BHD) syndrome, and von Hippel-Lindau disease occurred through either germline mutations seen in oncogenes/tumor suppressor genes or loss/gain of chromosomes [13]. Although the incidence of hereditary RCC is low, the discovery of the genetic background giving rise to their development enabled the identification of molecular pathologies for sporadic RCCs [14].

ccRCC is the major subtype of renal epithelial malignancies among RCC tumors [15]. It originates from the proximal convoluted tubules and its histological examination points out a clear cytoplasm that is rich in lipid and glycogen [16]. ccRCC can be either familial or sporadic. In both cases, the main underlying reason for ccRCC development is the loss of *VHL* tumor suppressor gene [17]. The main advantage of this malignant subtype is the availability of the targeted therapies owing to the elucidation of the molecular mechanisms participating in its cancerogenesis.

Multilocular cystic renal neoplasm of low malignant potential is classified as a variant of ccRCC because of the presence of mutated *VHL* gene and clear cytoplasm [18]. However, this subtype has a good prognosis and exhibits complete cure without any observed metastasis compared to ccRCC [16].

Papillary RCC (pRCC) is the second predominant RCC subtype accounting for 10-15 per cent of all RCC tumors [15]. pRCC originates from the proximal tubules and exhibits papillary architecture with a cytoplasm containing few organelles [16]. The histological analysis reveals two types of pRCC that differ from each other through their genetic background. Hereditary papillary renal carcinoma (HPRC) is a low-grade hereditary type I pRCC with a rare clear cytoplasm. Hereditary leiomyomatosis and renal cell cancer (HLRCC) is the type II pRCC demonstrating granular eosinophilic cytoplasm and aggressive behavior with poor prognosis [19]. Mutated proto-oncogene *c-MET* and *fumarate hydratase* (*FH*) genes are associated for the development of type I and type II pRCC, respectively [20, 21]. Trisomy of chromosomes 7 and 17, and the loss of Y chromosome are the common chromosomal abnormalities observed in pRCC [22].

The third frequently observed RCC subtype is the **chromophobe** RCC (chRCC) accounting for 5 per cent of all renal epithelial tumors [23]. It originates from the type B intercalated cells constituting the collecting duct and shows pale cells with reticulated cytoplasm during histological investigation [16]. The disease is mostly associated with BHD syndrome and occupies a less aggressive profile with a 7 per cent metastasis of all cases compared to chRCC [24].

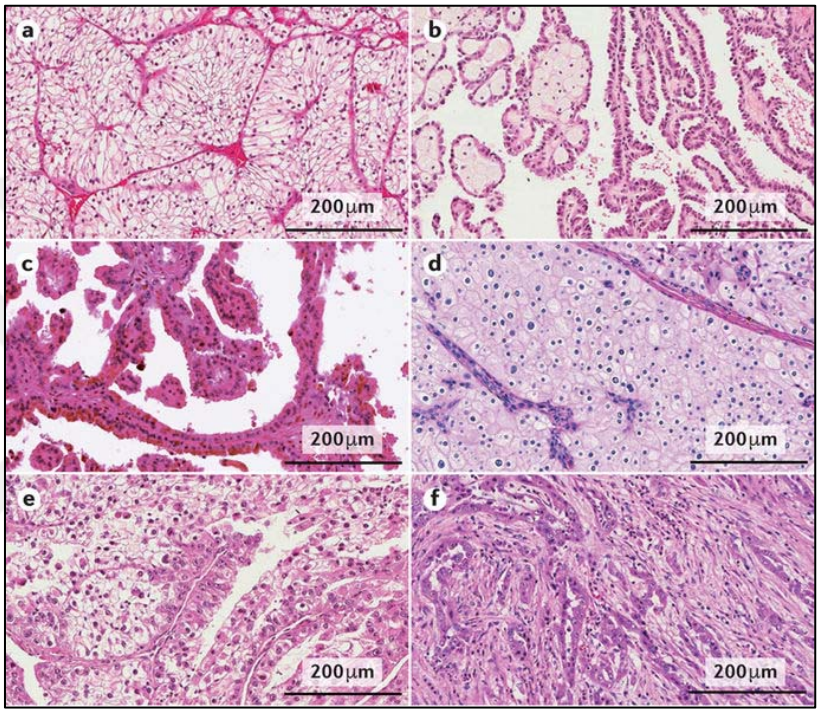

Figure 1.1. Subtypes of RCC tumors characterized by their histopathology. **a**. clear cell; **b**. papillary type I; **c**. papillary type 2; **d**. chromophobe; **e**. MiT family translocation; **f**. collecting duct [25]

Renal oncocytome is the benign variant of RCC originating from the type A intercalated cells constituting the collecting duct with eosinophilic cytoplasm [26]. Like chRCC, the disease is also developed in patients with BHD syndrome and it is difficult to distinguish from chRCC [24].

Collecting Duct carcinoma (CDC) is a rare variant of RCC corresponding to less than one per cent of RCC tumors [26]. It originates from principle cells of medullary collecting duct and has a basophilic cytoplasm [27]. Collecting duct carcinoma is highly aggressive and

found in advanced stage with already developed metastasis. Indeed, mortality is observed for 60-70 per cent of patients with metastatic CDC within two years after diagnosis [16].

Renal medullary carcinoma is another remarkably aggressive and rare form of RCC tumors [28]. The disease exhibits eosinophilic cytoplasm and is considered as a variant of CDC, as it arises from the collecting duct in renal medulla [27]. However, renal medullary carcinoma, which is linked to the sickle cell anemia is mostly observed in earlier ages compared to CDC [29] .

Besides these well characterized malignant subtypes of RCC, a number of ongoing studies uncovers new variants of renal tumors that have been validated by World Health Organization (WHO) in 2016 [30].

Hereditary leiomyomatosis and RCC syndrome–associated RCC (HLRCC-associated RCC) is an example for rare renal neoplasms. HLRCC-associated RCC contains eosinophilic cytoplasm with papillary architecture and originates from germline mutation in *FH* gene [31, 32]. The disease has poor prognosis.

Like HLRCC-associated RCC, **succinate dehydrogenase–deficient RCC (SDH-deficient RCC)** arises from germline mutations in succinate dehydrogenase (*SDH*) gene and is mostly observed in young patients [33]. The disease shows a clear cell histology with vacuolated or eosinophilic material and loss of SDHB expression [34].

Another rare subtype of RCC is the **tubulocystic RCC**. According to histopathological examination, the disease contains multiple cysts and exhibits tubular structure with eosinophilic cytoplasm [35, 36]. Trisomy of chromosome 17 was validated in tubulocystic RCC tumors [37].

Clear cell papillary RCC (CCP-RCC) and acquired cystic disease–associated RCC (ACD-RCC) are the two subtypes for end-stage renal disease, which develop after long-term hemodialysis and have a indolent behavior [23]. **CCP-RCC** is characterized by clear cytoplasm with tubular and papillary structure [38]. In comparison to ACD-RCC, this type of end-stage renal cell neoplasm shows no loss or gains in the chromosome 7 as well as an intact VHL gene [39-41]. **ACD-RCC** has a eosinophilic and clear cytoplasm with papillary

architecture. The presence of calcium oxalate crystals has been also reported [42]. The disease displays gains in chromosome 7 and 17 [38].

1.2. SIGNALING PATHWAYS IN CLEAR CELL RENAL CELL CARCINOMA

Cancer is a neoplastic disease originating from the unlimited growth of normal cells and its development is a multistep process. Therefore, a healthy cell requires some biological capabilities such as sustained proliferation, evading growth suppressors, and enabling immortality to be differentiated into a cancer cell. Especially in solid tumors, cancer progression follows the steps of activated invasion, induced angiogenesis and metastasis. These biological processes are summarized as hallmarks of cancer in a comprehensive review that Hanahan and Weinberg published in 2000 [43]. Under physiological conditions, the signaling pathways mediating these biological processes are strictly controlled and abnormalities seen in these signaling pathways are mostly associated with tumorigenesis.

ccRCC is the predominant malignant subtype with an incidence of 80-90 per cent among the other subtypes of RCC tumors. It is a epithelial neoplasm with high metastatic potential. Indeed, almost 30 per cent of ccRCC patients suffer from metastasis already at the diagnosis [10]. The high incidence of the disease drew the attention of many researchers to investigate the underlying signaling pathways contributing to its tumorigenesis. Owing to their attempt, VHL/ hypoxia-inducible factor 1 α (HIF-1α) and phosphatidylinositol 3-kinase (PI3K) /AKT protein kinase B (AKT) / mammalian target of rapamycin (mTOR) pathways were characterized as the main drivers for ccRCC cancerogenesis [44].

1.2.1. VHL/HIF-1α Pathway

The high vascularity and metastatic potential of ccRCC points out that angiogenesis is indispensible for its pathogenesis. In fact, deregulation of angiogenic signaling driven by hypoxia is reported for RCC tumors [44]. Besides being a common characteristic of solid

tumors, hypoxia plays a fundamental role especially for RCC malignancy, as most of ccRCC tumors have mutated *VHL* tumor-suppressor gene [45].

Hypoxia as a signaling mechanism is driven by the hypoxia inducible factors (HIFs) and occurs when the physiological oxygen level decreases below 5 per cent (Figure 1.2). HIF proteins are transcription factors and especially hypoxia-inducible factor 1 and 2 (HIF-1/2) initiate the transcription of over 200 hypoxia-inducible genes that are known to regulate cellular processes such as angiogenesis, metastasis, and apoptosis [46, 47]. HIF-1α and HIF-1β proteins together forms the heterodimeric HIF-1 protein [48]. HIF-1α has an oxygen-dependent degradation domain (ODDD) that enables the oxygen sensitivity and is expressed under hypoxic conditions, whereas HIF-1β lacks this domain and is constitutively active [49].

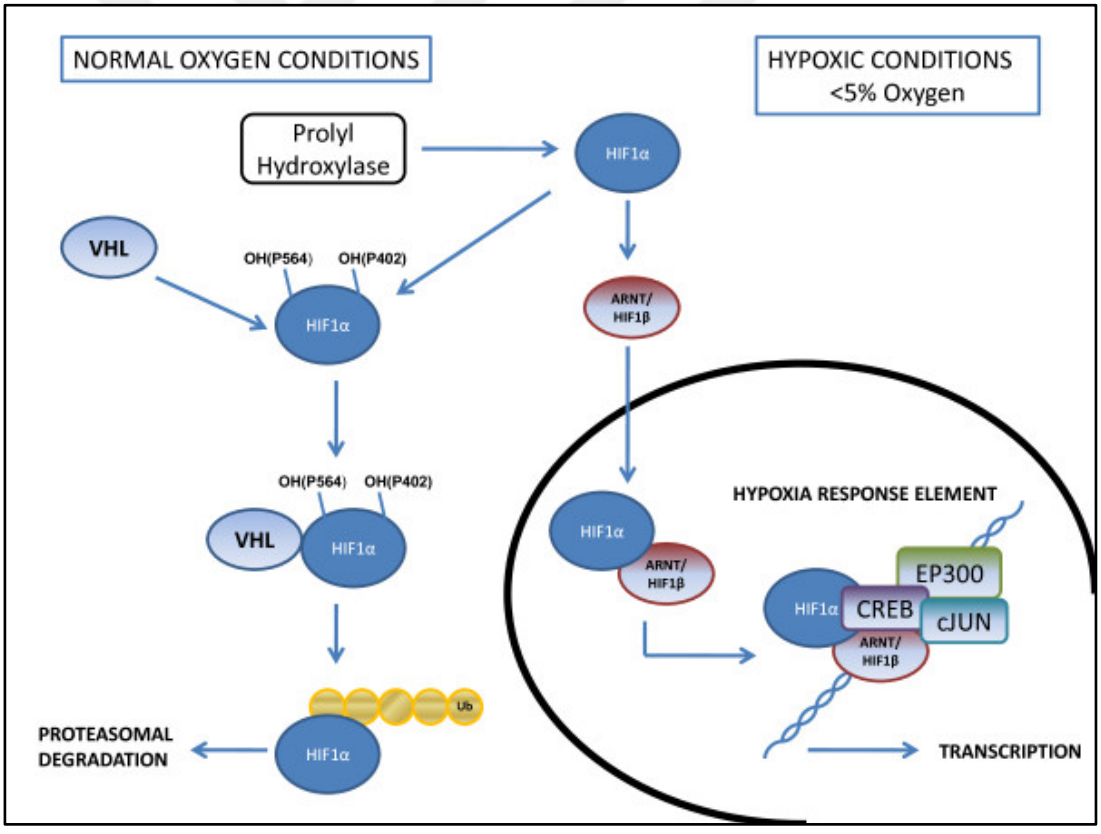

Figure 1.2. VHL/HIF-1α pathway [50]

Under normoxia, enzyme prolyl-hydroxylase (PHD) uses oxygen together with ferrous iron to oxidize HIF-1α protein [51]. The hydroxylated HIF-1α is recognized by E3 ubiquitin ligase complex comprised of VHL, elongin B, elongin C, and Cullin-2 proteins.

VHL protein within the complex then binds to and ubiquitinates the hydroxylated HIF-1α for its proteosomal degradation by 26S proteosome, which results in the inhibition of hypoxia- inducible gene expression [52]. However, PHD cannot hydroxylate the HIF-1α protein upon the hypoxic conditions, so that HIF-1α protein translocates into nucleus through aryl hydrocarbon receptor nuclear translocator (ARNT) [53, 54]. In nucleus, the binding of HIF-1α/1ß heterodimer to hypoxia response elements (HREs) triggers the recruitment of the cofactors including cAMP responsive element binding protein (CREB), E1A binding protein p300 (EP300), and jun proto- oncogene (c-JUN) to initiate the transcription of hypoxia-inducible genes, including as platelet-derived growth factor (PDGF) and vascular endothelial growth factor (VEGF), which are necessary for angiogenesis (Figure 1.2) [50, 54].

Previous studies have reported the elevated levels of HIF-1α in solid tumors such as breast, prostate, and renal carcinoma, where metastasis plays a crucial role in their malignancy. In case of renal cell carcinoma, overexpression of HIF proteins is mostly associated with the loss of *VHL* gene [55]. Especially, 80 per cent of ccRCC shows a sporadic feature with a point mutation in *VHL* gene and 4 per cent of patients with mRCC have hereditary history where *VHL* gene inheritably mutated [56, 57]. In either case, mutated VHL protein abolishes the hypoxic signaling because it can not fulfill its function of ubiquitination, which prevents the proteosomal degradation of HIF-1α [58]. In this regard, the loss of function of both alleles of *VHL* gene in ccRCC that causes to constitutive activation of HIF-1α/2α even under normoxic conditions explains the high vascularity and the metastatic potential of ccRCC [54]. Based on few studies, the high levels of HIF-2α were also reported to be associated with RCC tumorigenesis [59].

In addition to the regulation of angiogenesis in solid tumors under hypoxic conditions, the transcription factor HIF-1α can mediate the transcription of numerous hypoxia-inducible genes that have diverse roles in broad spectrum of biological processes such as metabolism and proliferation. In this regard, *GLUT1* and *GLUT3* can be given as example for HIF-1α target genes other than *VEGF* [46]. It was reported that HIF-1α changes the direction of metabolism from tricarboxylic acid (TCA) cycle to glycolytic pathway through expression of GLUT1 protein at the early onset of RCC tumor formation [60].

1.2.2. PI3K/AKT/mTOR Pathway

PI3K/AKT/mTOR pathway is one of the central intracellular signal transduction pathways regulating a wide variety of crucial processes such as growth, survival, proliferation, migration of cells, and angiogenesis as a respond to extracellular or intracellular stimuli [61]. PI3K/AKT/mTOR pathway consist of different kinases and proteins that can also participate in other signaling cascades by interacting indirectly or directly with their components. This interplay provides a complex network localizing PI3K/AKT/mTOR pathway in the center. Any dysregulation in the steps of the PI3K/AKT/mTOR signaling cascade can affect other cellular mechanisms which can, in turn, result in tumorigenesis. In fact, overexpression or loss of function of some of pathway components has been validated in numerous cancer types [62], especially in RCC cancerogenesis [63].

1.2.2.1. PI3K/AKT Axis

PI3K belongs to the lipid kinase family that phosphorylates phosphatidylinositol (PtdIns) lipids [64]. There are three classes of PI3K that differ from each other by the selectivity of lipid substrates and class I PI3K responds specifically to growth factors, cytokines, and hormones [65]. PI3K itself forms a heterodimer with regulatory p85α and catalytic p110α subunits [65]. Growth factors such as epidermal growth factor (EGF), platelet-derived growth factors (PDGF), insulin-like growth factor (IGF) and VEGF secreted through either paracrine or autocrine signaling bind to their corresponding receptor tyrosine kinases (RTKs) located on plasma membrane [66].

Upon the growth factor binding, RTKs undergo auto-phosphorylation at tyrosine residues on their cytoplasmic domain that tethers PI3K and thereby inducing its kinase activity [63]. Activated PI3K phosphorylates the membrane phospholipid phosphatidylinositol-4,5-bisphosphate (PIP2) to generate phosphatidylinositol-3,4,5- trisphosphate (PIP3). PIP3, then, enables the recruitment of phosphoinositide-dependent kinase 1 (PDK1) and AKT to cell membrane through their pleckstrin homology (PH) domains, which catalyzes the phosphorylation of activation loop of AKT at Thr308 by PDK1 (Figure 1.3) [67]. In addition to Thr308 phosphorylation, AKT is phosphorylated at Ser473 located in the

hydrophobic motif by mTOR complex 2 (mTORC2) and this dual phosphorylation on different residues causes the maximum kinase activity of AKT [68, 69]. AKT is responsible for the regulation of different processes such as glucose transport and protein synthesis by mediating the phosphorylation of a variety of proteins. The AKT's substrate specificity is determined by the phosphorylation of either Thr308 or Ser473 residues. In fact, effector proteins of p-AKT-Thr308 are identified as glycogen synthase kinase-3 (GSK-3) and tuberous sclerosis complex 2 (TSC2), whereas p-AKT-Ser473 targets the forkhead box O1/3a (FoxO1/3a) protein [70]. Dephosphorylation of Thr308 residue by protein phosphatase 2 (PP2) and Ser473 residue by PH domain leucine-rich repeat phosphatase (PHLPP) abrogates the signal transduction through AKT [71].

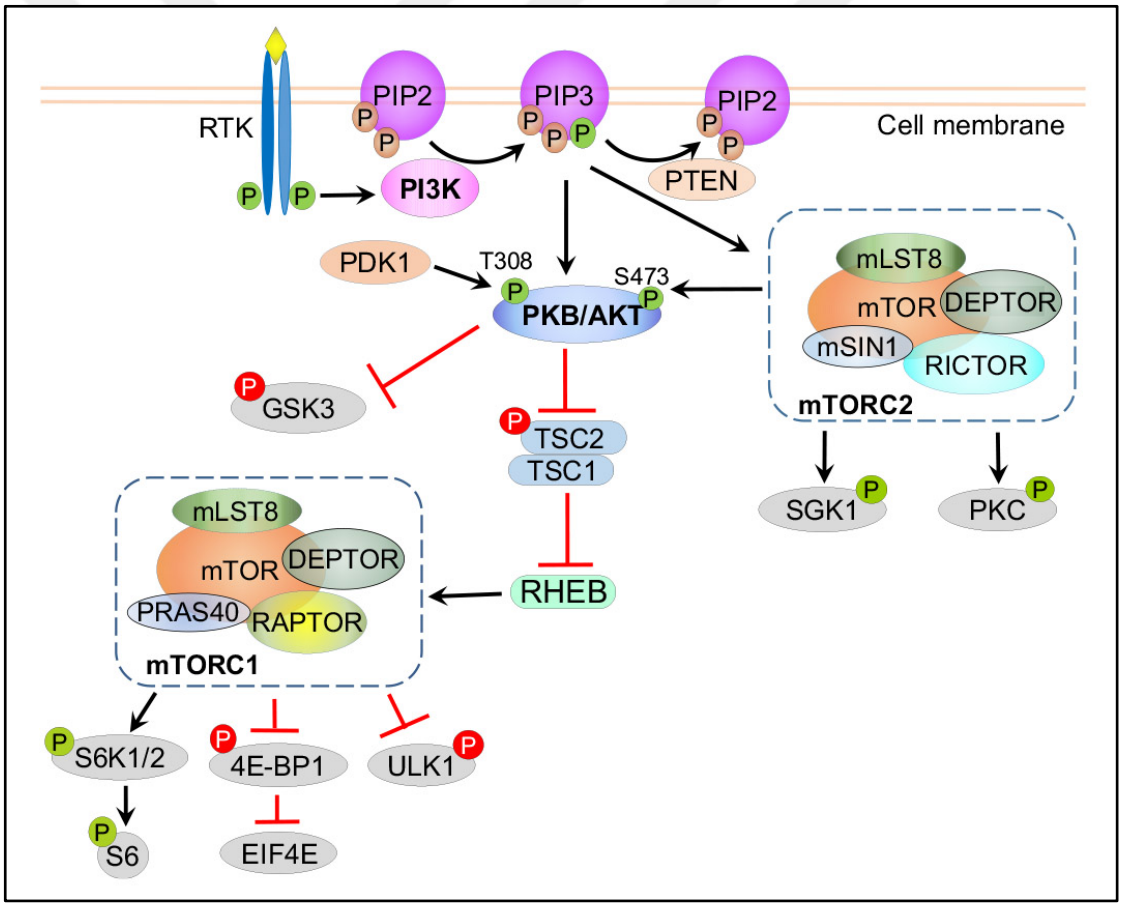

Figure 1.3. PI3K/AKT/mTOR pathway [72]

1.2.2.2. mTOR Pathway

AKT kinase has a broad spectrum of effector proteins that participate in metabolism, proliferation, angiogenesis, and translation (Figure 1.3) [71]. The well-studied downstream effector of AKT is mTOR that is a serine/threonine kinase acting as the main molecular switch for the regulation of cell proliferation, survival, growth, and metabolism [73]. mTOR, a member of the phosphatidylinositol kinase-related kinase (PIKK) family, is identified through the discovery of antifungal compound rapamycin. Rapamycin is able to form a complex together with FK506-binding protein 12 (FKBP12) protein, which then binds to FKBP12-rapamycin binding (FRB) domain that is located between FAT and kinase domain of mTOR protein. The binding of FKBP12-rapamycin complex to FRB causes inhibition of mTOR's kinase activity (Figure 1.4) [74]. There are two functionally distinct multi-protein complexes that have the mTOR as a catalytic subunit within the complex. mTOR complex 1 (mTORC1) and mTORC2 are composed of different components and they differ in the biological processes that they mediate through their downstream target proteins [75]. mTORC1 complex consists of mTOR, regulatory-associated protein of mTOR (Raptor), proline-rich AKT substrate 40 kDa (PRAS40), DEP-domain-containing mTOR-interacting protein (Deptor) and mammalian lethal with Sec13 protein 8 (mLST8) and regulates cell growth, cell cycle progression, macromolecule biogenesis or metabolism [75]. The activity of mTORC1 complex is selectively regulated by the PI3K/AKT pathway in response to growth factors.

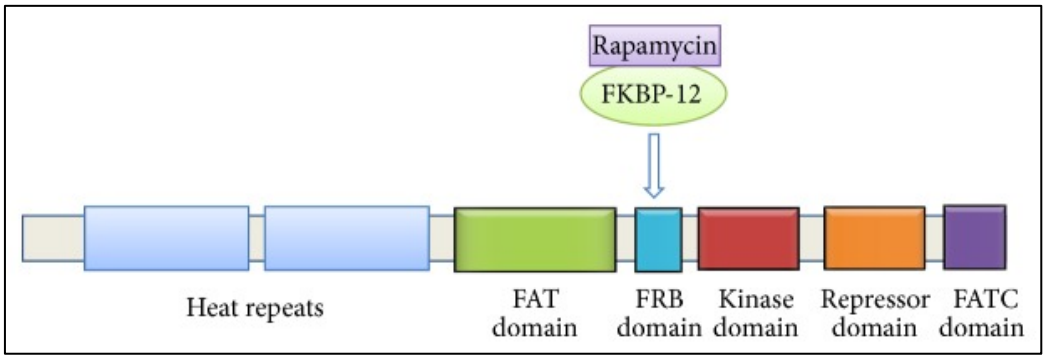

Figure 1.4. Structural organization of mTOR kinase [76]

Once phosphorylated by PDK1 at Thr308, AKT is released from the plasma membrane and phosphorylates TSC2 (tuberin) protein within the tuberous sclerosis complex (TSC1/2)

[77]. TSC2 is a GTPase-activating protein (GAP) for Ras homolog enriched in brain (Rheb), a positive regulator of mTORC1 [78]. AKT catalyzes the phosphorylation of TSC2 to prevent TSC2-mediated inhibition of Rheb, so that GTP-Rheb can not be converted into GDP-Rheb [79]. GTP-loaded Rheb interacts with mTORC1 complex through direct binding that triggers the kinase activity of mTOR [80]. AKT further controls the complex formation and the activity of mTORC1 by phosphorylating PRAS40, the inhibitory subunit of mTORC1, at Thr246 residue [81]. In addition to AKT, PRAS40 is also subjected to phosphorylation by mTOR at Ser221 residue to enable the substrate binding of Raptor [82, 83]. Thereby, activated mTOR performs the phosphorylation of eukaryotic translation initiation factor 4E binding protein 1 (4E-BP1) and 70kDa ribosomal protein S6 kinase 1 (S6K1) proteins, the mTORC1's downstream targets, to initiate translation [84, 85].

4E-BP1 is a small translation repressor protein that is responsible from the suppression of cap-dependent translation by direct binding to the eukaryotic initiation factor 4E (eIF4E) [86]. The inhibitory effect of 4E-BP1 protein on eIF4E is reversed through the phosphorylation of 4E-BP1, which occurs sequentially at threonine 37 (Thr37), threonine 46 (Thr46), threonine 70 (Thr70), and serine (Ser65) residues by the active mTOR kinase [87]. Briefly, phosphorylation of 4E-BP1 leads to its dissociation from eIF4E, so that free eIF4E can bind to 5' cap of mRNAs giving rise to the assembly of translation initiation machinery [88]. In addition to 4E-BP1 protein, activated mTOR kinase executes the phosphorylation of another target protein, S6K1, at Thr389. This phosphorylation event triggers the kinase activity of S6K1 resulting in the phosphorylation of ribosomal protein S6 at Ser235/236 and/or Ser240/244, a fundamental subunit of ribosomes, to facilitate the ribosome biogenesis [89, 90]. In addition to S6 phosphorylation, S6K1 can also phosphorylate S6K1 aly/REF-like target (SKAR) to stimulate mRNA biogenesis or eukaryotic translation initiation factor 4B (eIF4B) and programmed cell death 4 (PDCD4) to enable the cap-dependent translation. In addition, eukaryotic translation elongation factor 2 kinase (eEF2K), another target protein of S6K1, takes place in the translation elongation (Figure 1.5) [91].

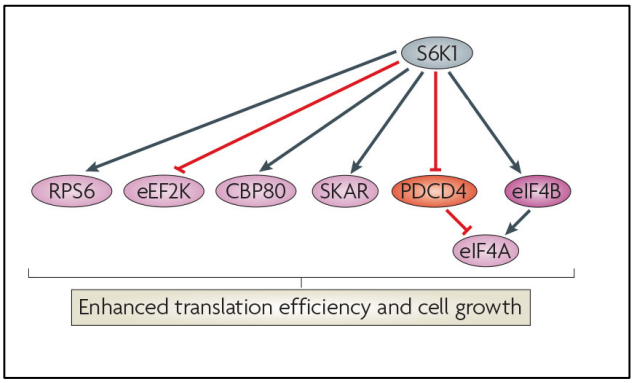

Figure 1.5. The downstream target proteins of S6K1, adapted from Ma and Blenis 2009 [91]

mTOR, rapamycin-insensitive companion of mTOR (Rictor), mammalian lethal with Sec13 protein 8 (mLST8), Deptor, and mammalian stress-activated protein kinase interacting protein (mSin1) form mTORC2 complex (Figure 1.3). The conserved function of the complex is the maintenance of cell survival and the regulation of cytoskeletal organization [75]. Like mTORC1, the activity of mTORC2 is controlled by the growth factors through PI3K/AKT axis [92], however, the direct mechanism for this regulation still remains unclear. Depending on the type of growth factor, mTORC2 phosphorylates a different target protein. AKT, protein kinase C alpha (PKCα), and serum glucocorticoid-induced protein kinase 1 (SGK1) and are AGC kinases and characterized as downstream effectors for mTORC2 [93]. The signaling triggered by growth factors initiates the auto-phosphorylation of mTOR at Ser2481, which is believed to be the marker for an active mTORC2 complex [94]. Active mTORC2, then, phosphorylates its well-studied substrate, AKT, at Thr450 and Ser473, which controls promotes cell survival by phosphorylating the pro-apoptotic proteins such as procaspase-9, BAD, and apoptosis signal regulation kinase 1 (ASK1) [69, 95]. Additionally, AKT together with SGK1 phosphorylated at Ser422 by mTORC2 can block apoptosis by targeting the transcription factors, FoxO1/3a, that is responsible for the transcription of genes coding the cell cycle inhibitors [70, 96]. In addition, mTORC2 participates in the regulation of actin cytoskeleton by activating PKCα that further elevates the migration potential of cells [97].

1.2.2.3. Regulation of PI3K/AKT/mTOR Pathway

PI3K/AKT/mTOR pathway mediates the signal transduction induced by growth factors to promote critical cellular processes that maintain the vitality of cells. Owing to its pivotal role, pathway is strictly regulated by feedback loops that act either upstream or downstream of the signaling cascade to prevent development of any cellular abnormalities. A lipid phosphatase, phosphatase and tensin homolog on chromosome 10 (PTEN), is an upstream negative regulator of PI3K and performs the dephosphorylation of PIP3 into PIP2 resulting in the interruption of signal transduction from RTKs to mTOR through AKT [98]. Loss of PTEN function caused by mutations or deletions was observed in a variety of human cancers including kidney cancer [99].

Additionally, the signal trafficking through PI3K/AKT axis can be blocked by mTORC1 complex, where mTORC1 counteracts its own activity by inducing the negative feedback mechanisms. In this regard, PI3K pathway was inhibited by mTORC1 through phosphorylation of growth factor receptor–bound protein 10 (Grb10) that serves as a negative regulator of the insulin-induced PI3K/AKT signal cascade [100]. In another mechanism, S6K1 phosphorylates insulin receptor substrate 1 (IRS1) at Ser302 to block growth factor-induced signaling of PI3K/AKT [101]. Furthermore, S6K1 inhibits mTORC2-mediated AKT phosphorylation at S473 by phosphorylating Rictor at Thr1135 site upon growth factor stimulus [102, 103].

1.2.2.4. mTOR Pathway and Renal Cell Carcinoma

Human cancers are mostly associated with the gain-of-function or loss-of-function mutations and abnormalities observed in the regulation of molecular mechanisms, especially those mediating the cell survival. mTOR pathway, the main regulator of cell survival, has been intensively reported as being affected in many types of cancers such as non-small cell lung carcinoma (NSCLC), breast cancer, colon cancer, and kidney cancer [62]. The participation of mTOR pathway in renal diseases ranges from the polycystic kidney disease to intrarenal inflammation and RCC [104]. In many types of cancer, the studies revealed that the mutations affecting this cell signaling pathway are considered as

oncogenic. Especially, *PTEN*, the negative regulator of PI3K, is listed as the second tumor suppressor gene after *p53* gene as being frequently mutated in human cancers. Besides *PTEN*, *PIK3CA* coding for catalytic subunit p110α of PI3K is another gene that is highly mutated in cancers after *KRAS* oncogene. However, mutations in *PTEN* and/or *PIK3CA* are not frequently observed in RCC, when the importance of PI3K/AKT/mTOR pathway for RCC tumorigenesis is considered [63].

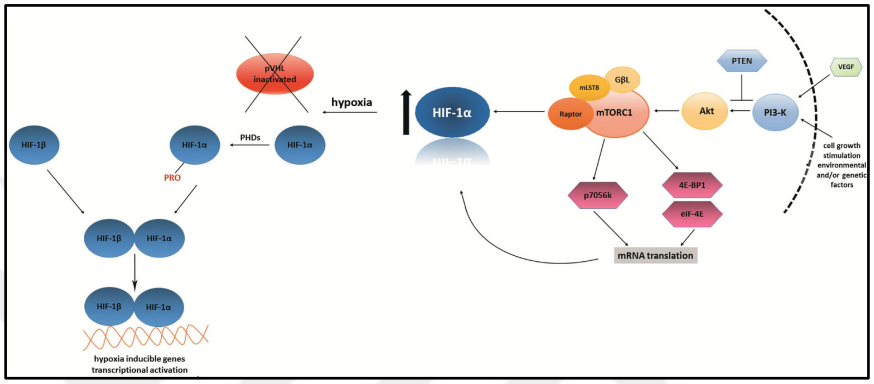

Figure 1.6. Interplay between HIF/VHL and PI3/AKT/mTOR pathways, adapted from Bielecka *et al.* 2014 [45]

The angiogenic signaling mediated by VHL/HIF-1α pathway is the major contributor of high vascularity and metastatic potential in ccRCC. Almost 75 per cent of ccRCC tumors are characterized as being *VHL*-deficient [45]. The *VHL* deficiency ensures the stabilization of HIF-1α protein that executes the angiogenesis through constitutive transcription of VEGF under growth factor stimulation [49]. The autocrine signaling of VEGF facilitates the interplay between VHL/HIF-1α pathway and PI3K/AKT/mTOR signaling that provides a positive feedback loop by participating in the translation of HIF-1α protein (Figure 1.6) [63, 105]. In fact, the upregulation of HIF-1α and HIF-2α was observed in RCC tumors [59, 106]. The overexpression of HIF-2α mediated by mTORC2 seems to be more critical in RCC tumorigenesis ratifying a pro-proliferative feature [107, 108]. This cross talk between two pathways implements a complex signaling network that is essential for RCC development. Additionally, it also explains the high activity of mTOR signaling, although the occurrence of mutations in genes such as *PTEN* and *PIK3CA* is a rare event in RCC [109].

1.2.3. Feedback Loops Activating mTOR Pathway

The acquired drug resistance is the major limitation confronted during cancer treatment with the current molecularly targeted therapies. Different molecular mechanisms facilitating or promoting the drug resistance was proposed for various cancer types. In general, resistance mechanisms mediate the activation of survival pathways or down-regulation of programmed cell death [110]. Besides their particular role in regulating these critical survival processes, they can also induce epithelial mesenchymal transition (EMT) and epigenetic modifications or alter the drug metabolism leading to the inactivation of drugs [111]. Among many malignant and solid tumors, mRCC tumors that have already showed resistance to the traditional therapies tend to enable insensitivity to the targeted agents [112]. A number of feedback mechanisms are proposed that dedicatedly coordinate the interplay between signaling cascades to provide a survival advantage to mRCC tumors [113]. The activation of PI3K/AKT pathway, loss of negative feedback loops or overexpression of anti-apoptotic proteins are the main examples for the characterized resistance mechanisms participating in the failure in drug response for mRCC tumors.

1.2.3.1. Loss of Negative Feedback Loops

AKT activation mostly serves as a possible biomarker for the acquired everolimus resistance observed in mRCC tumors [114]. Generally, the loss negative feedback loops activates the signaling cascade through PI3K/AKT axis, and thereby, they fully participate in the development of drug-resistance [115].

A negative feedback loop activated by mTORC1 is responsible to block IGF signaling using S6K1 protein. IGF signaling is responsible for the maintenance of cell growth, proliferation, and metabolism [116]. The signal transduction begins through the binding of IGF-1 to its corresponding receptor tyrosine kinase, IGF-R1, located on the cell membrane. The interaction of IGF-R1 with its ligand triggers the recruitment of the adaptor protein, IRS-1, to the cytoplasmic region of the RTK [117]. IRS-1, further, interacts with p85α subunit of PI3K to activate PI3K/AKT/mTOR pathway [118]. The active mTOR pathway, further, regulates the expression of IRS-1 through S6K1 protein. Besides, S6K1

phosphorylates IRS-1 protein at Ser302 to block the IGF-induced signaling cascade [101]. In case of rapalog treatment, the loss of S6K1 activation causes the stabilization of IRS-1 that contributes to the stimulation of PI3K/AKT axis by IGF signaling [119]. Everolimus resistance mediated-IGF signaling was observed in prostate cancer and acute myeloid leukemia [119, 120]. Moreover, IGF-induced AKT phosphorylation was reported in the multiple myeloma cells, rhabdomyosarcoma cell lines and xenograft mouse models [121, 122].

The loss of S6K1 as a consequence of mTORC1 inhibition also influence the RAS/ mitogen-activated protein kinase (MAPK) pathway through PI3K-dependent IGF-1/IRS-1 signaling [123]. MAPK pathway is a complex network of kinases that are responsible for the transduction of extracellular stimuli to nucleus to activate the corresponding genes regulating the cell growth, cell differentiation, cell proliferation, and apoptosis [124]. The interplay between mTOR and MAPK pathways was first shown by Carracedo *et al.*, where they proposed a negative feedback regulation of MAPK pathway by mTORC1 [123]. Their study showed an increase in the protein levels of phosphorylated extracellular signal-related kinase (ERK), the final executer of MAPK pathway, in the tumor samples of metastatic melanoma, breast and colon cancer derived from patients treated with everolimus [123]. Therefore, the activation of MAPK pathway is accepted as a feedback loop for the adaptive rapalog resistance [115].

In addition to the above mentioned feedback loops, another reason for the acquired rapalog resistance observed in mRCC tumors is the molecular switch from mTORC1 to mTORC2. Differently from mTORC1, mTORC2 complex is rapamycin insensitive and this insensitivity is provided by its constituent rictor [125] that is phosphorylated by S6K1 at Thr1135 [102, 103, 126]. Phosphorylated rictor blocks the mTORC2 complex to phosphorylate AKT at Ser473, thus providing a negative feedback loop [69]. Upon rapalog treatment, mTORC1 can not activate S6K1, and thereby loses its inhibitory effect on mTORC2, which causes the constitutive activation of AKT observed in rapalog-resistant mRCC [127, 128].

Additionally, active mTORC2 provides an interplay between mTOR and HIF pathways by upregulating the overexpression of HIF-2α that plays a major role in tumorigenesis [129]. HIF-2α is predominantly expressed in kidney and mediate the transcription of genes

including *VEGF* and *Cyclin D1* [130, 131]. Elevated levels of HIF-2α was also reported in mRCC as a critical player for its pathogenesis [107]. As mTORC2 is insensitive to rapamycin, rapamycin analogs could not downregulate HIF-2α expression, which limits the efficacy of mTORC1 targeted therapy in mRCC.

Mutations that occur in *FKBP12* or *mTOR* genes can also participate in the adaptive rapalog resistance, as they will impair the interaction of rapamycin and its analogs with FKBP12 or the rapamycin-FKBP12 complex with mTOR [113].

1.2.3.2. FKBP Proteins

FK506 binding proteins (FKBPs) belong to the immunophilin family that bind to the naturally occurring immunosuppressive agents, FK506 (tacrolimus) and rapamycin. FKBPs mainly act as chaperons as they participate in biochemical functions such as protein folding and protein trafficking. Besides their regulatory role during T-cell activation, they exhibit neuroprotective effects as they have been found to be abundantly expressed in neurons [132]. FK506 binding affinity and peptidylprolyl cis/trans isomerase (PPIase) activity are conserved in the canonical family members such as FKBP12, FKBP51, and FKBP52. FKBP38 is the non-canonical protein of the family as it neither possess PPIase activity nor binding affinity for FK506 due to lack of amino acid Trp59 residue within the FK506 binding domain (FKBD) [133, 134].

In comparison to FKBP12 that contains only FKBD domain, FKBP38 is a high molecular weight protein comprising FKBD, three units of tetratricopeptide repeats (TPRs), calmodulin binding domain (CBD), and transmembrane domain (Figure 1.7) [132, 133]. TPR domains enable the interaction of FKBP38 with anti-apoptotic proteins, including Bcl-2 and Bcl-xL [135], while through the FKBP-C within FKBD domain, FKBP38 interacts with Rheb and mTOR [136]. FKBP38 also associates with presenilin 1/2 and S4 subunit of proteosome through the TPR domains [137, 138]. The presence of a transmembrane domain in the structure enables FKBP38 to anchor at membranes of mitochondria and ER suggesting that FKBP38 protein can perform various undefined functions within the cells.

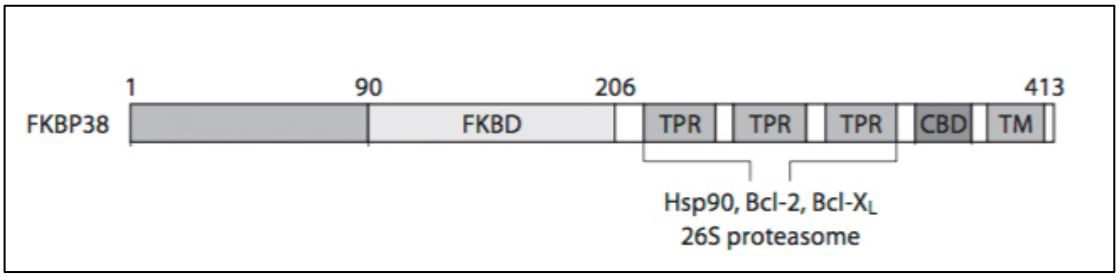

Figure 1.7. Domain organization of FKBP38, adapted from Kang *et al.* 2008 [132]

The relation of FKBP38 protein with mTOR pathway was first identified through a yeast two-hybrid screen performed to determine the putative interaction partners of Rheb [139]. The studies reported that the inhibitory effect of FKBP38 on mTORC1 complex, which is characterized by a decrease in the phosphorylation of mTORC1's downstream effector proteins, was lost through the interaction of FKBP38 with Rheb·GTP in the presence of insulin and nutrients (Figure 1.8) [136, 139, 140].

Besides mTOR and Rheb, Bcl-2 protein has been validated as an interacting partner of FKBP38 [142]. Bcl-2 has an unstructured flexible loop between BH4 and BH3 domains that is subjected to posttranslational modifications (PTMs) such as c-Jun N-terminal kinase (JNK)-mediated phosphorylation at Thr56, Ser70, and Ser87 [143]. The studies revealed that the specific binding of FKBP38 to this flexible loop prevents the phosphorylation of Bcl-2, and thereby, its proteosomal degradation [134]. FKBP38 interaction with the flexible loop protects Bcl-2 protein from the caspase-mediated cleavage, as Asp34 residue located at this unstructured loop of Bcl-2 protein was identified as a cleavage site for caspase 3 [135, 144]. This interaction further enables the localization of Bcl-2 protein into mitochondrial outer membrane (MOM), which results in the inhibition of apoptosis [142]. In fact, the knockdown of FKBP38 by siRNA was reported to reduce the Bcl-2 protein level concomitant with the induction of apoptosis, which was characterized by PARP cleavage and increased caspase 3 activity [145]. According to these findings, the interplay between FKBP38 and Bcl-2 has been suggested to maintain the chemoresistance in cancer cells overexpressing Bcl-2 protein [135].

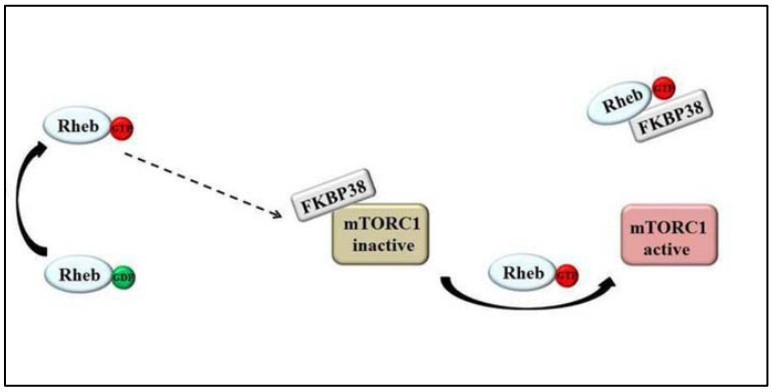

Figure 1.8. Interaction between FKBP38 and mTOR/ Rheb, adapted from Zheng *et al.* 2014 [141]

Besides the regulation of mTORC1 activity through competing with FKBP38, the interaction of Rheb with FKBP38 also contributes to apoptotic process. According to the study of Ma *et al.*, Rheb blocks the FKBP38-Bcl-2 interaction under the nutrient-rich conditions, once Bcl-2 is transported to mitochondrial outer membrane, suggesting an inhibitory role of Rheb on apoptosis [84]. Additionally, a recent paper proposed a regulatory role for FKBP38 during the interplay between Bcl-2 and mTORC1 complex, where it demonstrated that the association of the decreased mTORC1 activity with the siRNA-silenced Bcl-2 protein [146].

1.3. BCL-2 FAMILY MEDIATED APOPTOSIS

Apoptosis is the term used for a programmed cell death mechanism playing a major role in the regulation of diverse biological functions including maintenance of tissue homeostasis, elimination of damaged cells and pathogens. Besides, apoptosis is a necessary process occurring during embryogenesis. The hallmarks of apoptosis have been characterized according to the morphological changes that a cell undergoes during cell death process. Cell shrinkage, chromosomal condensation, DNA fragmentation can be given as main examples for the morphological alterations [147].

Extrinsic and intrinsic apoptotic pathways are two fundamental signal transduction pathways of apoptosis mediating cell death by respectively transducing extracellular and intracellular death signals to caspase cascade. Although both induce the activation of

caspase cascade at the final step of the apoptotic program, the mechanisms how they mediate the execution of apoptosis as well as the components that are involved in the process are quite different. Extrinsic apoptosis is a receptor-mediated cell death whose activation is triggered upon the binding of extracellular death-inducing ligands to death receptors located on plasma membrane, whereas intrinsic apoptosis initiates mitochondrion-mediated cell death as a response to intracellular abnormalities and tightly regulated by the orchestra of Bcl-2 family members [148].

Considering the extensive contribution of apoptosis in cell homeostasis, any aberrant regulation of proteins involved in apoptotic process can cause cancer development and severe disorders [149]. Besides, cancer cells have the ability of evading apoptosis to sustain their survival, which is one of the current limitations confronted during cancer treatment. To circumvent this problem, therapeutic agents targeting specifically apoptotic proteins were developed showing therapeutic benefits in the management of several malignancies [150].

1.3.1. Bcl-2 Family

Bcl-2 protein, the first identified member of the family, was determined as a transcript of *bcl-2* gene that was discovered near breakpoint between chromosomes 14 and 18 in human follicular B-cell lymphoma [151]. The translocation of *bcl-2* gene under the *immunoglobulin heavy chain* (*IgH*) gene enhancer Eμ results in the constitutive expression of Bcl-2, which is suggested to associate with pathogenesis of the lymphoma [152]. Instead of promoting cell proliferation, which is attributed to oncogenes, Bcl-2 provides a survival advantage for B-cell lymphoma [153, 154]. The intensive study in this field resulted in the discovery of other Bcl-2-related genes such as Bcl-xL, another negative regulator of apoptosis [155]. The first insights about the structural organization of Bcl-2 and its relatives came from the NMR analysis of Bcl-xL. This study revealed that Bcl-xL protein consists of seven α helices, a flexible loop between α1 and α2, and four Bcl-2 homology (BH) regions [156]. According to the findings obtained during last decades, a number of Bcl-2-related proteins were identified and divided into three classes (Figure 1.9). These proteins differ in their activities that they perform during apoptosis as well as in the

number of BH domains in their structure. The class of anti-apoptotic Bcl-2 proteins is comprised of Bcl-2, Bcl-xL, Bcl-w, A1, and Mcl-1 and responsible for the inhibition of apoptotic induction, whereas Bax, Bak, and Bok, the pro-apoptotic proteins, carry out the initiation process. The proteins in both groups contain four BH domains and nine α helices in their structure [157].

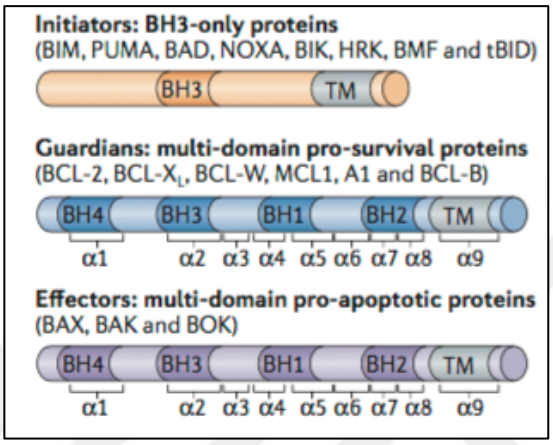

Figure 1.9. The Bcl-2 family, adapted from Czabotar *et al.* 2014 [157]

The execution of apoptosis merely based on the direct interaction between anti- and pro-apoptotic Bcl-2 proteins on MOM. Before their association, however, these proteins require the communication with BH3-only proteins that comprised the third class of the family. As the name indicates, these proteins possess only BH3 domain in their structure and play a balancing role between their pro- and anti-apoptotic counterparts [158]. Bim, Bid, Bik, Bad, Bmf, Hrk, Puma, Noxa, and Bnip3 are the examples of BH3-only proteins [159]. The structural differences in BH3 domain provides BH3-only proteins a target selectivity to act either as sensitizers or activators [147, 160]. Indeed, Bim, Puma, and tBid (the active form of Bid) have a broad selectivity enabling them to interact with both pro- or anti- survival Bcl-2 proteins [150]. Among sensitizers, Bad and Bmf targets specifically Bcl-2, Bcl-xL, and Bcl-w, whereas A-1 and Mcl-1 are the binding partners of Noxa [161]. This precise and organized interplay between Bcl-2 family members is maintained by their protein-protein interaction through the conserved BH3 domain [162, 163].

1.3.2. Execution of Intrinsic Apoptosis through MOMP

The main characteristic of the intrinsic apoptosis is the disruption of the mitochondrial outer membrane (MOM) integrity [159]. As a response to apoptotic stimuli, MOM undergoes permeabilization that is carried out by pro-apoptotic Bax and Bak proteins [164]. Bax and Bak differ by their cellular localization as well as through binding affinities for their anti-apoptotic counterparts [165, 166]. Under physiological conditions, the binding of corresponding anti-apoptotic Bcl-2 proteins inhibits Bax and Bak [167]. Bak that is constitutively bound to MOM interacts primarily with Bcl-xL and Mcl-1, whereas Bax is free in cytoplasm and targets Bcl-2 and Bcl-xL for binding once translocated onto MOM. Like Bak, Bcl-2 is also tightly bound to MOM, whereas Bcl-xL, Bcl-w, and Mcl-1 require conformational changes to be inserted into MOM (Figure 1.10) [168].

Upon apoptotic stimuli, the sensitizer BH3-only proteins (Bad, Bik, Bmf, Bnip3, Noxa, and Hrk) interacts with pro-survival proteins to interrupt their association with Bak or Bax. These sensitizer BH3 proteins do not possess the ability of direct binding to Bax and Bak [170]. Meanwhile, activator BH3-only proteins (Bim, Puma, and tBid, the cleaved form of Bid) that are able to interact both anti- and pro-apoptotic proteins, translocate to the MOM through their mitochondria targeting sequences (MTS). This binding of BH3-only proteins to MOM recruits cytosolic Bax to the MOM where it interacts with the membrane-bound Bak [171]. This interaction further leads to a conformational change in Bax's α1 helix to catalyze the insertion of α5, 6 and 9 helices into the MOM [172]. Bax stably inserted into MOM can reciprocally dimerize with other Bax or Bak proteins through its α2 helix corresponding to BH3 domain [173]. These Bax/Bax homodimers or Bax/Bak heterodimers can oligomerize and, thereby form a pore about 5 nm in diameter on the MOM [174]. The pore formation can now enables the cytochrome c leakage into cytosol [175]. The continuous oligomerization further increases the diameter of already existing pore resulting in the efflux of larger proteins such as pro-caspase 9 and Smac/Diablo. Under the presence of ATP, the interaction of cytosolic cytochrome c with Apaf-1 recruits pro-caspase 9 in order to form a wheel-like structure named apoptosome [176]. Apoptosome complex triggers the proteolytic cleavage of pro-caspase 9 into active caspase 9 that initiates cellular destruction by the activating of caspase 3, 6 and 7 [177, 178].

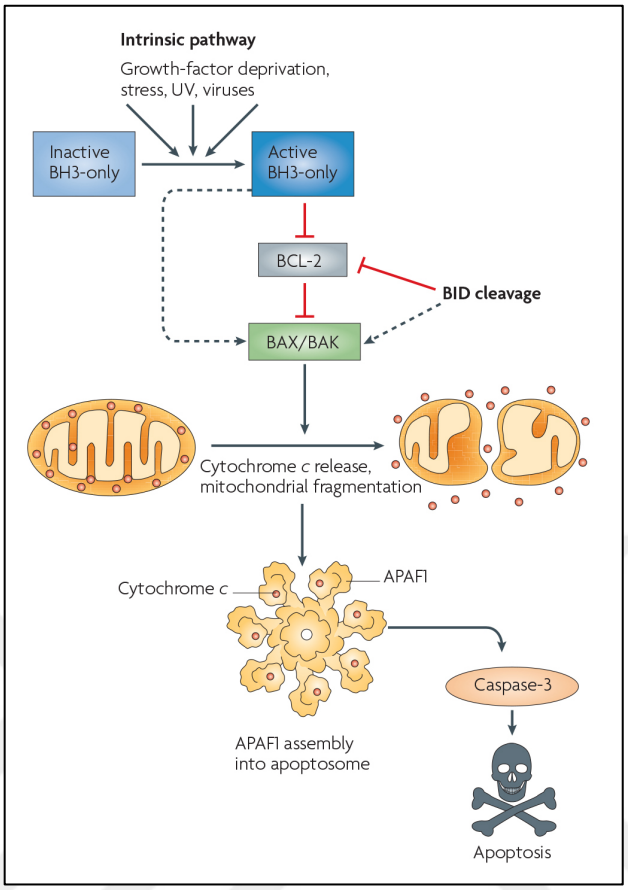

Figure 1.10. Mechanism of intrinsic apoptosis, adapted from Youle and Strasser 2008 [169]

1.4. TREATMENT OF METASTATIC RCC

Renal cell carcinoma is the prominent malignancy of kidney and accounts for 2-3 per cent of all adult tumors [3]. 70-75 percent of RCC patients are diagnosed with ccRCC at locally advanced stage, where almost 20-30 per cent of patients suffers from metastasis [179]. Radical nephrectomy, nephron sparing surgery (especially for bilateral RCC and RCC having high risk of tumor growth, and for patients with solitary kidney only), and laparoscopic nephrectomy (radical or partial) are the surgical operations for the localized mRCC [180]. In addition, minimal alternative treatments such as cryoablation, percutaneous radiofrequency (RF) or microwave therapy are the other medical attentions [181]. Although the surgery increases the survival rate about 85 per cent, patients are susceptible to the development of metastasis during follow-up period [182]. Low response

rate and resistance observed with standard chemotherapeutics during treatment of mRCC indicates that mRCC patients might benefit more from systemic therapy [183, 184]. In this regard, the cytokine therapy with high-dose interleukin 2 (IL-2) showed tumor regression that is durable for 10 months, whereas no durable response was observed with interferon-α (IFN-α) [185, 186]. The disadvantage of IL-2 therapy was the toxicity-associated severe side effects including capillary leak syndrome (CLS), arrhythmia, hypotension, nausea, vomiting, and diarrhea, which requires the selection of patients without organ failure as well as an intensive observation of patients during therapy [187, 188]. Therefore, the lack of survival benefit and the elevated toxicity of immunotherapy with IL-2 and IFN-α interfered with their use in mRCC treatment [189, 190].

The identification of signaling mechanisms participating in RCC tumorigenesis gave rise to the development of targeted therapy, which is accepted as the first treatment option for patients suffering from cytokine-refractory mRCC. Reports revealed that the use of the novel agents ameliorate the advantage of survival rate about two fold [191]. There are seven therapeutic agents currently used in clinic for mRCC treatment. These agents, namely sorafenib, sunitinib, bevacizumab, pazopanib, axitinib, temsirolimus, and everolimus are divided into two main groups according to their target mechanisms [192]. The first group is composed of sorafenib, sunitinib, pazopanib, and axitinib, which are tyrosine kinase inhibitors (TKIs) specifically targeting the highly expressed VEGFR. In addition to TKIs, bevacizumab can also be used as it is an humanized antibody against VEGF. The first group, therefore, is responsible for the suppression of RCC progression through the inhibition of angiogenesis [193, 194]. The second group of drugs contains temsirolimus and everolimus, so called rapalogs, that target mTOR pathway, the main mediator of cell growth, cell survival, cell proliferation and angiogenesis [73]. All molecular targeted agents mentioned here are further divided into two groups according to their administration line. Sunitinib, pazopanib, bevacizumab, and temsirolimus are used in the first-line setting, whereas sorafenib, axitinib, and everolimus are administered to mRCC patients as a second-line therapy [194].

1.4.1. Molecular Targeted Therapy

ccRCC, the most prevalent subtype of RCC tumors, is a epithelial neoplasm with a high metastatic potential. Metastasis is mostly observed during diagnosis or follow-up period after the surgery of patients diagnosed with advanced RCC. The identification of the molecular aspects underlining the tumor-associated vasculature of mRCC paved the way for the idea of the targeted therapy. Hence, many therapeutic agents were developed to specifically target the molecular mechanisms defining RCC tumorigenesis. Currently, there are seven therapeutics approved by FDA for the curative therapy of ccRCC as alternative cancer treatment to immunotherapy which exhibits a low efficacy. These therapeutics listed in Table 1.1 are classified as TKIs and mTOR inhibitors, and their aim is to increase the PFS of mRCC patients by blocking the VEGF-mediated angiogenesis in endothelial cells.

Table 1.1. List of drugs approved for the treatment of patients diagnosed with advanced and/or metastatic RCC

Generic Name	**Brand Name**	**FDA Approval (Year)**	**Target Molecule**	**Administration Line**
Sorafenib	Nexavar	2005	Raf-1, VEGFR (1,2,3), PDGFR-β, Flt-3, c-kit	2nd Line
Sunitinib	Sutent	2006	VEGFR-2, PDGFR	1st Line
Pazopanib	Vatrient	2009	all VEGF and PDFG receptors	1st Line
Axitinib	Inlyta	2012	VEGFR (1,2,3)	2nd Line
Bevacizumab	Avastin	2009	VEGF-A isoforms	1st Line
Temsirolimus	Torisel	2007	mTOR	1st Line
Everolimus	Afinitor	2009	mTOR	2nd Line

1.4.1.1. Tyrosine Kinase Inhibitors

TKIs inhibit a wide variety of tyrosine kinase receptors and disrupt the signal transduction activating angiogenic signaling. Their action mechanism is very similar, although they differ from each other in the duration of PFS and side effects that they exhibit [195]. Sorafenib is a first-generation TKI approved by FDA in 2005 for the treatment of patients with advanced RCC tumors [196]. Sorafenib targets the RAF/MEK/ERK pathway especially by inhibiting a broad spectrum of RTKs including VEGFR 1-2-3, PDGFR-β, Flt-3, c-kit, and as well as serine threonine kinase Raf-1[197]. Sorafenib monotherapy is accepted as the second line treatment for patients with cytokine-refractory and intermediate risk mRCC and shows a PFS of 5.5 months [198]. Diarrhea, nausea and hypertension were reported as severe side effects of sorafenib [199].

Sunitinib is another first generation TKI approved by FDA in 2006 as standard cure for the advanced ccRCC patients [196]. VEGFR-2 and PDGFR-α are the target molecules inhibited more potently among the other RTKs by sorafenib [200]. The agent administered in the first-line setting showed a PFS of 11 months in treatment-naïve patients and overall survival (OS) of 26.4 months [201, 202]. In addition to adverse effects including diarrhea, nausea, and fatigue observed with sorafenib treatment, the most severe site effect reported for sunitinib monotherapy is the cardiac toxicity [203, 204].

Pazopanib is a second generation multitargeted TKI developed to block all VEGF and PDGF receptors [205]. FDA approved the use of pazopanib for mRCC patients in 2009 which provides PFS about 9.2 months in treatment-naïve patients or patients subjected to the cytokine therapy [206, 207]. Pazopanib monotherapy is administered in the first-line setting for good or intermediate risk mRCC patients as an alternative to sunitinib monotherapy due to its tolerability [188, 194]. In addition to gastrointestinal side effects, hepatotoxicity was observed with pazopanib treatment [199, 208].

The third generation TKI, axitinib, selectively inhibits the VEGFR-1, 2, and 3 [209]. In 2012, the drug was approved by FDA for standard treatment of mRCC patients with failure to immunotherapy in a second-line setting with a PFS of 6.7 months [210]. In addition to gastrointestinal symptoms as adverse effects, the drug exhibits a higher risk of hypertension compared to the other TKIs [211, 212].

Another comprehensive subject in the field of molecular targeted therapy is the therapeutic benefit of monoclonal antibodies that are utilized to target specific proteins participating in the angiogenic signaling. Bevacizumab is a monoclonal humanized antibody designed to particularly neutralize all isoforms of pro-angiogenic VEGF-A [213]. FDA gave approval for bevacizumab in 2009 to be utilized as the first-line treatment together with IFN-α [196]. The combination of bevacizumab with IFN-α increased PFS up to 10.2 months for good or intermediate risk mRCC patients [214]. Hypertension, anorexia and fatigue are reported as adverse effects of bevacizumab and IFN-α combination therapy [215].

1.4.1.2. mTOR Inhibitors

mTOR inhibitors are designed to suppress the tumor cell growth, cell proliferation and neovascularization by inhibiting the activity of mTOR. They are the derivatives of rapamycin that forms a complex with its intracellular receptor, FKBP12 [216]. This complex exclusively binds to mTOR's FRB domain to impair the interaction between mTOR and raptor, thereby preventing the initiation of translation by mTORC1 [217]. In comparison to mTORC1, mTORC2 is insensitive to rapamycin and this insensitivity is attributed to the existence of rictor, the regulatory protein for mTOR kinase in complex 2 [125]. However, it was reported that rapamycin-insensitivity of mTORC2 can be reversed by the prolonged treatment of rapamycin through the disruption of complex formation [69, 218].

There are currently two mTOR inhibitors, temsirolimus and everolimus, which were approved by FDA for the therapy of patients with metastatic ccRCC [196]. Both temsirolimus and everolimus are analogues of rapamycin that was identified as an antifungal antibiotic isolated from the bacteria *Streptomyces hygroscopicus* [74]. Initially, rapamycin showed the ability to suppress the immune response that enabled its use in organ allografting to inhibit the rejection [219]. In fact, FDA approved the use of rapamycin in combination with cyclosporine in clinic for the patients undergone renal allografts [220, 221]. Almost a few years later after its discovery, investigations performed in solid tumors such as colon and brain pointed out the antitumor activity of rapamycin [222]. Growing evidence of *in vitro* studies further revealed that rapamycin causes growth arrest of cells originated from cancers including SCLC, neuroblastoma, prostate cancer, B-

cell lymphoma, and osteosarcoma [223]. Further, Luan *et al.* suggested that rapamycin treatment could block tumor growth and progression of metastasis in *in vivo* model of murine RCC [224]. Although *in vitro* and *in vivo* studies could potentiate the use of rapamycin in clinic, the low solubility in water made its clinical utility impossible [223]. In comparison to rapamycin, its analogue temsirolimus exhibited better solubility that facilitates its intravenous administration [196]. Therefore, temsirolimus is approved by FDA in 2009 for the cure of advanced RCC patients as the first-line therapy [196, 225]. The monotherapy with temsirolimus showed a PFS of 3.8 months for the poor risk mRCC patients who were not subjected to any treatments with targeted agents [226]. Additionally, the drug provided therapeutic benefit for patients diagnosed with non-clear cell RCC as well as for patients who did not undergo nephrectomy [227, 228]. Rash and mucotitis are the adverse events reported for temsirolimus treatment [226].

Everolimus (RAD001) is the second mTOR inhibitor approved by FDA in 2009 for the treatment of sorafenib/sunitinib refractory mRCC patients as a second-line therapy [229]. In comparison to temsirolimus, everolimus is an orally bioavailable agent. A phase I study performed to estimate the convenient dose of everolimus demonstrated good response in solid tumors including RCC [230]. Phase II trial with advanced mRCC patients showed antitumor activity of everolimus [231]. Later, Motzer *et al.* conducted a phase III trial with 416 mRCC patients who were subjected to prior TKI therapy. The study revealed a median PFS for 4.9 months. The observed adverse effects were dyspnea and fatigue. Importantly, the side effects associated with TKI treatment were not reported for everolimus monotherapy [232]. Of note, a recent meta analysis performed by Pal *et al.* indicated that any agent of TKI chosen for the first-line therapy did not affect the consequence of everolimus treatment in a second-line setting [233]. The promising efficacy of everolimus observed for mRCC opened the way to investigate its potent therapeutic role in other malignancies. In this regard, there are ongoing phase II trials that study the antitumor effect of everolimus in several cancers such as mantle cell lymphoma, gliablastoma and breast cancer [234]. Besides its therapeutic success, the main issue confronted with rapalog treatment is the limitation of the therapy due to the development of drug resistance [97]. In fact, the acquired resistance against rapalogs causes to insufficiency of therapy to decrease the mortality rate and/or increase the duration of PFS. The studies investigating the possible reasons for the generation of resistance draw attention towards the feedback loops

and the interconnected molecular mechanisms that are activated upon the inhibition of mTOR pathway [115].

1.4.2. Recent Advances in mRCC Treatment

The limited response of mRCC patients to current treatments has accelerated the search for other molecular targeted agents providing better efficiency and less toxicity. Recent advances revealed that there are a number of new therapeutics that are still under investigations in terms of clinical trials. The main purpose of these novel therapeutics is to overcome the rapalog-resistance encountered during mRCC treatment. Given the suggested participation of several feedback loops activated by PI3K/AKT axis and mTORC2 complex in the acquired rapalog resistance, several attempts were performed to develop novel therapeutics targeting those pathways. In fact, molecular targeted agents such as NVP-BEZ235, GDC0980, BEZ235, GDC0890 and GSK1059615 have been designed to block specifically both PI3K and mTOR kinases, whereas AZD8055 and AZD2014 solely target mTORC1/mTORC2 [235]. Among these drugs, especially NVP-BEZ235, and AZD2014 were tested in mRCC patients to compare their efficiency with the rapalog treatment.

NVP-BEZ235 is a dual-drug targeting ATP-binding domain of pan class I PI3K and mTOR kinase. Although preclinical study revealed the growth arrest both *in vitro* and *in vivo* settings, phase II study has been terminated due to severe adverse affects [236, 237]. In addition, phase I study is completed, which is conducted for the use of BEZ235 in combination with everolimus in 2015. However, the results of the study has not been reported yet. In comparison to NVP-BEZ235, AZD2014 is designed to merely inhibit mTOR kinase activity in mTORC1 and mTORC2 complexes. According to preclinical study indicating the higher efficiency of AZD2014 compared to rapamycin and RAD001, investigation for dose determination was performed as phase I trial in patients with the advanced solid tumors and the convenient dose for phase II was reported [238, 239]. However, phase II study conducted in VEGF-refractory mRCC patients was terminated due to the adverse effects that decrease the efficiency of AZD2014 in terms of PFS in comparison to everolimus [240].

Therefore, the development of novel therapy strategies is still the urgent need for the treatment of mRCC patients.

1.4.3. New Approaches Targeting Evasion of Apoptosis

Cancer cells can change their genetic background to affect the process of signaling mechanisms playing a pivotal role in cell survival. Enormous data obtained through investigations about cancer initiation and progression have enabled the characterization of essential cancer hallmarks that utilize the complex interplay between cellular processes [43]. In this regard, evasion of apoptosis, one of these hallmarks, is the major strategy used by cancer cells to develop resistance against standard anti-cancer therapies as well as molecular targeted therapies.

The attempts made to characterize apoptotic process led to the identification of Bcl-2 family proteins that play a crucial role in cancer biology. Owing to their significant impact on cancerogenesis, researchers performed structure-based development of drugs in order to target only pro-survival members of Bcl-2 family. Among the others, Bcl-2 protein is the most studied member of the family targeted by these agents.

1.4.3.1. Bcl-2 Targeted Therapy

During the last decades, investigations performed in various solid tumors revealed the tremendous contribution of anti-apoptotic Bcl-2 protein in their tumorigenesis as well as the resistance against conventional therapies. Besides the standard anti-cancer therapies that use cytotoxic agents such as cisplatin or doxorubicin, the acquired resistance to novel molecular targeted agents is also suggested to associate with the overexpressed anti-apoptotic Bcl-2 protein [241-243].

The importance of *bcl-2* gene in the pathogenesis of cancer has been first identified in human follicular B-cell lymphoma [152]. Later, Vaux *et al.* suggested the role of Bcl-2 protein in cell survival by the study performed with lymphoid and myeloid cell lines [153]. Besides hematological malignancies, expression of Bcl-2 protein was recorded in solid tumors including neuroblastoma, malignant melanoma, androgen-independent prostate

carcinoma, NSCLC, SCLC, and esophageal squamous cell carcinoma [244-248]. Additionally, the immunohistochemical analysis carried out in RCC tumors also indicated the overexpression of Bcl-2 [243, 249-253]. However, the association of the elevated Bcl-2 level with resistance to apoptosis was first mentioned for multidrug resistant SCLC [248, 254] and later reported in chronic lymphocytic leukemia (CLL) and SCLC [255-257]. Besides Bcl-2, Bcl-xL has been also suggested to be an indicator of chemo-resistance observed in multiple myeloma [258]. As its elevated level negatively modulates the cytotoxicity of anti-tumor therapeutics, several BH3 mimetics were developed in order to attenuate the interaction of anti-apoptotic Bcl-2 proteins with their pro-apoptotic and BH3-only counterparts.

Among several Bcl-2 inhibitors, obatoclax (GX15-070) was developed as pan-Bcl-2 inhibitor [259]. Although obatoclax inhibited more potently Bcl-2, Bcl-xL, and Mcl-1, it could not induce the "Bcl-2 relief of inhibition" on Bax/Bak activation which is determined as a necessary mechanism of action for BH3 mimetic [260].

Further attempts were performed to find out a compound binding to hydrophobic groove of Bcl-xL protein. Chemical structure of the compound discovered through screening of a chemical library was revised to increase the binding affinity against Bcl-xL and, thus ABT-737 was developed [261]. Besides Bcl-xL, ABT-737 has the ability to inhibit Bcl-2 and Bcl-w, as they possess a structure similarity. However, other anti-apoptotic proteins including Mcl-1 and A1 are not the targets of ABT-737 because they exhibit different structural properties [261]. The efficiency ABT-737 was first investigated in hematological diseases as well as in SCLC, where it provided pronounce implications for clinical developments [262, 263]. Preclinical trials performed in CLL and myeloma have shown that ABT-737 was able to induce Bcl-2-mediated apoptosis through displacing the pro-apoptotic Bax and Bak from Bcl-2 [262, 264].

Because of the solubility problems, ABT-263 (navitoclax), orally bioavailable analog of ABT-737, was developed and used in clinical trials [265]. Phase I study of ABT-263 conducted in patients suffering from refractory lymphoid malignancies revealed PFS of 25 months. Thrombocytopenia, lymphopenia and diarrhea were the reported adverse effects [266]. Another phase I carried out eight SCLC patients reported the safety and tolerability of ABT-263. Documented side effects were the dose-dependent thrombocytopenia,

diarrhea, nausea, vomiting, and fatigue [267]. In comparison to phase I and II studies, however, the phase II of ABT-263 conducted in patients with recurrent SCLC showed limited single agent efficiency with thrombocytopenia as adverse effect [268]. In order to circumvent the development of thrombocytopenia that is the major limitation confronted with ABT-263 treatment, another orally available agent, ABT-199, was developed, which merely targets the Bcl-2 protein [269].

The duration of response as 20.5 months was reported as a result of phase I study conducted with refractory CLL patients which was compared to the phase II trial carried out in high risk AML patients [270]. Neutropenia, diarrhea and fatigue are the adverse effects observed in both trials. According to the promising outcome of phase trials, ABT-199 is currently the prominent agent for hematological malignancies used in clinic.

1.5. AIM OF THE STUDY

RCC is the prominent type of kidney cancer and accounts for 2-3 per cent of all adult tumors [3]. Among several histopathological subtypes, ccRCC comprises the majority of RCC cases and displays an aggressive malignant profile [15]. In fact, tumor has already developed resistance to the standard anti-cancer therapies in 20-30 per cent of patients diagnosed with ccRCC at advanced or metastatic stage [10].

According to studies performed in last decades, VHL/HIF and mTOR pathways have been identified to play an essential role in ccRCC tumorigenesis [44]. The loss of *VHL* gene has been reported in most of the ccRCC tumors, which causes overexpression of HIF proteins that regulate the initiation of angiogenesis through growth factors such as EGF and VEGF as well as the induction of mTOR pathway, the main mediator of cell survival [54, 55, 104]. In fact, the elevated activity of the mTOR pathway has been associated with ccRCC tumorigenesis [62]. In this regard, everolimus, FDA-approved mTOR kinase inhibitor, is used in clinic to provide a therapeutic advantage for the treatment of advanced RCC [271]. However, the expected efficacy of the everolimus therapy could not be achieved due to the acquired everolimus-resistance that circumvents mTOR inhibition and further results in the tumor recurrence [192, 272].

Among several feedback loops, the overexpression of anti-apoptotic Bcl-2 protein has been suggested to play a role in the acquired drug resistance, as its overexpression was reported in hematological disorders, solid tumors as well as in RCC [244, 246, 253]. However, its contribution to rapalog resistance was reported only in prostate intraepithelial neoplasia [273]. Owing to its association with cancer survival as a prominent biomarker, several small BH3 mimicking molecules have been developed in order to activate the apoptotic process by blocking the interaction of anti-apoptotic Bcl-2 protein with its pro-apoptotic counterparts [150]. In this regard, the preclinical efficiency of ABT-737, a BH3 mimetic, have been investigated in several cancer types including lymphoma and SCLC [262, 263]. However, the anti-cancer effect of ABT-737 on everolimus-resistant RCC tumors has not been tested yet. Given the suggested role of high Bcl-2 protein levels in the development of everolimus-resistance in mRCC tumors, this thesis aimed to investigate the anti-tumor effect of ABT-737 alone or everolimus-ABT-737 combination using Bcl-2 overexpressing RCC cell lines and established RCC xenograft mouse model. In this regard, the aim of this thesis was to complete the preclinical study of everolimus-ABT-737 combination therapy that is needed prior to clinical trials for mRCC patients.

Another aim of the thesis is to clarify the molecular mechanism for the interplay between mTOR and Bcl-2 pathway. Our second hypothesis was to test whether the crosstalk between two pathways depends on FKBP38 protein, as it can interact with both mTOR kinase and Bcl-2 protein under the regulation of Rheb [139, 142]. In support of our hypothesis, FKBP38 was reported to participate in Bcl-2-mediated mTORC1 regulation, where knockdown of Bcl-2 correlated with the attenuation of mTORC1 activity [146]. Therefore, this thesis aimed to determine the participation of FKBP38 protein as a scaffold between mTOR and Bcl-2 in everolimus-resistant mRCC.

2. MATERIALS

2.1. INSTRUMENTS

2.1.1. Instruments used for Cell Culture Experiments

CO_2 incubator (Thermo Fisher Scientific, USA), Laminar Flow Cabinet (ESCO Labculture Class II Biohazard Safety Cabinet 2A, Singapore), Low-Speed Centrifuge (Gyrozen 416, Korea), Microscope Primo Vert (Zeiss, Germany), Shaking Water Bath (Stuart, UK), 80°C freezer (Thermo Forma -86°C ULT Freezer, USA)

2.1.2. Instruments used for Cell Death

FACS Calibur (BD Biosciences, USA)

2.1.3. Instruments used for SDS-PAGE and Western Blot

ChemiDOC XRS+Gel Imaging System (Bio-Rad Universal Hood 2, USA), Gyro-Rocker (Stuart, UK), Magnetic Stirrer (MR 3004 Heidolph, Germany), Mikro 22 R Centrifuge (Hettich Zentrifugen, Germany), Mini Trans-Blot Cell Blotting System (Bio-Rad 170-3935, USA), Mini-PROTEAN Tetra Cell Electrophoresis System (Bio-Rad 165-8001, USA), Multi-Rotator (BioSan Multi Bio RS-24, Latvia), pH/ ORP/ Temperature Bench Meter (Milwaukee Mi151, USA), Pierce G2 Fast Blotter (Thermo Fisher Scientific 62287, USA), SpectraMax Paradigm (Molecular Devices Multi-Mode Detection Platform, USA), TS-1 Thermo-Shaker (INOVIA Technology, UK), Vortex (Stuart SA8, UK), Weighing Machine (Shimadzu Corporation TW423L, Japan)

2.2. EQUIPMENTS

15 ml and 50 ml Conical Bottom Centrifuge Tube, Screw Cap (Axygen, USA), Pipette Tips (10, 200, and 1000 µl) (SPL Life Sciences, Korea), Bright-Line Hemocytometer (Sigma Aldrich Z359629, Germany), Cell Culture Dish (60 mm x 15 mm) (SPL Life Sciences 20060, Korea), Cell Culture Dish, 100 mm (SPL Life Sciences 200200, Korea), Cell Culture Flask T-150 (SPL Life Sciences, Korea), Cryo Tubes two ml (TPP 89020, Switzerland), Electronic pipette (CAPP aid, Denmark), Filter 0.22/0.45 µm (Santorius Stedim Biotech, Germany), Graduated Cylinder 50, 250, 500, and 1000 ml (Isolab, Germany), Microcentrifuge Tubes 0.5, 1.5, and two ml (CAPP, Denmark), Micropipettes two, 10, 20, 100, 200, and 1000 µl (Eppendorf Research, Germany), Serological pipets two, 5, 10, and 25 ml (Isolab, Germany), Tissue Culture Flask T-25 (TPP 90025 or 90026, Switzerland), Tissue Culture Flask T-75 (TPP 90075 or 90076, Switzerland), Tissue Culture Test Plates 6-well, 12-well, 24-well, and 96-well (TPP, Switzerland)

2.3. DRUGS

ABT-737 (Selleck Chemicals S1002, USA), Aphidicolin (Santa Cruz Biotechnology sc-201535, USA), Everolimus (Selleck Chemicals S1120, USA)

2.4. CHEMICALS

2.4.1. Chemicals used for Cell Culture

Amphotericin B (Gibco 15290018, Thermo Fisher Scientific, USA), Cell Proliferation Reagent WST-1 (Roche 11644807001, Switzerland), DMSO (Dimethyl Sulphoxide) (Santa Cruz Biotechnology sc-202581, USA), DMEM with L-glutamine (Gibco 41966-029, Thermo Fisher Scientific, USA), Heat inactivated Fetal Bovine Serum (FBS) (Gibco 10500-056, Thermo Fisher Scientific, USA), L-glutamine Solution (Sigma Aldrich G7513, Germany), McCoy's 5A (modified) (Gibco 26600-023, Thermo Fisher Scientific, USA), Penicillin-Streptomycin (Gibco 15140-122 Thermo Fisher Scientific, USA), Phosphate

Buffered Saline (PBS) (Lonza BE17-517Q, Switzerland), RPMI-1640 Medium (Sigma Aldrich R8758, USA), Trypsin 10x (Lonza BE02-007E, Switzerland)

2.4.2. Chemicals used for Cell Death

Annexin V-FLUOS Staining Kit (Roche 11988549001, Switzerland)

2.4.3. Chemicals used for Co-Immunoprecipitation

EDTA (Merck 324503, Germany), Phenylmethanesulfonyl fluoride (Sigma Aldrich 78830, Germany), Protein A-Agarose (Santa Cruz Biotechnology sc-2001, USA), Protein G Plus Agarose (Santa Cruz Biotechnology sc-2002, USA), Sodium Deoxycholate (Sigma Aldrich D6750, USA)

2.4.4. Chemicals used for SDS-PAGE and Western Blot

2-Propanol (Sigma Aldrich 24137, Germany), Acrylamide/Bis-acrylamide, 30 per cent solution (Sigma Aldrich A3574, Germany A), Albumin, Bovine Serum (Bioshop Canada ALB001, Canada), Amersham Full-Range Rainbow Molecular Weight Marker (GE Healthcare RPN800E, USA), Ammonium persulfate (APS) (Sigma Aldrich A3678, Germany), Dodecyl sulfate sodium salt (Sigma Aldrich L3771, Germany), Ethanol (Sigma Aldrich 32221, USA), Glycine (Santa Cruz Biotechnology sc-29096B, USA), Immobilon-P Membrane, PVDF, 0.45 µm (Millipore IPVH00010, USA), Immobilon-PSQ PVDF Membrane, 0.2µm (Merck ISEQ00010, Germany), Isopropanol extra pure (Sigma Aldrich I9516, Germany), Laemmli Buffer 2x Concentrate (Sigma Aldrich S3401, Germany), Mercaptoethanol (Merck 805740, Germany), Methanol (Sigma Aldrich 34885, Germany), Mitochondria Isolation Kit for Cultured Cells (Thermo Fisher Scientific 89874, USA), Nitrocellulose membrane (0.22 µm) (GE Healthcare RPN3032D, USA), Nitrocellulose membrane (0.45 µm) (GE Healthcare RPN303D, USA), Protein Assay Dye Reagent Concentrate (Bio-Rad 5000006, USA), Protein Assay Reagent A (Bio-Rad 5000113, USA), Protein Assay Reagent B (Bio-Rad 5000114, USA), RIPA Buffer (Santa Cruz

Biotechnology sc-24948, USA), Sodium Azide (Sigma Aldrich S2002, Germany), Sodium Chloride (Merck 106404, Germany), Sodium Hydroxide (Sigma Aldrich 06203, Germany), Tris Ultra Pure (MP Biomedical 819623, France), Trizma hydrochloride (Fisher Scientific BP153-1, USA), TWEEN® 20 Detergent (Merck 655204, Germany), WesternBright Sirius HRP Substrate (Advansta K-12043, USA), Whatman 3MM CHR Blotting Paper (GE Health Care3030-917, USA)

2.5. ANTIBODIES

2.5.1. Primary Antibodies

4E-BP1 (CST 9452S, USA), AKT (CST 9272S, USA), Anti-Bcl-2 (phospho S87) (Abcam Ab73985, UK), Bad (CST 9239P, USA), Bax (CST 5023P, USA), Bcl-2 (CST 2870P and 15071S, USA), Bcl-xL (CST 2764P, USA), Bim (CST 2933P, USA), Caspase 9 (CST 9502S, USA), CDK2 (CST 2546S, USA), CDK4 (CST 12790S, USA), Cleaved caspase 3 (CST 9664S, USA), Cyclin D3 (CST 2936S, USA), Cyclin E1 (CST 4129S, USA), Cyclin D1 (CST 2978S, USA), Cytochrome c (CST 4272S, USA), FKBP38 (Abcam ab24450, UK), FKBP38 (Millipore ABS992, USA), FKBP38 (Novus NBP1-77909, USA), Mcl-1 (CST 5453P, USA), mTOR (CST 2972S, USA), Noxa (CST 14766S, USA), $p27^{Kip1}$ (CST 3686S, USA), P53 (CST 2524S, USA), p70S6K (CST 9202S, USA), pan-Actin (CST 8456S, USA), PARP (CST 9542P, USA), Phospho-4E-BP1 (Ser65) (CST 9451S, USA), Phospho-4E-BP1 (Thr37/46) (CST 2855S, USA), Phospho-4E-BP1 (Thr70) (CST 9455S, USA), Phospho-AKT (Ser473) (CST 4060S, USA), Phospho-AKT (Thr308) (CST 9275S, USA), Phospho-Bad (Ser136) (CST 4366S, USA), Phospho-Bcl-2 (Ser70) (CST 2827P, USA), Phospho-Bcl-2 (Thr56) (CST 2875P, USA), Phospho-mTOR (Ser2448) (CST 5536S, USA), Phospho-mTOR (Ser2481) (CST 2974S, USA), Phospho-p70 S6 Kinase (Thr389) (CST 9205S, USA), Phospho-Rictor (Thr1135) (CST 3806S, USA), Phospho-S6 Ribosomal Protein (Ser235/236) (CST 4858S, USA), Phospho-S6 Ribosomal Protein (Ser240/244) (CST 2215S, USA), Puma (CST 4976P, USA), Rheb (CST 13879S, USA), Rictor (CST 2104S, USA), S6 (CST 2317S, USA), SDH5 (CST 14445, USA), B-Actin (Sigma Aldrich A5316, Germany)

2.5.2. Secondary Antibodies

Anti-mouse IgG peroxidase conjugate (Sigma Aldrich A4416, Germany), Anti-rabbit IgG, HRP-linked antibody (CST 7074S, USA or Sigma Aldrich A0545, Germany), Normal Mouse IgG (Santa Cruz Biotechnology sc-2025, USA), Normal Rabbit IgG (Santa Cruz Biotechnology sc-2027, USA)

2.6. CELL LINES

A-498, Human Primary Kidney Epithelial Carcinoma, Adherent (ATCC HTB-44, USA), ACHN, Human Metastatic Renal Cell Carcinoma (lung), adherent (ATCC CRL-1611, USA), Caki-1, Human Metastatic Kidney Clear Cell Carcinoma (Skin), Adherent (ATCC HTB-46, USA), Caki-2 Human Primary Clear Cell Carcinoma of Human Kidney, Adherent (ATCC HTB-47, USA), HEK-293, Human Embryonic Kidney Epithelial, Adherent (ATCC CRL-1573, USA), RenCa, Mouse Renal Epithelial Adenocarcinoma, Adherent (ATCC CRL-2947, USA), $RenCa^{res}$, Everolimus-resistant Mouse Renal Epithelial Adenocarcinoma (generated during the study by Ayşe Hande Nayman)

3. METHODS

3.1. CELL CULTURE

3.1.1. Cell Thawing

The cryo tubes were taken from liquid nitrogen and the frozen cell suspension was allowed to thaw at room temperature. Later, the cell suspension (1 ml) was added drop by drop to 4 ml of complete growth medium and the mixture was subjected to centrifugation at 300 *x g* for 5 minutes. The cell pellet was resuspended in complete growth medium and transferred to appropriate culture dish/flask and incubated in a humidified mammalian cell culture incubator at 37ºC and 5 per cent CO_2. After 24 hours incubation, the medium was replaced with fresh complete growth medium.

3.1.2. Culturing Conditions

All cell lines used during the thesis were purchased from American Type Culture Collection (ATCC). A-498 (primary human kidney carcinoma), ACHN (metastatic human kidney carcinoma), and HEK-293 (human embryonic kidney cell 293) cells were cultured in DMEM medium supplemented with 10 per cent (v/v) FBS, 100 µg/ml streptomycin, and 100 units/ml penicillin. RenCa (mouse murine renal adenocarcinoma) and $RenCa^{res}$ (everolimus-resistant mouse murine renal adenocarcinoma) cells were grown in RPMI-1640 medium containing 15 per cent (v/v) FBS, 100 µg/ml streptomycin, and 100 units/ml penicillin. Caki-1 (ccRCC skin metastasis) and Caki-2 (primary human RCC) cells were maintained in McCoy's 5A medium supplemented with 10 per cent (v/v) FBS, 100 µg/ml streptomycin, and 100 units/ml penicillin. All cell lines were cultured in the humidified incubator at 37ºC and 5 per cent CO_2.

3.1.3. Cell Passaging

The cells that reached 70-80 per cent confluency were subjected to passaging. For the passaging, the cells were washed with 1x DPBS, followed by the incubation with 0.05 per cent (w/v) trypsin at 37°C for 5 minutes. The cell suspension was collected and mixed with complete growth medium to inhibit the trypsin's enzyme activity. The suspension was then centrifuged at 300 *x g* for 5 minutes. The cell pellet was resuspended in growth media and cultured in appropriate cell culture flasks.

3.1.4. Calculation of Cell Number

The cell suspension prepared for passaging (described in Section 3.1.2.) was used to determine the cell number. 10 µl of cell suspension was pipetted into the hemocytometer and the upper left and upper right quarters of the chamber of hemocytometer were counted. The average number was calculated and the total amount of cells in 1 ml complete growth medium was determined. The formula for the calculation used was:

Cell number / ml = Average of total cell counts x dilution factor x depth of hemocytometer

3.1.5. Generation of Everolimus-resistant RenCa Cells

Drug resistant RenCa cells were generated by exposure to the increasing concentrations of everolimus as described in [274]. RenCa cells were initially seeded at a density of 5 x 10^3, cells/well in 96-well plate containing RPMI-1640 medium supplemented with 10 per cent (v/v) FBS, 100 µg/ml streptomycin, and 100 units/ml penicillin. Next day, the cell monolayer was washed with 1x DPBS and the cells were grown in complete growth medium containing 1 µM everolimus for 72 hours. Following 72 hours, cells were sub-cultured in complete growth medium with increased concentration of everolimus (10 µM) for additional 72 hours. Following 72 hours of drug treatment, cells were transferred to 6-well plate containing complete growth medium without everolimus and allowed to grow for 2 weeks. Following this period, cells were re-exposed to 1 µM everolimus for

additional 2 weeks period. RenCa cells that showed exponential proliferation in the presence of everolimus were designated as everolimus-resistant RenCa ($RenCa^{res}$) cells.

3.1.6. Cryopreservation of Cells

The freezing solution was prepared by mixing 10 per cent (v/v) DMSO (dimethyl sulfoxide) with 90 per cent FBS (v/v). Cells were washed with 1xDBPS and trypsinized as described in Section 3.1.2. The cell pellet was resuspended in 1 ml of freezing solution and transferred into cryo tubes, which were immediately placed to -80°C freezer for 2-3 days. Vials were finally transferred into liquid nitrogen containing tanks for a long-term storage.

3.2. DETERMINATION OF THE EFFECT OF DRUG TREATMENT ON RCC CELL LINES

3.2.1. Cell Viability Assay

The cell viability assay was performed to determine the cytostatic doses of everolimus and ABT-737, and the cytotoxic effect of their combination on cells. A-498, Caki-1, RenCa, and HEK-293 cells were subjected to 4 hours serum starvation prior to the cell viability assay. Following starvation, A-498, RenCa, and $RenCa^{res}$ cells were seeded at a density of 5×10^3 cells/well in 96-well plate, whereas cell density was 1×10^4 cells/well in 96-well plate for Caki-1 and HEK-293 cells. After 24 hours, A-498, Caki-1, HEK-293, and $RenCa^{res}$ cells were treated either with increasing concentrations of everolimus or ABT-737 or in combination of both drugs at chosen concentrations for 24, 48 and 72 hours. RenCa cells were subjected only to increasing concentrations of everolimus and neither to ABT-737 nor combinatorial treatment. Following the incubation time, WST-1 cell viability assay was performed according to the manufacturer's protocol. 5 µl of WST-1 reagent was mixed with 45 µl of complete growth medium and cells were incubated with the total amount of 50 µl at 37°C for 1 hour. Following 1 hour incubation, the absorbance was measured at 450/630 nm using the spectrophotometer. In parallel, cell viability assay was

performed for the cells seeded in 96-well plate at pre-determined number to establish a standard curve.

3.2.1.1. Isobolograms

A-498 and Caki-1 cells were subjected to 4 hours serum starvation prior to the cell viability assay. Following starvation, A-498 cells were seeded at a density of 5 x 10^3 cells/well in 96-well plate, whereas cell density was 1 x 10^4 cells/well in 96-well plate for Caki-1 cells. After 24 hours, A-498 were subjected to treatment with either 1-50 µM everolimus or 1-10 µM ABT-737. Caki-1 cells were treated either with 1-50 µM concentrations of everolimus or 1-50 µM concentrations of ABT-737 for 72 hours. Following the incubation time, the analysis of the effect of individual drugs on cell viability was performed by WST-1 cell viability assay as described in Section 3.2.1.

3.2.2. Cell Death Assay

A-498, Caki-1, RenCa, and $RenCa^{res}$ cells were subjected to 4 hours serum starvation prior to culture for the cell death assay. Following starvation, Caki-1 and A-498 cells were seeded in a 6 well-plate at a density of 3,5 x 10^5 and 3 x 10^5 cells/well, respectively, whereas RenCa and $RenCa^{res}$ cells were seeded at a density of 3,5 x 10^5 cells/ well in 6-well plate. After 24 hours of culturing in a humidified incubator at 37ºC and 5 per cent CO_2, cells were subjected to either single drug treatments or combinatorial treatment for 24, 48 and 72 hours and the control group were treated with the vehicle DMSO. Following incubation with drugs, the growth medium containing the dead cells was centrifuged at 350 *x g* for 10 minutes. In mean time, the cell monolayer was washed with 1x DPBS and trypsinized at 37°C for 5 minutes followed by the centrifugation at 350 *x g* for 10 minutes. After centrifugation processes, both cell pellets were gathered with 1 ml of 1x DPBS and counted. The cell number was counted and 1 x 10^5 cells were transferred into a new 1.5 ml eppendorf tubes to perform Annexin-V Fluos Staining assay according to the manufacturer's protocol. Briefly, cells were centrifuged at 300 *x g* for 10 minutes followed by incubation with 2 µl Annexin-V labeling reagent and/or PI solution prepared in 98 µl of incubation buffer under dark conditions for 15 minutes. The samples were supplied with

400 µl of 1x DPBS and 30,000 cells were analyzed by flow cytometry. Gating was performed with control cells incubated without Annexin V or PI.

3.3. DETERMINATION OF THE EFFECT OF COMBINATON TREATMENT ON PROTEIN LEVELS

3.3.1. Isolation of Total Protein Extracts for Analysis of mTOR Pathway, Cell Cycle and Bcl-2 Family Proteins

A-498, RenCa and RenCa^{res} (3 x 10^5 cells/well), and Caki-1 (3,5 x 10^5 cells/well) cells were serum starved for 4 hours and seeded into 6-well plates followed by drug treatment for 24 hours. After 24 hours, cell monolayer was washed with 1x DPBS and cells were scraped with 30 µl RIPA (Radio immunoprecipitation assay) lysis buffer supplemented with 1mM sodium orthovanadate (Na_3VO_4), 2 mM PMSF and 1 per cent (v/v) protease inhibitor cocktail. Sonication of samples by 4 cycles at 60 per cent power with three second pulses on ice was followed by centrifugation at 10,000 rpm and 4°C for 10 minutes. The supernatants was transferred into sterile 1.5 ml eppendorf tubes and stored at -20°C for 1-2 days or -80°C for long-term storage.

3.3.2. Isolation of Total Protein Extracts for Analysis of Caspase Cascade

A-498, RenCa and RenCa^{res} (3 x 10^5 cells/well), and Caki-1 (3,5 x 10^5 cells/well) cells were serum starved for 4 hours and seeded into 6-well plates followed by drug treatment for 24 hours. After 24 hours, dead cells in the growth medium was collected by centrifugation at 350 *x g* for 10 minutes. The cell monolayer was washed with 1x DPBS and isolation of total proteins was performed by scraping the cells from surface with RIPA lysis buffer supplemented with 1 mM sodium orthovanadate (Na_3VO_4), 2 mM PMSF and 1 per cent (v/v) protease inhibitor. Isolated protein extracts and precipitated dead cells were combined and sonicated by 4 cycles at 60 per cent power with three second pulses on ice. The samples were, then, centrifuged at 10,000 rpm for 10 minutes at 4°C. The supernatants was transferred into sterile 1.5 ml eppendorf tubes and stored at -20°C for short-term storage (1-2 days) or -80°C for long-term storage.

3.3.3. Isolation of Total Protein Extracts for Detection of FKBP38 Protein

A-498 (3 x 10^5 cells/well), and Caki-1 (3,5 x 10^5 cells/well) cells were serum starved for 4 hours and seeded into 6-well plates followed by drug treatment for 24 hours. After 24 hours, dead cells in the growth medium was collected by centrifugation at 350 *x g* for 5 minutes. 200 µl of supernatant was left and adjusted to 1ml with 1x DPBS. Samples were subjected to an impulse until 5,000 *x g* or 13,000 rpm and 4°C first and centrifuged at 350 *x g* for 5 minutes at 4°C subsequently. Meanwhile, cell monolayer was washed with 1x DPBS and cells were scraped in IP buffer (50 mM Tris-HCl pH 7.4, 0.25 per cent sodium deoxycholate, 150 mM NaCl, 5 mM EDTA, 0.1 M PMSF, and 1 per cent protease inhibitor) or RIPA buffer supplemented with 1 mM Na_3VO_4, 2 mM PMSF and 1 per cent (v/v) protease inhibitor. Cell lysates were combined and sonicated for 1 cycle at the lowest power with one pulse on ice.

3.3.4. Determination of Protein Concentration by Lowry Method

BSA standards ranging from 0.25 to 1 mg/ml concentration was prepared and total protein extracts were diluted 1:10 with dH_2O. The determination of protein concentration was performed according to Lowry method. Briefly, 25 µl of protein assay reagent A and 5µl of samples (BSA standards or proteins) were placed into the well of 96-well plate subsequently and mixed with 200 µl protein assay reagent B. The mixture was incubated at room temperature for 15 minutes and absorbance was measured at 750 nm by using microplate reader. A standard curve was established with absorbance values of BSA standards to determine the unknown concentration of protein extracts.

3.3.5. Sodium Dodecyl-sulfate Polyacrylamide Gel Electrophoresis (SDS-PAGE)

Proteins isolated from the cell line of interest were separated according to their molecular weight by SDS-PAGE technique. SDS-PAGE was performed with 30-100 µg of proteins that were denatured with 2x Laemmli buffer (125 mM Tris-HCl pH 6.8, 20 per cent (v/v) glycerol, 4 per cent (v/v) SDS, 10 per cent (v/v) 2-b-mercaptoethanol, and 0.004 per cent

bromophenol blue) at 95°C for 5 minutes. Stacking and separating polyacrylamide gels were prepared according to Table 3.1 and 3.2.

Table 3.1. The solutions for separating polyacrylamide gel

Solutions	**6 per cent**	**8 per cent**	**10 per cent**	**12 per cent**	**15 per cent**
1.5 M Tris/ 0.4 per cent SDS pH 8.8	3.75 ml	3.75 ml	1.25 ml	1.25 ml	1.25 ml
50 per cent Glycerol	-	-	400 µl	400 µl	400 µl
Acrylamide / bisacrylamide (29:1)	3 ml	4 ml	1.65 ml	2 ml	2.5 ml
dH_2O	8.25 ml	7.25 ml	1.7 ml	1.35 ml	850 µl
10 per cent APS	50 µl	50 µl	50 µl	50 µl	50 µl
TEMED	10 µl	10 µl	5 µl	5 µl	5 µl

First, separating gel with the percentage of interest was prepared by mixing the solutions in the same order as written in Table 3.1. The mixture was poured between the glasses of casting gel and isopropanol was pipetted on top of the solution to avoid any contact with air. After the polymerization of the gel, isopropanol was discarded and the gel surface was washed with dH_2O to remove any remaining isopropanol.

Table 3.2. The solutions for stacking polyacrylamide gel

Solutions	**4 per cent**
0.5 M Tris/ 0.4 per cent SDS pH 6.8	1.25 ml
Acrylamide / bisacrylamide	500 µl
dH_2O	3.25 ml
10 per cent APS	40 µl
TEMED	10 µl

Then, the solutions for stacking gel was mixed in the same order as given in Table 3.2. and the mixture was poured on the separating gel surface. 10-well comb with a thickness of 1 mm was placed into the stacking gel. The comb was removed carefully after stacking gel was polymerized. Gel plates placed into PROTEAN Tetra cell Electrophoresis apparatus that was filled with electrode running buffer consisting of 25 mM Tris pH 8.5, 192 mM glycine, and 0.1 per cent (w/v) SDS. Denatured proteins were loaded into the slots provided by the 10-well comb. Electrophoresis was initiated with 70V, until the proteins reached the borderline of separating gel and the voltage was then increased up to 100V for the rest of the electrophoresis. The running of the proteins through the system was ceased, when the dye bromophenol blue completely migrated out off the separating gel.

3.3.6. Western Blot Analysis

SDS-PAGE technique was followed by Western blot to transfer separated proteins onto membranes with a pore size of 0.22 or 0.45 μm electrophoretically. The transfer of proteins was performed by two different transfer systems, mini Trans-Blot Cell Blotting System for wet blot transfer and Pierce G2 Fast blotter for semi-dry transfer.

3.3.6.1. Wet Transfer

Blotting sponge pads, Whatman papers, nitrocellulose or PVDF membrane, and gel were soaked in ice-cold transfer buffer composed of 25 mM Tris-Base pH 8.3, 192 mM glycine and 20 per cent (v/v) methanol. PVDF membrane was incubated with methanol for 5 minutes before usage. So-called gel sandwich was prepared by placing a blotting sponge pad, two sheets of Whatman paper, membrane, gel, two sheets of Whatman paper and one blotting sponge pad onto each other in a blotting cassette. The blotting cassette and a frozen ice container were placed into the blotting apparatus filled with one liter of ice-cold transfer buffer. The transfer was performed by a current of 250 mA for 1 hour.

3.3.6.2. Semi-dry Transfer

Semi-dry transfer was performed for the proteins with a molecular weight more than 200 kDa. Briefly, Whatman papers, membranes and gel were soaked in ice-cold transfer buffer composed of 25 mM Tris-Base pH 8.3, 192 mM glycine, 0.05 per cent SDS, and 20 per cent (v/v) methanol and placed onto Pierce G2 Fast blotter in the following order, three sheets of Whatman paper, membrane, gel, and three sheets of Whatman paper. The transfer was performed by 2.5V for 15 minutes.

3.3.6.3. Antibody Incubation

After the transfer, the membrane was blocked with blocking solution (5 per cent (w/v) non-fat milk powder in 1x TBS-T buffer consisting of 1 M Tris-HCl pH 7.4, 9 per cent NaCl, and 0.5 per cent Tween 20) at room temperature for 1 hour under gentle agitation. Following blocking, the incubation of membrane with primary antibody of interest that was prepared with a proper dilution in blocking solution was performed at 4°C overnight under rotation. Next day, the membrane was washed three times with 1x TBS-T for 5 minutes, followed by incubation with secondary antibody at room temperature for 1 hour under gentle agitation. The secondary antibody was then removed by washing the membrane three times with 1x TBS-T for 5 minutes. After removing the secondary antibody, the membrane was stored in 1x DPBS until detection. The immuno-detection was performed by incubating the blots with WesternBright Sirius HRP Substrate at room temperature for 1 minute and the visualization of signals was carried out with ChemiDOC XRS+Gel Imaging System.

3.4. DETECTION OF BCL-2 OR MTOR INTERACTION WITH FKBP38 PROTEIN

3.4.1. Preparation of Beads Suspension

Protein A/G beads were used for the co-immunoprecipitation experiments. 50 µl of the beads, already as slurry, was transferred into new 1.5 ml eppendorf tubes and spin down at 600 *x g* for one minute at 4ºC. The beads were washed three times with washing buffer (50 mM Tris-HCl pH 7.4, 0.25 per cent sodium deoxycholate, 150 mM NaCl, 5 mM EDTA and 0.1 M PMSF), followed by centrifugation at 300 *x g* for 1 minute at 4ºC.

3.4.2. Co-Immunoprecipitation

A-498 cells were serum starved for 4 hours prior to seeding at a density of 3 x 10^5 cells/well in a 6-well plate and incubated in complete growth medium in a humidified incubator at 37ºC and 5 per cent CO_2 over night. Next day, cells were subjected to either 1 µM Everolimus or 5 µM ABT-737 or their combinatorial treatment for 24 hours. After incubation with drugs, the cell monolayer was washed with 1xDPBS and scraped with 200 µl washing buffer (50 mM Tris-HCl pH 7.4, 0.25 per cent sodium deoxycholate, 150 mM NaCl, 5 mM EDTA, 0.1 M PMSF, and 1 per cent protease inhibitor) to isolate total protein extracts. The concentration of isolated proteins were measured as described in the Section 3.3.4. 150-200 µg of proteins were taken for the immunoprecipitation and the volume was adjusted to 150 µl with washing buffer. The samples were pre-cleared with 0.5 µg of non-specific IgG (rabbit/mouse) at 4ºC for 1 hour under rotation. Pre-cleared protein samples were incubated with protein A or G beads at 4ºC for 90 minutes on rotator. After centrifugation at 600 *x g* for one minute at 4ºC, the supernatants were transferred into fresh 1.5 ml eppendorf tubes and incubated with proper amount of antibody of interest at 4ºC for 90 minutes under rotation. Next, immune complexes were precipitated with beads at 4ºC for 2 hours, followed by the centrifugation at 600 *x g* for one minute at 4ºC. The supernatants were transferred into fresh eppendorf tubes and stored at -80ºC freezer. The samples were supplied with 20 µl of 2x Laemmli buffer and heated at 95ºC for 5 minutes and used either directly for Western blot or stored at -80ºC.

3.5. *IN VIVO* EXPERIMENTS

3.5.1. Handling and Care of Animals

6-8 weeks old male Balb/c mice were bred and maintained in the animal facility of Yeditepe University (Turkey) in accordance with and approved by Animal Care and Welfare Committee of Yeditepe University (Turkey).

3.5.2. Mice Xenograft Model and Pathological Analysis

The Balb/c male mice with the age between 6-8 weeks were separated into four groups as being control, everolimus, ABT-737 and combination of both drugs. $RenCa^{res}$ cells cultured in RPMI-1640 supplemented with 15 per cent (v/v) FBS, 100μg/ml streptomycin, 100 units/ml penicillin, and 1 μM everolimus in a humidified incubator at 37°C and 5 per cent CO_2 were injected subcutaneously in the dorsal side of the mice at a density of 15 x 10^6 per mouse. Following the fourth day of inoculations, mice were injected at peritoneum every other day with vehicle control, everolimus (2 mg/kg) [275], ABT-737 (75 mg/kg) or the combination of everolimus (2 mg/kg), ABT-737 (75 mg/kg) for a period of 21 days [264]. DMSO diluted with 1x DPBS was used as vehicle control. After 21 days, mice were sacrificed and organs including brain, thymus, heart, lung, stomach, guts, liver, kidney, spleen, testis, and tumor tissue, if any observed, were isolated and immediately stocked in 10% formalin for pathological analysis. Hematoxylin and eosin (H&E) staining was carried out to characterize tumor tissue [276].

3.6. ANALYSIS OF DATA

3.6.1. Analysis of Western Blots

The bands on Western blots were visualized by ChemiDOC XRS+Gel Imaging System. The densitometric analysis of band's intensity was carried out by using ImageJ software.

Blots presented in the figures were chosen as the representative of at least three independent experiments.

3.6.2. Statistical Analysis

Data were obtained from three to six independent experiments and presented as means ± standard deviation (SD). Regarding in vitro experiments, each graph shows the mean ± S.D of three independent experiments, each performed in triplicate. The significant analysis of treatment groups was performed by one-way ANOVA followed by Tukey post-hoc test using GraphPad Prism 6 (GraphPad Software, USA). p value less than 0.05 was considered as statistically significant. Asterisk in graphs indicates the statistical significance between control group and everolimus and/or ABT-737 treatment groups. * $P \leq 0.05$, ** $P \leq 0.01$, *** $P \leq 0.001$, **** $P \leq 0.0001$.

The formula established by Chou-Talalay was used to calculate the combination index (CI) [277]. CI value less than 1 was considered as synergistic and CI more than 1 was defined as antagonistic.

The significance analysis of tumor weights of mice from different treatment cohorts was performed by two-tailed Student t-test.

4. RESULTS

4.1. DETERMINATON OF PROTEIN LEVELS OF ANTI-APOPTOTIC BCL-2 FAMILY MEMBERS IN RCC CELL LINES

In order to find out the model cell lines that exhibit a high level of Bcl-2 protein, basal levels of anti-apoptotic Bcl-2 proteins were determined in the primary site A-498 and Caki-2 as well as in the metastatic site Caki-1 and ACHN RCC lines using Western blot analysis as described in Section 3.3.6.

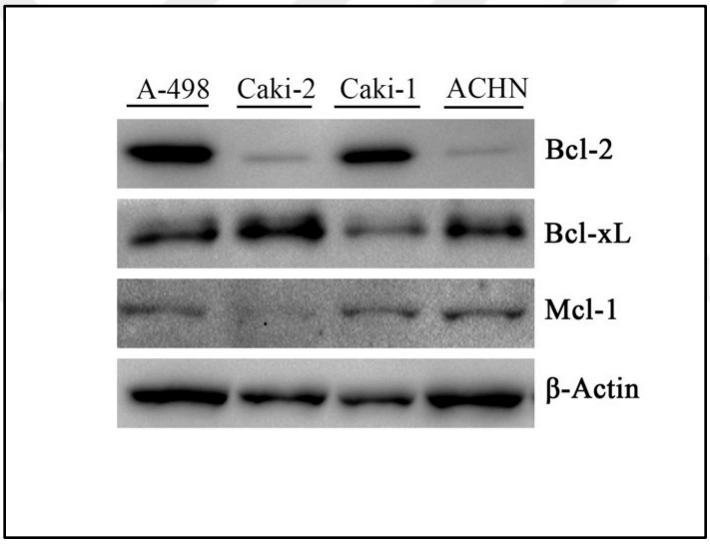

Figure 4.1. Identification of basal protein levels of anti-apoptotic Bcl-2 family members. Western blot analysis was performed with four different RCC cell lines to compare expression of Bcl-2 (26 kDa), Bcl-xL (30 kDa), and Mcl-1 (40 kDa) proteins. To ensure equal protein loading 38 kDa-protein β-actin was utilized.

All four RCC cell lines used in this experiment showed different expression levels of anti-apoptotic proteins (Figure 4.1). In fact, only the primary site A-498 and metastatic site Caki-1 cells exhibited elevated levels of Bcl-2 protein. While the protein level of Bcl-2 was barely detectable in Caki-2 and ACHN, the Bcl-xL protein levels was found to be higher in these cell lines compared to A-498 and Caki-1 cells. Basal Mcl-1 protein was

detected in A-498, Caki-1, and ACHN in very low levels compared to other anti-apoptotic proteins. Caki-2 cells did not show Mcl-1 protein expression.

According to Western blot analysis, A-498 and Caki-1 cells were chosen as the model cell lines to analyze the therapeutic effect of everolimus and ABT-737 combination in subsequent experiments.

4.2. DETERMINATION OF THE CYTOTOXIC DOSES OF EVEROLIMUS AND ABT-737

4.2.1. Effect of Everolimus and/or ABT-737 Combination on the Viability of A-498 Cells

Before analyzing the therapeutic effect of everolimus and ABT-737 combination on cell viability, A-498 cells were subjected to increasing concentrations of everolimus or ABT-737 for 24, 48, and 72 hours. Dose-dependent effect of monotherapies on A-498 cell viability and proliferation was determined by WST-1 viability assay as described in Section 3.2.1. Absorbance values obtained for the cell viability of control cells was considered as 100 per cent at 24 hours. In parallel, a standard curve was drawn to translate the absorbance values into cell number, where absorbance values corresponded to different cell densities including 1 x 10^3, 2 x 10^3, 3 x 10^3, 4 x 10^3, and 5 x 10^3 cells/well.

The effect of 1 and 5 μM everolimus concentration was a dose dependent decrease in cell viability with time (Figure 4.2a). In comparison to control cells, 15 per cent and 17 per cent decrease observed in A-498 cell viability at 24 hours were followed by 53 per cent and 45 per cent decrease for 1 and 5 μM everolimus after 72 hours, respectively. The viability of A-498 cells was declined about 20 per cent after 10 μM everolimus concentration at 24 hours. After 48 and 72 hours, the cell viability of the control A-498 cells recorded respectively as 140 and 170 per cent compared to 10 μM everolimus treatment which showed a 45 per cent decrease in cell viability. Starting from 24 hours, no decrease in cell number below 2 x 10^3 was observed when cells were subjected to the increasing doses of everolimus (Figure 4.2b). Taken together, the cell viability and cell proliferation results indicated a cytostatic effect of everolimus on A-498 cells. Based on

these results, 1 µM concentration of everolimus was chosen as the minimum effective drug dose for the combinatorial treatment with ABT-737.

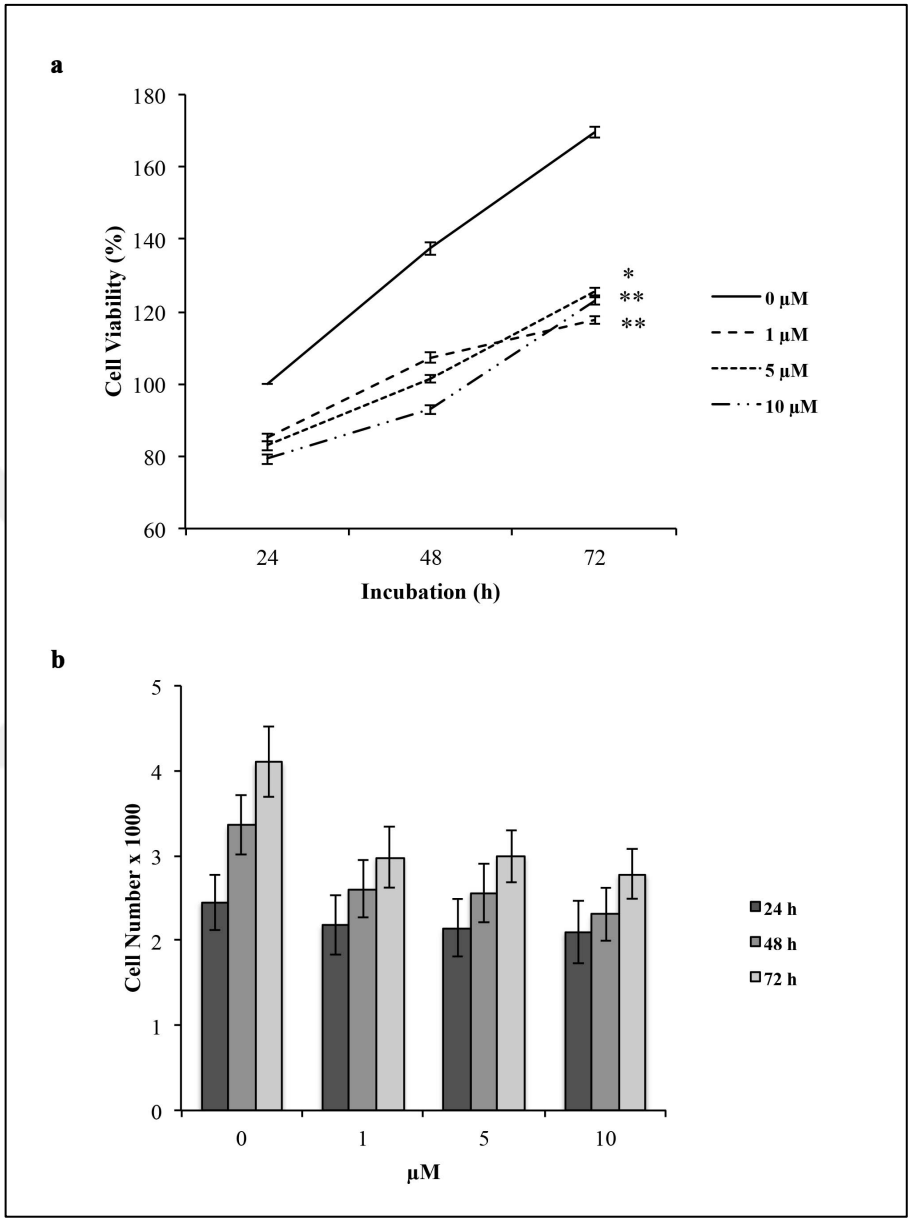

Figure 4.2. Determination of the cytostatic doses of everolimus for A-498 cells. Increasing doses of everolimus were utilized to treat A-498 cells for 24, 48, and 72 hours. DMSO was used to treat control cells (0 µM). (a) The cell viability of control cells measured by WST-1 viability assay at 24 hour was set to 100 per cent. (b) The initial cell number/well was 2 x 10^3 at the start of the experiment.

The cell viability and proliferation obtained from ABT-737 monotherapies for 24, 48, and 72 hours were demonstrated in Figure 4.3. When compared to the vehicle (DMSO) treated A-498 (control) cells at the indicated time points, the decrease in A-498 cell viability caused by 1 μM ABT-737 monotherapy was not significant, but cytostatic (Figure 4.3 a and b). However, a dose- and time-dependent cytotoxicity was observed with 5 and 10 μM concentrations of ABT-737.

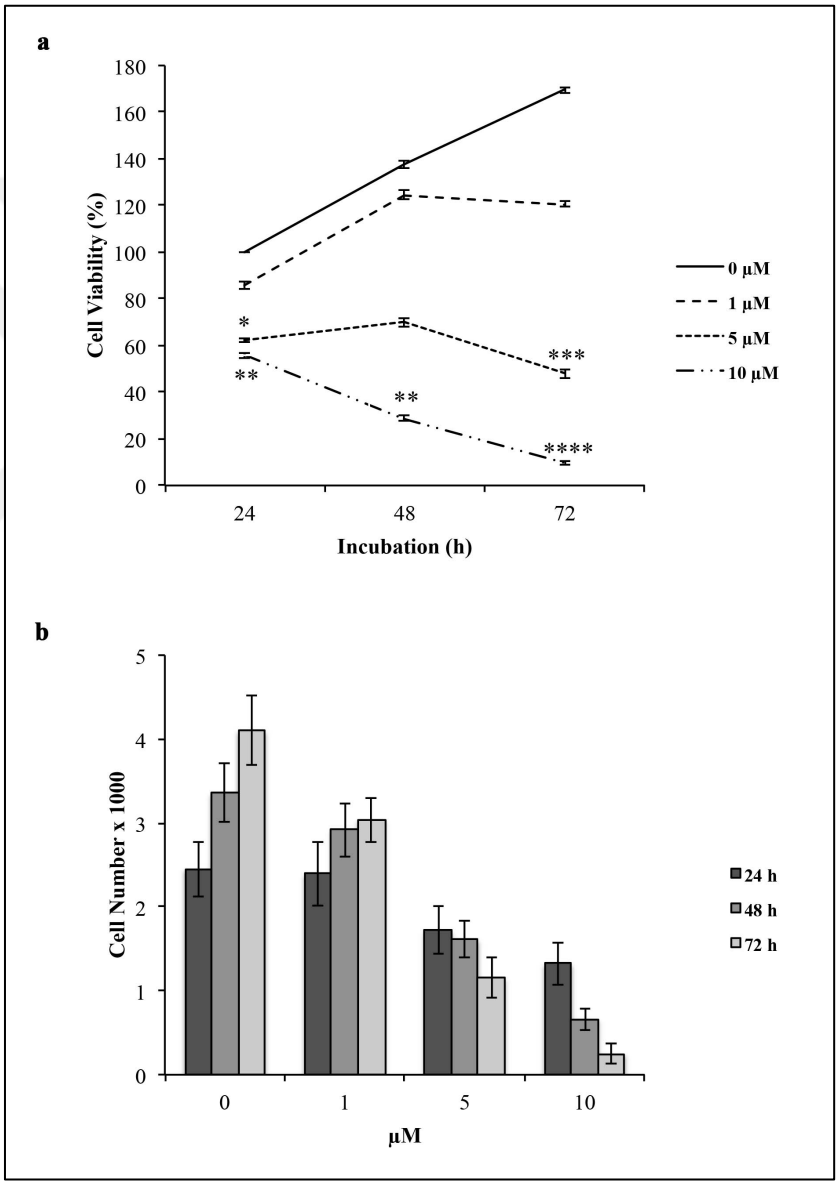

Figure 4.3. Determination of the cytostatic doses of ABT-737 for A-498 cells. Increasing doses of ABT-737 were utilized to treat A-498 cells for 24, 48, and 72 hours. DMSO was used to treat control cells (0 μM). (a) The cell viability measured for control cells at 24 hours was set to 100 per cent. (b) 2 x 10^3 cells /well were seeded at time t_0.

In fact, 5 µM ABT-737 led to 67 per cent and 122 per cent decrease in cell viability while 137 per cent and 170 per cent viability was detected for the control cells at 48 and 72 hours, respectively. Only 10 per cent of A-498 cells remained viable after 72 hours treatment with 10 µM ABT-737 (Figure 4.3a).

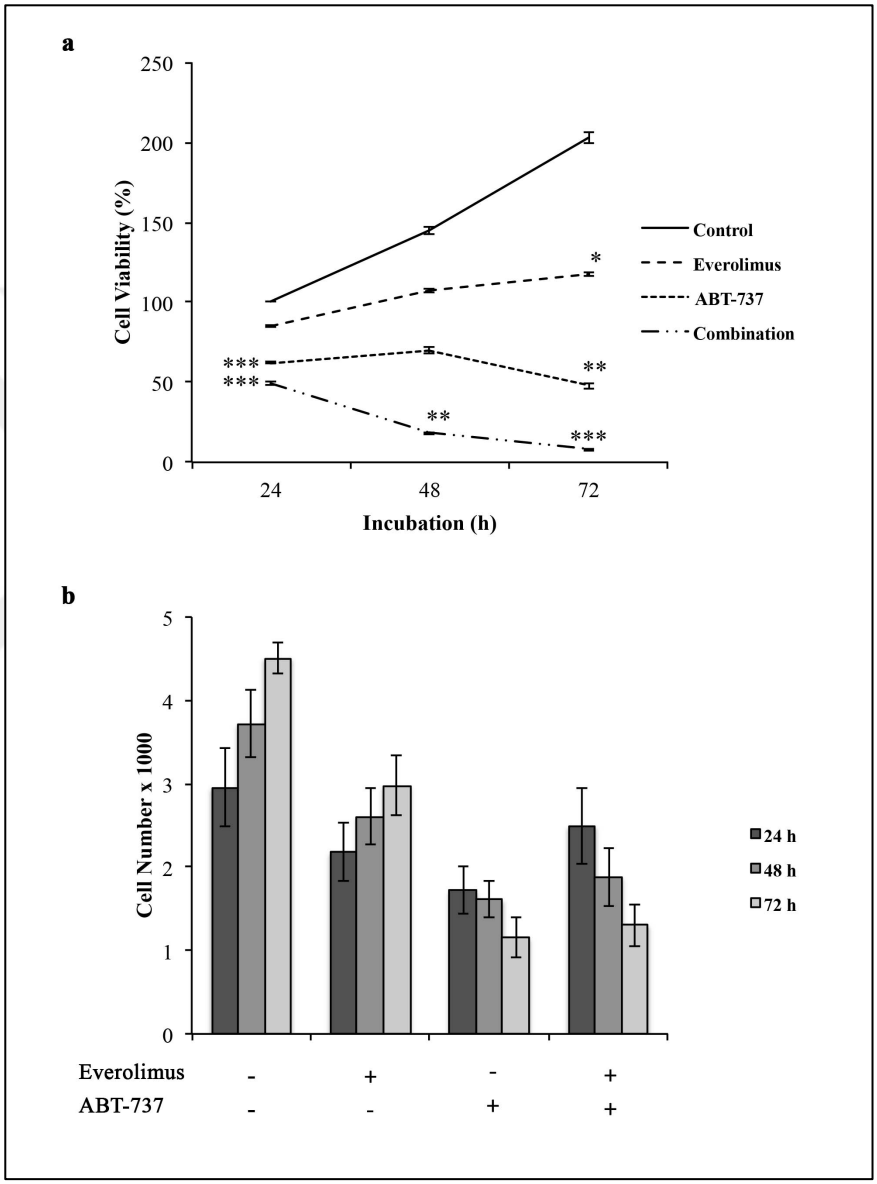

Figure 4.4. Determination of the cytotoxic effect of everolimus-ABT-737 combination on A-498 cells. A-498 cells were exposed to everolimus (1 µM) and/or ABT-737 (5 µM) for indicated hours. DMSO-treated A-498 cells were considered as control (0 µM). (a) The viability of control cells measured by WST-1 viability assay at 24 hours was set to 100 per cent. (b) 2 x 10^3 cells/well were seeded at the start of the experiment.

In validation with the cell viability data, a significant reduction in cell number was observed after 10 μM ABT-737 regimen. In fact, initial 2 x 10^3 cell number was diminished to 250 cells per well after 72 hours (Figure 4.3b). Based on these viability results, 5 μM ABT-737 concentration was decided as the effective concentration for the combinatorial treatment.

Following the determination of everolimus and ABT-737 concentrations, the cytotoxic effect of dual-drug combination (1 μM everolimus with 5 μM ABT-737) was analyzed in A-498 cells in a time-dependent manner. A 50 per cent decrease was observed in the cell viability after 24 hours treatment (Figure 4.4a and 4b). After 48 hours, the co-treatment resulted in a 75 per cent decrease in cell viability, when compared to the control A-498 cells (100 per cent viability). The cytotoxic effect of combination regimen was even more potent after 72 hours treatment, as only 8 per cent A-498 cells remained viable. Altogether, these findings indicated that ABT-737-dependent anti-cancer effect is more potent in primary site A-498 cells when combined with everolimus.

4.2.2. Effect of Everolimus and/or ABT-737 Combination on the Viability of Caki-1 Cells

In order to determine the lowest effective dose of everolimus and ABT-737, Caki-1 cells were treated with various concentrations of both drugs for 24, 48, and 72 hours. The effect of single drug treatments on cell viability and proliferation was analyzed by WST-1 viability assay as described in Section 3.2.1. The absorbance value of control cells at 24 hours was considered as 100 per cent for the viability analysis. Meanwhile, absorbance values obtained from cells seeded at different densities, including 5 x 10^3, 1 x 10^4, 1.5 x 10^4, and 2 x 10^4 cells/ well, were translated into cell number via a standard curve.

The impact of everolimus monotherapy on Caki-1 cell viability and cell proliferation was demonstrated in Figure 4.5. 1, 5, and 10 μM concentrations of everolimus showed no impact on the Caki-1 cell viability at 24 hours, as similar absorbance values were recorded for each concentration (Figure 4.5a). However, 1 μM everolimus led to an average of 10 per cent decrease in cell viability at 48 and 72 hours, whereas an average of 14 per cent decrease in viability was observed with 5 μM everolimus at the same time points. The

highest drug concentration (10 µM) diminished the viability of Caki-1 cells about 24 and 25 per cent upon 48 and 72 hours treatment, respectively. In parallel to these viability results shown in Figure 4.5a, analysis of the proliferation data pointed out the cytostatic effect of everolimus at increasing doses on Caki-1 cells, as no reduction in cell number was recorded in comparison to control cells. In fact, the cell number was increased to 14,211 upon 10 µM everolimus regimen at 72 hours (Figure 4.5b). All together, these results indicated the possible everolimus resistance of Caki-1 cell line.

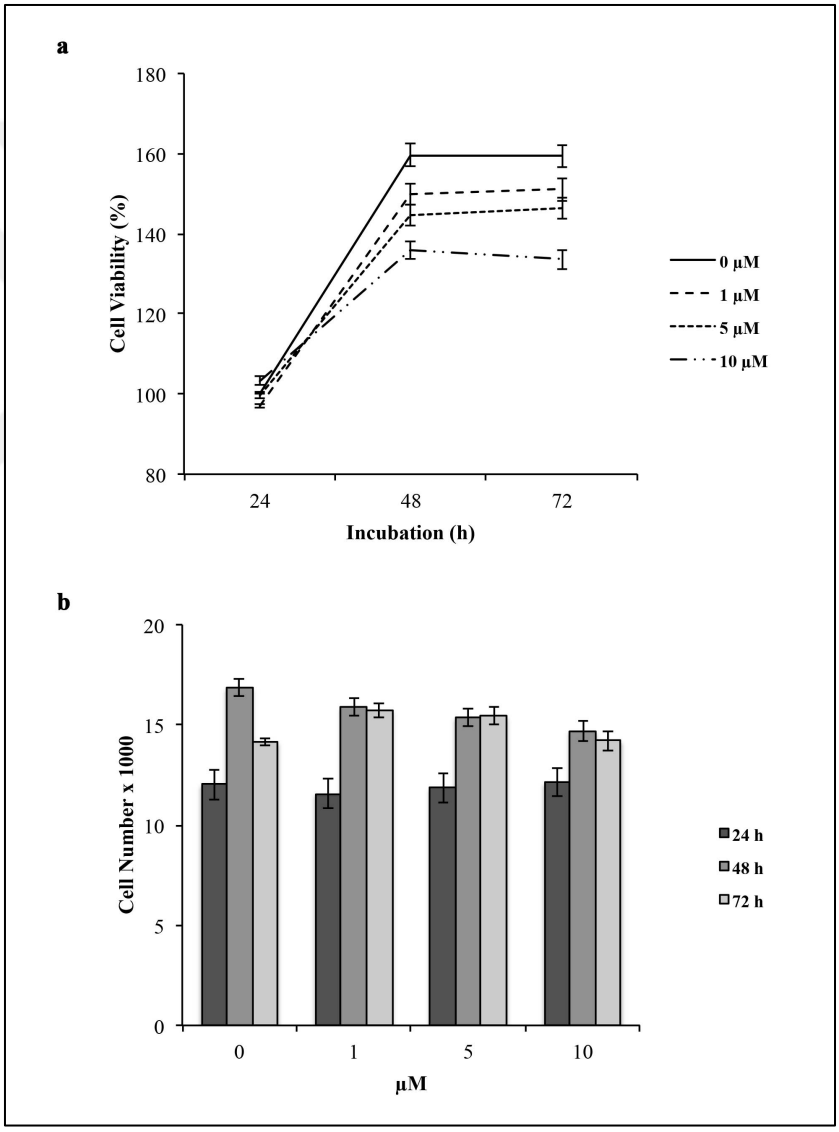

Figure 4.5. Determination of the cytostatic doses of everolimus for Caki-1 cells. Increasing everolimus doses were utilized to expose Caki-1 cells to -24, 48, and 72 hours treatments. DMSO was used to treat control cells (0 µM). (a) The cell viability of control cells was set to 100 per cent at 24 hours. (b) 1 x 10^4 cells/well were seeded at the time t_0.

In line with the results obtained from everolimus treatment, ABT-737 monotherapy did not show a significant reduction in viability of Caki-1 cells (Figure 4.6a). In fact, 1 μM ABT-737 concentration decrease cell viability about 12 per cent at 72 hours. When compared to control cells, the reduction in cell viability was more pronounced with 5 μM ABT-737, where 19 and 38 per cent decrease was observed at 48 and 72 hours, respectively. Additionally, the proliferation of Caki-1 cells was not affected by each concentration at 24 and 48 hours, as similar cell numbers were calculated for each concentration (Figure 4.6b). The highest decline in the cell viability (31 per cent) was recorded with 10 μM ABT-737 at 24 hours, which was followed by 41 and 54 per cent reductions at 48 and 72 hours, respectively. The observed decrease was related to the cytostatic effect of the drug, as the calculated cell number was 10,573 after 72 hours of the treatment (Figure 4.6b). In comparison to A-498 cells, a more resistant profile to ABT-737 monotherapy was observed in Caki-1 cells.

Based on single drug treatments, 1 μM everolimus and 10 μM ABT-737 were chosen to analyze the effect of their combination on Caki-1 cells' viability and proliferation (Figure 4.7). A time-dependent decrease in the Caki-1 viability was observed upon treatment with everolimus-ABT-737 combination. When compared to the viability of control cells at 48 and 72 hours, the combinatorial drug treatment hampered the viability to 38 per cent at 48 hours, which was followed by a 98 per cent decrease in the viability at 72 hours (Figure 4.7a). Only 20 per cent of Caki-1 cells remained viable after the combination regimen for 72 hours, which corresponded to 3.329 cells (Figure 4.7b). Thereby, data presented here pointed out the cytotoxic effect of everolimus and ABT-737 combination on Caki-1 cells.

Similar to A-498 cells, the combination of everolimus with ABT-737 potentiated the anti-cancer effect of everolimus in Caki-1 cells that exhibit high level of the anti-apoptotic Bcl-2 protein.

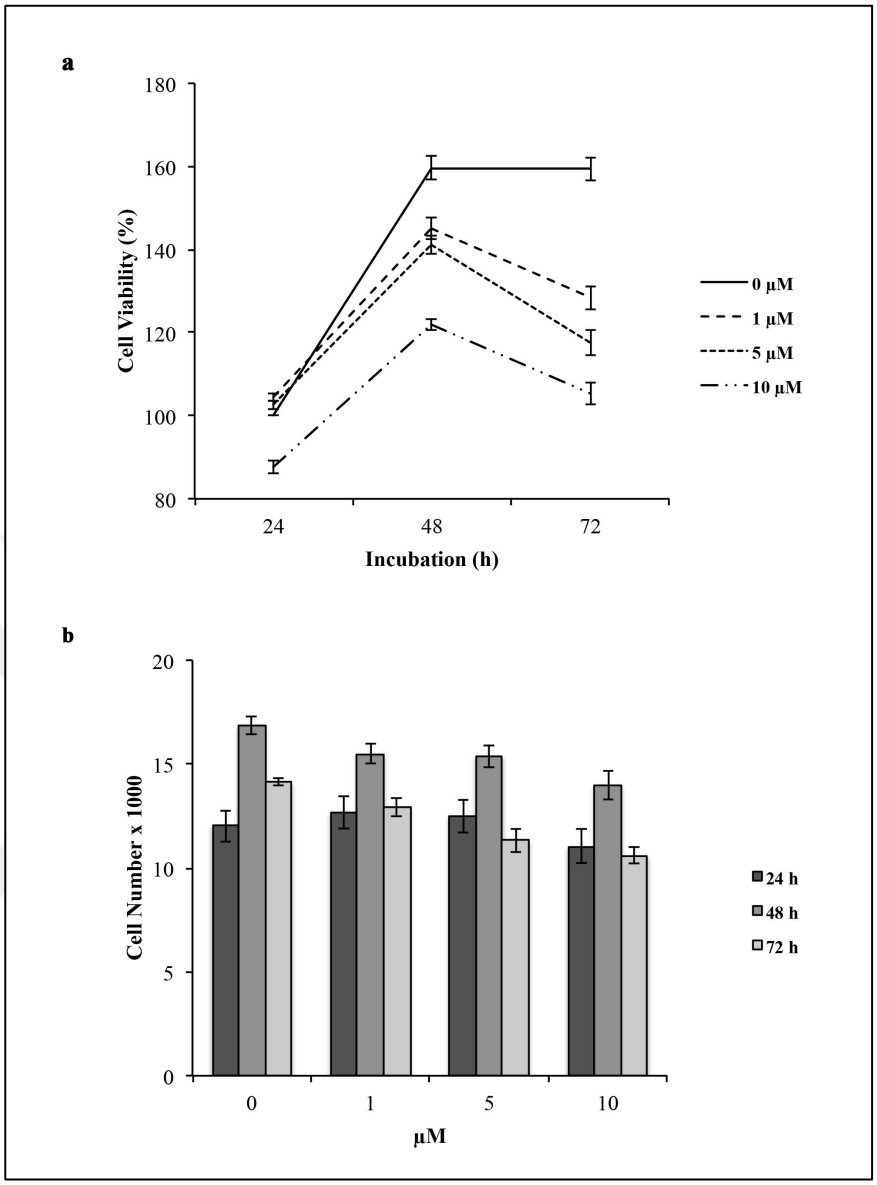

Figure 4.6. Determination of the cytostatic doses of ABT-737 for Caki-1 cells. Increasing ABT-737 concentration were used in treatments of Caki-1 cells for indicated hours. DMSO was used to treat control cells (0 µM). (a) The viability of control cells was set to 100 per cent at 24 hours. (b) Initial number of cells seeded was 1 x 10^4 cells/well.

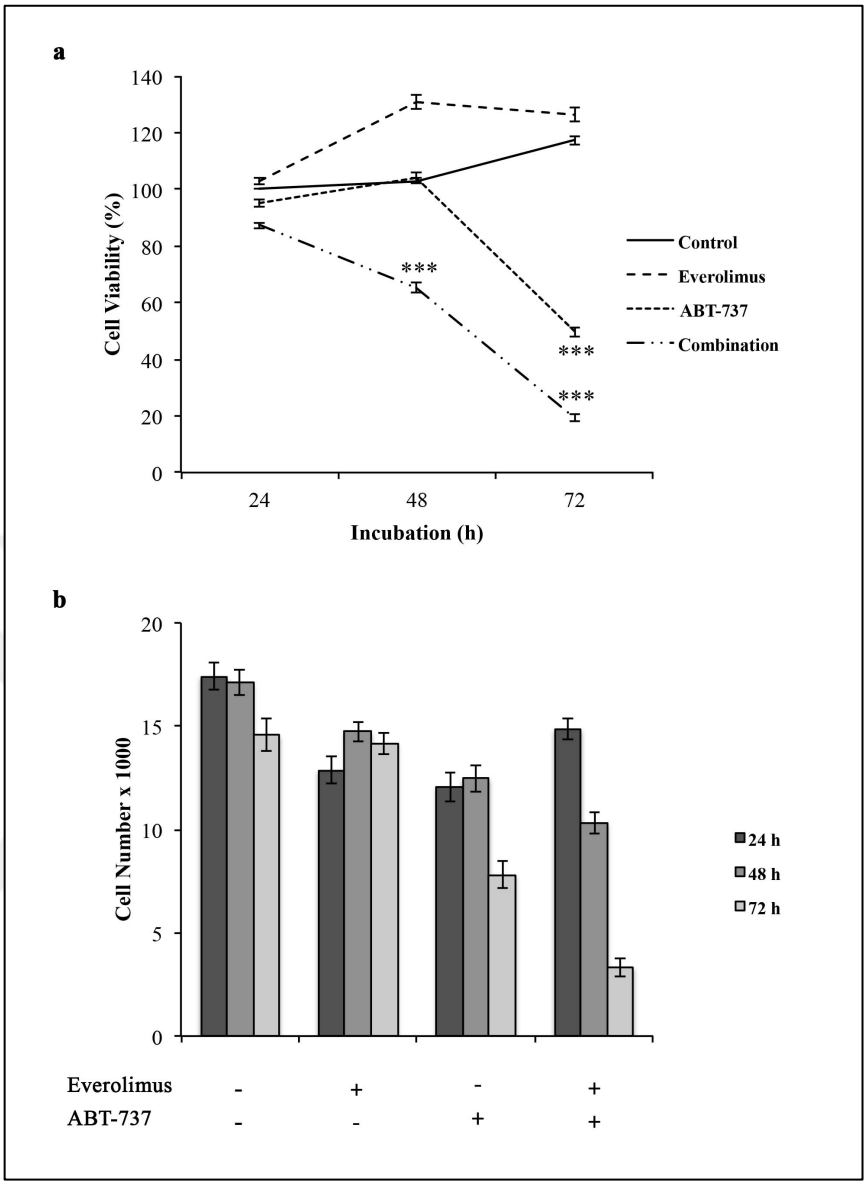

Figure 4.7. Determination of the cytotoxic effect of everolimus-ABT-737 combination on Caki-1 cells. 1 µM everolimus and/or 10 µM ABT-737 doses were used to treat Caki-1 cells for indicated hours. DMSO-treated Caki-1 cells were considered as control (0 µM). (a) The viability of control cells measured by WST-1 viability assay at 24 hours was set to 100 per cent. (b) 1 x 10^4 cells/well were seeded at the start of the experiment.

4.2.3. Effect of Everolimus and/or ABT-737 Combination on the Viability of HEK-293 Cells

In order to answer the question, whether everolimus and ABT-737 combination exerts a cytotoxic effect on the viability of healthy kidney cells, human embryonic kidney 293 (HEK-293) cell line was used as control cell line. Prior to the combinatorial regimen, HEK-293 cells were treated with the increasing concentrations of individual drugs for 24, 48 and 72 hours. The viability of cells was measured by WST-1 viability assay (Section 3.2.1), where the viability of control cells was considered as 100 per cent at 24 hours. In parallel, HEK-293 cells were seeded at an increasing density of 5 x 10^3, 7.5 x 10^3, 1 x 10^4, 1.25 x 10^4, 1.5 x 10^4, and 2 x 10^4 cells/well to draw a standard curve using absorbance values. The standard curve was then used to calculate the actual cell number at the indicated time points after treatments.

Figure 4.8 shows the effect of everolimus and ABT-737 monotherapies on viability and proliferation of HEK-293 cells. According to the results, 1 μM everolimus caused a 12 per cent decrease in the viability of HEK-293 cells at 24 hours, which is followed by an average of 29 per cent reduction at 48 and 72 hours (Figure 4.8a). A similar response was observed when HEK-293 cells were subjected to 5 μM everolimus regimen that decreased the cell viability about an average of 30 per cent upon 48 and 72 hours treatments compared to control cells. In comparison to 1 and 5 μM concentrations, 10 μM everolimus led to a 20 per cent reduction in HEK-293 viability after 24 hours. The decrease was more pronounced when the duration of treatment was increased. In fact, 46 per cent decrease in viability of HEK-293 cells was recorded after 48 hours of treatment, which was recovered at 72 hours. The calculated cell number after each treatment indicated no effect of everolimus monotherapy on cell proliferation at all three time points when compared to the initial cell number (Figure 4.8b).

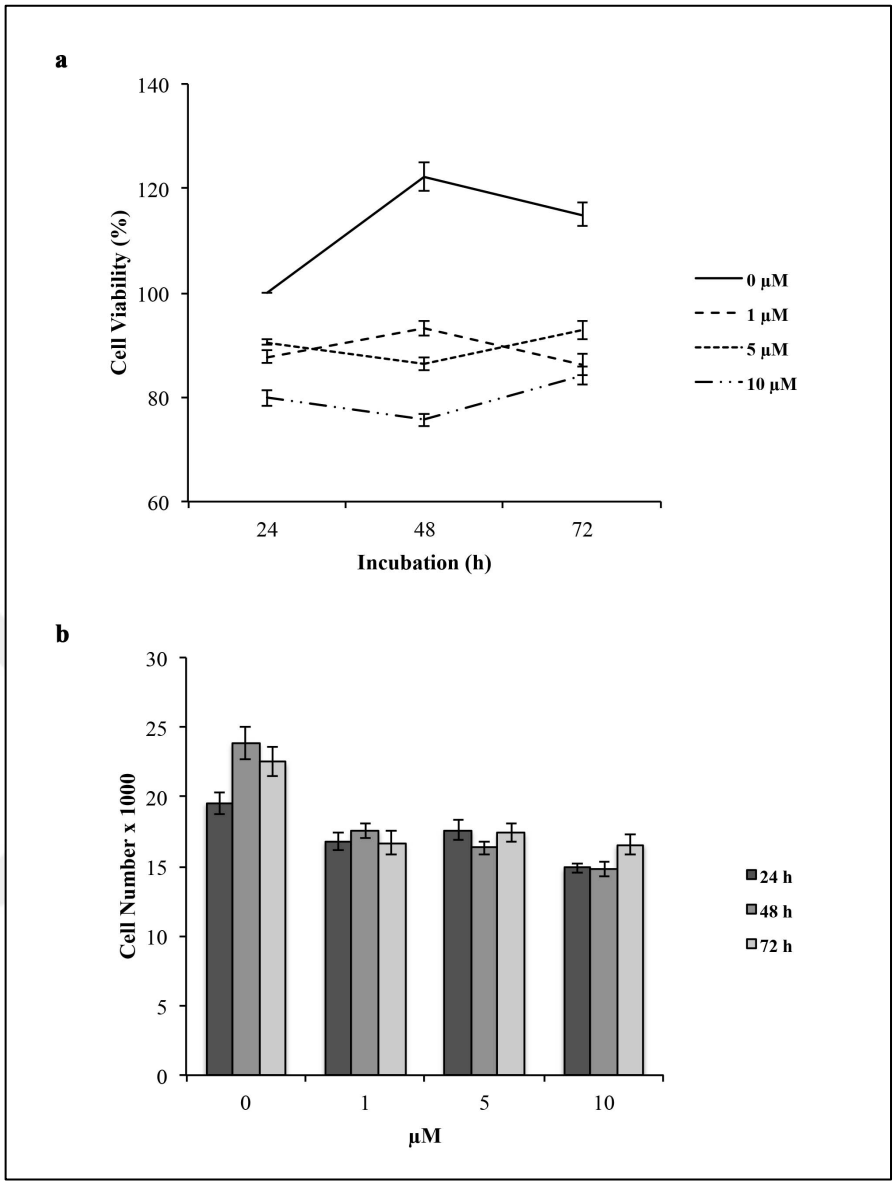

Figure 4.8. Determination of the cytostatic doses of everolimus for HEK-293 cells. The increasing concentrations of everolimus were utilized for the treatment of HEK-293 cells at indicated hours. DMSO-treated HEK-293 cells were considered as control (0 µM). (a) The viability of control cells set to100 per cent at 24 hours. (b) 1 x 10^4 cells/well was seeded at time t_0.

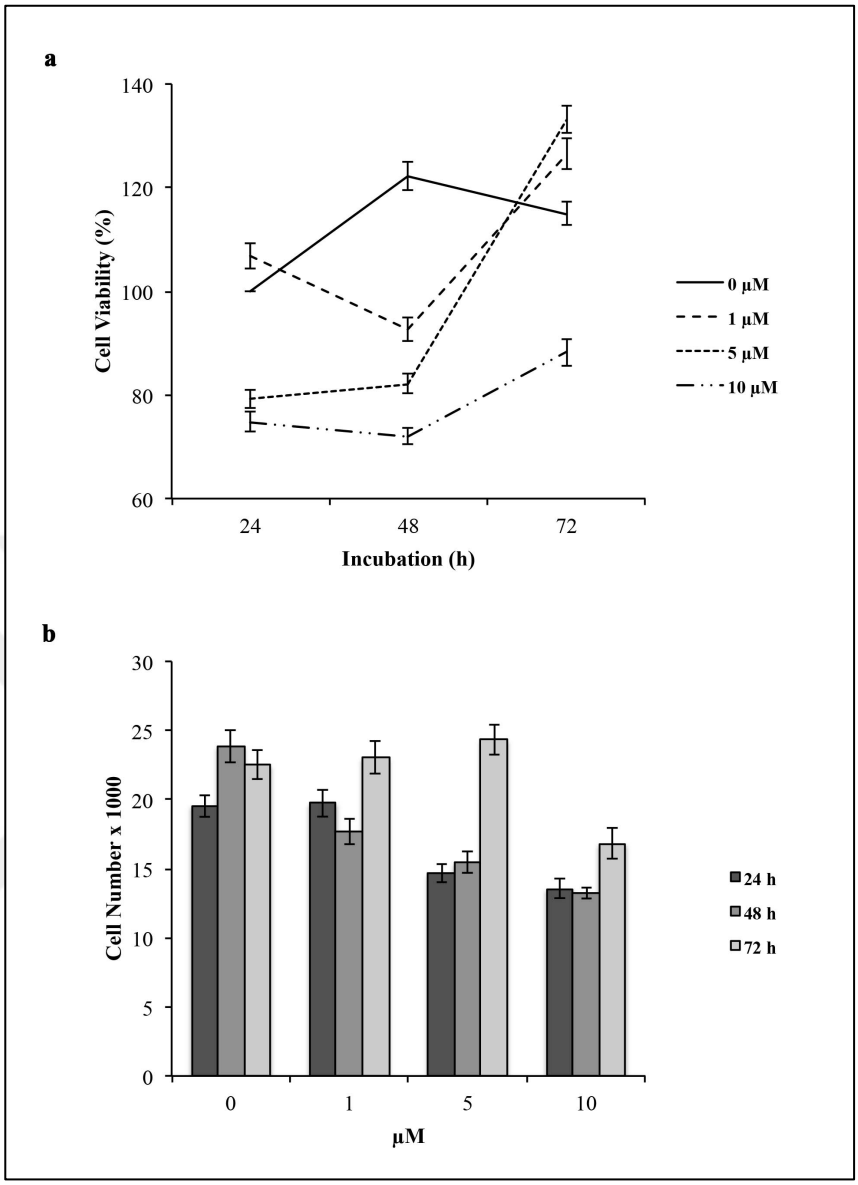

Figure 4.9. Determination of the cytostatic doses of ABT-737 for HEK-293 cells. HEK-293 cells were exposed to increasing ABT-737 dosed for indicated treatment hours. DMSO-treated HEK-293 cells were considered as control (0 µM). (a) The viability of control cells set to100 per cent at 24 hours. (b) 1 x 10^4 cells/well were seeded at time t_0.

Similar to everolimus monotherapy, no significant reduction in the cell viability was observed with different concentrations of ABT-737 (Figure 4.9a), although HEK-293 cells showed a different profile of response against each treatment. Upon 1 µM ABT-737 treatment, 29 per cent decrease observed in HEK-293 viability at 48 hours was recovered by the cells at 72 hours, where 127 per cent of cells were calculated as viable compared to the control cells at the same time point. At 24 hours, the average reduction of 23 per cent

recorded for the cell viability upon treatment with 5 and 10 μM ABT-737 concentrations was increased up to 40 and 50 per cent at 48 hours, respectively. In consistence with 1 μM ABT-737 dose, the cytostatic effect of 5 and 10 μM ABT-737 concentrations observed after 24 and 48 hours was recovered by the cells when the duration of treatment time was increased to 72 hours. In fact, only 18 and 27 per cent reduction in viability were observed for these two concentrations at 72 hours, respectively. Additionally, the proliferation data indicated that HEK-293 cells could proliferate even under the highest ABT-737 concentration at the indicated time points (Figure 4.9b).

HEK-293 cells were further used to investigate the role of combination therapy on the cell viability and proliferation. The combination of 1 μM everolimus with 5 μM ABT-737 led to a time-dependent increase in the cell viability when compared to the control cells at 24 hours (Figure 4.10a). In that, 57 per cent increase in the cell proliferation recorded upon the combinatorial treatment at 48 hours was restored to 85 per cent at 72 hours, indicating no cytostatic effect of dual-drug treatment (Figure 4.10b).

Altogether, these results demonstrated that everolimus and ABT-737 exerted their cytotoxic effect merely on the model RCC cell lines of RCC, A-498 and Caki-1 cells, and not on the healthy kidney HEK-293 cells.

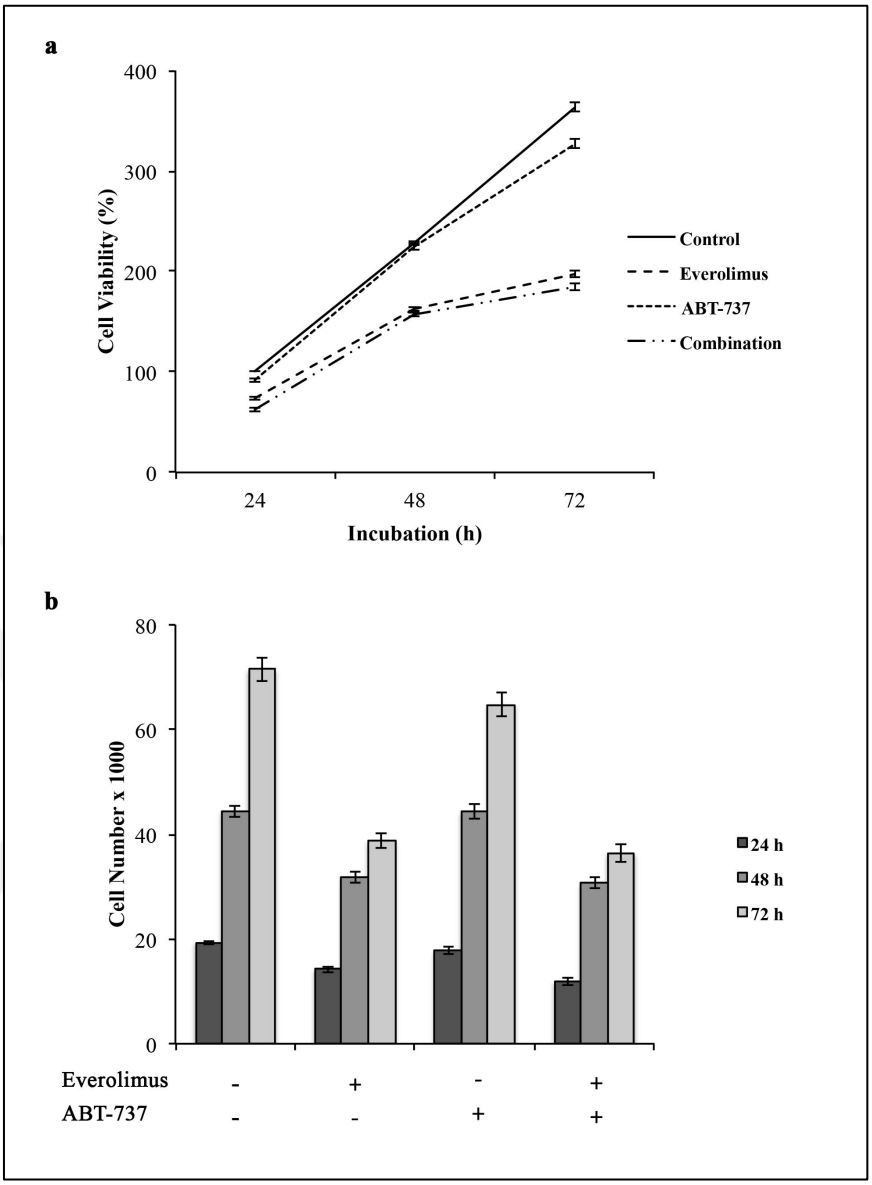

Figure 4.10. Determination of the effect of combination therapy on the cell viability of HEK-293 cells. The treatments with everolimus (1 µM) and/or ABT-737 (5 µM) were performed in HEK-293 cells for 24, 48, and 72 hours. HEK-293 cells treated with DMSO were considered as control (0 µM). (a) The viability of control cells measured by WST-1 viability assay at 24 hours was set to100 per cent. (b) 1 x 10^4 cells/well were seeded at the start of the experiment.

4.3. ANALYSIS OF THE SYNERGY BETWEEN EVEROLIMUS AND ABT-737

The synergy between individual drugs used in a combination during cancer therapy is determined by the analyses of isobologram and combination index (CI) [278]. The CI less than 1 defines the synergy, whereas CI more than 1 points out the additive effect of the drugs in the combination [277]. In order to determine whether everolimus-ABT-737 combination demonstrates a synergistic effect on A-498 and Caki-1 cells, combination index was calculated using the classic isobologram analyses. In this regard, A-498 and Caki-1 cells subjected to a wide range of everolimus and ABT-737 concentrations were used to define the lethal doses (LD) 30, 50, 70, 90 for each drug at 72 hours by WST-1 cell viability assay.

Figure 4.11 shows that the increasing concentrations of everolimus (0-50 μM) and ABT-737 (0-10 μM) led to a continuous decrease in the viability of A-498 cells, when treated for 72 hours. According to Figure 4.11a, 30 per cent decrease in the viability was observed at 12.7 μM everolimus concentration. LD50 and LD70 were recorded with an average of 37.5 and 47 μM of everolimus, respectively. 50 μM everolimus was defined as LD90 for the drug, when only 10 per cent of A-498 cells remained viable.

A-498 cells were more prone to ABT-737 treatment, which led to a continuous decrease in the cell viability with lower concentrations compared to everolimus, indicating the possible everolimus resistance of this RCC cell line (Figure 4.11b). Indeed, LD30 was defined at 2 μM concentration after the treatment of cells with ABT-737. Only a further 0.7 μM increase in the concentration led to the 50 per cent decrease in the viability, whereas 30 per cent of cells remained viable after ABT-737 regimen of 4.7 μM dose. Additionally, 10 μM, the highest concentration of drug tested in the study, led to the 90 per cent decrease (LD90) in the viability of A-498 cells.

According to the isobologram showing distribution of the obtained LD values, the calculated CI was 0.32 for LD90, indicating the synergistic effect of both drugs for A-498 cells, when 1μM everolimus and 5 μM ABT-737 were used in a combination (Figure 4.11c).

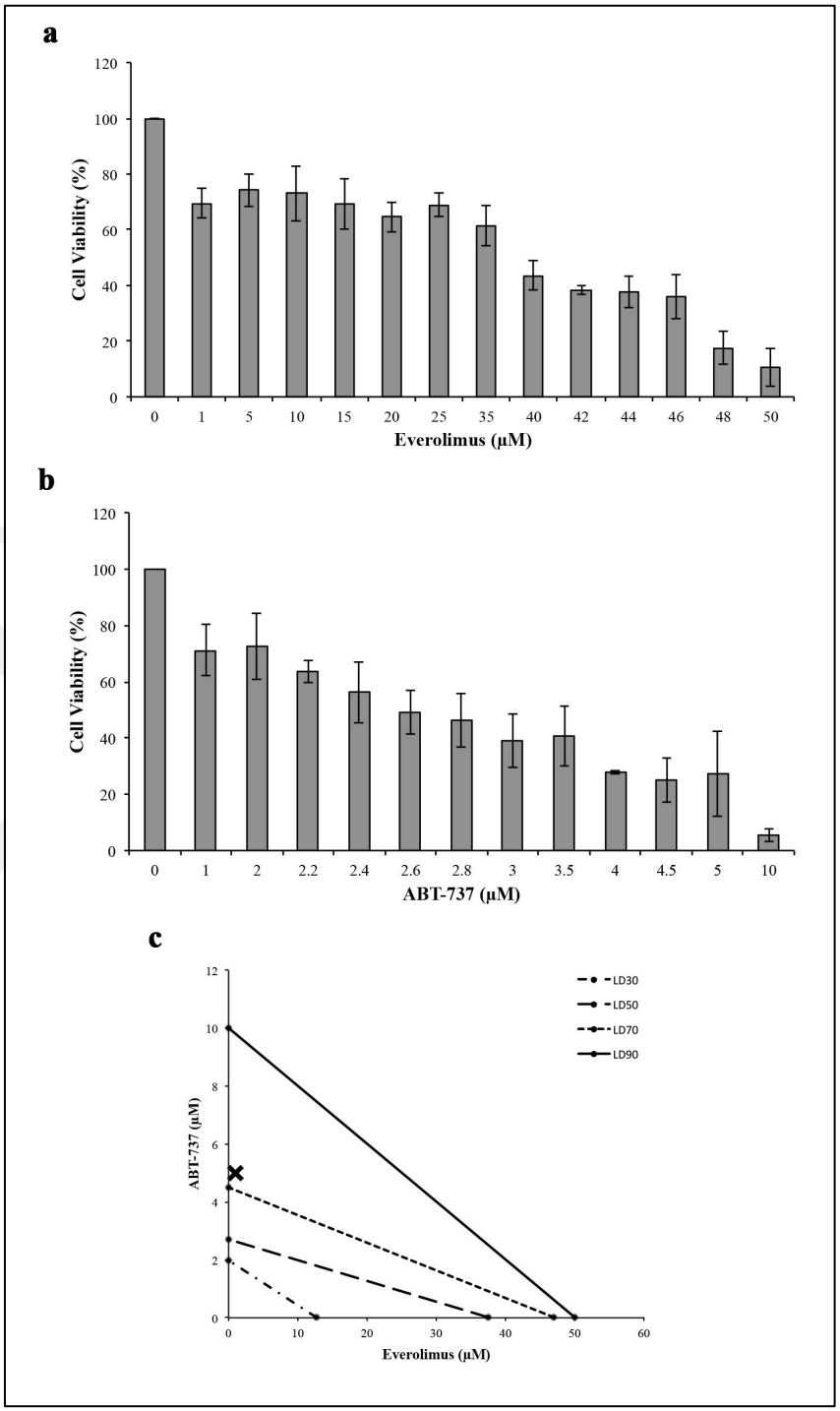

Figure 4.11. Effect of everolimus or ABT-737 on the viability of A-498 cells. A-498 cells were exposed to increasing doses of (a) everolimus (1-50 µM) and (b) ABT-737 (1-10 µM) for 72 hours. DMSO-treated A-498 cells were considered as control (0 µM). The viability of control cells set to100 per cent. (c) Isobologram was drawn with concentrations of each drug giving LD30, LD50, LD70, and LD90. x shows the concentrations of each drugs used in the combination.

In comparison to A-498 cells, Caki-1 cells showed a more resistant profile to both everolimus and ABT-737 concentrations tested (Figure 4.12a). In fact, LD30 was recorded when Caki-1 cells were treated with 42 μM everolimus. 45 and 46 μM everolimus concentrations led to 50 and 70 per cent decrease in the cell viability. Interestingly, all LD values were calculated within the narrow range of everolimus doses between 42 and 48 μM, in that 10 per cent of cells (LD90) remained viable after the treatment with 48 μM everolimus.

In comparison to A-498 cells, higher ABT-737 concentrations were required for the 50 and 90 per cent reduction in the viability of Caki-1 cells (Figure 4.12b). 10 μM dose of ABT-737 caused to 30 per cent decrease in the Caki-1 viability, where 90 per cent reduction was recorded with the same dose for A-498 cells. Further 2.5 μM increase in the concentration diminished the viability of Caki-1 cells about 50 per cent. The calculated LD50 and LD90 were obtained with an average of 17.5 and 36.7 μM doses of ABT-737.

Based on the isobologram drawn with the calculated LD values, CI value of 0.685 was recorded for the LD40 pointing out the synergistic effect of everolimus and ABT-737 on Caki-1, when 1 μM everolimus was used in combination with 10 μM ABT-737 for the treatment of Caki-1 cells (Figure 4.12c).

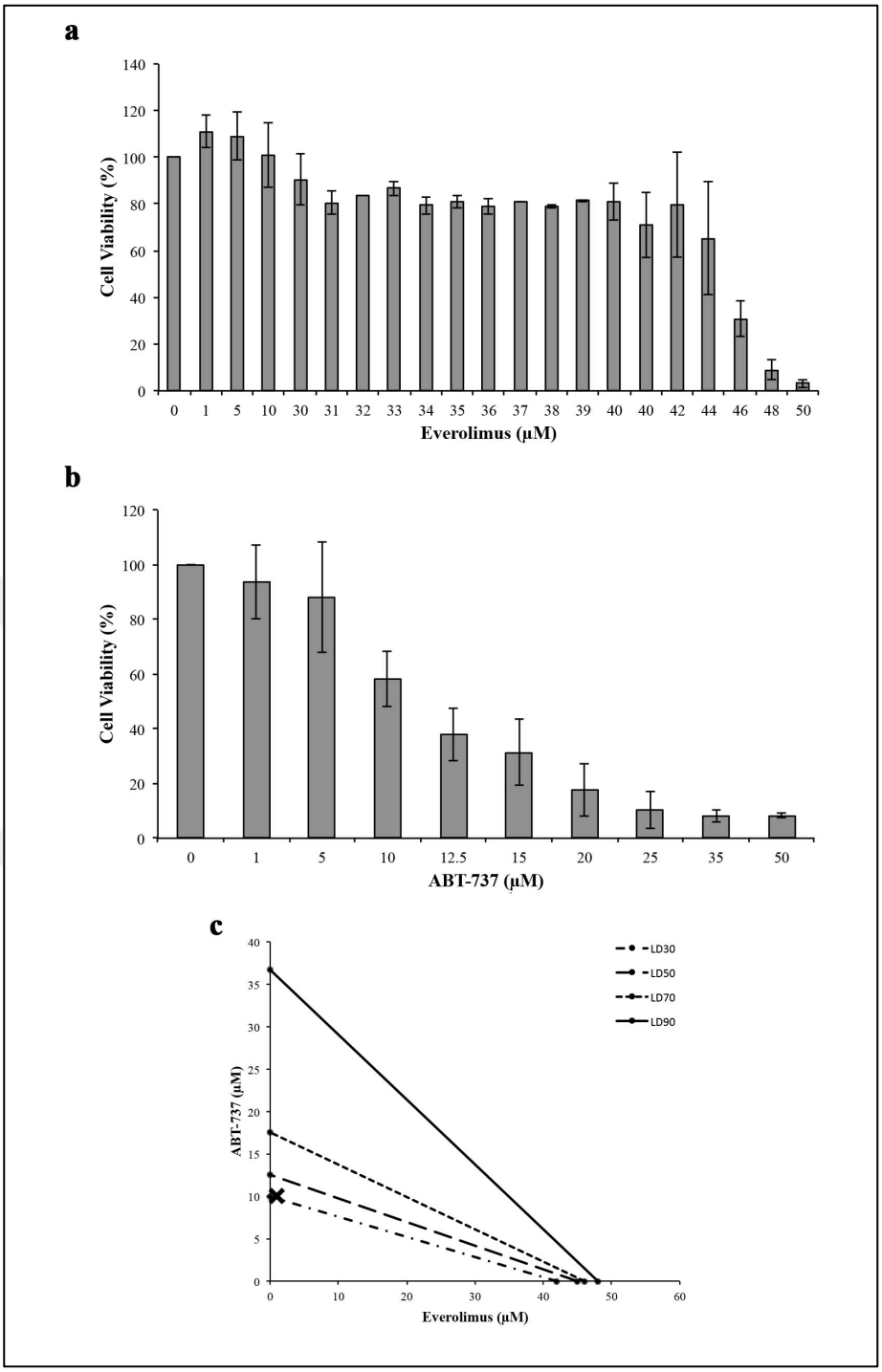

Figure 4.12. Effect of everolimus or ABT-737 on the viability of Caki-1 cells. Caki-1 cells were exposed to increasing concentrations of (a) everolimus and (b) ABT-737 for 72 hours-treatment. DMSO-treated Caki-1 cells were considered as control (0 µM). The viability of control cells set to 100 per cent. (c) Isobologram was drawn with concentrations of each drug giving LD30, LD50, LD70, and LD90. x shows the concentrations of each drugs used in the combination.

4.4. ANALYSIS OF EVEROLIMUS ABT-737 COMBINATION AT MOLECULAR LEVEL

4.4.1. Effect of Everolimus and/or ABT-737 Combination on Cell Cycle

Previous results demonstrated that the combination of everolimus with ABT-737 exerts anti-proliferative effect on both primary site A-498 and metastatic site Caki-1 cells. Therefore, the reduction in the number of cells raised the question whether the co-treatment of both drugs altered the cell cycle mechanism. In order to answer this question, Western blot analysis was performed as described in Section 3.3.6 using the cell lysates obtained from A-498 and Caki-1 cells that were subjected to either monotherapy or the combination therapy for 24 hours.

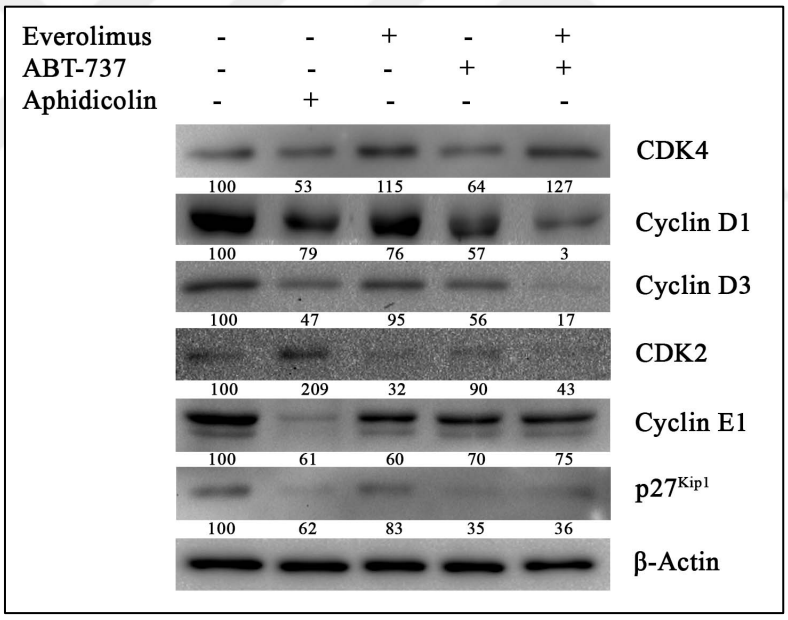

Figure 4.13. Effect of everolimus-ABT-737 combination on the cell cycle players in A-498 cells. Cell lysates of A-498 cells that were treated either with 1 μM everolimus and/or 5 μM ABT-737 for 24 hours were used to determine protein levels of CDK4 (30 kDa), Cyclin D1 (36 kDa), Cyclin D3 (31 kDa), CDK2 (33 kDa), Cyclin E1 (48-56 kDa), and $p27^{Kip1}$ (27 kDa) by Western blot. To ensure equal protein loading 38 kDa-protein β-actin was utilized. One representative blot was shown. The average percentage values were calculated according to densitometric analysis of at least three independent experiments and set as 100 per cent for control cells.

The analysis of cell cycle in A-498 cells treated either with 1 μM everolimus and/or 5 μM ABT-737 or left untreated was shown in Figure 4.13. Compared to untreated control cells, everolimus monotherapy led to 24 and 5 per cent decrease in Cyclin D1 and Cyclin D3 levels, whereas an average of 43.5 per cent reduction was recorded for both proteins upon ABT-737 regimen, respectively. However, the combination of both drugs diminished the protein levels of Cyclin D1 and Cyclin D3 about 97 and 83 per cent, respectively. Everolimus therapy led to 27 per cent increase in CDK4 level when compared to ABT- monotherapy that decreased the protein level about 34 per cent. This result suggests that the combination therapy might cause cell cycle arrest at G_1 phase that is regulated by the Cyclin D-CDK4 complex. The complex formed by Cyclin E1 and CDK2 that regulates the G_1/S transition was also affected by the everolimus-ABT-737 combination as 25 and 57 per cent reduction in Cyclin E1 and CDK2 levels were recorded, respectively. Although, ABT-737 regimen led to a slight decrease (10 per cent) in CDK2 protein level, everolimus monotherapy resulted in a more significant reduction in CDK2 protein (68 per cent) levels compared to the combination regimen. Interestingly, reduced of $p27^{Kip1}$, the G_1/S inhibitor, level was detected upon ABT-737 monotherapy and combination therapy, which was more pronounced compared to everolimus regimen.

Figure 4.14 shows the changes in cell cycle protein levels for Caki-1 cells after treatment with 1 μM everolimus and/or 10 μM ABT-737. Everolimus regimen led to 46 and 66 per cent reductions in Cyclin D1 and Cyclin D3 protein levels, respectively. In contrast with everolimus treatment, ABT-737 monotherapy exhibited an increase in Cyclin D1 protein level, whereas the drug caused a 49 per cent reduction in Cyclin D3 level. Upon combination therapy, the decrease detected in Cyclin D3 level was more pronounced than the one in Cyclin D1 protein. Although everolimus treatment led to a 58 per cent decrease in CDK4 protein expression, the reduction observed upon the combinatorial treatment was only 31 per cent. In line with these results, ABT-737 monotherapy also caused a slight decrease in CDK4 protein level. Similarly, the 72 per cent decrease recorded for Cyclin E1 level after everolimus monotherapy was brought up to 21 per cent of the control levels upon combination regimen. ABT-737 treatment also led to a lower decline in Cyclin E1 level by 38 per cent than everolimus regimen. On the other hand, the reduction in CDK2 level was detected less in cells treated with everolimus than its combination with ABT-737 than ABT-737 alone. The co-treatment of cells with everolimus and ABT-737 seemed to

favor the inhibition of cell cycle as the reduced level of $p27^{Kip1}$ protein was recovered upon combinatorial regimen.

Altogether, these data suggest that combination of everolimus with ABT-737 might induce the cell cycle arrest at G_1 phase for both A-498 and Caki-1 cells.

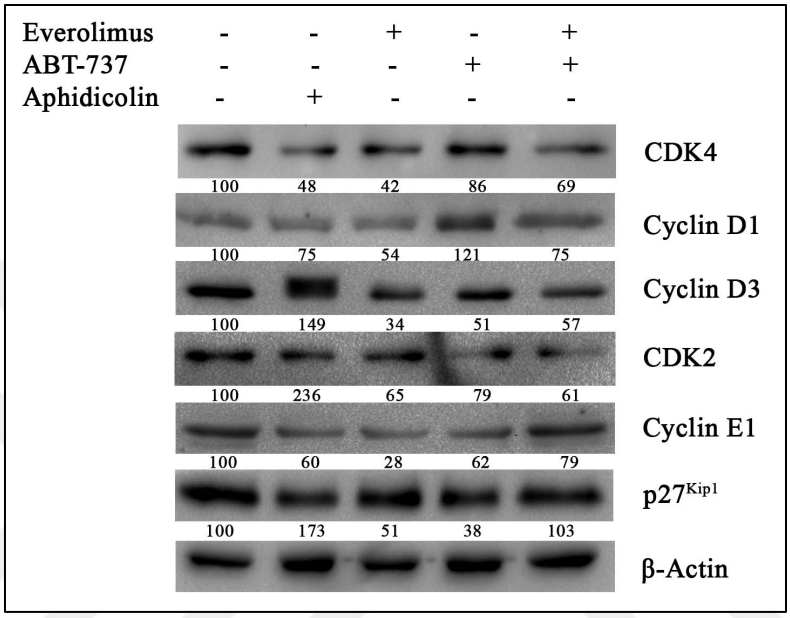

Figure 4.14. Effect of everolimus-ABT-737 combination on the cell cycle proteins in Caki-1 cells. Cell lysates of Caki-1 cells that were treated either with 1 μM everolimus and/or 10 μM ABT-737 for 24 hours were used to determine protein levels of CDK4 (30 kDa), Cyclin D1 (36 kDa), Cyclin D3 (31 kDa), CDK2 (33 kDa), Cyclin E1 (48-56 kDa), and $p27^{Kip1}$ (27 kDa) by Western blot. To ensure equal protein loading 38 kDa-protein β-actin was utilized. One representative blot was shown. The average percentage values were calculated according to densitometric analysis of at least three independent experiments and set as 100 per cent for control cells.

4.4.2. Effect of Everolimus and/or ABT-737 Combination on mTOR Pathway

As everolimus targets mTOR pathway, the effect of everolimus and/or ABT-737 on the mTOR molecular mechanism was analyzed following the cell cycle. In this regard, Western blot analysis was performed to determine the changes of protein levels of mTOR

pathway components. The analysis carried out in the cell lysates of A-498 and Caki-1 cells that were subjected to either monotherapies or combination therapy for 24 hours.

mTOR pathway mediates its regulatory function through two main complexes, mTORC1 and mTORC2, that differ from each according to their upstream regulators and downstream target proteins executing distinct cellular processes [75]. Therefore, the impact of combinatorial treatment was examined in three parts. The initiation of mTORC1 activity depends on its upstream regulator, AKT, that undergoes a phosphorylation at Thr308 by PDK1 [67]. In comparison to control and everolimus-treated A-498 cells, 56 per cent increase was observed in phosphorylated AKT at Thr308 after ABT-737 monotherapy, which was further increased up to 128 per cent upon combination therapy (Figure 4.15). In contrast, a 37 per cent decrease was observed for the basal AKT level in A-498 cells treated with ABT-737 alone. The combination of ABT-737 with everolimus further decreased AKT level about 50 per cent in A-498 cells.

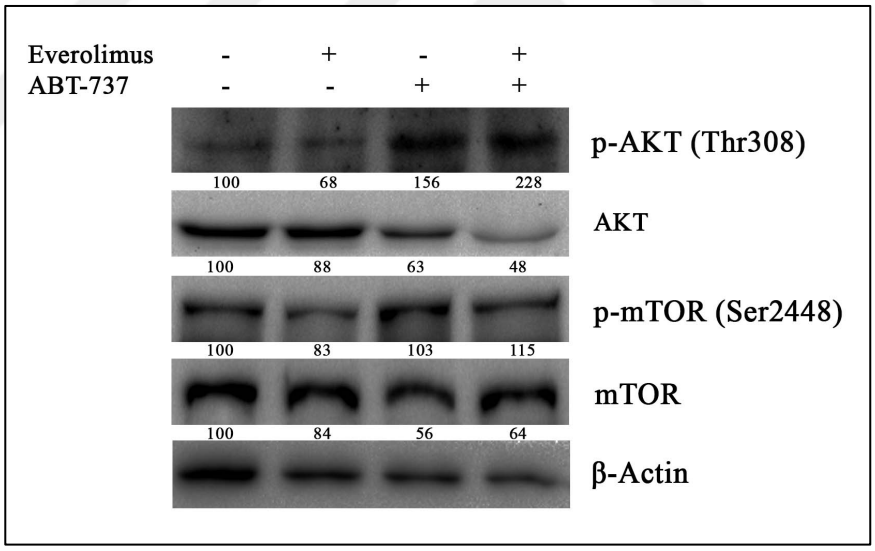

Figure 4.15. Effect of everolimus-ABT-737 combination on the upstream regulators of mTORC1 pathway in A-498 cells. A-498 cells were treated with 1 μM everolimus and/or 5 μM ABT-737 for 24 hours and cell lysates were used to determine levels of p-AKT (Thr308) (60 kDa), AKT (60 kDa), p-mTOR (Ser2448) (289 kDa), and mTOR (289 kDa) proteins by Western blot analysis. To ensure equal protein loading 38 kDa-protein β-actin was utilized. One representative blot was shown. The average percentage values were calculated according to densitometric analysis of at least three independent experiments and set as 100 per cent for control cells.

In Caki-1 cells, everolimus led to a 43 per cent decrease in p-AKT protein level, while no change in p-AKT protein was observed after ABT-737 regimen (Figure 4.16). The combination therapy, however, resulted in 130 per cent increase in p-AKT protein. The basal AKT protein was affected negatively by each treatment which was evident by an 30 decrease in the endogenous AKT protein level in Caki-1 cells.

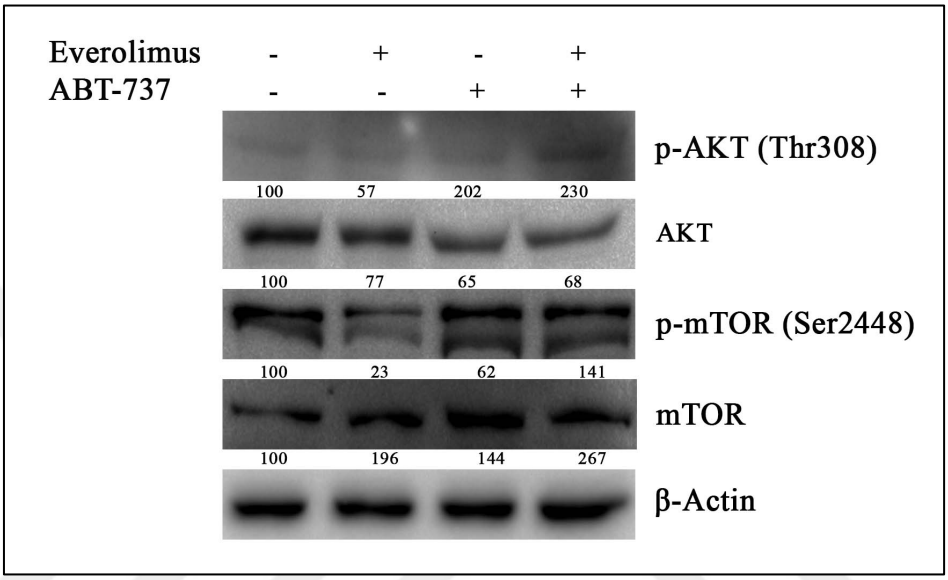

Figure 4.16. Effect of everolimus-ABT-737 combination on the upstream regulators of mTORC1 pathway in Caki-1 cells. Caki-1 cells were treated with 1 μM everolimus and/or 10 μM ABT-737 for 24 hours and cell lysates were used to determine levels of p-AKT (Thr308) (60 kDa), AKT (60 kDa), p-mTOR (Ser2448) (289 kDa), and mTOR (289 kDa) proteins by Western blot analysis. To ensure equal protein loading 38 kDa-protein β-actin was utilized. One representative blot was shown. The average percentage values were calculated according to densitometric analysis of at least three independent experiments and set as 100 per cent for control cells.

The activity of mTORC1 is characterized by the phosphorylation of its downstream target proteins. Therefore, the inhibitory effect of dual-drug therapy on mTORC1 activity was analyzed through the determination of phosphorylated mTORC1's effector proteins. Everolimus and combination regimen drastically diminished the expression of p-S6K1 protein in A-498 and Caki-1 cells, while no effect of ABT-737 regimen on p-S6K1 level recorded for both cell lines (Figure 4.17 and 4.18). In comparison to Caki-1 cells, the

reduction in basal S6K1 level in response to each drug treatment was more pronounced in A-498 cells.

As S6 protein is the downstream target of S6K1, the loss of its phosphorylation at Thr389-S6K1 caused the complete loss of S6 phosphorylation at Ser235/236 and Ser240/244 in A-498 cells after the combinatorial treatment. In accordance, ABT-737 and combination regimen diminished the basal S6 level about 68 and 86 per cent, respectively (Figure 4.17). Similar to A-498 cells, almost 75 per cent decrease was recorded for the phosphorylated S6 protein at Ser235/236 and Ser240/244 regions in Caki-1 cell after everolimus and the combination treatment. Interestingly, Caki-1 cells showed an 131 and 172 per cent increase in the basal S6 protein when treated with ABT-737 or its combination with everolimus, respectively (Figure 4.18).

Reduced levels for phosphorylated 4E-BP1, another well-known effector of mTORC1 complex, was evident in A-498 cells in the presence of everolimus (Figure 4.18). More than 50 per cent decline in the levels of 4E-BP1 Thr37/45 and Thr70 was recorded for everolimus treated A-498 cells. Although, in the presence of ABT-737 similar decline in 4E-BP1 (Thr70) levels was observed, the phosphorylation of 4E-BP1 at Thr37/45 was not affected by ABT-737 regimen in A-498 cells. In Caki-1 cells, everolimus and combination regimen could only diminish the protein level of p-4E-BP1 at Ser65 Thr70 (Figure 4.18), whereas ABT-737 regimen increased the level of p-4E-BP1 at Thr70.

Interestingly, ABT-737 exhibited different effect on basal 4E-BP1 protein expression in both cell lines. In fact, ABT-737 caused to a slight decrease in 4E-BP1 level of A-498 cells when used alone or in combination with everolimus, whereas a significant increase in 4E-BP1 level was observed in Caki-1 cells under the presence of ABT-737. Taken together, the results showed that the addition of ABT-737 to everolimus regimen could sustain the inhibitory effect of everolimus on mTORC1 activity in both A-498 and Caki-1 cells.

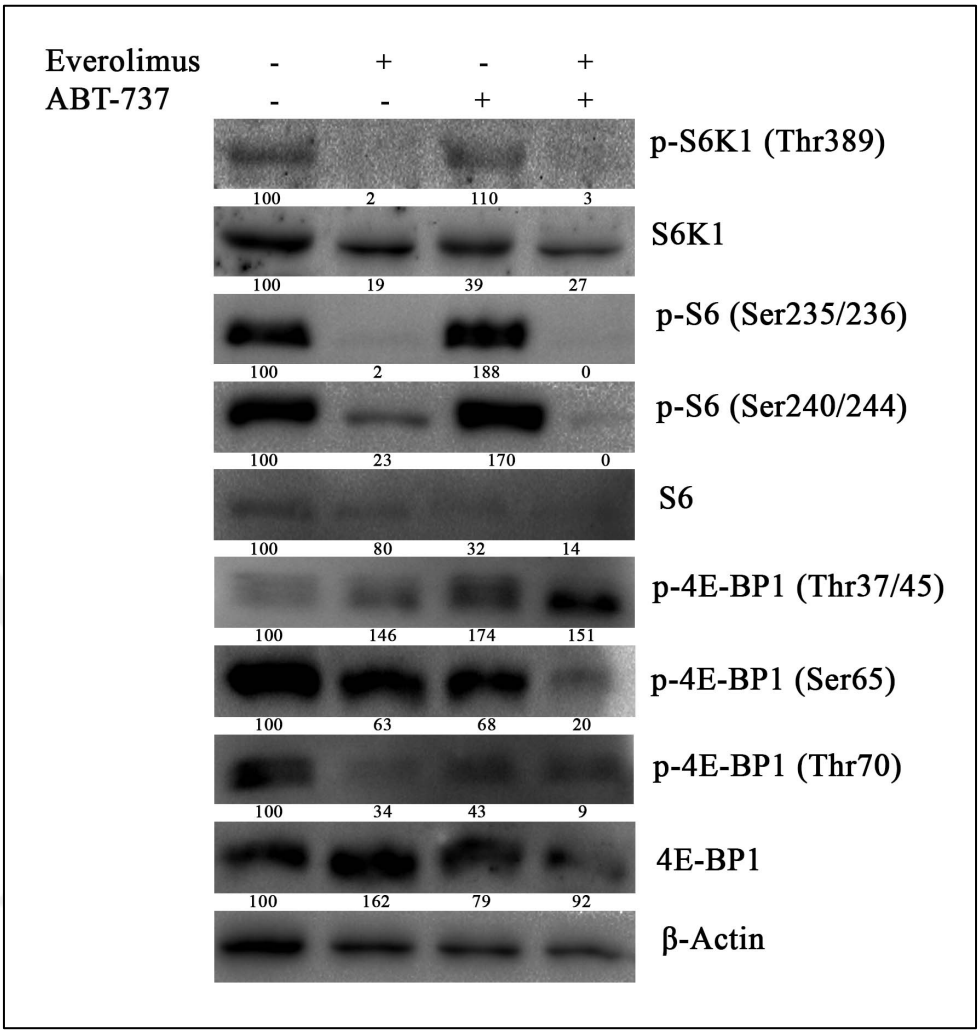

Figure 4.17. Effect of everolimus-ABT-737 combination on the downstream target proteins of mTOR pathway in A-498 cells. Cell lysates of A-498 cells treated with 1 μM everolimus and/or 5 μM ABT-737 for 24 hours were used to determine levels of p-S6K1 (Thr389) (70-85 kDa), S6K1 (70-85 kDa), p-S6 (Ser235/236) (32 kDa), p-S6 (Ser240/244) (32 kDa), S6 (32 kDa), p-4E-BP1 (Thr37/45) (15-20 kDa), p-4E-BP1 (Ser65) (15-20 kDa), p-4E-BP1 (Thr70) (15-20 kDa), and 4E-BP1 (15-20 kDa) proteins by Western blot. As loading control, β-Actin (38 kDa) was used. The average percentage values were calculated according to the densitometric analysis of at least three independent experiments and set as 100 per cent for control cells.

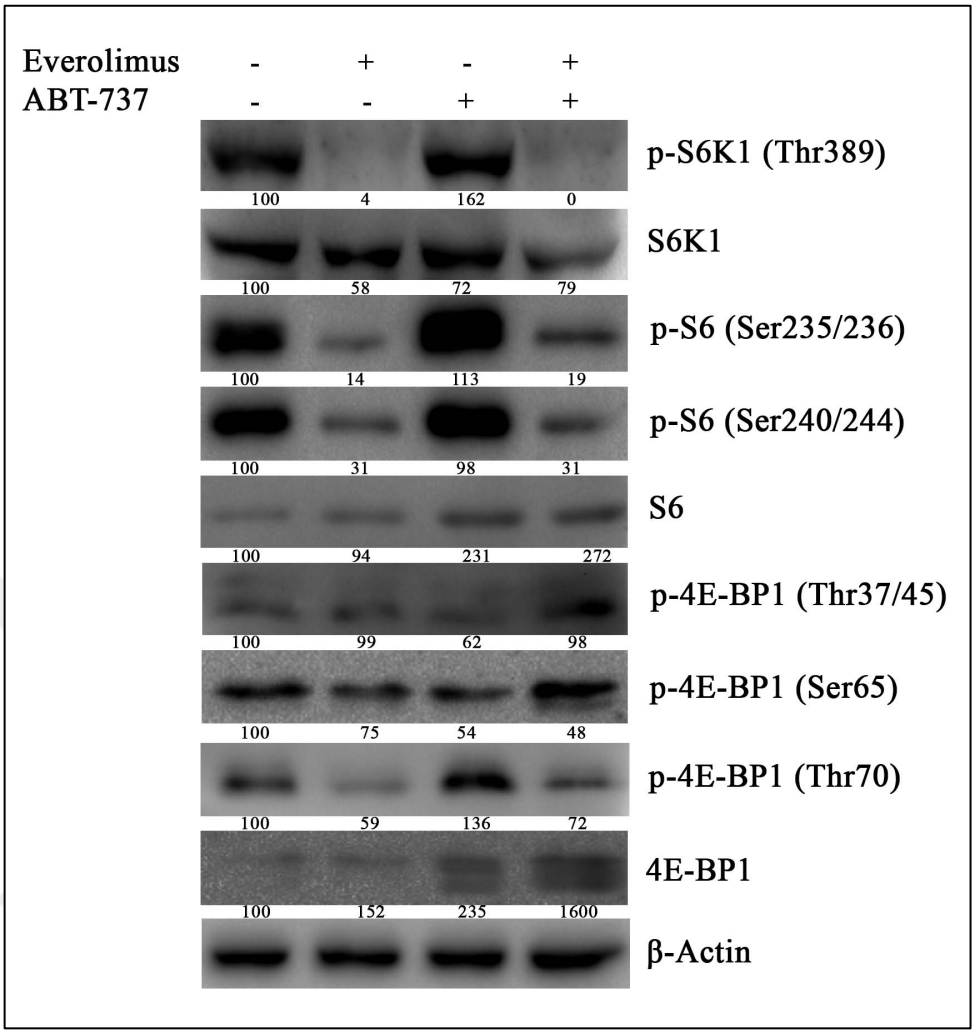

Figure 4.18. Effect of everolimus-ABT-737 combination on the downstream target proteins of mTOR pathway in Caki-1 cells. Cell lysates of Caki-1 cells treated with 1 μM everolimus and/or 10 μM ABT-737 for 24 hours were used to determine levels of p-S6K1 (Thr389) (70-85 kDa), S6K1 (70-85 kDa), p-S6 (Ser235/236) (32 kDa), p-S6 (Ser240/244) (32 kDa), S6 (32 kDa), p-4E-BP1 (Thr37/45) (15-20 kDa), p-4E-BP1 (Ser65) (15-20 kDa), p-4E-BP1 (Thr70) (15-20 kDa), and 4E-BP1 (15-20 kDa) proteins by Western blot. As loading control, β-Actin (38 kDa) was used. One representative blot was shown. The average percentage values were calculated according to the densitometry analysis and set as 100 per cent for control cells.

One of the feedback loops characterized in RCC as being activated upon acquired everolimus resistance is the molecular switch from mTORC1 to mTORC2 complex [115]. Under normal conditions, the activity of mTORC2 is regulated indirectly by mTORC1

through which mTORC2 exhibits rapamycin insensitivity. Therefore, cell lysates of A-498 and Caki-1 cells that were subjected to mono- or combination therapies for 24 hours were next used in Western blot in order to determine whether the combination therapy can affect the mTORC2 complex activation. The phosphorylation of S6K1 at Thr389 by mTORC1 complex activates S6K1 which in turn catalyzes the phosphorylation of Rictor protein at Thr1135 [102, 125]. Hence, the presence of phosphorylated Rictor protein indicates the active mTORC2 complex.

In A-498 and Caki-1 cells, the reduced p-Rictor level were observed after everolimus and combination regimen, whereas ABT-737 regimen caused to a slight increase in p-Rictor protein level (Figure 4.19 and 4.20). These results indicates that Rictor protein could not be phosphorylated due to the lack of p-S6K1 protein observed in both cell lines after everolimus and combination regimen (Figure 4.17 and 4.18). As ABT-737 had no effect on S6K1 phosphorylation, the p-Rictor could be detected in both cell lines. In comparison to A-498 cells, where ABT-737 and dual-drug regimen led to a slight decrease in basal Rictor level, an increase in endogenous Rictor protein was detected in Caki-1 cells in response to the same treatments.

mTORC2 complex provides a negative feedback loop in cells that develop resistance to rapalogs. In fact, mTORC2 complex catalyzes the phosphorylation of AKT at Ser473 that further activates the mTORC1 complex [119, 128]. In A-498 cells, the level of phosphorylated AKT at Ser473 was decreased about 26 and 36 per cent upon everolimus or ABT-737 regimen. The reduced p-AKT level was more pronounced upon dual-drug combination (57 per cent) (Figure 4.19). However, Caki-1 cells showed an average of 17 per cent increase in p-AKT protein level upon ABT-737 and combination treatments, whereas everolimus caused to a reduction in p-AKT level for this cell line (Figure 4.20). In contrast, the reduced level of basal AKT was detected in both cell lines after each treatment type. These results indicate that mTORC2 complex is regulated differently in both cell lines. Everolimus and combination regimen decreased the level of phosphorylated mTOR at Ser2481 in A-498 and Caki-1 cells, while an increase in p-mTOR was detected in both RCC cell lines upon ABT-737 treatment. In A-498 cells, each treatment caused a slight decrease in the basal mTOR level in comparison to Caki-1 cells which exhibited high endogenous mTOR level in response to mono- and combination therapies.

Altogether, these data suggested that the combination treatment might suppress the activity of mTORC2 complex in A-498 cells. In contrast, the activation of mTORC2 complex as a result of mTORC1 suppression was not affected by the dual-drug therapy in Caki-1 cells.

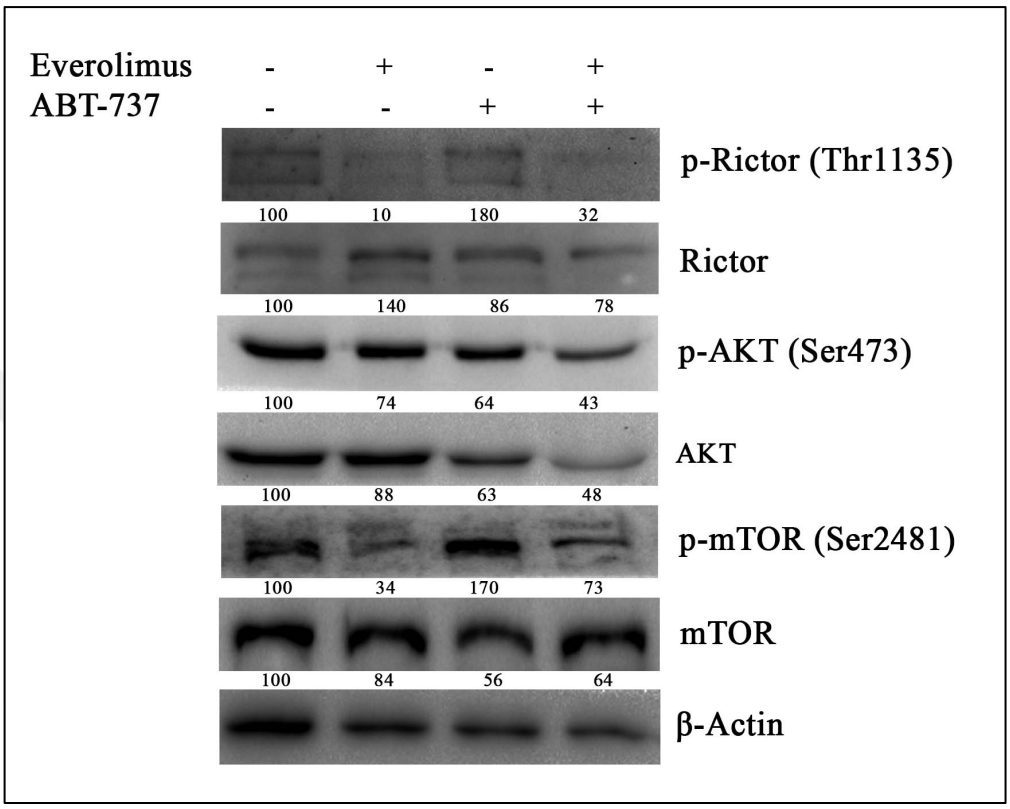

Figure 4.19. Effect of everolimus-ABT-737 combination on the mTORC2 complex in A-498 cells. Protein extracts of A-498 cells treated with 1 μM everolimus and/or 5 μM ABT-737 for 24 hours were used to determine p-Rictor (Thr1135) (200 kDa), Rictor (200 kDa), p-mTOR (Ser2481) (289 kDa), mTOR (289 kDa), p-AKT (Ser473) (60 kDa), and AKT (60 kDa) protein levels by Western blot analysis. To ensure equal protein loading 38 kDa-protein β-actin was utilized. One representative blot was shown. The average percentage values were calculated according to densitometric analysis of at least three independent experiments and set as 100 per cent for control cells.

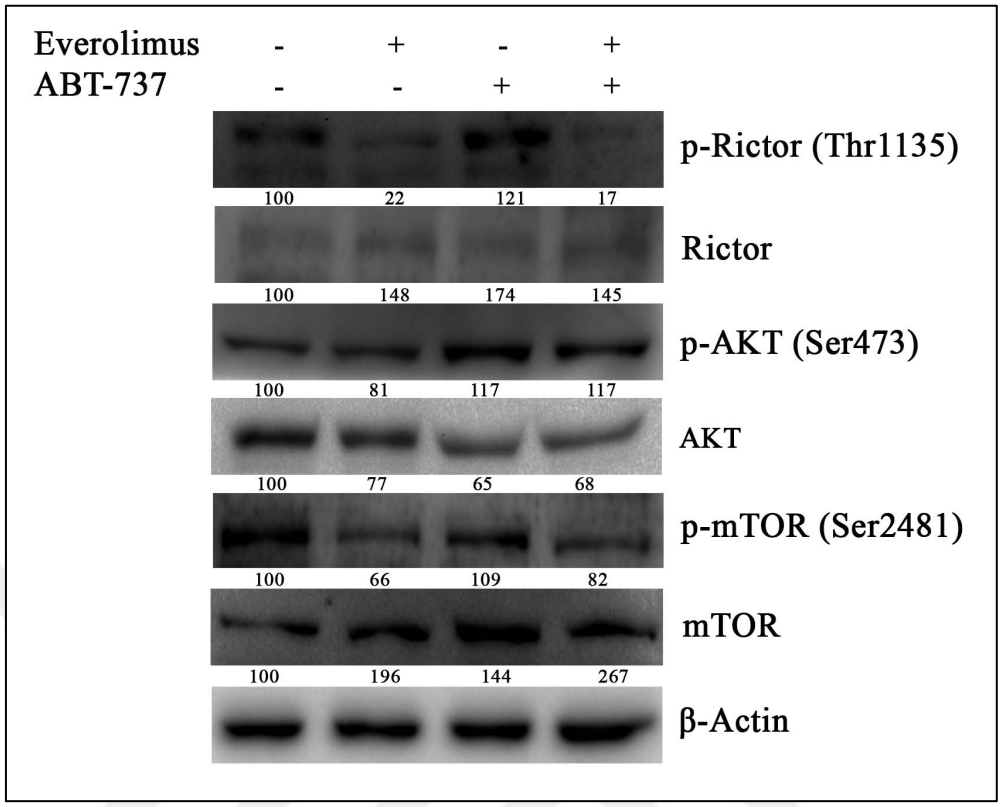

Figure 4.20. Effect of everolimus-ABT-737 combination on the mTORC2 complex in Caki-1 cells. Protein extracts of Caki-1 cells treated with 1 μM everolimus and/or 10 μM ABT-737 for 24 hours were used to determine p-Rictor (Thr1135) (200 kDa), Rictor (200 kDa), p-mTOR (Ser2481) (289 kDa), mTOR (289 kDa), p-AKT (Ser473) (60 kDa), and AKT (60 kDa) by Western blot. As loading control, β-Actin (38 kDa) was used. One representative blot was shown. The average percentage values were calculated according to the densitometry analysis and set as 100 per cent for control cells.

4.5. EFFECT OF EVEROLIMUS AND ABT-737 COMBINATION ON CELL DEATH

4.5.1. Apoptotic Effect of Everolimus and ABT-737 Combination

In A-498 and Caki-1 cells, the cytotoxic effect of everolimus and ABT-737 combination was shown with WST-1 viability, suggesting that the reduction of cell number might be due to induced cell death. In order to determine the apoptotic response against the

combination therapy, Annexin V-PI staining was performed as described in Section 3.2.2 on A-498 and Caki-1 cells that were subjected to either monotherapy or combination therapy for 24, 48, and 72 hours.

In consistence with cell viability data, percentages of A-498 cells that enter in early and late apoptosis was 2 per cent and 7 per cent at 24 hours after everolimus regimen, respectively (Figure 4.21b). The increased duration of treatment did not significantly change the number of apoptotic cells at 48 and 72 hours (Figure 4.22 and 4.23). In comparison to everolimus, a significant induction of apoptosis was observed upon ABT-737 regimen and its combination with everolimus even after 24 hours where apoptosis was demonstrated in more than 60 per cent of A-498 cells (Figure 4.21). Compared to control cells, the induction of apoptosis was much more pronounced when cells were treated with ABT-737 monotherapy and combination therapy for 48 and 72 hours (Figure 4.22 and 4.23).

These results indicated that the decrease in A-498 cell viability observed as a response to combination therapy was due to the induction of apoptosis. In order to investigate this apoptotic response at the molecular level, the protein expressions of caspases were analyzed by Western blot performed with the cell lysates of A-498 cells subjected to 1 μM everolimus and/or 5 μM ABT-737 for 24 hours (Figure 4.24).

In consistence with results obtained from Annexin-V staining, ABT-737 monotherapy and its combination with everolimus increased the protein level of cleaved caspase 9, as well as cleaved caspase 3, the effector of active caspase 9. As the cleaved PARP is another indicator for the active apoptotic mechanism, the observation of the increase in its cleaved form under the same conditions indicated the induction of cell death.

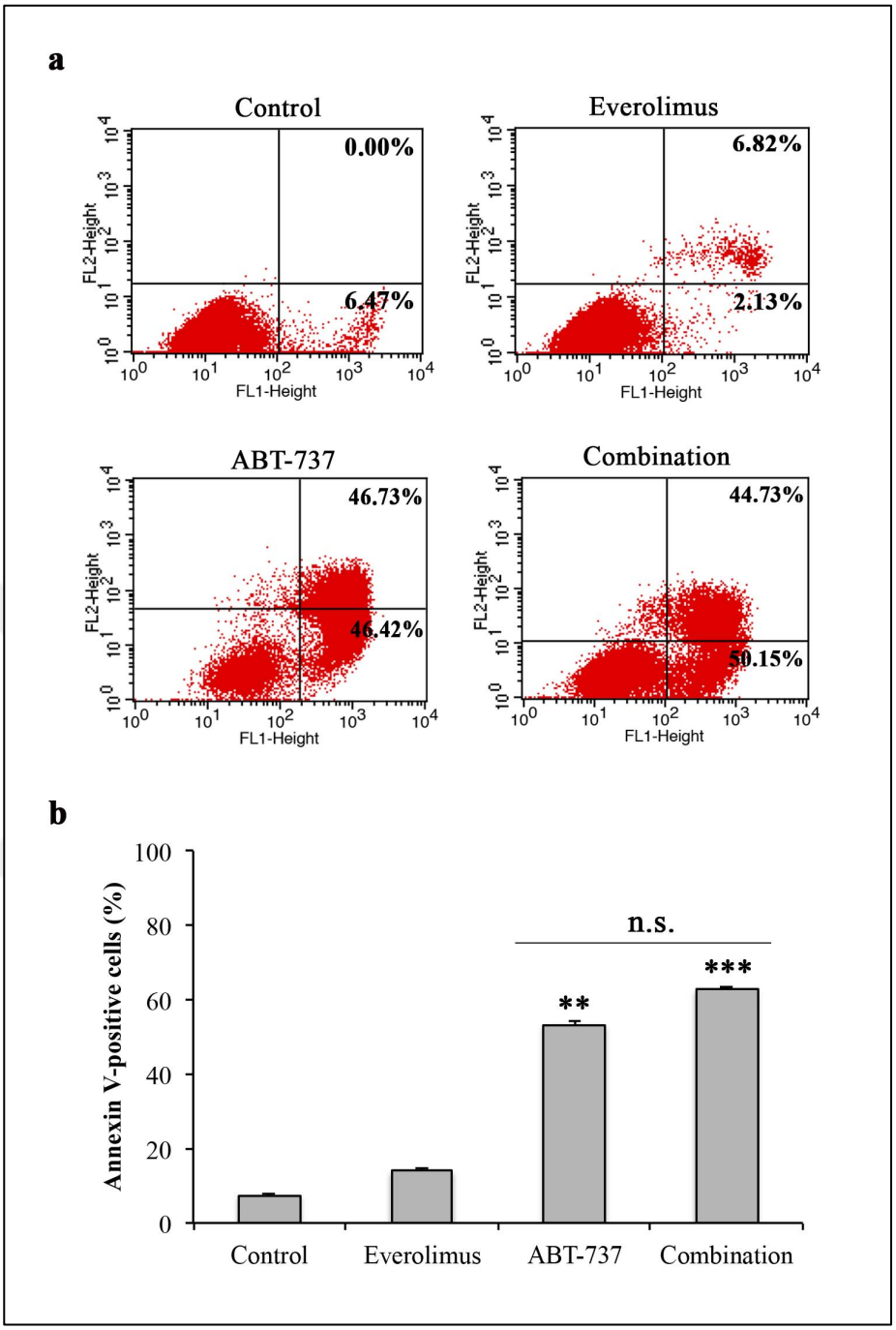

Figure 4.21. Effect of everolimus-ABT-737 combination on A-498 cell death at 24 hours. (a) Cell death of A-498 cells subjected to 1 µM everolimus and/or 5 µM ABT-737 was analyzed by Annexin-V/PI staining. The numbers of cells entered in early apoptosis (bottom right) and late apoptosis (top right) cells were shown as percentages in histogram images. (b) Graphical representation of percentages for Annexin V-positive cells (early and late apoptosis) were shown.

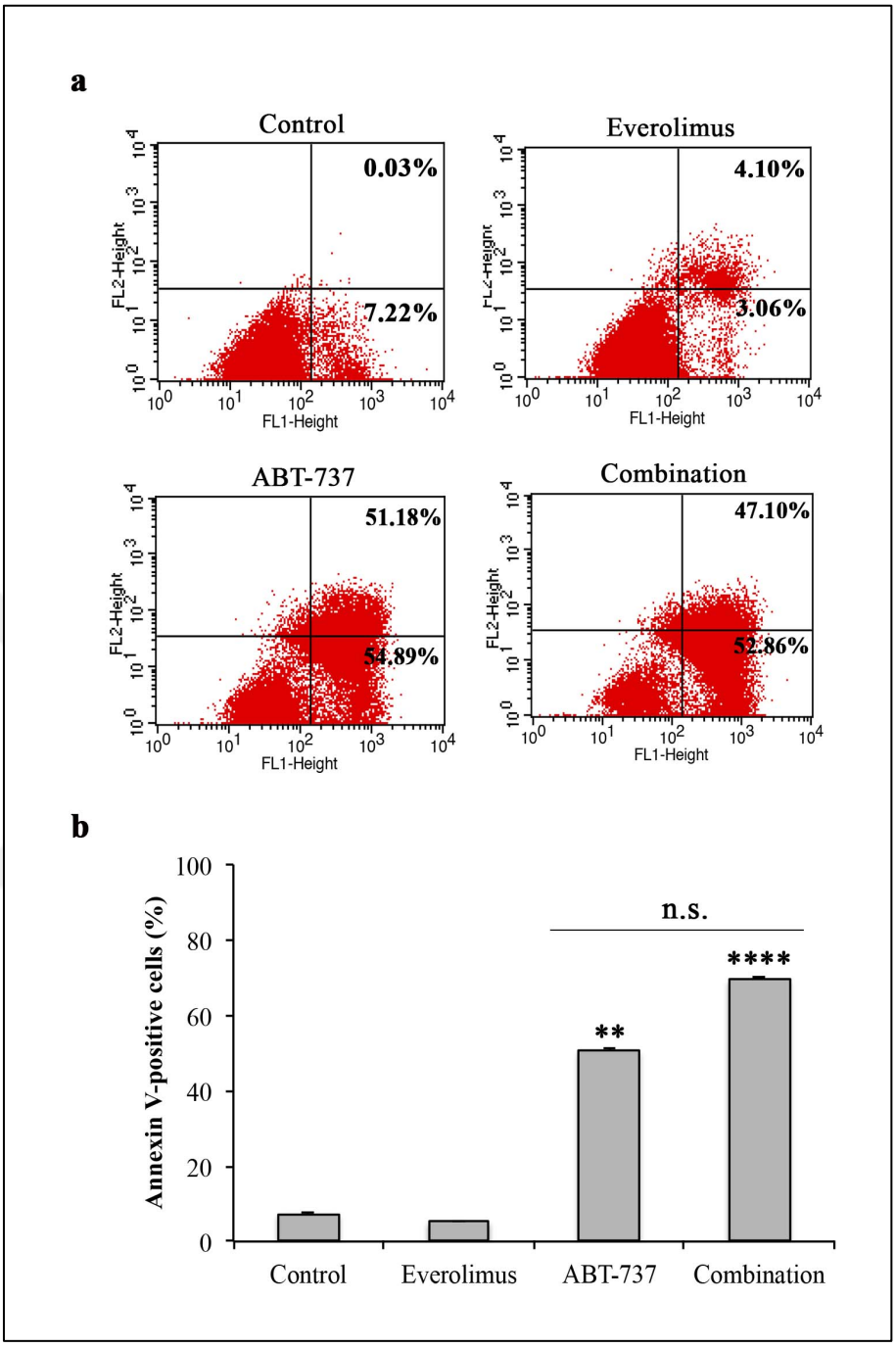

Figure 4.22. Effect of everolimus-ABT-737 combination on A-498 cell death at 48 hours. (a) Cell death of A-498 cells undergone treatment with 1 µM everolimus and/or 5 µM ABT-737 was analyzed by Annexin-V/PI staining. The numbers of cells in early apoptosis (bottom right) and late apoptosis (top right) cells were shown as percentages in histogram images. (b) Graphical representation of percentages for Annexin V-positive cells (early and late apoptosis) were shown.

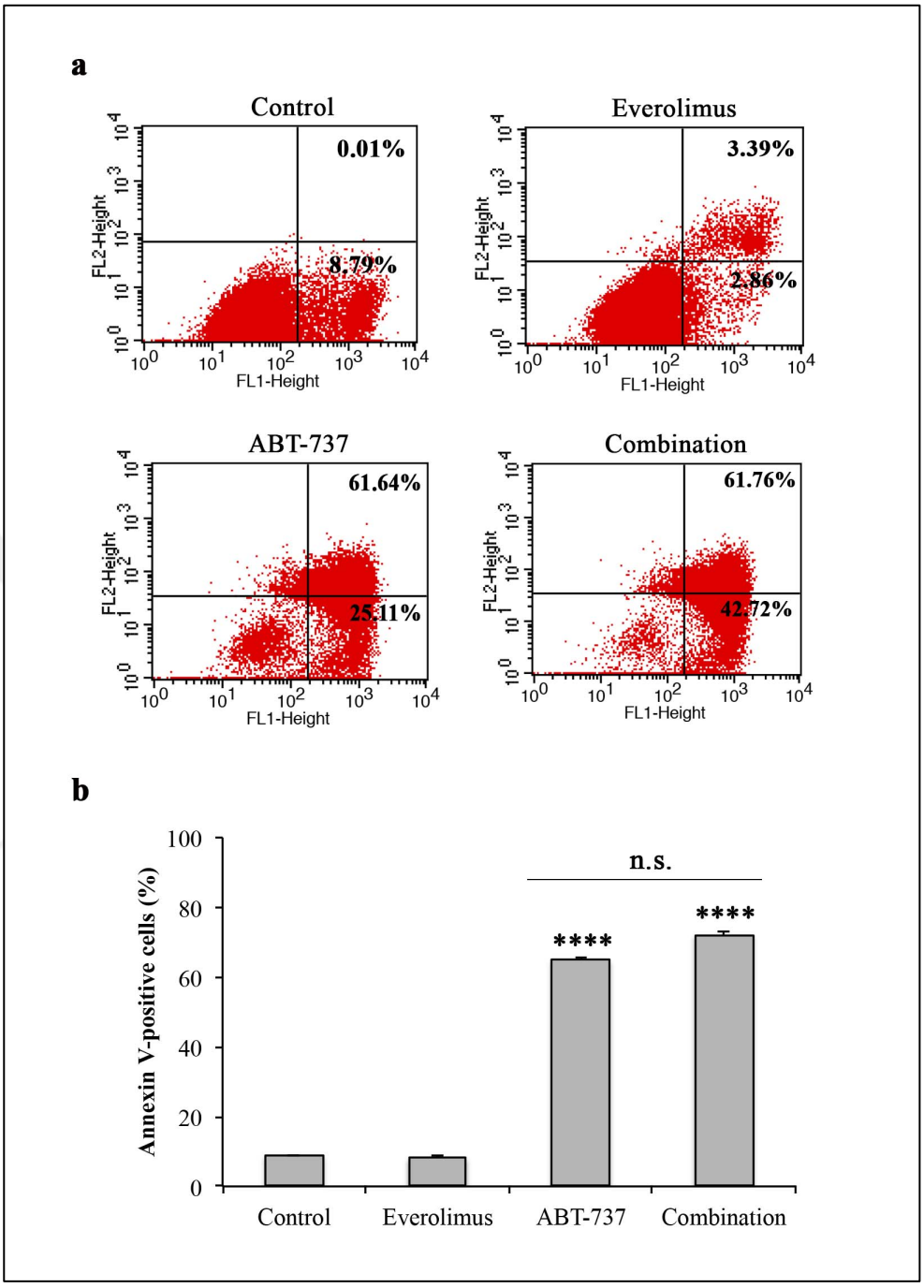

Figure 4.23. Effect of everolimus-ABT-737 combination on A-498 cell death at 72 hours. (a) A-498 cells were treated with 1 µM everolimus and/or 5 µM ABT-737 to analyze cell death by Annexin-V/PI staining. The numbers of cells entering in early apoptosis (bottom right) and late apoptosis (top right) cells were shown as percentages in histogram images. (b) Graphical representation of percentages for Annexin V-positive cells (early and late apoptosis) were shown.

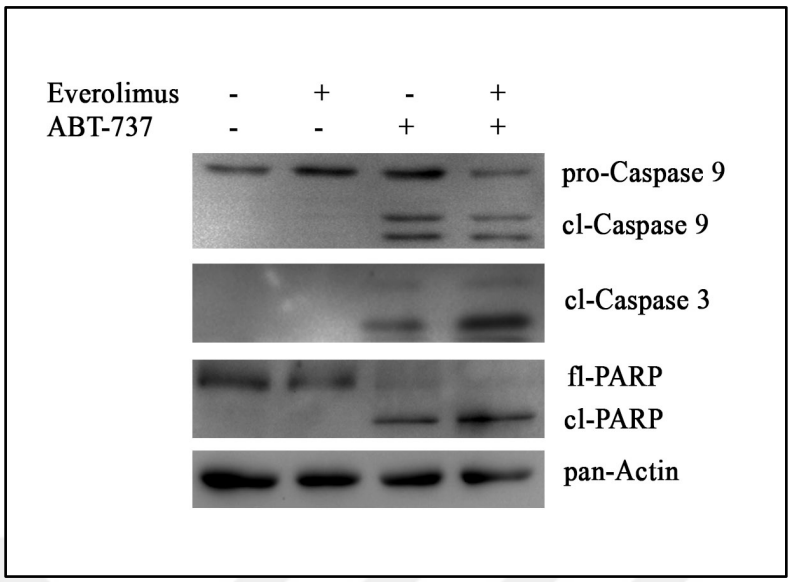

Figure 4.24. Effect of everolimus-ABT-737 combination on apoptotic mechanism of A-498 cells. A-498 cells were undergone everolimus (1 μM) and/or ABT-737 (5 μM) regimens for 24 hours were used to determine the protein expression of caspase 9 (47, 37, 35 kDa), caspase 3 (17, 19 kDa), and PARP by Western blot analysis. To ensure equal protein loading 45 kDa-protein pan-actin was utilized.

An average of 7 per cent of Annexin-V stained Caki-1 cells was recorded after the treatment with 1 μM everolimus for 24 and 48 hours, where an average of 5 per cent cells were found in late apoptosis (Figure 4.25). In comparison to A-498 cells, the significant induction of cell death was observed only after 72 hours of treatment with ABT-737 and its combination with everolimus (Figure 4.27) in Caki-1 cells. ABT-737 monotherapy resulted in 14 per cent and 19 per cent late apoptosis at 24 and 48 hours, which was increased significantly up to 60 per cent at 72 hours, whereas no significant change was observed in early apoptosis (Figure 4.25 and 4.26). At the end of 72 hours, 64 per cent of Caki-1 cells were stained positive for Annexin-V (Figure 4.27).

In comparison to ABT-737 regimen, 10 per cent and 8 per cent late apoptosis were recorded after everolimus-ABT7-737 combination at 24 and 48 hours, respectively (Figure 4.25 and 4.26). Similar to single ABT-737 regimen, 58 per cent of cells were characterized as being apoptotic in response to the combination regimen for 72 hours (Figure 4.27).

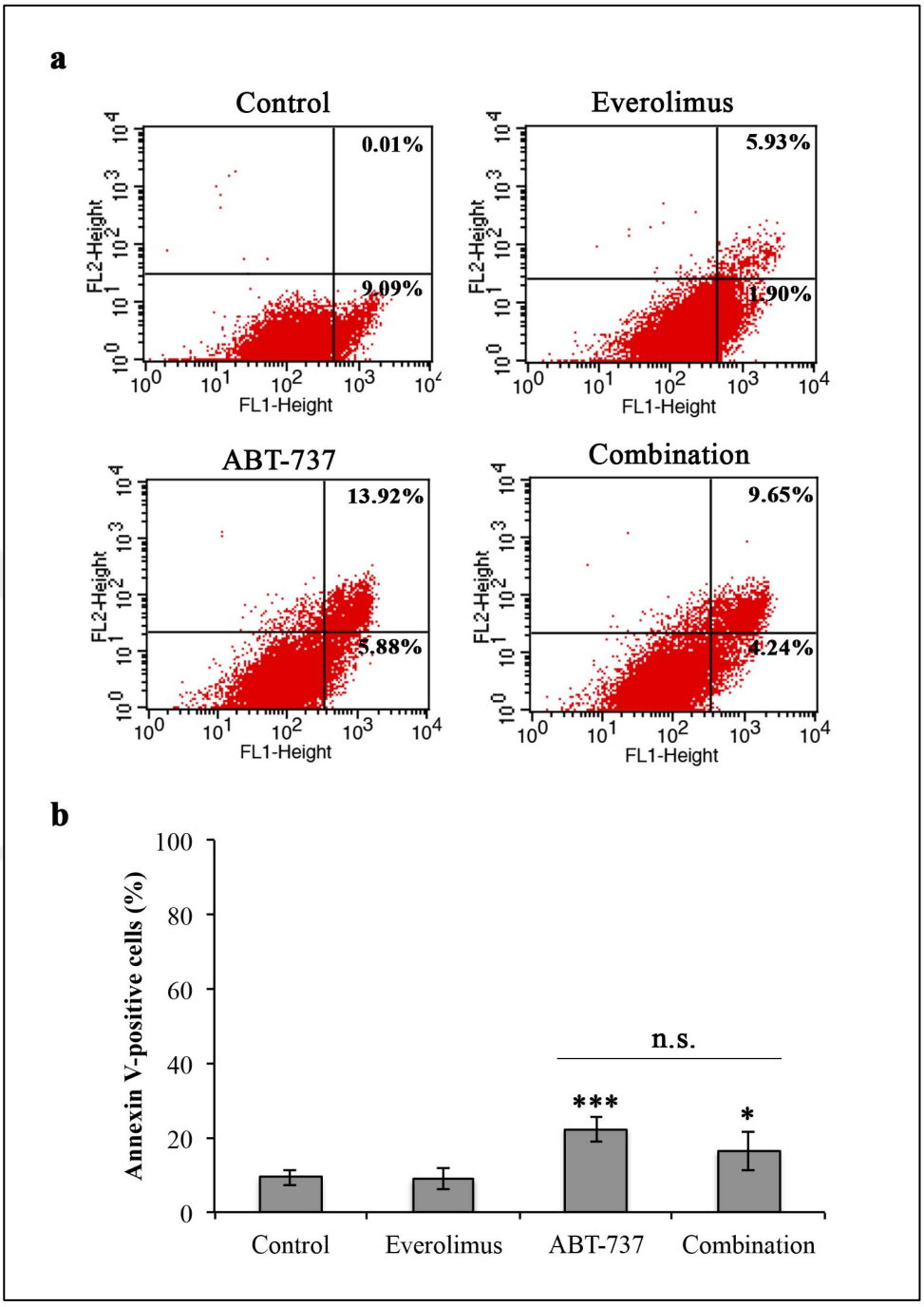

Figure 4.25. Effect of everolimus-ABT-737 combination on Caki-1 cell death at 24 hours. (a) Annexin-V/PI staining was carried out to analyze the cell death of Caki-1 cells undergone treatment with 1 μM everolimus and/or 10 μM ABT-737. The numbers of cells entered in early apoptosis (bottom right) and late apoptosis (top right) cells were shown as percentages in histogram images. (b) Graphical representation of percentages for Annexin V-positive cells (early and late apoptosis) were shown.

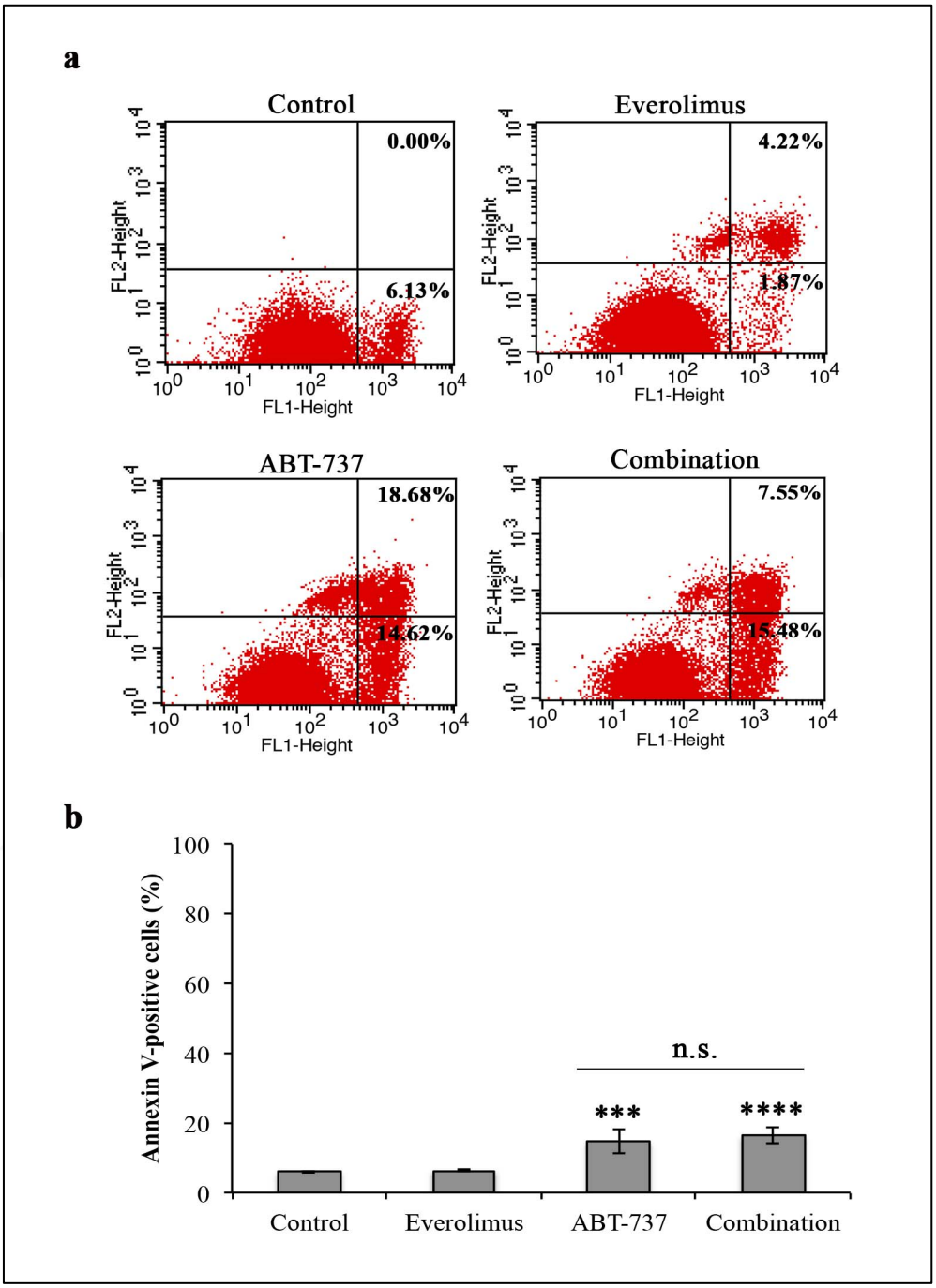

Figure 4.26. Effect of everolimus-ABT-737 combination on Caki-1 cell death at 48 hours. (a) Cell death of Caki-1 cells subjected to everolimus (1 µM) and/or ABT-737 (10 µM) was analyzed by Annexin-V/PI staining. The numbers of cells in early apoptosis (bottom right) and late apoptosis (top right) cells were shown as percentages in histogram images. (b) Graphical representation of percentages for Annexin V-positive cells (early and late apoptosis) were shown.

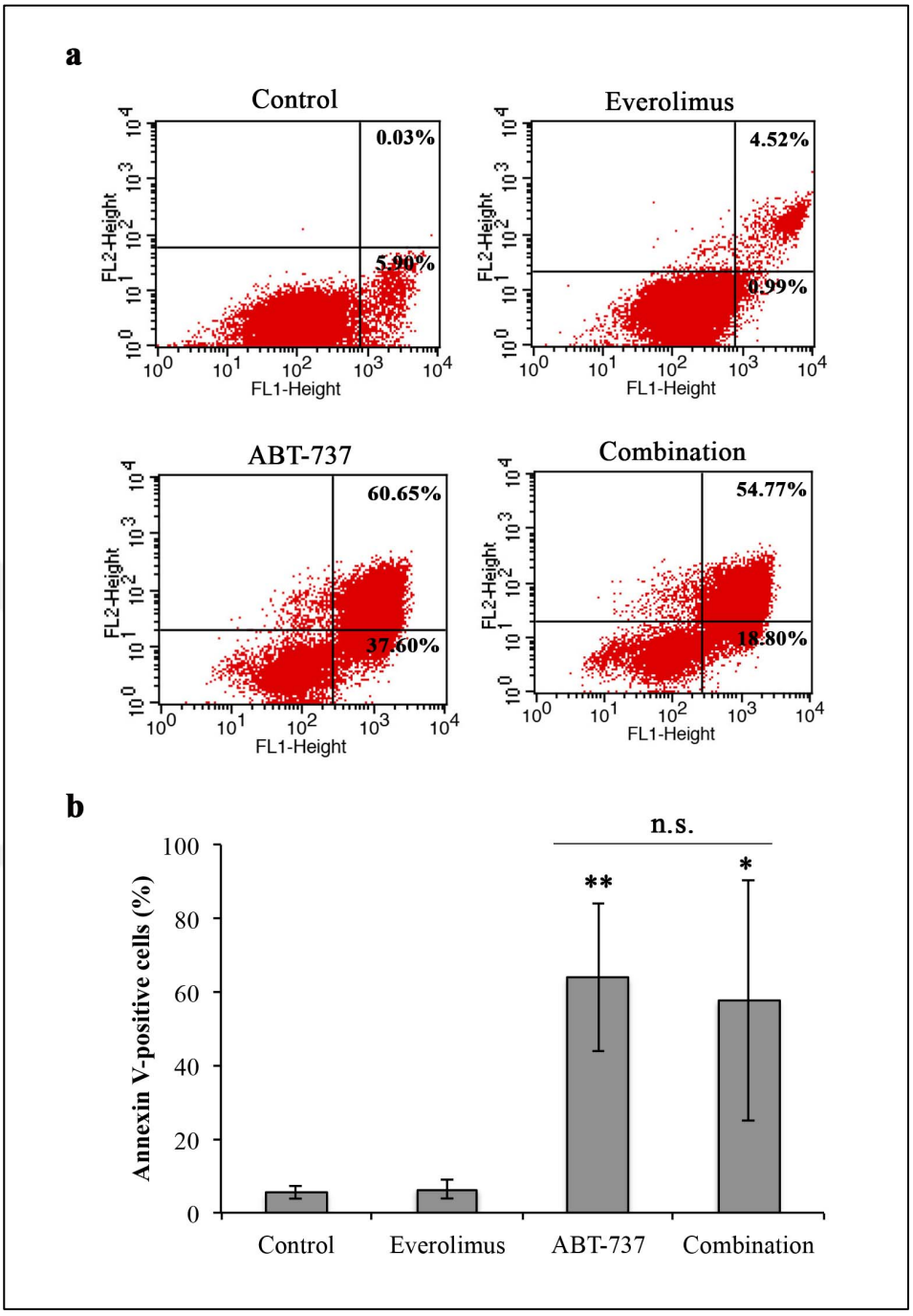

Figure 4.27. Effect of everolimus-ABT-737 combination on Caki-1 cell death at 72 hours. (a) Caki-1 cells were subjected to everolimus (1 μM) and/or ABT-737 (10 μM) treatments in order to analyze cell death determined by Annexin-V/PI staining. The numbers of cells entered in early apoptosis (bottom right) and late apoptosis (top right) cells were shown as percentages in histogram images. (b) Graphical representation of percentages for Annexin V-positive cells (early and late apoptosis) were shown.

The effect of combination therapy on Caki-1 apoptosis was further investigated at the molecular level. Therefore, Caki-1 cells were subjected to everolimus (1 μM) and/or ABT-737 (10 μM) regimen in order to analyze their protein extracts by Western blot.

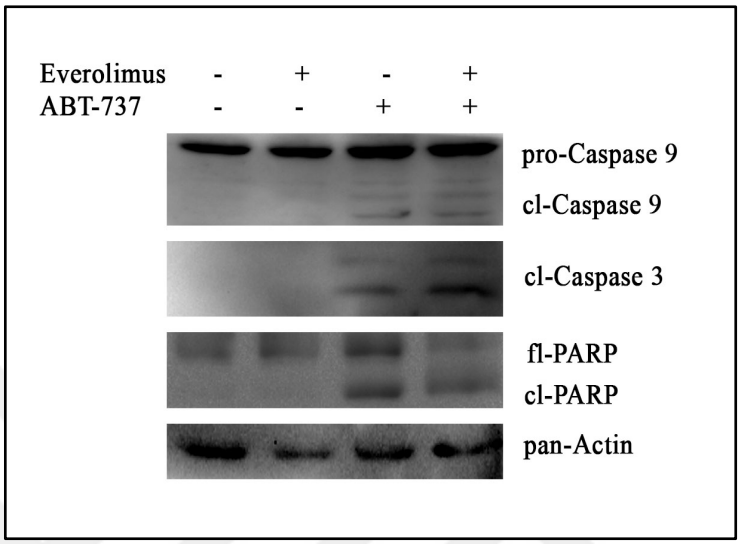

Figure 4.28. Effect of everolimus-ABT-737 combination on the apoptotic mechanism of Caki-1 cells. Protein extracts of A-498 cells subjected to everolimus (1 μM) and/or ABT-737 (10 μM) regimens for 24 hours were used to determine the protein expression of caspase 9 (47, 37, 35 kDa), caspase 3 (17, 19 kDa), and PARP by Western blot. To ensure equal protein loading 45 kDa-protein pan-Actin was utilized.

In support of the Annexin V data, an increase in levels of cleaved caspase 9 and cleaved caspase 3 were observed in Caki-1 cells once subjected to ABT-737 or combination regimen, compared to the control and everolimus-treated cells. Interestingly, the level of cleaved PARP was more pronounced in cells undergone single ABT-737 treatment than in cells co-treated with everolimus and ABT-737 (Figure 4.28).

Taken together, the data presented here suggested that ABT-737 alone or in combination with everolimus triggers the apoptotic response in Bcl-2 overexpressing A-498 and Caki-1 cells that were insensitive to everolimus treatment.

4.5.2. Effect of Everolimus and ABT-737 Combination on Bcl-2 Family Members

In order to understand the molecular mechanism underlining the apoptotic response observed in A-498 and Caki-1 cells when they were subjected to everolimus-ABT-737 combination, the alterations in the expression levels of Bcl-2 family proteins were investigated by Western blot analysis as described in Section 3.3.6.

The stability of Bcl-2 protein is regulated through the phosphorylation of amino acids located between BH4 and BH3 domains of the protein [144]. Therefore, the alterations in the protein level of phosphorylated Bcl-2 at Ser70 might indicate the effect of the everolimus-ABT combination therapy on the integrity of Bcl-2 protein, as BH3 region of Bcl-2, Bcl-xL, and Bcl-w is the specific target of ABT-737. In A-498 cells, everolimus treatment led 50 per cent decrease in the phosphorylation of Bcl-2 in comparison to basal Bcl-2 protein, which was increased up to 40 per cent upon everolimus regimen (Figure 4.29). In comparison to everolimus regimen, single ABT-737 treatment exerted an inhibitory effect on the Bcl-2 phosphorylation in A-498 cells as evidenced by 30 per cent fold decrease in the p-Bcl-2 protein level. The decrease in p-Bcl-2 was recorded only as 80 per cent when cells were subjected to combination therapy. These reduced p-Bcl-2 levels correlated with 60 and 80 per cent reduction in the basal Bcl-2 protein levels observed in A-498 cells treated ABT-737 monotherapy and combination therapy, respectively.

In addition to Bcl-2, ABT-737 also showed an blocking effect on the protein expression of Bcl-xL in A-498 cells. In fact, cells treated either with ABT-737 or dual-drug combination demonstrated a respective 10 and 50 per cent decrease in Bcl-xL levels. Upon everolimus treatment, the expression of Bcl-xL protein was increased up to 20 per cent in A-498 cells. In comparison to Bcl-2 and Bcl-xL, however, everolimus exhibited no effect on Mcl-1 protein level. As expected increase of 67 and 47 per cent was recorded in Mcl-1 protein for A-498 cells exposed to ABT-737 or dual-drug combination as Mcl-1 is not the target protein of ABT-737.

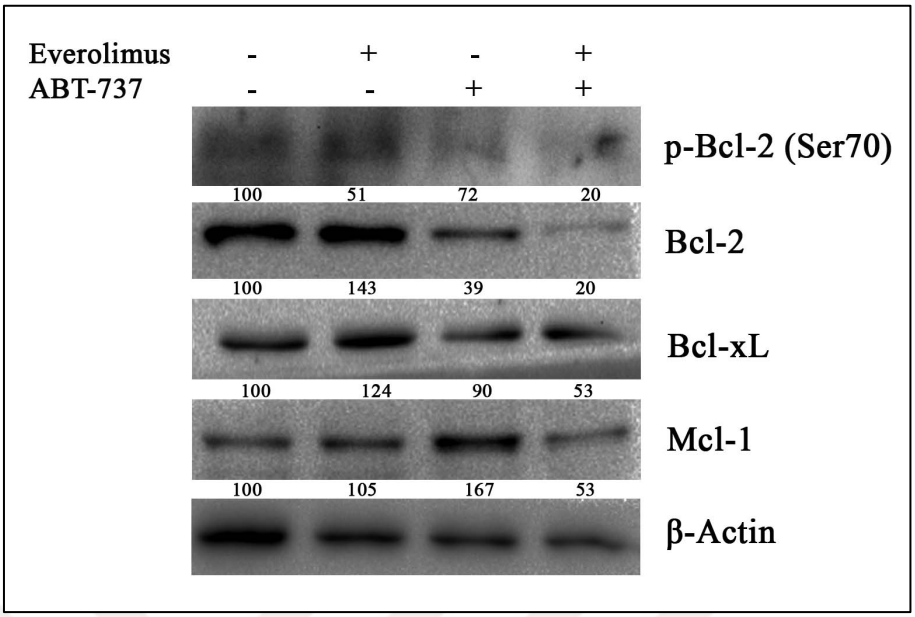

Figure 4.29. Effect of everolimus-ABT-737 combination on the anti-apoptotic Bcl-2 family proteins of A-498 cells. Western blot was carried out with cell lysates of A-498 cells subjected to everolimus (1 μM) and/or ABT-737 (5 μM) regimen for 24 hours to determine p-Bcl-2 (Ser70) (28 kDa), Bcl-2 (26 kDa), Bcl-xL (30 kDa), and Mcl-1 (40 kDa) protein levels. To ensure equal loading, β-Actin (38 kDa) was used. The average percentage values were calculated according to the densitometry analysis of at least three independent experiments and set as 100 per cent for control cells.

In Caki-1 cells, treatment with either everolimus or ABT-737 demonstrated an average of 16 per cent decrease in p-Bcl-2 levels (Figure 4.30). The combination of both agents, however, inhibited the phosphorylation of Bcl-2 as evidenced by 90 per cent decrease in the protein expression. Compared to control cells, a slight increase (4 per cent) in the basal expression levels of Bcl-2 protein was detected in the everolimus-treated Caki-1 cells. In line with the results obtained for A-498 cells, ABT-737 monotherapy and dual-drug therapy decreased the endogenous Bcl-2 level respectively about 21 and 29 per cent, indicating the amount of Bcl-2 protein correlated with its phosphorylated derivative.

In comparison to Bcl-2, the endogenous expression level Bcl-xL, another target protein of ABT-737, increased up to 20 and 50 per cent in response to everolimus and ABT-737 treatment in Caki-1 cells, respectively. However, 33 per cent decrease in Bcl-xL level recorded upon the combination regimen indicated that both agents can synergistically

effect the basal Bcl-xL levels in Caki-1 cells. Similar to A-498 cells, an average of 70 per cent increase in the endogenous Mcl-1 level was recorded in Caki-1 cells undergone ABT-737 single treatment or co-treatment with both drugs. No effect of everolimus therapy on the expression of Mcl-1 protein was detected.

Altogether, these results suggested that the elevated level of Bcl-2 protein observed in both control and everolimus-treated A-498 and Caki-1 cells could be diminished in the presence of ABT-737.

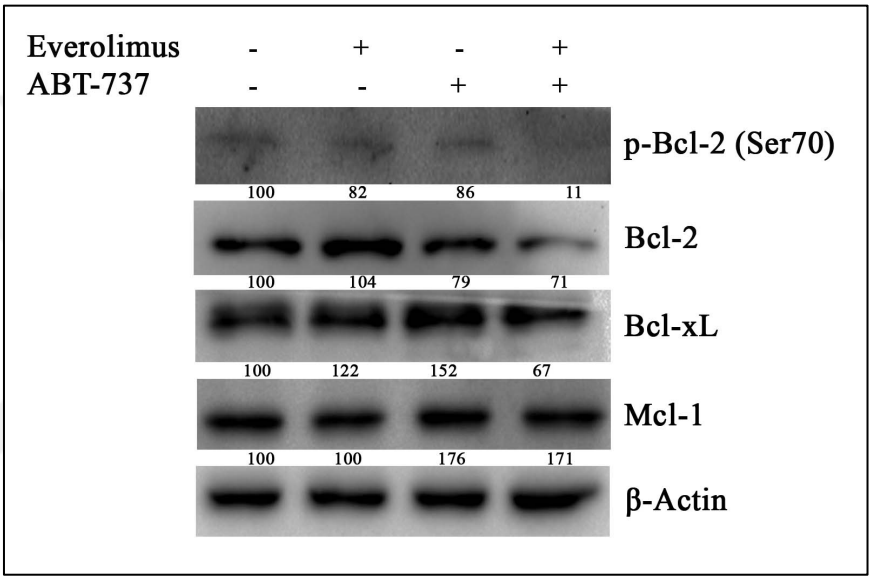

Figure 4.30. Effect of everolimus-ABT-737 combination on the anti-apoptotic Bcl-2 family proteins of Caki-1 cells. Cell lysates of Caki-1 cells subjected to 1 μM everolimus and/or 10 μM ABT-737 regimen for 24 hours were used to determine p-Bcl-2 (Ser70) (28 kDa), Bcl-2 (26 kDa), Bcl-xL (30 kDa), and Mcl-1 (40 kDa) protein levels by Western blot. To ensure equal loading, 38 kDa protein β-Actin was utilized. One representative blot was shown. The average percentage values were calculated according to the densitometry analysis and set as 100 per cent for control cells.

The interplay between BH3-only proteins and their anti- and pro-apoptotic counterparts enables the pore formation on the mitochondrial membrane, which is a prerequisite for the initiation of caspase cascade [160]. In this regard, the expression levels of BH3-only proteins were investigated in A-498 and Caki-1 cells treated with everolimus and/or ABT-737 in order to understand the cytotoxic effect of the dual-drug therapy at molecular level. The analysis of pro-apoptotic Bax levels in A-498 cells revealed no change in response to

mono- or combo-drug treatment (Figure 4.31). As an activator BH3-only protein, Bim interacts with both the pro-apoptotic Bax and anti-apoptotic Bcl-2 [279, 280]. Upon the apoptotic signal, Bim disrupts the Bcl-2-Bax/Bak interaction through binding to Bcl-2 [262]. Therefore, the upregulation of Bim protein has been associated with the induction of cell death. In A-498 cells, ABT-737 and combination regimen led to a respective 7 and 8 fold increase in the endogenous Bim_L level. This finding indicated that the cell death assocaited with the use of ABT-737 either alone or in combination might be through Bim-dependent pathway. Bad is a sensitizer BH3-only protein and is only active when serine residue at the position 136 is dephosphorylated [281]. In A-498 cells, treatment with everolimus led to 15 fold increase in p-Bad level, while a 60 per cent reduction in the basal Bad protein was observed. The significant increase (77 fold) detected for p-Bad protein level was more pronounced in ABT-737-treated cells than in cells co-treated with everolimus and ABT-737 (48 fold). Although ABT-737 monotherapy led to 2 fold increase in the endogenous Bad level, only 0.3 fold decrease in basal Bad level was observed upon the combination therapy.

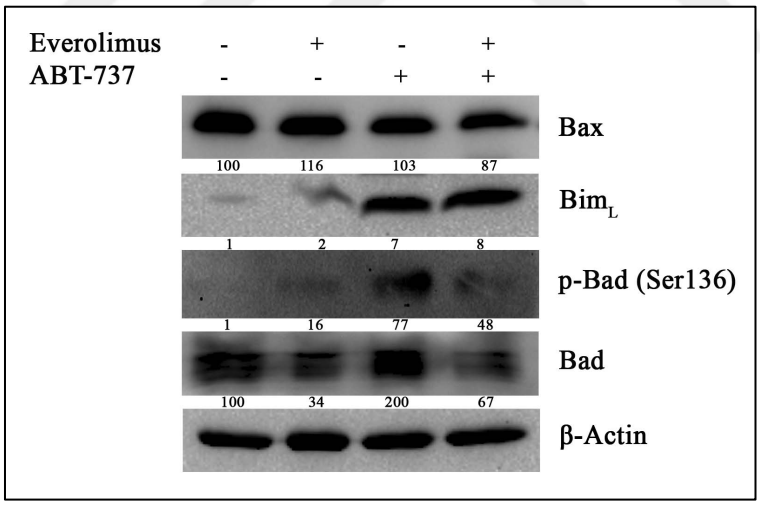

Figure 4.31. Effect of everolimus-ABT-737 combination on the Bcl-2 family members of A-498 cells. In order to determine levels of p-Bad (Ser136) (23 kDa), Bad kDa), Bax (20 kDa), and Bim_L (15 kDa) proteins, Western blot was performed with protein extracts of A-498 cells exposed to everolimus (1 μM) and/or ABT-737 (5 μM) for 24 hours. To ensure equal protein loading 38 kDa protein β-Actin was utilized. Blots show one representative experiment. The average percentage values were calculated according to the densitometry analysis and set as 100 per cent for control cells.

The analysis of endogenous Bax protein in Caki-1 cells revealed that monotherapies induced the expression of Bax protein at about 40 per cent (Figure 4.32). In cells co-treated with everolimus and ABT-737, the protein level of Bax was increased up to 90 per cent which indicates the possible accumulation of the protein in response to the dual-drug combination. In Caki-1 cells, ABT-737 monotherapy and its combination with everolimus led to 21 and 12 fold increase in the expression levels of Bim_L protein, respectively. No change in basal Bim_L protein level was observed in the control and everolimus-treated cells. The single treatment with everolimus or ABT-737 led to a respective 8 and 12 fold increase in p-Bad levels, while a 0.8 fold decrease was recorded in cells undergone treatment with the dual-drug combination. In comparison to control cells, the everolimus regimen did not alter the basal level of Bad protein, however, a significant 6 fold increase in the endogenous Bad levels was observed in the presence of ABT-737. The increase in Bad protein level was 11 fold in cells co-treated with everolimus and ABT-737.

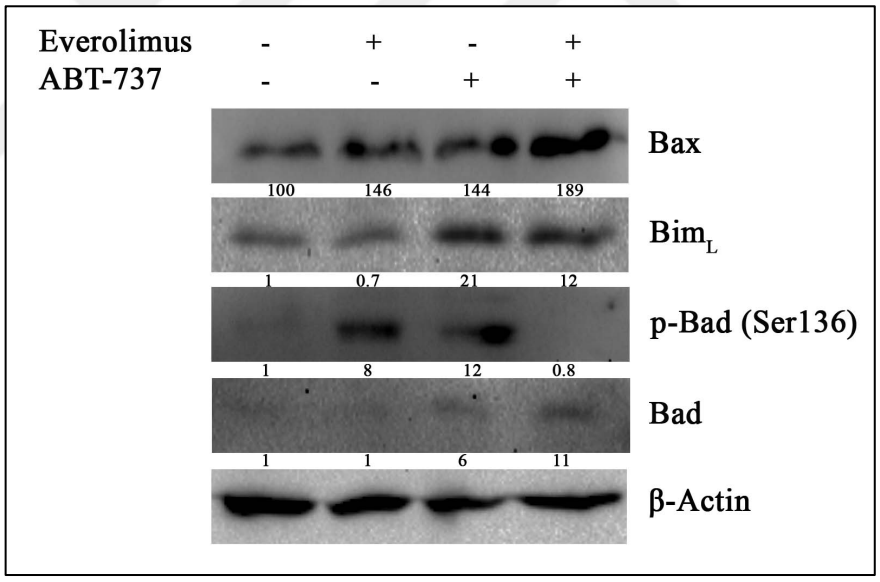

Figure 4.32. Effect everolimus-ABT-737 combination on the Bcl-2 family members of Caki-1 cells. Protein extracts of Caki-1 cells exposed to everolimus (1 μM) and/or ABT-737 (10 μM) regimens for 24 hours were used to determine levels of p-Bad (Ser136) (23 kDa), Bad kDa), Bax (20 kDa), and Bim_L (15 kDa) proteins by Western blot. To ensure equal protein loading 38 kDa protein β-Actin was utilized. The average percentage values were calculated according to the densitometric analysis of at least three independent experiments and set as 100 per cent for control cells.

4.5.3. Role of p53 in Apoptosis Triggered by Combination Therapy

Puma and Noxa, the other BH3-only proteins, interact with pro-survival Bcl-2 proteins to remove their inhibition on Bax/Bak-mediated pore formation in MOM [170]. The transcription factor p53 contributes to the initiation of apoptotic program, where p53 triggers transcription of Puma and Noxa [282]. Besides, p53 can activate Bax/Bak proteins through acting like a BH3-only protein itself [283]. To further understand the apoptotic process executed by ABT-737 and its combination with everolimus at a molecular level, the protein expressions of p53, Puma, and Noxa were analyzed in A-498 and Caki-1 cells by Western blot.

Compared to control and everolimus-treated A-498 cells, treatment with ABT-737 or its combination with everolimus led to a 57 per cent and 62 per cent decrease in p53 protein levels, respectively (Figure 4.33). The reduction observed in the expression of Puma protein was recorded as 70 and 50 per cent respectively in A-498 cells treated either with everolimus or ABT-737. In line with the reduced p53 protein level, expression of Puma protein diminished about 85 per cent in cells as a response to dual-drug combination. Compared to control cells, everolimus monotherapy did not alter the levels of Noxa protein, while a 20 per cent increase in the protein level was documented in A-498 cells undergone ABT-737. The combination regimen further increased the Noxa protein level up to 40 per cent. Although the decline observed in Puma expression under the presence of ABT-737 correlated with decrease p53 levels, the induction of Noxa protein level under the same conditions was not related to p53.

In parallel to A-498 cells, no difference in p53 protein levels was observed in everolimus-treated Caki-1 cells compared to control (Figure 4.34). ABT-737 monotherapy, however, led to 33 per cent decrease in level of p53 protein which was decrease to undetectable levels when Caki-1 cells were exposed to everolimus-ABT-737 regimen. The similar expression levels of Puma and Noxa were found in control cells and cells treated with everolimus which was in line with the results obtained for p53 under the same treatment conditions. In contrast to the decline p53 levels, 2 fold and 4 fold increase in Puma and Noxa levels were recorded in Caki-1 cells, once treated with ABT-737, respectively. Upon

the combination treatment, the level Puma protein was increased by 1.3 fold, while the recorded fold of increase was 2 fold for Noxa protein.

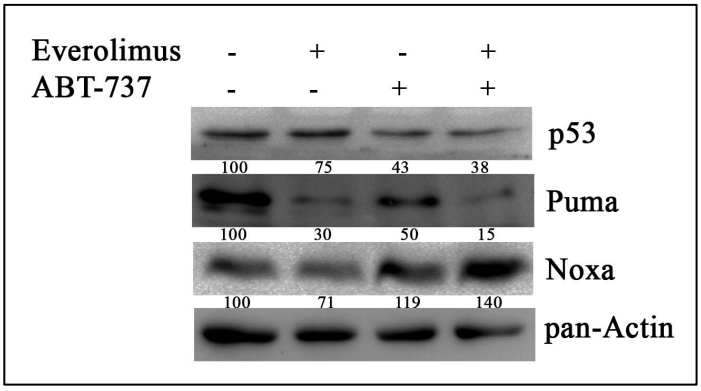

Figure 4.33. Effect of everolimus-ABT-737 combination on the p53 pathway of A-498 cells. Protein levels of p53 (53 kDa), Puma (23 kDa), and Noxa (10 kDa) was determined in protein extracts of A-498 cells subjected to everolimus (1 μM) and ABT-737 (5 μM) treatment for 24 hours. As loading control, pan-Actin (45 kDa) was used. The average percentage values were calculated according to the densitometry analysis and set as 100 per cent for control cells.

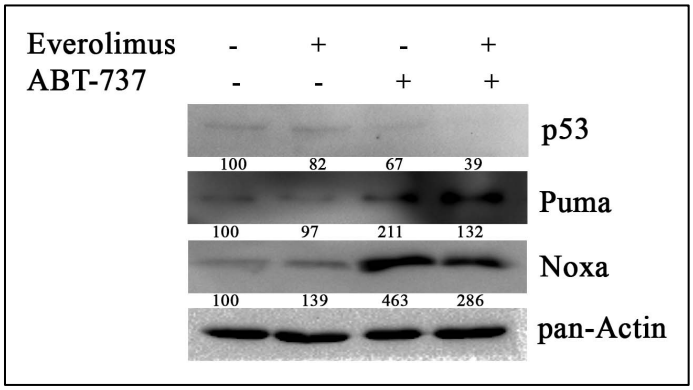

Figure 4.34. Effect of everolimus-ABT-737 combination on the p53 pathway of Caki-1 cells. Protein levels of p53 (53 kDa), Puma (23 kDa), and Noxa (10 kDa) was determined in protein extracts of Caki-1 cells subjected to everolimus (1 μM) and ABT-737 (10 μM) treatment for 24 hours. As loading control, pan-Actin (45 kDa) was used. The average percentage values were calculated according to the densitometry analysis and set as 100 per cent for control cells.

4.6. CHARACTERIZATION OF EVEROLIMUS RESISTANCE OF RENCA CELL LINE

4.6.1. Effect of Everolimus and/or ABT-737 on the Cell Viability of RenCa Cells

Following *in vitro* experiments showing anti-cancer effect of everolimus-ABT-737 combination, animal studies were carried out to investigate the combination therapy's anti-tumor effect using mouse murine RCC cell line, RenCa cells. Before starting *in vivo* experiments, the response of RenCa cells to everolimus and ABT-737 was investigated by WST-1 viability assay as described in Section 3.2.1. The absorbance value of control cells at 24 hours was considered as 100 per cent for the viability analysis. Meanwhile, absorbance values obtained from cells seeded at different densities including 2.5 x 10^3, 5 x 10^3, 7.5 x 10^3, and 1 x 10^4 cells/well were translated into cell number via a standard curve.

The effect of everolimus regimen on RenCa cell viability and proliferation was shown in Figure 4.35. Starting from the 24 hours, a significant dose-dependent decrease in the cell viability was observed in RenCa cells subjected to everolimus treatment (Figure 4.36a). Each everolimus concentration caused a significant reduction in the viability of RenCa cells at 72 hours. Especially, 85 per cent reduction in the viability was recorded in cells treated with 10 μM everolimus at 72 hours. In parallel to the cell viability data, at 72 hours 10 μM everolimus regimen led to a 84 per cent decline in cell number below the initial seeding density of the control cells (Figure 4.36b) suggesting that everolimus exhibits a cytotoxic effect on RenCa cells.

In comparison to everolimus monotherapy, no significant change in the viability was evident in RenCa cells treated with either 1 or 5 μM dosed of ABT-737 (Figure 4.36). At 24 hours, cells responded to 1 μM ABT-737 treatment by increasing their viability up to 14 per cent. Similar results were obtained for cells treated with 5 and 10 μM concentrations of ABT-737 at 24 hours (Figure 4.36a). An average of 12 per cent decline in the cell viability was observed upon 1 and 5 μM ABT-737 doses at 48 and 72 hours. In comparison to 1 and 5 μM ABT-737 doses, the highest ABT-737 concentration (10 μM) decreased the viability of RenCa cells about 34 and 58 per cent at 48 and 72 hours, respectively. In addition to cell

viability data, 5474 cells were counted upon 10 µM ABT-737 at 72 hours, which indicated the cytostatic effect of ABT-737 on RenCa cells (Figure 4.36b).

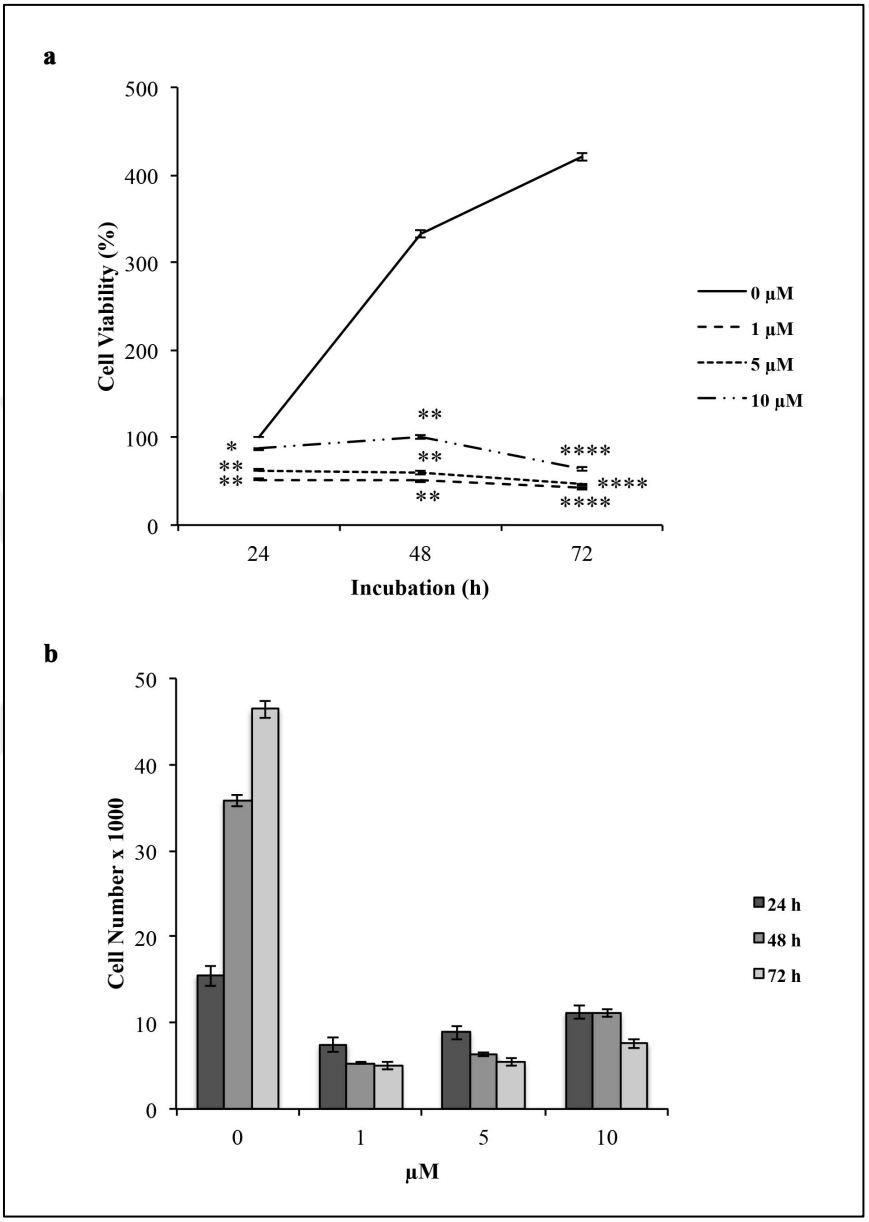

Figure 4.35. Response of RenCa cells to everolimus. RenCa cells were exposed to 1, 5, and 10 µM concentrations of everolimus for 24, 48, and 72 hours. DMSO-treated RenCa cells were considered as control (0 µM). (a) The viability of control cells measured by WST-1 viability assay at 24 hours set to 100 per cent. (b) 5 x 10^3 cells/well were seeded at time t_0.

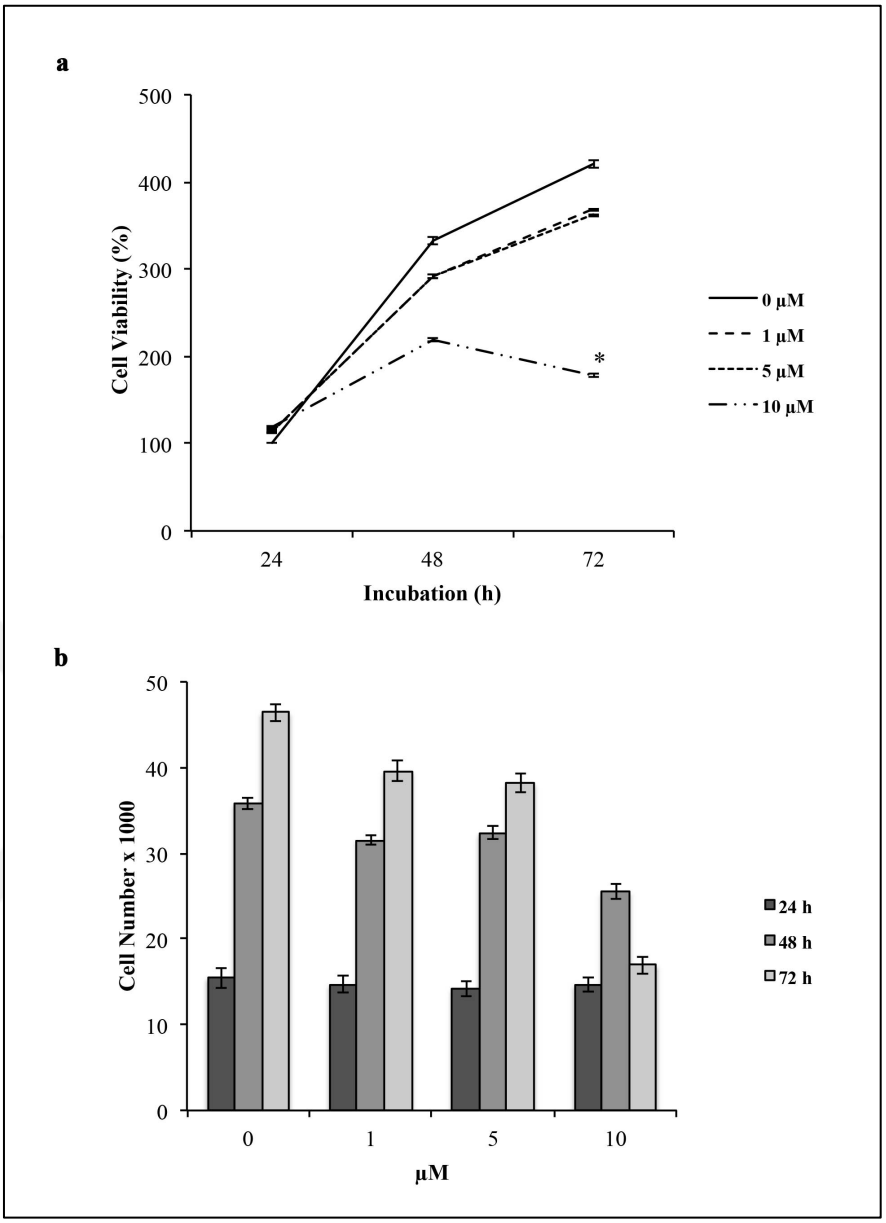

Figure 4.36. Response of RenCa cells to ABT-737. RenCa cells were undergone ABT-737 regimen (1, 5, and 10 µM doses) for 24, 48, and 72 hours. DMSO-treated RenCa cells were considered as control (0 µM). (a) The viability of control cells was set to 100 per cent at 24 hours. (b) 5 x 10^3 cells/well were seeded at the start of the experiment.

4.6.2. Generation of Everolimus-resistant RenCa Cell Line

In order to overcome the everolimus sensitivity of RenCa cells, everolimus-resistant RenCa cell line was generated by culturing the cells at low everolimus concentrations

(Section 3.1.5). The acquired everolimus resistance was investigated by WST-1 viability assay, where RenCa^{res} cells were undergone increasing everolimus concentrations for indicated hours. The absorbance values of control cells at 24 hours were considered as 100 per cent for viability analysis. In parallel, the cell proliferation was determined using the standard curve drawn with the absorbance values obtained from cells seeded at different densities including 2.5 x 10^3, 5 x 10^3, 7.5 x 10^3, and 1 x 10^4 cells/well.

The graphs presented in Figure 4.37 shows the effect of everolimus on the viability and proliferation of everolimus-resistant RenCa cells. A 20 per cent increase in the cell viability in RenCa^{res} cells was observed with the highest everolimus concentration (10 μM) at 24 hours in comparison to parental RenCa cells (Figure 4.37a). The increase in cell viability observed with 10 μM everolimus was more pronounced at 48 and 72 hours. In consistence with the viability data, an 66 per cent increase in the RenCa^{res} cell number was recorded for 10 μM everolimus regimen at 72 hours (Figure 4.37b). All together, this finding pointed out the acquired everolimus resistance for RenCa^{res} cells.

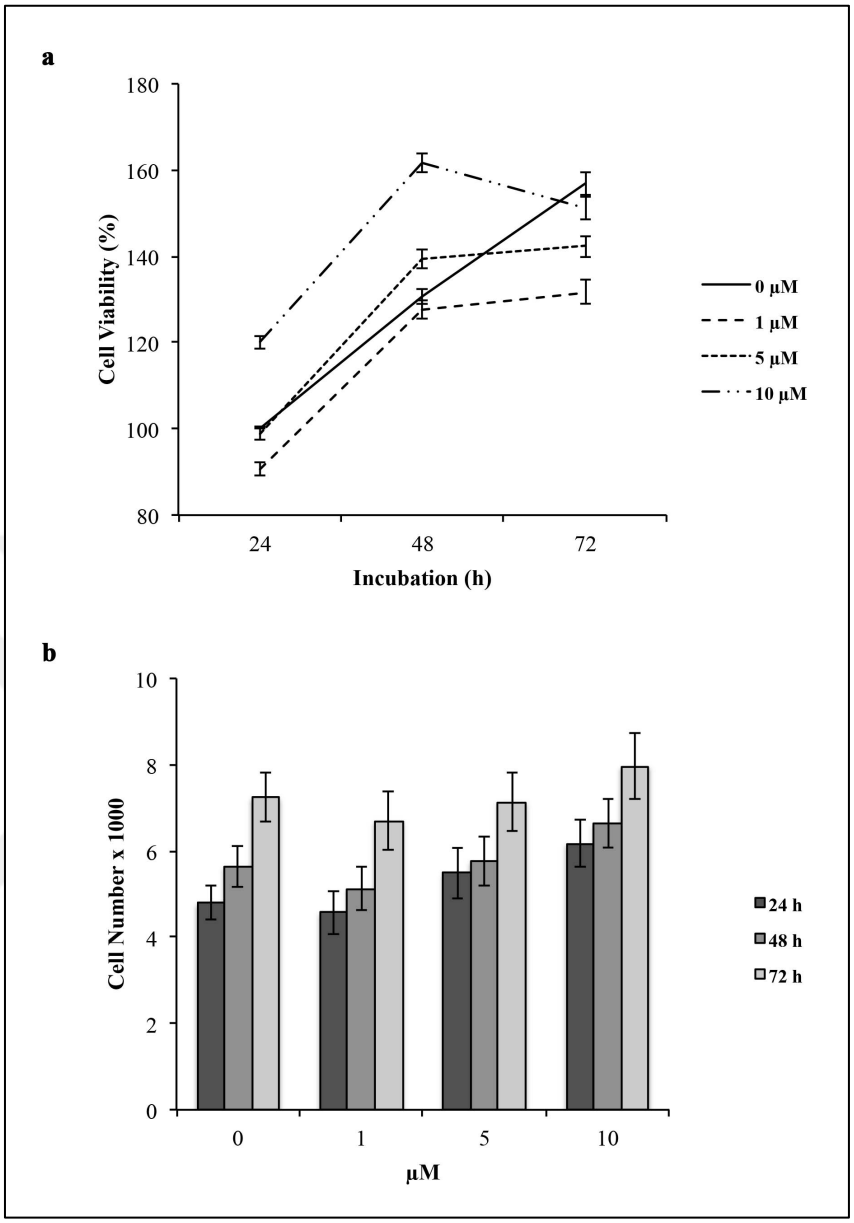

Figure 4.37. Analysis of the acquired everolimus resistance in RenCa^{res} cells. RenCa^{res} cells were treated with 1, 5, and 10µM everolimus concentrations 24, 48, and 72 hours. DMSO-treated RenCa^{res} cells were considered as control (0 µM). (a) The viability of control cells measured by WST-1 viability assay at 24 hours was set to 100 per cent. (b) 5 x 10^3 cells/well were seeded at the time t_0.

4.6.3. Effect of ABT-737 on The Cell Viability of RenCa^{res} Cells

RenCa^{res} cells were further used to analyze the effect of ABT-737 on the cell viability by WST-1 viability assay. In this regard, RenCa^{res} cells were undergone ABT-737 regimen with increasing doses together with 1 μM everolimus for 24, 48, and 72 hours. For the viability analysis, the graph was drawn according to the absorbance value of control cells at 24 hours which was considered as 100 per cent. Meanwhile, the proliferation rate was calculated by the standard curve that was drawn with absorbance values obtained from cells seeded at different densities including 2.5 x 10^3, 5 x 10^3, 7.5 x 10^3, and 1 x 10^4 cells/well.

At 1, 5 μM, and 10 μM ABT-737 treatments, RenCa^{res} cells did not change their survival rate (Figure 4.38a), in that a sequential increase in the viability of RenCa^{res} cells was recorded at increasing treatment hours. For instance, a 45 per cent increase in the cell viability was observed at 72 hours upon 10 μM ABT-737 regimen. However, at 15 μM ABT-737 17 caused a 23 per cent reduction in the viability of RenCa^{res} after 72 hours. The significant decrease (81 per cent) in the RenCa^{res} cell viability was recorded only with 20 μM of ABT-737 at 72 hours. The observed decline was related to the cytotoxic effect of the drug at 20 μM concentration, as the calculated cell number was 2460 after 72 hours of the treatment (Figure 4.38b).

In order to understand whether the decrease observed in the cell number was a consequence of induced apoptosis, RenCa^{res} cells treated with 20 μM ABT-737 were analyzed with Annexin V staining as described in Section 3.2.2. Figure 4.39 shows that 20 μM ABT-737 led to the initiation of apoptotic response in RenCa^{res} cells upon 72 hours treatment as evidenced by 51 per cent increase in the cells entering early apoptosis.

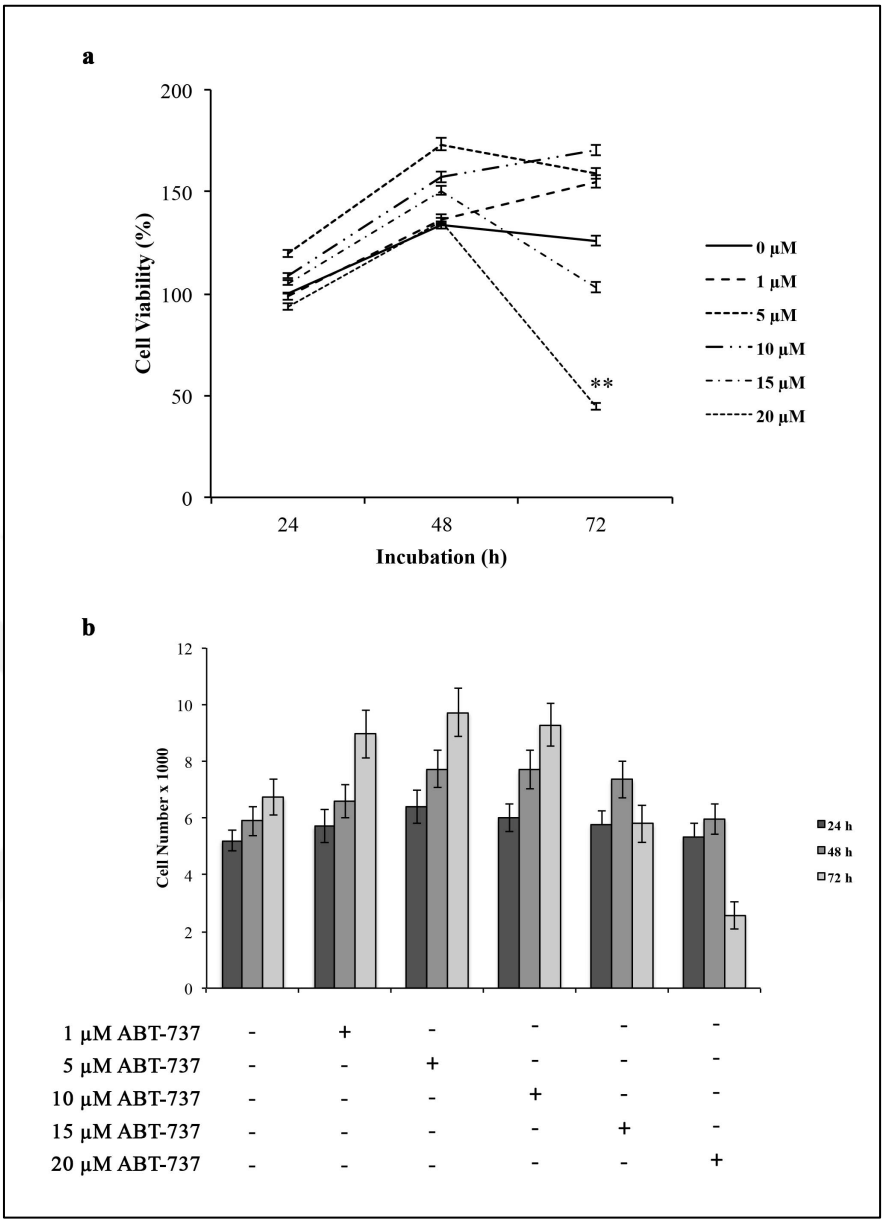

Figure 4.38. Effect of ABT-737 on the cell viability of RenCa^{res} cells. RenCa^{res} cells were subjected to treatment with increasing ABT-737 concentrations concomitant with 1µM everolimus for 24, 48, and 72 hours. Everolimus-treated (1 µM) cells were considered as control. (a) The viability of control cells was set to 100 per cent at 24 hours. (b) 5 x 10^3 cells/well were seeded at the start of the experiment.

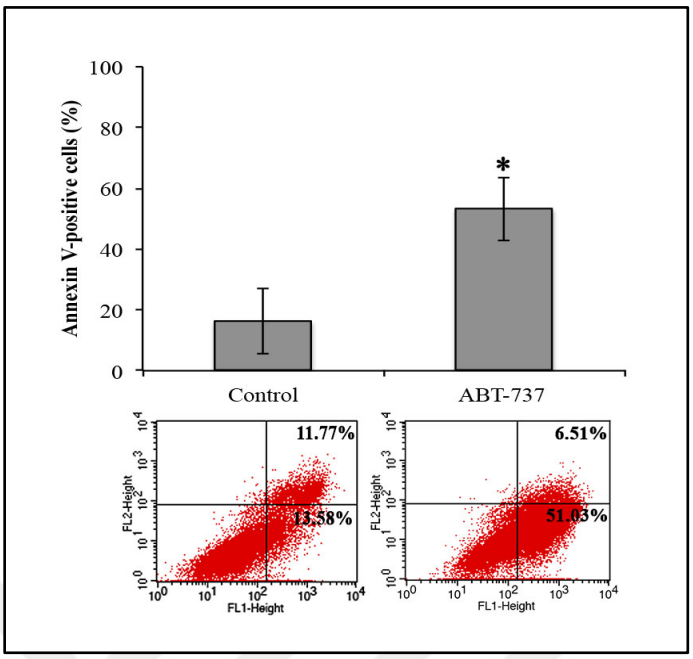

Figure 4.39. Effect of ABT-737 treatment on parental RenCa and RenCa^{res} cell death. Annexin-V/PI staining was utilized to analyze cell death of RenCa and RenCa^{res} cells treated with 20 µM ABT-737. The graphical representation of percentages for Annexin V-positive cells (early and late apoptosis) were shown (n = 3) and the numbers of cells entered in early apoptosis (bottom right) and late apoptosis (top right) cells were shown as percentages in histogram images.

4.6.4. Effect of The Acquired Everolimus Resistance on mTOR Pathway

Everolimus together with is intracellular receptor FKBP12 inhibits the kinase activity of mTOR [216]. In order to investigate the effect of the acquired everolimus resistance on mTOR pathway, cell lysates of parental RenCa and RenCa^{res} cells were used to determine the differences in the protein expression of mTOR pathway components by Western blot technique.

According to data presented in Figure 4.40, a slight decrease was observed in the phosphorylated mTOR at Ser2448 in RenCa^{res} cells compared to the parental RenCa cells, while no difference was detected in the basal mTOR levels in both cell lines. In RenCa^{res} cells, a complete suppression of S6K1 phosphorylation was observed. The acquired drug resistance, however, did not affect the basal S6K1 protein level in RenCa^{res} cells compared

to the control parental RenCa cells. The loss of phosphorylated S6K1 further resulted in almost 100 per cent reduction in the phosphorylation of S6 protein at Ser235/236 and Ser240/244 in RenCa^{res} cells, while an increase in the endogenous S6 protein was observed in these cells. Additionally, the phosphorylation of 4E-P1 protein at Ser65 decreased about 39 per cent in RenCa^{res} cells compared to the control RenCa cells, which was concomitant with a reduction in the endogenous 4E-BP1 levels. Taken together, these results indicated the suppression of mTORC1 pathway in RenCa^{res} cells, albeit a continuous cell proliferation was recorded in the presence of everolimus (Figure 4.37).

Secondly, the effect of the acquired everolimus resistance on mTORC2 complex was investigated in the parental RenCa and RenCa^{res} cells by Western blot analysis. Compared to RenCa cells, the phosphorylation of Rictor was decreased about 92 per cent in RenCa^{res} cells indicating the effect of mTORC1 inhibition (Figure 4.41). The expression of basal Rictor protein, however, was not affected in RenCa^{res} cells. Albeit 45 per cent increase in the basal AKT level was recorded for RenCa^{res} cells, the phosphorylation of AKT was decreased about 30 per cent in indicating the inactivation of mTORC2 complex.

Altogether, these findings suggest that RenCa^{res} cells found alternative pathways to mTORC1 and mTORC2 that facilitate their proliferation and survival.

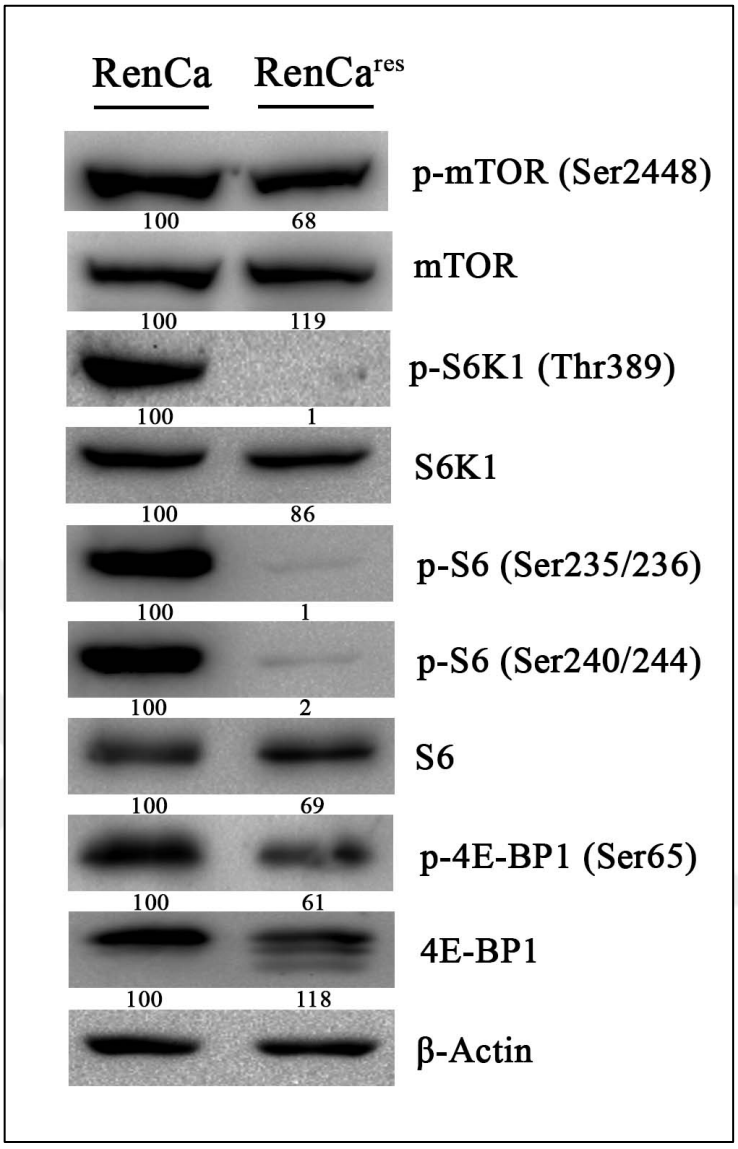

Figure 4.40. Effect of the acquired everolimus resistance on the mTORC1 complex of RenCa and RenCa^{res} cells. Cell lysates of RenCa and RenCa^{res} cells were used to determine levels of p-mTOR (S2448) (289 kDa), mTOR (289 kDa), p-S6K1 (Thr389) (70-85 kDa), S6K1 (70-85 kDa), p-S6 (Ser235/236) (32 kDa), p-S6 (Ser240/244) (32 kDa), S6 (32 kDa), p-4E-BP1 (Ser65) (15-20 kDa), and 4E-BP1 (15-20 kDa) proteins by Western blot analysis. To ensure equal protein loading 38 kDa-protein β-Actin was utilized. The average percentage values were calculated according to the densitometry analysis and set as 100 per cent for parental RenCa cells.

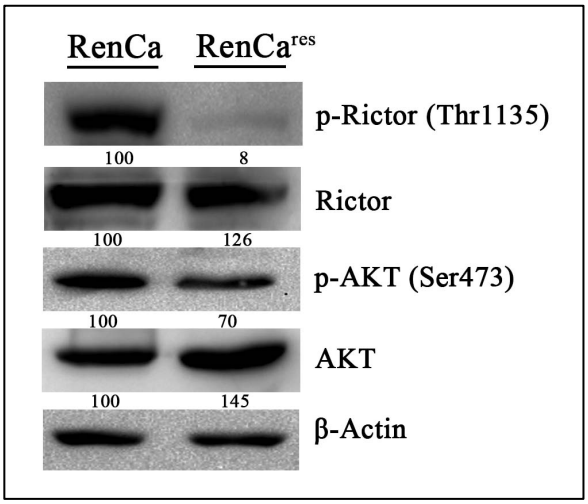

Figure 4.41. Effect of everolimus-ABT-737 combination on the mTORC2 complex of RenCa and RenCa^{res} cells. Protein extracts of RenCa and RenCa^{res} cells treated were used to determine p-Rictor (Thr1135) (200 kDa), Rictor (200 kDa), p-AKT (Ser^{473}) (60 kDa), and AKT (60 kDa) protein levels. As loading control, β-Actin (38 kDa) was used. The average percentage values were calculated according to the densitometry analysis and set as 100 per cent for parental RenCa cells.

4.6.5. Effect of The Acquired Everolimus Resistance on Pro-survival Bcl-2 Family Proteins

As the over-expression of pro-survival Bcl-2 protein provides a survival advantage to cancer cells under the presence of cytotoxic agents, the expression levels of Bcl-2 and other pro-survival Bcl-2 proteins were investigated in RenCa^{res} cells by Western blot analysis.

Supporting this hypothesis, 19 per cent and 35 per cent increase in Bcl-2 and Bcl-xL protein levels were observed in RenCa^{res} cells, respectively, while RenCa^{res} cells exhibited a 28 per cent reduction in the basal Mcl-1 protein level compared to the parental RenCa cells (Figure 4.42). These results suggest that RenCares might overcome the inhibitory effect of everolimus on cell survival by overexpressing Bcl-2 and Bcl-xL proteins.

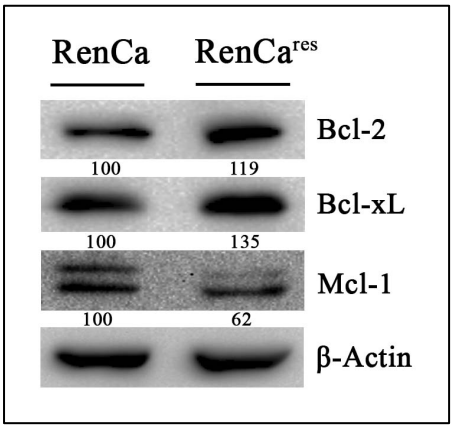

Figure 4.42. Effect of the acquired everolimus resistance on the anti-apoptotic Bcl-2 family proteins of RenCa and RenCa^{res} cells. Cell lysates of RenCa and RenCa^{res} cells were used to determine levels of Bcl-2 (26 kDa), Bcl-xL(30 kDa), and Mcl-1 (40 kDa) proteins. As loading control, β-Actin (38 kDa) was used. The average percentage values were calculated according to the densitometry analysis and set as 100 per cent for parental RenCa cells.

4.7. THERAPEUTIC IMPACT OF EVEROLIMUS AND ABT-737 COMBINATION ON RENCA^{RES} TUMOR MODEL

To characterize the anti-tumor effect of everolimus and ABT-737, an RCC xenograft mouse model was established using RenCa^{res} cells generated. Briefly, Balb/c mice (6-8 weeks old) were undergone subcutaneous injections with RenCa^{res} cells and randomized in four different groups, where each group consisted of eight animals. Following the fourth day of the cell inoculation, mice were subjected to the monotherapies or combination therapy every other day.

Figure 4.43 shows a representative picture of mice in each group, where the tumor formation was observed in control, everolimus and ABT-737 cohorts. In the control cohort, which received DMSO as vehicle control, all animals (n=8) developed tumors (Figure 4.43a). The incidence of tumor formation was four out of eight animals in the group of mice subjected to the treatment with 2 mg/kg everolimus (Figure 4.43b), while three out of eight animals in the ABT-737 (75 mg/kg) treatment cohort developed tumors (Figure

4.43c). No tumor growth was documented in the combination cohort indicating the synergistic anti-tumor effect of everolimus-ABT-737 combination (Figure 4.43d).

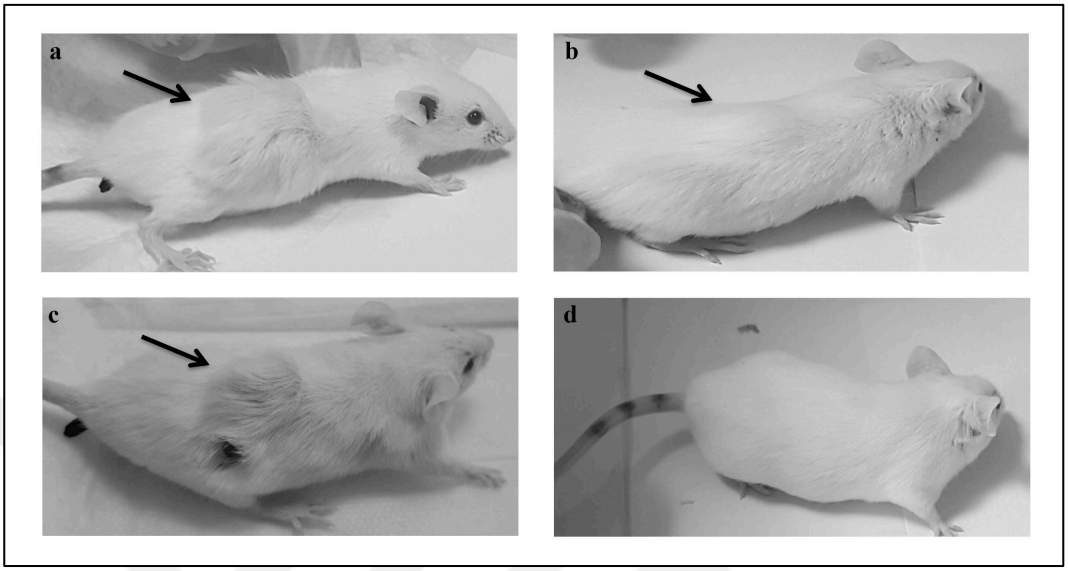

Figure 4.43. Effect of everolimus-ABT-737 combination on the tumor growth. Balb/c mice were divided randomly into four groups (n = 8) and exposed to the vehicle control (DMSO), 2mg/kg everolimus, 75mg/kg ABT-737 or the co-treatment of single drug doses every other day. Representative pictures of Balb/c mice exhibiting tumor development were shown for (a) control cohort, (b) everolimus cohort, (c) ABT-737 cohort, and (d) everolimus-ABT-737 cohort. Tumors were indicated with an arrow.

Following 21 days of the drug treatment, sacrification of animals were carried out and their organs as well as the tumor tissues, if any observed, were isolated. Figure 4.34 demonstrates the isolated tumors from animals in control, everolimus and ABT-737 cohorts. In comparison to control cohort and ABT-737 treatment cohort, the size of the tumors isolated from mice that undergone everolimus treatment was smaller (Figure 4.44a). The weight of the isolated tumor tissues was proportional to their size (Figure 4.44b). In fact, the calculated tumor weight was 0.1 g in average for the everolimus group, whereas the average weight of tumor tissues was recorded as 2.0 g and 1.8 g for the control and ABT-737 cohorts, respectively.

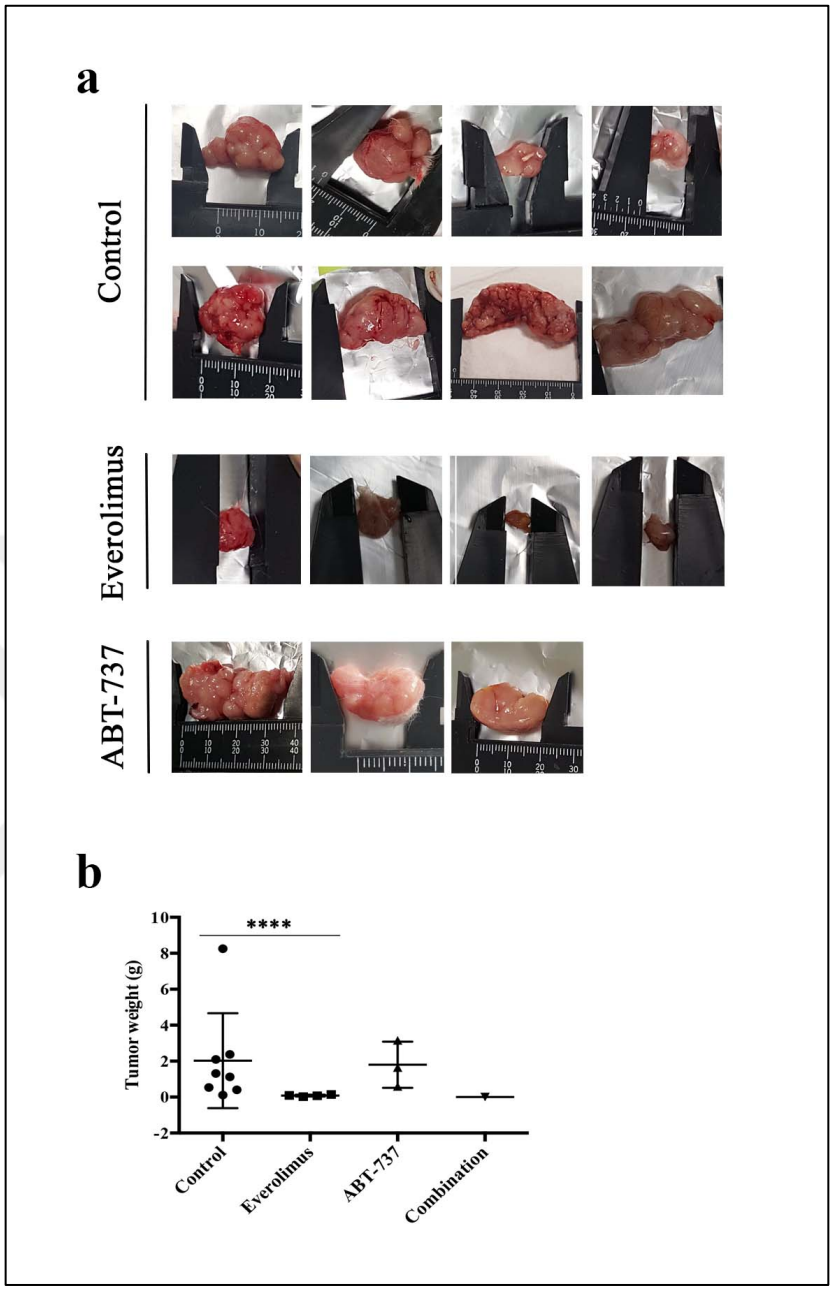

Figure 4.44. Anti-tumor effect of everolimus-ABT-737 combination on RenCa^{res} xenograft mice model. (a) Pictures represent the tumors isolated from Balb/c mice in three different groups subjected to treatments with vehicle control (DMSO) or everolimus, or ABT-737. (b) Graph shows the distribution of the isolated tumor weights.

Further, the tumors isolated from the corresponding treatment groups underwent Hematoxylin and Eosin staining for their histopathological examination (Figure 4.45). For all isolated tumor tissues, high nuclear pleomorphism, a feature of malignant neoplasms as

well as the histological architecture of RCC, was prevalent indicating the successful generation of RCC xenograft mouse model [284] (Table 4.1).

Table 4.1. Characterization of isolated tumor tissues of Balb/c mice used in the study.

	Animal	Tumor Type	Grade/Necrosis
Control	1	RCC	4/+
	2	RCC	5/+
	3	RCC	4/+
	4	RCC	5/+
	5	RCC	4/+
	6	RCC	4/+
	7	RCC	4/+
	8	RCC	4/+
Everolimus	**Animal**	**Tumor Type**	**Grade/Necrosis**
	1	RCC	5/+
	5	RCC	4/-
	6	RCC	2/-
	8	RCC	5/+
ABT-737	**Animal**	**Tumor Type**	**Grade/Necrosis**
	1	RCC	5/-
	2	RCC	5/-
	8	RCC	5/

* - = no necrosis; + = necrosis.

Six of the tumors developed in mice of the control group had a tumor grade of 4, whereas mice in the ABT-737 treatment cohort showed development of tumors with grade 5. In the everolimus cohort, two out of four mice demonstrated that tumors had a grade of 4, whereas the other tumors were identified as grade 2 and 4. Additionally, pathological analysis of the isolated organs (brain, thymus, heart, lung, stomach, spleen, liver, kidney, intestine, and testis) implicated no signs of toxicity or metastatic lesions for the animals of any treatment cohorts.

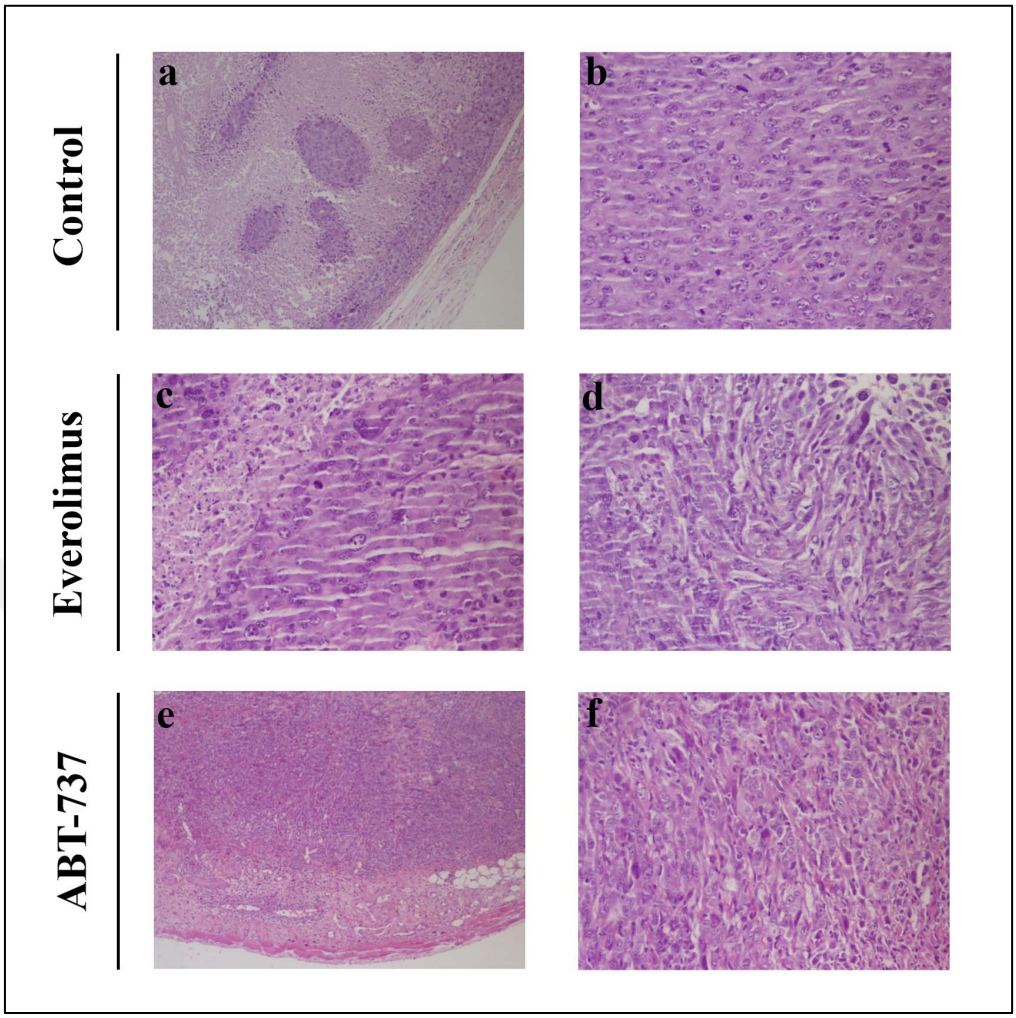

Figure 4.45. Histopathological analysis of the tumors samples. Hematoxylin and eosin staining was utilized to stain tumors isolated from Balb/c mice in three different groups subjected to treatments with either vehicle control (DMSO) or everolimus, or ABT-737. (a) Tumor with extensive necrosis in soft tissue, (b) Tumor containing pleomorphism and extensive mitosis, (c) Solid tumor in soft tissue, (d) Pleomorphic tumor cells with eosinophilic and clearly visible nucleoli, (e) Tumor showing extreme nuclear pleomorphism, giant cells with necrosis (f) sarcomatoid dedifferentiation.

Importantly, no change was monitored in the body weight of mice subjected to the monotherapies as well to the combination therapy indicating that the injected doses of everolimus and ABT-737 were tolerable (Figure 4.46).

Collectively, the data suggest that ABT-737 could synergistically potentiate the anti-tumor effect of everolimus.

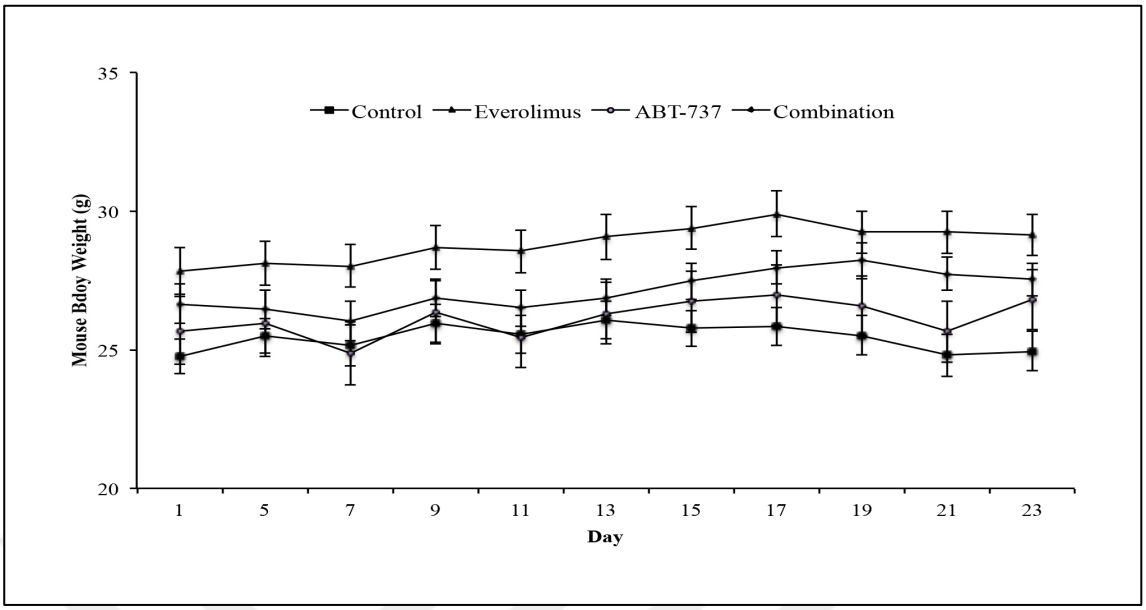

Figure 4.46. Effect of everolimus-ABT-737 combination on the mouse body weight.

4.8. CHARACTERIZATION OF FKBP38 INTERACTION WITH MTOR AND BCL-2 IN A-498 CELLS

The ability of FKBP38 protein to interact both with mTOR and Bcl-2 raises the possibility for its function as a scaffold protein between two distinct pathways regulated by mTOR or Bcl-2, respectively [135, 139]. In light of this data, the role of FKBP38 protein in the crosstalk of mTOR or Bcl-2 pathway was investigated only in A-498 cells as the CI calculated for A-498 indicated higher synergistic effect for the everolimus and ABT-737 combination for A-498 cells than Caki-1 cells. In this regard, the protein extracts of A-498 cells were used in co-immunoprecipitation (Co-IP) assay. The interaction of FKBP38 protein with either mTOR or Bcl-2 was further analyzed by Western blot. As it was shown in Figure 4.47a, FKBP38 protein was co-precipitated with endogenously expressed mTOR protein in A-498 cells under the physiological conditions. Interestingly, when the order of pull-down was switched, co-purification of mTOR protein was not observed when FKBP38 protein was precipitated. In comparison to FKBP38-mTOR interaction, the interaction of FKBP38 with Bcl-2 protein was more pronounced in A-498 cells that possess high level of Bcl-2 protein under physiological conditions (Figure 4.47b).

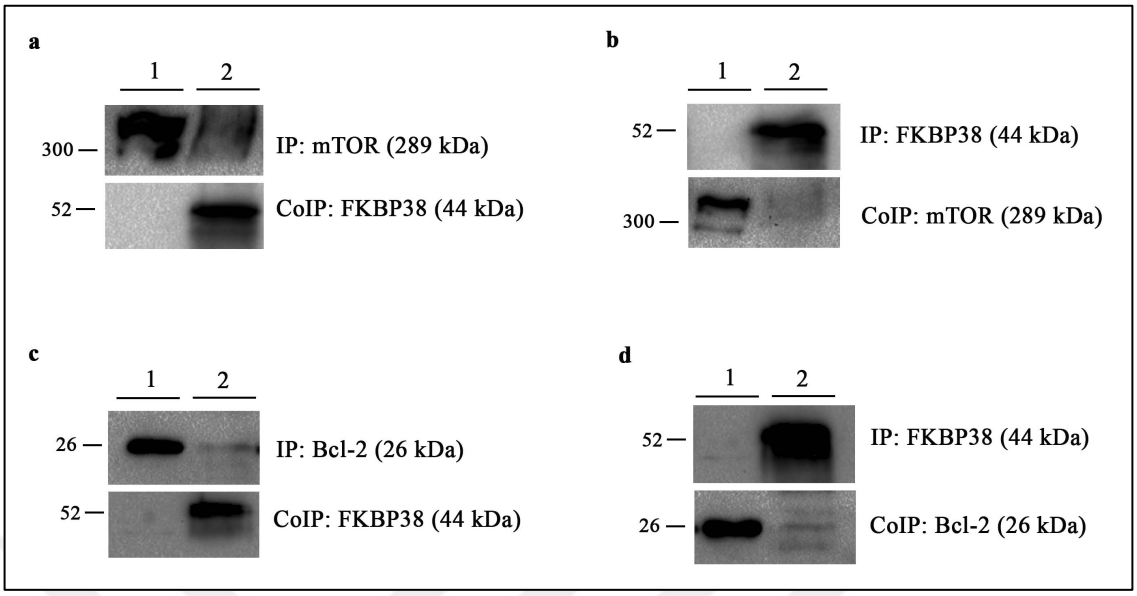

Figure 4.47. Analysis of FKBP38 interaction with mTOR or FKBP38 in A-498 cells. Protein extracts of A-498 cells were used to immuno-precipitate endogenous proteins by (a) mTOR, (b and d) FKBP38, and (c) Bcl-2 antibodies. (a and c) FKBP38, (b) mTOR; (d) Bcl-2 antibodies were used to detect co-immunoprecipitated proteins. Lane 1 indicates input, while Lane 2 indicates IP/Co-IP.

In order to understand whether the combination therapy regulates the FKBP38-mTOR interaction, Co-IP experiments were performed with the cell lysates of A-498 cells subjected to either monotherapies or combination therapy for 24 hours. Western blot analysis was carried to out to detect immuno-precipitated proteins of interest.

mTOR-FKBP38 interaction was observed in cells upon everolimus and ABT-737 monotherapies as evidenced by the presence of protein band for FKBP38 (52 and 76 kDa) as shown in Figure 4.48. In comparison to monotherapies, the interaction of FKBP38 with mTOR was reduced upon the combinatorial treatment indicating that the combination of everolimus with ABT-737 disrupts the mTOR-FKBP38 interaction. In contrast to the results shown in Figure 4.48, there was no change in mTOR and FKBP38 protein interaction in A-498 cells treated with either monotherapies of combination therapy (Figure 4.49).

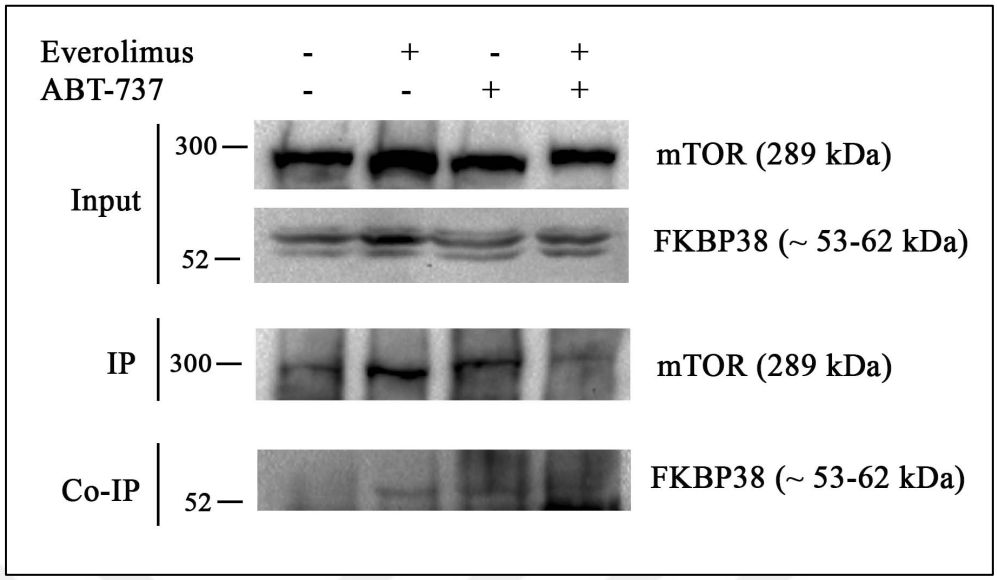

Figure 4.48. Effect of everolimus-ABT-737 combination on FKBP38-mTOR interaction in A-498 cells. 24 hours everolimus (1 μM) and/or ABT-737 (5 μM) regimen was carried out in A-498 cells in order to use its protein extracts to precipitate mTOR protein with mTOR antibody, which then analyzed by Western blot using FKBP38 antibody.

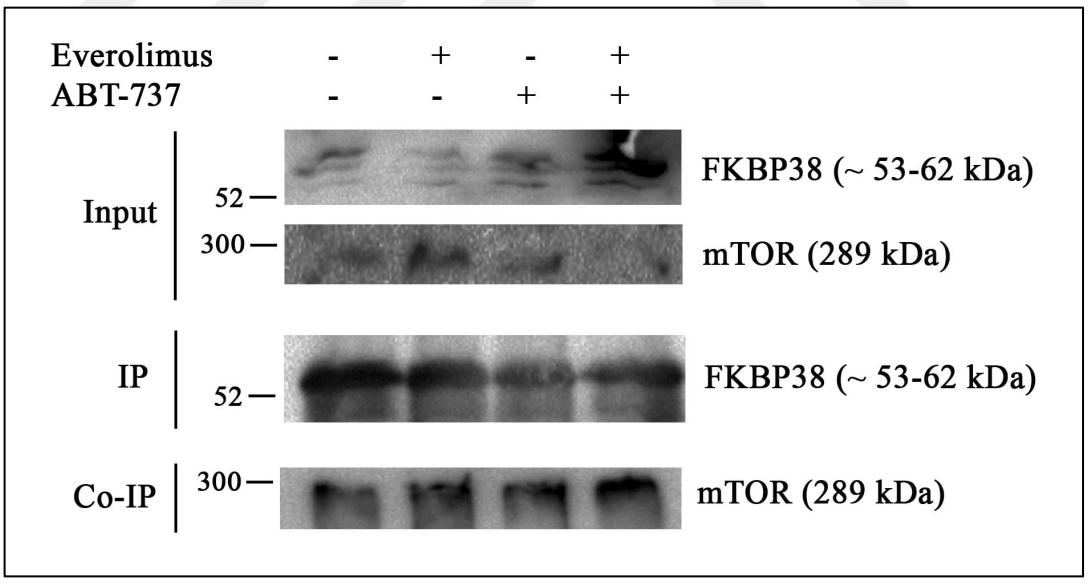

Figure 4.49. Effect of everolimus-ABT-737 combination on FKBP38-mTOR interaction in A-498 cells. Protein extracts of A-498 cells that were subjected to 24 hours regimen of everolimus (1 μM) and/or ABT-737 (5 μM) were used to precipitate FKBP38 protein with FKBP38 antibody and then mTOR protein was analyzed using mTOR antibody.

The protein extracts of A-498 cells undergone regimen with everolimus and/or ABT-737 were further used in Co-IP experiments to determine the impact of drug regimens on the interaction of FKBP38-Bcl-2. As shown in Figure 4.50, none of the drug treatments abolished the interaction of FKBP38 with Bcl-2 in A-498 cells. In contrast to this result, the reduced interaction of FKBP38 protein with Bcl-2 was observed when A-498 cells were subjected to ABT-737 treatment or its combination with everolimus (Figure 4.51).

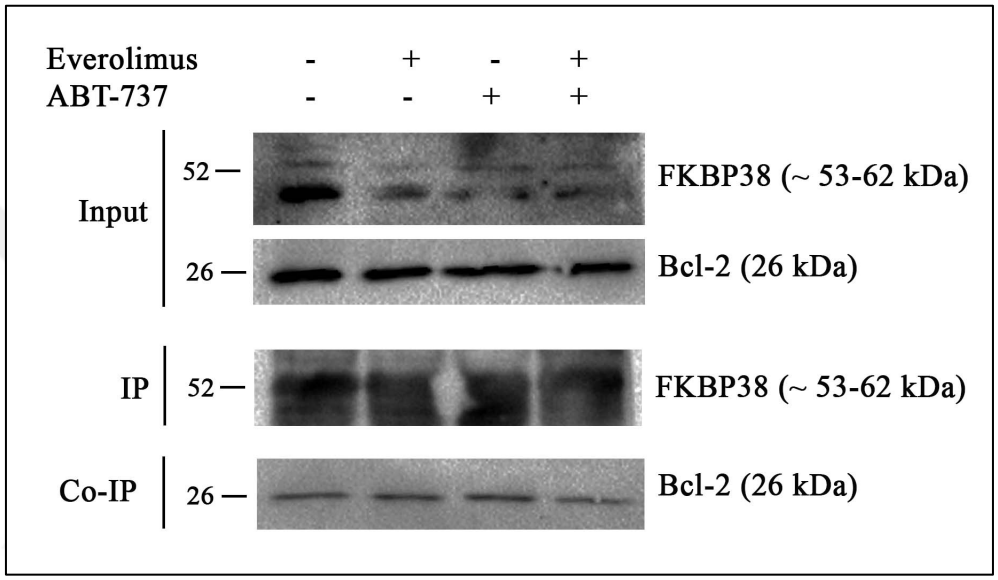

Figure 4.50. Effect of everolimus-ABT-737 combination on FKBP38-Bcl-2 interaction in A-498 cells. Protein extracts of A-498 cells undergone 24 hours regimen of everolimus (1 μM) and/or ABT-737 (5 μM) were used to precipitate FKBP38 protein with FKBP38 antibody. Co-immunoprecipitation of Bcl-2 was detected using Bcl-2 antibody.

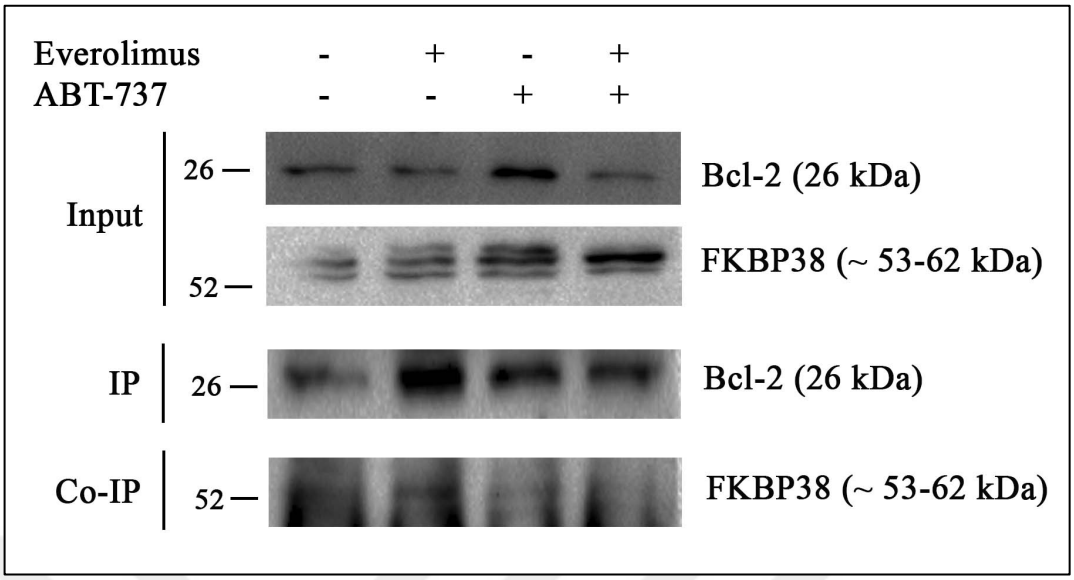

Figure 4.51 Effect of everolimus-ABT-737 combination on FKBP38-Bcl-2 interaction in A-498 cells. Protein extracts of A-498 cells that undergone 24 hours regimen of everolimus (1 μM) and/or ABT-737 (5 μM) were used to precipitate Bcl-2 protein with Bcl-2 antibody and then analyzed by Western blot using FKBP38 antibody.

5. DISCUSSION

During the last decades, comprehensive research has been performed in order to understand the molecular nature of RCC tumorigenesis. Accordingly, the reports revealed that the interplay between two main signal transduction pathways, HIF and PI3K/AKT/mTOR, mediates the control of initiation, progression, and especially metastasis observed in RCC tumors [44]. The discovery of these molecular mechanisms enabled the development of molecular therapeutics that have been used in clinic for patients suffering from advanced or metastatic RCC [44]. Owing to FDA approval, sorafenib/sunitinib-refractory mRCC patients are exposed to everolimus during their therapy [229, 271]. The low rate of progression free survival and the acquired resistance to everolimus are the clinical limitations of everolimus therapy leading to consideration of novel therapy strategies [285, 286]. Therefore, the identification of the several feedback loops contributing to everolimus resistance raised the idea of combination therapy [115].

As the elevated level of Bcl-2 protein has been implicated in a number of solid tumors impairing the sensitivity of cancer cells towards anti-cancer drugs, a BH3 inhibitor called ABT-737 has been developed in order to overcome the Bcl-2-mediated inhibition of apoptotic process. According to the literature, ABT-737 mono- or combo-therapy with different agents showed promising results for the treatment of several cancer types, where SCLC or thyroid cancer can be given as examples [263, 287]. As the anti-cancer effect of ABT-737 combination with everolimus has never been investigated in everolimus-resistant RCC where Bcl-2 protein might also have a role for RCC tumorigenesis, this thesis aimed to investigate for the first time in literature the chemotherapeutic potential of everolimus-ABT-737 combination for the advanced RCC.

Relying to the fact that ABT-737 mimics the BH3 domain of Bcl-2 and Bcl-xL proteins, the first attempt of this thesis was to characterize the endogenous levels of these proteins in different RCC cell lines. The results revealed that primary site A-498 and metastatic site Caki-1 cells exhibited high levels of Bcl-2 protein compared to other RCC cell lines Caki-2 and ACHN. In comparison to Bcl-2, the endogenous level of Mcl-1 protein was similar in all RCC cell lines tested. These results led to the selection of Bcl-2 overexpressing A-498

and Caki-1 cells as model cell lines to evidence the hypothesis proposing whether Bcl-2 protein plays a crucial role for RCC tumorigenesis.

Supporting to the report of Hassan *et al.* [288] showing the intrinsic resistance of A-498 cells to rapamycin, we showed that everolimus regimen exhibited no reduction in A-498 and Caki-1 cells viability. In comparison to everolimus, ABT-737 led to a dose- and time-dependent cytotoxicity in A-498 cells by inducing apoptotic process. This result was consistent with the literature showing a dose-dependent decrease in A-498 cell viability due to ABT-737 treatment [289]. In this study, the decrease in the viability of A-498 cells and the caspase activation was detected upon regimen with ABT-737-chloroquine, a lysosomal inhibitor. Although the influence of ABT-737 on Caki-1 cell viability seemed to be cytostatic, an intensive assessment of the apoptotic process in this cell line revealed that ABT-737 caused an elevated protein expression of cleaved PARP, caspase 9 and 3. In support of our finding, Zhu *et al.* reported the ABT-737-induced PI-staining as well as PARP-cleavage in Caki-1 cells. In the same report, the authors also demonstrated the anti-cancer effect of ABT-737 combination with a PI3K inhibitor, LY 244002 on Caki-1 cells, which resulted in the activation of caspase cascade [290]. There are also several research groups reporting the efficiency of everolimus combination with chemotherapeutic drugs for the therapy of mRCC. For example, the study conducted by Juengel *et al.* demonstrated the anti-cancer effect of everolimus combination with AEE788, a receptor tyrosine kinase inhibitor, with a decrease in the proliferation rate of A-498 and Caki-1 cells [291]. Additionally, another group addressed the effect of everolimus combination with an MEK1 inhibitor, Selumetinib on Caki-1 cells and showed that the dual-drug combination could attenuate the cell proliferation and cell cycle [292]. Supporting to literature, the results presented in this thesis that investigated the chemotherapeutic effect of everolimus combination with ABT-737 on RCC cell lines, showed that the everolimus and ABT-737 synergistically diminished the viability of A-498 and Caki-1 cells. The decrease we observed was associated with the increase in the number of apoptotic cells concomitant with the detection of cleaved apoptosis activators, caspase 9 and caspase 3.

The regulation and the progression of cell cycle requires the coordinated interplay between cyclin and CDK proteins [293]. Cyclin type D and type E are the major regulatory units of the G_1 phase. During G_1 phase, the complex formation between Cyclin D with CDK4

catalyzes the expression of Cyclin E1 that further regulates the G_1/S transition in a complex with CDK2 [293]. Since everolimus is designed to block the kinase activity of mTOR, which maintains the regulation of cellular mechanisms, the anti-proliferate effect of everolimus has been extensively investigated in several tumor cell lines, including RCC cells. The analysis of cell cycle revealed that everolimus treatment of A-498 and Caki-1 cells led to a reduction in the levels of Cyclin D1, CDK2, and Cyclin E1 proteins as well as elevated levels of CDK4 protein, which indicates everolimus-mediated G_0/G_1 arrest in both RCC cell lines [291]. In consistence with the literature, similar changes in the levels of cell cycle proteins in A-498 and Caki-1 cells undergone everolimus treatment were recorded in our experiments. We showed that, in addition to low Cyclin D1 levels, the everolimus regimen led to downregulation in protein expression of Cyclin D3 and upregulation of $p27^{Kip1}$ levels in both A-498 and Caki-1 cells. The elevated $p27^{Kip1}$ protein levels in A-498 and Caki-1 cells have been also reported in another study published from the same group several years later [294]. As expected, everolimus-mediated G_0/G_1 arrest was in parallel with decreased levels of CDK2 protein detected for both A-498 and Caki-1 cells. We obtained similar alterations in cell cycle regulatory proteins including CDK4, Cyclin D3, CDK2, Cyclin E1, and $p27^{Kip1}$ proteins in both ABT-737-treated RCC cell lines, although ABT-737 targets a different mechanism than everolimus. To our knowledge, there is one research article in the literature demonstrating the inhibitory effect of ABT-737 monotherapy on the CDK2 activity in prostate carcinoma cells [295]. Further, we also documented that everolimus-ABT-737 combination led to the cell cycle attenuation as evidenced by the decrease recorded Cyclin D1, Cyclin D3, CDK2, Cyclin E1 and p27 in A-498 cells. For Caki-1 cells, there was a significant reduction CDK4, Cyclin D3 and CDK2 levels in response to the combination treatment. In contrast to our results, Jane *et al.* stated that the use of ABT-737 either alone or in co-treatment with dinaciclib, a cyclin-dependent kinase inhibitor, did not change the protein expression of CDK4, Cyclin D1, Cyclin D3, and CDK2 in malignant glioma cell lines [296]. These contradictory outcomes might indicate that cell type specific effect of ABT-737 on cell cycle or it might vary based on the chemotherapeutics used in the combinatorial setting with ABT-737.

The attenuation of the cell cycle recorded in A-498 and Caki-1 cells upon the combination therapy might be associated with the suppression of mTORC1 complex which mediates the translation of Cyclin D1 [297]. In fact, the reduced levels of proteins (CDK4, Cyclin D1,

Cyclin E1, and CDK2) in NSCLC and esophageal squamous cell carcinoma cells was associated with the loss of S6 phosphorylation [298, 299]. Additionally, a more recent study also reported that p-S6 depletion observed in Caki-1 cells as a result of the combinatorial treatment with RAD001 with selumetinib, MEK1 inhibitor, caused cell cycle arrest at G_1 phase [292]. In support of the literature, treatment of A-498 and Caki-1 cells with everolimus resulted in the complete suppression of mTORC1 complex as evidenced by the decreased levels of phosphorylated mTOR downstream effector proteins, S6K1 and 4E-BP1 (Section 4.4.2). As expected, the presence of ABT-737 neither affected mTORC1 activity, nor interfered with the activity of everolimus in A-498 and Caki-1 cells. In fact, the combination therapy abrogated the mTORC1 activity in both RCC cell lines, where almost complete reduction of p-S6K1, and p-4E-BP1 was recorded. Similar results were also obtained by Juengel *et al.* for the A-498 and Caki-1 cells co-treated with RAD001 with the receptor tyrosine kinase inhibitor AEE788 [291].

mTORC2 activity is one of the feedback loops whose activation is related to everolimus-resistance observed in RCC tumors [115]. The activity of mTORC2, which is regulated by p-S6K1 protein, indicator of the active mTORC1 complex, is characterized through the ability of the complex by phosphorylating AKT at Ser473 [102]. Although mTORC2 is insensitive to rapamycin, the long-term treatment with drug may disrupt the mTORC2 complex formation, resulting in the decreased levels of p-AKT (Ser473) [218]. Sarbassov *et al.* reported that the rapamycin leads to a differential response in p-AKT -Ser473 levels in cancer cell lines depending on their rapamycin-sensitivity or -insensitivity [218]. In fact, the mTORC2 complex might be still active in rapamycin-insensitive cell lines. In response to everolimus treatment A-498 and Caki-1 cells showed reduced p-S6K1 levels resulting in a decrease in p-Rictor levels since p-S6K1 was responsible for the phosphorylation of Rictor. This reduction in p-Rictor levels was correlated with the slight decrease observed in the p-AKT (Ser473) levels suggesting that everolimus alone can partially block the mTORC2 activity (Section 4.4.2). Interestingly, similar to everolimus treatment a more prominent decrease in p-AKT (Ser473) level was observed in ABT-737-treated A-498 cells, in parallel with a decline in the basal AKT levels. According to the study performed by Hurvitz *et al.* a panel of 49 breast cancer cell lines, which have sensitive, intermediate or resistant profile to everolimus, exhibited variable expressions of AKT protein [300]. However, in Caki-1 cells an increase in p-AKT (Ser473) was observed due to ABT-737

treatment despite the reduced basal AKT levels. A similar increase in p-AKT (Ser473) levels was evident in Caki-1 cells co-treated with everolimus and ABT-737, although the combination therapy led to the inactivation of mTORC1 complex. In a recent study, the phosphorylation of SIN1, mTORC2 complex component, at Thr88 by AKT was reported [301]. Two years later, Yang *et al.* reported that p-AKT (Thr308)-mediated catalysis of SIN1 phosphorylation might provide a activating loop for mTORC2 activation [302]. In this report, p-SIN1-mediated mTORC2 activity catalyzed AKT phosphorylation at Ser473 [302]. These findings led to suggest that the upregulation of p-AKT (Ser473), we observed in Caki-1 cells subjected to everolimus-ABT-737 combination, might depend on the elevated p-AKT (Thr308). This result might also indicate the role of possible feedback mechanisms that are activated by Caki-1 cells to overcome the anti-cancer effect of the combination treatment.

The intrinsic apoptosis is mediated by cross-talk between the proteins of Bcl-2 family, where BH3-only proteins play pivotal roles. During the apoptotic switch, these proteins act either as activators or sensitizers to block the function of anti-apoptotic proteins [157]. Bim is an activator BH3-only protein and has the ability to interact both with pro-apoptotic Bax and anti-apoptotic proteins including Bcl-2, Bcl-xL, and Bcl-w [279, 280]. The binding of Bim to the hydrophobic groove of Bcl-2 protein initiates the apoptotic process, as it abrogates Bcl-2 interaction with pro-apoptotic Bax or Bak [262]. Depending on its prominent participation in the apoptotic cascade, the reduction of Bim protein expression which was detected in different solid tumors, is accepted as a hallmark for tumorigenesis [303]. In this regard, Weber *et al.* showed in ovarian cancer cells, that the elevated Bim expression was associated with cell death mediated by ABT-737-regimen [304]. In consistence with this finding, the ABT-737 monotherapy led to the induction of Bim protein expression in A-498 and Caki-1 cells (Section 4.5.2). Besides the effect of the single use of ABT-737 on Bim protein, the combination of ABT-737 with other agents revealed similar results [290, 305]. For example, the combination of ABT-737 with PI3K/mTOR inhibitors, including NVP-BEZ235 and BEZ23 triggered apoptotic response in ovarian carcinoma cells and human myeloid leukemia cells due to upregulation of Bim [306, 307]. In addition to PI3K/mTOR inhibitors, the combination of ABT-737 with gefitinib or erlotinib, the EGFR tyrosine kinase inhibitors, also led to the initiation of Bim-dependent cell death mediated in lymphoma cell lines [305]. The upregulation of Bim has

also been further implicated in the cell death triggers by ABT-737 combination with another PI3K inhibitor, LY294002 in RCC cell lines, 786-O, Caki-1, and 769-P cells [146]. In line with these literature, the induction of apoptosis in A-498 and Caki-1 co-treated with everolimus and ABT-737 might be Bim-dependent. The reason for the elevated Bim levels we observed in A-498 and Caki-1 cells might depend on the (i) the disruption of Bcl-2-Bim interaction by ABT-737 or (ii) ABT-737-mediated reduction of Bcl-2 levels observed in A-498 and Caki-1 cells. In support to our results, Alharbi *et al.* also showed the reduced mRNA levels of Bcl-2 protein in primary CLL cells upon ABT-737 regimen [308]. Although reduction in the pro-survival Bcl-2 protein was obvious in A-498 and Caki-1 cells, interestingly no alteration in the Bax protein level was detected for A-498 cells, suggesting that A-498 cells might induce apoptosis by the upregulation of Bak rather than Bax protein. However, ABT-737 monotherapy and the combination therapy induced the expression of Bax protein in Caki-1 cells, which was consistent with the previous report showing the elevated Bax levels upon the knockdown of Bcl-2 protein in HeLa cells [145].

In comparison to Bim, sensitizer BH3-only protein Bad indirectly activates Bax by neutralizing Bcl-2, Bcl-xL, and Bcl-w [160, 309]. Bad undergoes PTM such as phosphorylation at several serine residues. The phosphorylation of serine at position 136 is mediated by AKT protein whose activity depends on its phosphorylation at Ser473 through mTORC2 complex [67]. Regarding to this fact, Bad provides a link between mTOR pathway and intrinsic apoptosis [281]. The phosphorylation of Bad is a prerequisite for the recognition by 14-3-3 proteins that mediate the proteosomal degradation of Bad [310]. Only non-phosphorylated Bad can interact with Bcl-2, Bcl-xL, and Bcl-w [311]. According to the study performed by Liu *et al.*, rapamycin induces Bad phosphorylation specifically at Ser136 through activated ERK1/2 and AKT, which results in a decrease in the half-life of basal Bad levels in human lung cancer cells [312]. In the same report, the author claimed that the rapamycin-resistance might be associated with the increased p-Bad levels. In parallel to literature, our results demonstrated that everolimus treatment increased the phosphorylation of Bad (Ser136) in A-498 and Caki-1 cells, which was concomitant with a decrease observed in the basal Bad levels. As shown by Liu *et al*, Bad phosphorylation that we observed can be partially mediated by ERK1/2 since a slight downregulation of AKT-phosphorylation (Ser473) in A-498 and Caki-1 cell lines was detected upon everolimus treatment. Bad plays an indirect role during the initiation of apoptosis induced by ABT-737

treatment [313]. Findings in the literature stated that ABT-737 regimen led to the increased expression of basal Bad protein in different human cancer cell lines [314, 315]. In support of this, we also detected an increase in basal Bad levels in A-498 and Caki-1 cells subjected to ABT-737 monotherapy. Albeit to the reduced p-AKT-Ser473 levels, a significant induction in p-Bad levels was observed in A-498 cells in the presence of ABT-737 again suggesting that ERK1/2 might be the responsible kinase for Bad phosphorylation [312]. In Caki-1 cells, however, the elevated p-Bad levels detected upon ABT-737 regimen was most probably the result of the upregulated AKT phosphorylation at Ser473. The difference in the phosphorylation mechanisms of Bad between A-498 and Caki-1 cells suggests that two different signal transduction pathways were in play for the everolimus resistance observed in these cell lines. In spite of the elevated level of p-AKT, everolimus-ABT-737 combination completely suppressed the phosphorylation of Bad in Caki-1 cells.

Puma and Noxa are the other BH3-only proteins acting as sensitizers. Both proteins are regulated transcriptionally by p53 protein that is upregulated as a response to DNA damage [316]. Rapamycin treatment had no impact on the protein expression of p53 in human colon carcinoma [317] and MCF-7 cell lines [318], consistent with these findings our results demonstrated that everolimus monotherapy did not alter the expression of p53 protein in A-498 and Caki-1 cells. In comparison to everolimus regimen, the presence of ABT-737 drastically diminished p53 levels in both RCC cell lines. To our knowledge, there is only one study showing reduced p53 levels in the lungs from mice exposed to ionizing irradiation followed by ABT-737 treatment [319].

According to the study published by Kao *et al.*, the treatment of human colon carcinoma cells with rapamycin caused an increase in Puma protein levels [317]. In another study, however, the authors did not document any upregulation of Puma in JEKO-1 cells (mantle cell lymphoma cell line) undergone rapamycin treatment [320]. In parallel to this study, we observed no change in the expression of Puma protein in A-498 and Caki-1 cells subjected to everolimus regimen, suggesting that the effect of everolimus on Puma might be cell-type specific. In comparison to everolimus monotherapy, we documented contradictory results for A-498 and Caki-1 cells, when they were treated with ABT-737 or everolimus-ABT-737 combination. In A-498 cells, the presence of ABT-737 decreased the Puma levels which was in correlation with the reduced p53 protein levels, indicating that Puma may not play a

pivotal role for this cell line during ABT-737-induced apoptosis. However, elevated Puma levels were recorded in Caki-1 cells in response to ABT-737 monotherapy or combination therapy, albeit to the low expression of p53 protein, which suggest a p53-independent participation of Puma in ABT-737-induced apoptosis. To our knowledge, there is no reports in the literature showing the effect of ABT-737 on the protein expression of Puma protein. Nevertheless, the study of Garrison *et al.* demonstrated that Puma is required for apoptosis in primary connective tissue mast cell (CTMC) treated with ABT-737 [321]. The authors also claimed that Puma together with Bim can induce Bax/Bak activation in p53-dependent or -independent manner.

In parallel to Puma, we recorded no change in Noxa levels for everolimus-treated A-498 and Caki-1 cells. In support of our results, Müller *et al.* reported that rapamycin had no impact on Noxa protein levels in JEKO-1 cells [320]. In contrast to everolimus monotherapy, we demonstrated that the presence of ABT-737 significantly induced the expression of Noxa protein in A-498 and Caki-1 cells, albeit to the reduced p53 levels, indicating that the regulation of Noxa expression might be p53-independet. In consistence to our findings, Soderquits *et al.* claimed that UPR (unfolded protein response)-mediated Noxa transcription does not require p53 protein [322]. In addition, increased Noxa levels might play a role in ABT-737 response since Noxa is known to neutralize the Mcl-1 protein [323], which would evoke apoptotic resistance against ABT-737 treatment unless inactivated. In support of our hypothesis, a recent study showed that co-treatment of acute lymphoblastic leukemia (ALL) cells with ABT-737 and mTOR inhibitor CCI-779 developed resistance due to Mcl-1 overexpression [324]. In addition, Zall *et al.* reported that ABT-737 combination with chemotherapeutic drugs, including vinblastine, etoposide, or paclitaxel might sensitize several RCC cells including RCC-21, RCC-30, RCC-26A, and Caki-2 to apoptosis induction by inactivation of Mcl-1 through Noxa [323]. It was also reported that Noxa overexpression increased the sensitive response of SCLC cells to ABT-737 treatment [325, 326].

The animal studies were performed with $RenCa^{res}$ cells generated from parental RenCa cells in addition to our *in vitro* findings. Our results demonstrated that the acquired everolimus resistance provided $RenCa^{res}$ cells the survival advantage under the presence of everolimus, which have been already observed in everolimus-resistant A-498 and Caki-1

cells. The complete inhibition of mTOR pathway was evidenced through the reduced levels of phosphorylated S6K1 and 4E-BP1 proteins in RenCa^{res} cells (Section 4.6.4), which was in consistent with the data obtained for both human RCC cell lines undergone everolimus treatment (Section 4.4.2). Besides, our results indicated that the overexpression of Bcl-2 protein might be the key factor, which enables the survival of RenCa^{res} cells, when mTOR pathway was suppressed. All together, these results indicated a similar response between RenCa^{res} cells and A-498 and Caki-1 cell lines in terms of everolimus resistance.

In parallel to the anti-cancer effect of everolimus-ABT-737 combination *in vitro*, we further showed its anti-tumor effect in RCC xenograft mouse model. Tumor growth was detected with everolimus cohort with a medium incidence. Albeit low incidence, the tumor formation was also documented in mice treated with ABT-737. In parallel to our findings, a previous study demonstrated tumor formation in xenografts generated with different SCLC cell lines that exhibits variable sensitivities to ABT-737 [263]. In the same study, the authors also mentioned no tumor regression in primary SCLC xenografts due to ABT-737 treatment. In comparison to the injections with individual drugs (everolimus or ABT-737), we achieved a complete suppression of RenCa^{res} xenograft tumor development in mice co-treated with everolimus and ABT-737. In confirmation of our findings, a more recent study published by Zou *et al.* demonstrated that RAD001 combination with AZD6244, a MEK inhibitor, drastically diminished the tumor volumes observed in Caki-1 xenografts [292]. In addition, previous studies presented the antitumor efficiency and the therapeutic potential of rapamycin-ABT-737 combination in NSCLC xenograft model [327] and in SCLC PDX (patient-derived xenograft) models [328]. To note, we did not notice any toxicity in the animals in any treatment groups as well as no pathological changes in excised organs were detected.

In summary, the results presented in this thesis showed for the first time that the use of Bcl-2 inhibitor ABT-737 in a therapeutic combination with everolimus enhanced the anti-tumor effect of everolimus. Everolimus-ABT-737 combination induced attenuation of cell cycle as well as cell death in RCC cell lines, A-498 and Caki-1, and led to the regression of *in vivo* RenCa^{res} tumor growth. Therefore, our data open a new avenue for the clinical use of everolimus-ABT-737 combination and can provide a therapeutic benefit for the patients suffering from the advanced RCC.

6. FUTURE PROSPECTS: A PROPOSED MECHANISM FOR THE ANTI-CANCER EFFECT OF EVEROLIMUS-ABT-737 COMBINATION

The therapeutic potential of everolimus and ABT-737 combination indicated by the work presented in this thesis raised the question, whether there is a particular link between two main cellular mechanisms which were targeted by these agents. Recent studies demonstrated that FKBP38 acts as a scaffold protein between mTOR pathway and Bcl-2 family-mediated apoptosis, as FKBP38 can interact with both mTOR and Bcl-2 proteins [139, 142].

FKBP38 is a member of the FK506 protein family and mediates the inactivation of mTORC1 complex by binding to mTOR [139]. It was shown that Rheb disrupts FKBP38-mTOR interaction by binding to FKBP38 under the nutrient-rich conditions resulting in mTOR activation (Figure 6.1) [139]. In that, FKBP38 negatively regulates the mTORC1 activity by sensing the nutrient and amino acid availability. FKBP38 protein is also involved in the activation of anti-apoptotic Bcl-2 proteins by interacting with Bcl-2 and Bcl-xL proteins under the control of Rheb [142]. FKBP38 translocates Bcl-2 and Bcl-xL proteins to mitochondria. Once recruited, Rheb dissociates FKBP38 from Bcl-2/Bcl-xL and, thereby, enables Bcl-2/Bcl-xL mediated inhibition of Bax and/or Bak [84]. In addition, the regulation of FKBP38-Bcl-2 interaction by Rheb was not affected by rapamycin. Furthermore, a recent report claimed that the overexpression of Bcl-xL caused elevated activity of mTORC1, but not mTORC2, suggesting a competition between Bcl-2 and mTOR for binding to FKBP38 [146].

In light of these data, we proposed that FKBP38 regulates cell survival by interacting with the overexpressed Bcl-2 protein in everolimus-resistant A-498 and Caki-1 cells when its interaction with mTORC1 was blocked by everolimus. In other words, the cells might develop everolimus resistance by (i) overexpressing or (ii) activating Bcl-2 protein through FKBP38. The complicated interplay between FKBP38, mTOR, Bcl-2, and Rheb might clarify the observation of elevated Bcl-2 levels in rapalog-resistant mRCC.

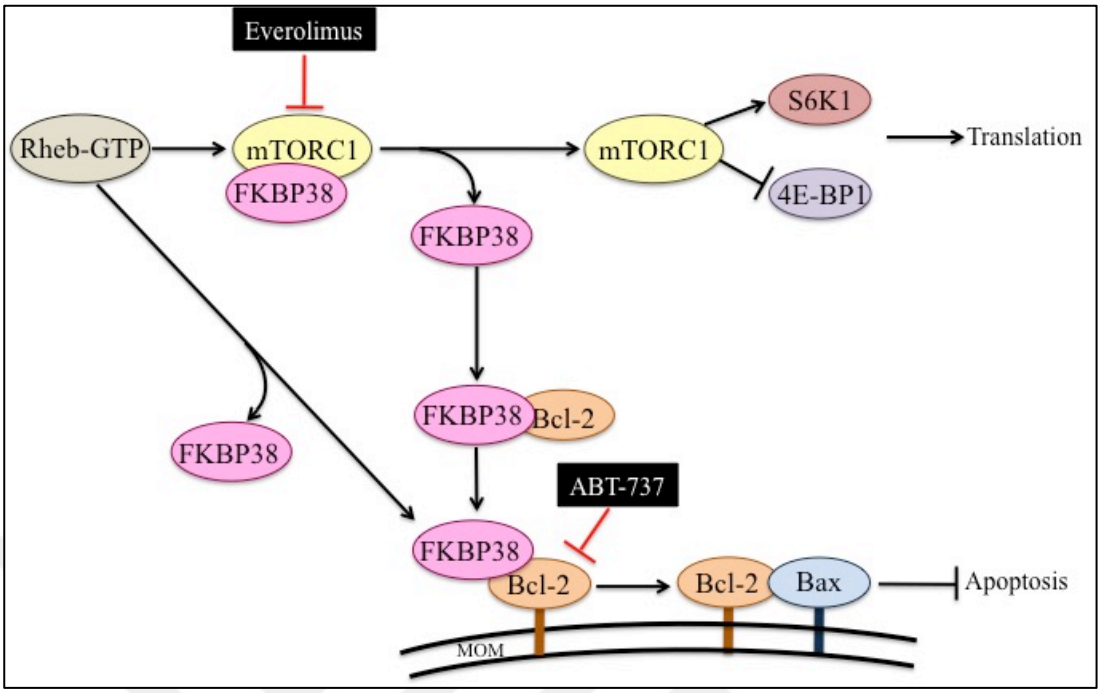

Figure 6.1. Interplay between FKBP38 and Rheb/mTOR/Bcl-2 proteins

Therefore, we hypothesize that the use of ABT-737 will disrupt FKBP38-Bcl-2 interaction, and thereby, induce apoptosis. To test our hypothesis, we characterized the effect of the mono- and combination therapies on FKBP38-mTOR and FKBP38-Bcl-2 interaction in A-498 cells. Results from mTOR-IP showed that ABT-737 did not effect the interaction between FKBP38 and mTOR in A-498 cells (Section 4.8). However, FKBP38-mTOR interaction was lost when A-498 cells were co-treated with everolimus and ABT-737, as expected. Interestingly, mTOR protein was detectable in response to each treatment type, when FKBP38 was precipitated. On the other hand, as expected, the interaction between FKBP38 and Bcl-2 was lost in A-498 undergone ABT-737 regimen or treatment with everolimus-ABT-737 combination, when Bcl-2 protein was precipitated. Interestingly, the presence of ABT-737 did not affect FKBP38-Bcl-2 interaction in cells, as Bcl-2 protein was detected, when FKBP38 protein was precipitated. There are several explanations for these contradictory results. On explanation is the possible overlapping of the antibodies with the region where the interaction of FKBP38 and mTOR/Bcl-2 occurs. The antibody of FKBP38 is produced with the epitope that targets the N-terminal region between 1-33 amino acids of FKBP38 protein. As this region is located downstream of FKBP and TPR domains of FKBP38 protein, where mTOR and Bcl-2 bind to, respectively, mTOR and Bcl-2 could be successfully co-immunoprecipitated. The epitope of Bcl-2 antibody

however was designed to target the amino acids located at the flexible loop of Bcl-2 protein, where FKBP38 interacts. Although mTOR antibody does not interferes with the FRB domain, the binding region of FKBP38 on mTOR protein, it targets the serine residues, which undergo phosphorylation events during the activation of mTOR kinase. Therefore, any PTM occurred at these regions of both Bcl-2 and mTOR proteins could interfere with the binding of antibody or FKBP38 protein. Therefore, the selection of appropriate antibodies in order to repeat the Co-IP experiments might provide reliable results in the future. Besides, these contradictory Co-IP results might also indicate an indirect interaction between FKBP38 and mTOR/Bcl-2, which is mediated by different protein(s). As another future plan, a mass spectrometry analysis can be performed in order to identify the putative linker protein(s) as well as the protein complexes, where FKBP38 participates in. Briefly, A-498 cells will be treated with everolimus and/or ABT-737 or left untreated and their cell lysates will be used in SDS-PAGE. The protein bands obtained for each treatment type will be compared and the candidate bands will be excised and analyzed by mas spectrometry.

REFERENCES

1. Souma T, Suzuki N, Yamamoto M. Renal erythropoietin-producing cells in health and disease. *Frontiers in Physiology.* 2015;6 (167):1-10

2. Ferlay J, Soerjomataram I, Dikshit R, Eser S, Mathers C, Rebelo M, Parkin DM, Forman D, Bray F. Cancer incidence and mortality worldwide: sources, methods and major patterns in GLOBOCAN 2012. *International Journal of Cancer.* 2015;136:E359-386.

3. Jemal A, Bray F, Center MM, Ferlay J, Ward E, Forman D. Global cancer statistics. *CA: A Cancer Journal for Clinicians.* 2011;61:69-90.

4. Gupta K, Miller JD, Li JZ, Russell MW, Charbonneau C. Epidemiologic and socioeconomic burden of metastatic renal cell carcinoma (mRCC): a literature review. *Cancer Treatment Reviews.* 2008;34:193-205.

5. Lindblad P. Epidemiology of renal cell carcinoma. *Scandinavian Journal of Surgery.* 2004;93:88-96.

6. Cumberbatch MG, Rota M, Catto JW, La Vecchia C. The role of tobacco smoke in bladder and kidney carcinogenesis: a comparison of exposures and meta-analysis of incidence and mortality risks. *European Urology.* 2016;70:458-466.

7. Anderson AS, Key TJ, Norat T, Scoccianti C, Cecchini M, Berrino F, Boutron-Ruault MC, Espina C, Leitzmann M, Powers H, Wiseman M, Romieu I. European code against cancer 4th edition: obesity, body fatness and cancer. *Cancer Epidemiology.* 2015;39:S34-45.

8. Decastro GJ, McKiernan JM. Epidemiology, clinical staging, and presentation of renal cell carcinoma. *Urologic Clinics of North America.* 2008;35:581-592

9. Maldazys JD, deKernion JB. Prognostic factors in metastatic renal carcinoma. *The Journal of Urology.* 1986;136:376-379.

10. Waalkes S, Becker F, Schrader AJ, Janssen M, Wegener G, Merseburger AS, Schrader M, Hofmann R, Stockle M, Kuczyk MA. Is there a need to further subclassify pT2 renal cell cancers as implemented by the revised 7th TNM version? *European Urology.* 2011;59:258-263.

11. Thoenes W, Storkel S, Rumpelt HJ. Histopathology and classification of renal cell tumors (adenomas, oncocytomas and carcinomas). The basic cytological and histopathological elements and their use for diagnostics. *Pathology - Research and Practice.* 1986;181:125-143.

12. Moch H. An overview of renal cell cancer: pathology and genetics. *Seminars in Cancer Biology.* 2013;23:3-9.

13. Zbar B, Klausner R, Linehan WM. Studying cancer families to identify kidney cancer genes. *Annual Review of Medicine.* 2003;54:217-233.

14. Haas NB, Nathanson KL. Hereditary kidney cancer syndromes. *Advances in Chronic Kidney Disease.* 2014;21:81-90.

15. Srigley JR, Delahunt B, Eble JN, Egevad L, Epstein JI, Grignon D, Hes O, Moch H, Montironi R, Tickoo SK, Zhou M, Argani P, Panel IRT. The International society of urological pathology (ISUP) vancouver classification of renal neoplasia. *The American Journal of Surgical Pathology.* 2013;37:1469-1489.

16. Muglia VF, Prando A. Renal cell carcinoma: histological classification and correlation with imaging findings. *Radiologia Brasileira.* 2015;48:166-174.

17. Kiuru M, Kujala M, Aittomaki K. Inherited forms of renal cell carcinoma. *Scandinavian Journal of Surgery.* 2004;93:103-111.

18. Halat S, Eble JN, Grignon DJ, Lopez-Beltran A, Montironi R, Tan PH, Wang M, Zhang S, MacLennan GT, Cheng L. Multilocular cystic renal cell carcinoma is a subtype of clear cell renal cell carcinoma. *Modern Pathology.* 2010;23:931-936.

19. Menko FH, Maher ER, Schmidt LS, Middelton LA, Aittomaki K, Tomlinson I, Richard S, Linehan WM. Hereditary leiomyomatosis and renal cell cancer (HLRCC): renal cancer risk, surveillance and treatment. *Familial Cancer.* 2014;13:637-644.

20. Schmidt L, Duh FM, Chen F, Kishida T, Glenn G, Choyke P, Scherer SW, Zhuang Z, Lubensky I, Dean M, Allikmets R, Chidambaram A, Bergerheim UR, Feltis JT, Casadevall C, Zamarron A, Bernues M, Richard S, Lips CJ, Walther MM, Tsui LC, Geil L, Orcutt ML, Stackhouse T, Lipan J, Slife L, Brauch H, Decker J, Niehans G, Hughson MD, Moch H, Storkel S, Lerman MI, Linehan WM, Zbar B. Germline and somatic mutations in the tyrosine kinase domain of the MET proto-oncogene in papillary renal carcinomas. *Nature Genetics.* 1997;16:68-73.

21. Lehtonen HJ. Hereditary leiomyomatosis and renal cell cancer: update on clinical and molecular characteristics. *Familial Cancer.* 2011;10:397-411.

22. Brunelli M, Eble JN, Zhang S, Martignoni G, Cheng L. Gains of chromosomes 7, 17, 12, 16, and 20 and loss of Y occur early in the evolution of papillary renal cell neoplasia: a fluorescent in situ hybridization study. *Modern Pathology.* 2003;16:1053-1059.

23. Lopez-Beltran A, Cheng L, Vidal A, Scarpelli M, Kirkali Z, Blanca A, Montironi R. Pathology of renal cell carcinoma: an update. *Analytical and Quantitative Cytopathology and Histopathology.* 2013;35:61-76.

24. Pavlovich CP, Walther MM, Eyler RA, Hewitt SM, Zbar B, Linehan WM, Merino MJ. Renal tumors in the Birt-Hogg-Dube syndrome. *The American Journal of Surgical Pathology.* 2002;26:1542-1552.

25. Hsieh JJ, Purdue MP, Signoretti S, Swanton C, Albiges L, Schmidinger M, Heng DY, Larkin J, Ficarra V. Renal cell carcinoma. *Nature Reviews. Disease Primers.* 2017;3:17009.

26. Valladares Ayerbes M, Aparicio Gallego G, Diaz Prado S, Jimenez Fonseca P, Garcia Campelo R, Anton Aparicio LM. Origin of renal cell carcinomas. *Clinical and Translational Oncology.* 2008;10:697-712.

27. Gupta R, Billis A, Shah RB, Moch H, Osunkoya AO, Jochum W, Hes O, Bacchi CE, de Castro MG, Hansel DE, Zhou M, Vankalakunti M, Salles PG, Cabrera RA, Gown AM, Amin MB. Carcinoma of the collecting ducts of Bellini and renal medullary carcinoma: clinicopathologic analysis of 52 cases of rare aggressive subtypes of renal cell carcinoma with a focus on their interrelationship. *The American Journal of Surgical Pathology.* 2012;36:1265-1278.

28. Liu Q, Galli S, Srinivasan R, Linehan WM, Tsokos M, Merino MJ. Renal medullary carcinoma: molecular, immunohistochemistry, and morphologic correlation. *The American Journal of Surgical Pathology.* 2013;37:368-374.

29. Davis CJ, Jr., Mostofi FK, Sesterhenn IA. Renal medullary carcinoma. The seventh sickle cell nephropathy. *The American Journal of Surgical Pathology.* 1995;19:1-11.

30. Moch H, Cubilla AL, Humphrey PA, Reuter VE, Ulbright TM. The 2016 WHO classification of tumours of the urinary system and male genital organs-part a: renal, penile, and testicular tumours. *European Urology.* 2016;70:93-105.

31. Tomlinson IP, Alam NA, Rowan AJ, Barclay E, Jaeger EE, Kelsell D, Leigh I, Gorman P, Lamlum H, Rahman S, Roylance RR, Olpin S, Bevan S, Barker K, Hearle N, Houlston RS, Kiuru M, Lehtonen R, Karhu A, Vilkki S, Laiho P, Eklund C, Vierimaa O, Aittomaki K, Hietala M, Sistonen P, Paetau A, Salovaara R, Herva R, Launonen V, Aaltonen LA, Multiple Leiomyoma C. Germline mutations in FH predispose to dominantly inherited uterine fibroids, skin leiomyomata and papillary renal cell cancer. *Nature Genetics.* 2002;30:406-410.

32. Merino MJ, Torres-Cabala C, Pinto P, Linehan WM. The morphologic spectrum of kidney tumors in hereditary leiomyomatosis and renal cell carcinoma (HLRCC) syndrome. *The American Journal of Surgical Pathology.* 2007;31:1578-1585.

33. Ricketts C, Woodward ER, Killick P, Morris MR, Astuti D, Latif F, Maher ER. Germline SDHB mutations and familial renal cell carcinoma. *Journal of the National Cancer Institute.* 2008;100:1260-1262.

34. Gill AJ, Hes O, Papathomas T, Sedivcova M, Tan PH, Agaimy A, Andresen PA, Kedziora A, Clarkson A, Toon CW, Sioson L, Watson N, Chou A, Paik J, Clifton-Bligh RJ, Robinson BG, Benn DE, Hills K, Maclean F, Niemeijer ND, Vlatkovic L, Hartmann A, Corssmit EP, van Leenders GJ, Przybycin C, McKenney JK, Magi-Galluzzi C, Yilmaz A, Yu D, Nicoll KD, Yong JL, Sibony M, Yakirevich E, Fleming S, Chow CW, Miettinen M, Michal M, Trpkov K. Succinate dehydrogenase (SDH)-deficient renal carcinoma: a morphologically distinct entity: a clinicopathologic series of 36 tumors from 27 patients. *The American Journal of Surgical Pathology.* 2014;38:1588-1602.

35. Yang XJ, Zhou M, Hes O, Shen S, Li R, Lopez J, Shah RB, Yang Y, Chuang ST, Lin F, Tretiakova MM, Kort EJ, Teh BT. Tubulocystic carcinoma of the kidney: clinicopathologic and molecular characterization. *The American Journal of Surgical Pathology.* 2008;32:177-187.

36. Amin MB, MacLennan GT, Gupta R, Grignon D, Paraf F, Vieillefond A, Paner GP, Stovsky M, Young AN, Srigley JR, Cheville JC. Tubulocystic carcinoma of the kidney: clinicopathologic analysis of 31 cases of a distinctive rare subtype of renal cell carcinoma. *The American Journal of Surgical Pathology.* 2009;33:384-392.

37. Zhou M, Yang XJ, Lopez JI, Shah RB, Hes O, Shen SS, Li R, Yang Y, Lin F, Elson P, Sercia L, Magi-Galluzzi C, Tubbs R. Renal tubulocystic carcinoma is closely related to papillary renal cell carcinoma: implications for pathologic classification. *The American Journal of Surgical Pathology.* 2009;33:1840-1849.

38. Tickoo SK, dePeralta-Venturina MN, Harik LR, Worcester HD, Salama ME, Young AN, Moch H, Amin MB. Spectrum of epithelial neoplasms in end-stage renal disease: an experience from 66 tumor-bearing kidneys with emphasis on histologic patterns distinct from those in sporadic adult renal neoplasia. *The American Journal of Surgical Pathology.* 2006;30:141-153.

39. Gobbo S, Eble JN, Grignon DJ, Martignoni G, MacLennan GT, Shah RB, Zhang S, Brunelli M, Cheng L. Clear cell papillary renal cell carcinoma: a distinct histopathologic and molecular genetic entity. *The American Journal of Surgical Pathology.* 2008;32:1239-1245.

40. Rohan SM, Xiao Y, Liang Y, Dudas ME, Al-Ahmadie HA, Fine SW, Gopalan A, Reuter VE, Rosenblum MK, Russo P, Tickoo SK. Clear-cell papillary renal cell carcinoma: molecular and immunohistochemical analysis with emphasis on the von Hippel-Lindau gene and hypoxia-inducible factor pathway-related proteins. *Modern Pathology.* 2011;24:1207-1220.

41. Zhou H, Zheng S, Truong LD, Ro JY, Ayala AG, Shen SS. Clear cell papillary renal cell carcinoma is the fourth most common histologic type of renal cell carcinoma in 290 consecutive nephrectomies for renal cell carcinoma. *Human Pathology.* 2014;45:59-64.

42. Cossu-Rocca P, Eble JN, Zhang S, Martignoni G, Brunelli M, Cheng L. Acquired cystic disease-associated renal tumors: an immunohistochemical and fluorescence in situ hybridization study. *Modern Pathology.* 2006;19:780-787.

43. Hanahan D, Weinberg RA. The hallmarks of cancer. *Cell.* 2000;100:57-70.

44. Banumathy G, Cairns P. Signaling pathways in renal cell carcinoma. *Cancer Biology & Therapy.* 2010;10:658-664.

45. Bielecka ZF, Czarnecka AM, Szczylik C. Genomic analysis as the first step toward personalized treatment in renal cell carcinoma. *Frontiers in Oncology.* 2014;4:194.

46. Harris AL. Hypoxia--a key regulatory factor in tumour growth. *Nature Reviews Cancer.* 2002;2:38-47.

47. Semenza GL. Targeting HIF-1 for cancer therapy. *Nature Reviews Cancer.* 2003;3:721-732.

48. Wang GL, Jiang BH, Rue EA, Semenza GL. Hypoxia-inducible factor 1 is a basic-helix-loop-helix-PAS heterodimer regulated by cellular O2 tension. *Proceedings of the National Academy of Sciences of the United States of America.* 1995;92:5510-5514.

49. Masoud GN, Li W. HIF-1alpha pathway: role, regulation and intervention for cancer therapy. *Acta Pharmaceutica Sinica B.* 2015;5:378-389.

50. Thirlwell C, Schulz L, Dibra H, Beck S. Suffocating cancer: hypoxia-associated epimutations as targets for cancer therapy. *Clinical Epigenetics.* 2011;3:9.

51. Masson N, Willam C, Maxwell PH, Pugh CW, Ratcliffe PJ. Independent function of two destruction domains in hypoxia-inducible factor-alpha chains activated by prolyl hydroxylation. *The EMBO Journal.* 2001;20:5197-5206.

52. Ohh M, Park CW, Ivan M, Hoffman MA, Kim TY, Huang LE, Pavletich N, Chau V, Kaelin WG. Ubiquitination of hypoxia-inducible factor requires direct binding to the beta-domain of the von Hippel-Lindau protein. *Nature Cell Biology.* 2000;2:423-427.

53. Pugh CW, Ratcliffe PJ. The von Hippel-Lindau tumor suppressor, hypoxia-inducible factor-1 (HIF-1) degradation, and cancer pathogenesis. *Seminars in Cancer Biology.* 2003;13:83-89.

54. Baldewijns MM, van Vlodrop IJ, Vermeulen PB, Soetekouw PM, van Engeland M, de Bruine AP. VHL and HIF signalling in renal cell carcinogenesis. *The Journal of Pathology.* 2010;221:125-138.

55. Maynard MA, Ohh M. Von Hippel-Lindau tumor suppressor protein and hypoxia-inducible factor in kidney cancer. *American Journal of Nephrology.* 2004;24:1-13.

56. Gnarra JR, Tory K, Weng Y, Schmidt L, Wei MH, Li H, Latif F, Liu S, Chen F, Duh FM, et al. Mutations of the VHL tumour suppressor gene in renal carcinoma. *Nature Genetics.* 1994;7:85-90.

57. Shen C, Kaelin WG, Jr. The VHL/HIF axis in clear cell renal carcinoma. *Seminars in Cancer Biology.* 2013;23:18-25.

58. Kaelin WG, Jr. Molecular basis of the VHL hereditary cancer syndrome. *Nature Reviews Cancer.* 2002;2:673-682.

59. Krieg M, Haas R, Brauch H, Acker T, Flamme I, Plate KH. Up-regulation of hypoxia-inducible factors HIF-1alpha and HIF-2alpha under normoxic conditions in renal carcinoma cells by von Hippel-Lindau tumor suppressor gene loss of function. *Oncogene.* 2000;19:5435-5443.

60. Mandriota SJ, Turner KJ, Davies DR, Murray PG, Morgan NV, Sowter HM, Wykoff CC, Maher ER, Harris AL, Ratcliffe PJ, Maxwell PH. HIF activation identifies early lesions in VHL kidneys: evidence for site-specific tumor suppressor function in the nephron. *Cancer Cell.* 2002;1:459-468.

61. Sato T, Umetsu A, Tamanoi F. Characterization of the Rheb-mTOR signaling pathway in mammalian cells: constitutive active mutants of Rheb and mTOR. *Methods in Enzymology.* 2008;438:307-320.

62. Azim H, Azim HA, Jr., Escudier B. Targeting mTOR in cancer: renal cell is just a beginning. *Targeted Oncology.* 2010;5:269-280.

63. Guo H, German P, Bai S, Barnes S, Guo W, Qi X, Lou H, Liang J, Jonasch E, Mills GB, Ding Z. The PI3K/AKT pathway and renal cell carcinoma. *Journal of Genetics and Genomics.* 2015;42:343-353.

64. Fruman DA, Meyers RE, Cantley LC. Phosphoinositide kinases. *Annual Review of Biochemistry.* 1998;67:481-507.

65. Vanhaesebroeck B, Guillermet-Guibert J, Graupera M, Bilanges B. The emerging mechanisms of isoform-specific PI3K signalling. *Nature Reviews Molecular Cell Biology.* 2010;11:329-341.

66. Tokunaga C, Yoshino K, Yonezawa K. mTOR integrates amino acid- and energy-sensing pathways. *Biochemical and Biophysical Research Communications.* 2004;313:443-446.

67. Alessi DR, James SR, Downes CP, Holmes AB, Gaffney PR, Reese CB, Cohen P. Characterization of a 3-phosphoinositide-dependent protein kinase which phosphorylates and activates protein kinase Balpha. *Current Biology.* 1997;7:261-269.

68. Alessi DR, Andjelkovic M, Caudwell B, Cron P, Morrice N, Cohen P, Hemmings BA. Mechanism of activation of protein kinase B by insulin and IGF-1. *The EMBO Journal.* 1996;15:6541-6551.

69. Sarbassov DD, Guertin DA, Ali SM, Sabatini DM. Phosphorylation and regulation of Akt/PKB by the rictor-mTOR complex. *Science.* 2005;307:1098-1101.

70. Guertin DA, Stevens DM, Thoreen CC, Burds AA, Kalaany NY, Moffat J, Brown M, Fitzgerald KJ, Sabatini DM. Ablation in mice of the mTORC components raptor, rictor, or mLST8 reveals that mTORC2 is required for signaling to Akt-FOXO and PKCalpha, but not S6K1. *Developmental Cell.* 2006;11:859-871.

71. Hers I, Vincent EE, Tavare JM. Akt signalling in health and disease. *Cell Signal.* 2011;23:1515-1527.

72. Yu JS, Cui W. Proliferation, survival and metabolism: the role of PI3K/AKT/mTOR signalling in pluripotency and cell fate determination. *Development.* 2016;143:3050-3060.

73. Sarbassov DD, Ali SM, Sabatini DM. Growing roles for the mTOR pathway. *Current Opinion in Cell Biology.* 2005;17:596-603.

74. Martel RR, Klicius J, Galet S. Inhibition of the immune response by rapamycin, a new antifungal antibiotic. *Canadian Journal of Physiology and Pharmacology.* 1977;55:48-51.

75. Guertin DA, Sabatini DM. Defining the role of mTOR in cancer. *Cancer Cell.* 2007;12:9-22.

76. Showkat M, Beigh MA, Andrabi KI. mTOR signaling in protein translation regulation: implications in cancer genesis and therapeutic interventions. *Molecular Biology International.* 2014;2014:686984.

77. Huang J, Manning BD. The TSC1-TSC2 complex: a molecular switchboard controlling cell growth. *Biochemical Journal.* 2008;412:179-190.

78. Wienecke R, Konig A, DeClue JE. Identification of tuberin, the tuberous sclerosis-2 product. Tuberin possesses specific Rap1GAP activity. *The Journal of Biological Chemistry.* 1995;270:16409-16414.

79. Tee AR, Manning BD, Roux PP, Cantley LC, Blenis J. Tuberous sclerosis complex gene products, Tuberin and Hamartin, control mTOR signaling by acting as a GTPase-activating protein complex toward Rheb. *Current Biology.* 2003;13:1259-1268.

80. Inoki K, Li Y, Xu T, Guan KL. Rheb GTPase is a direct target of TSC2 GAP activity and regulates mTOR signaling. *Genes & Development.* 2003;17:1829-1834.

81. Kovacina KS, Park GY, Bae SS, Guzzetta AW, Schaefer E, Birnbaum MJ, Roth RA. Identification of a proline-rich Akt substrate as a 14-3-3 binding partner. *The Journal of Biological Chemistry.* 2003;278:10189-10194.

82. Wang L, Harris TE, Lawrence JC, Jr. Regulation of proline-rich Akt substrate of 40 kDa (PRAS40) function by mammalian target of rapamycin complex 1 (mTORC1)-mediated phosphorylation. *The Journal of Biological Chemistry.* 2008;283:15619-15627.

83. Dibble CC, Cantley LC. Regulation of mTORC1 by PI3K signaling. *Trends in Cell Biology.* 2015;25:545-555.

84. Ma D, Bai X, Zou H, Lai Y, Jiang Y. Rheb GTPase controls apoptosis by regulating interaction of FKBP38 with Bcl-2 and Bcl-XL. *The Journal of Biological Chemistry.* 2010;285:8621-8627.

85. Fingar DC, Blenis J. Target of rapamycin (TOR): an integrator of nutrient and growth factor signals and coordinator of cell growth and cell cycle progression. *Oncogene.* 2004;23:3151-3171.

86. Haghighat A, Mader S, Pause A, Sonenberg N. Repression of cap-dependent translation by 4E-binding protein 1: competition with p220 for binding to eukaryotic initiation factor-4E. *The EMBO Journal.* 1995;14:5701-5709.

87. Gingras AC, Raught B, Gygi SP, Niedzwiecka A, Miron M, Burley SK, Polakiewicz RD, Wyslouch-Cieszynska A, Aebersold R, Sonenberg N. Hierarchical phosphorylation of the translation inhibitor 4E-BP1. *Genes & Development.* 2001;15:2852-2864.

88. Richter JD, Sonenberg N. Regulation of cap-dependent translation by eIF4E inhibitory proteins. *Nature.* 2005;433:477-480.

89. Rosner M, Hengstschlager M. Evidence for cell cycle-dependent, rapamycin-resistant phosphorylation of ribosomal protein S6 at S240/244. *Amino Acids.* 2010;39:1487-1492.

90. Ferrari S, Bandi HR, Hofsteenge J, Bussian BM, Thomas G. Mitogen-activated 70K S6 kinase. Identification of in vitro 40 S ribosomal S6 phosphorylation sites. *The Journal of Biological Chemistry.* 1991;266:22770-22775.

91. Ma XM, Blenis J. Molecular mechanisms of mTOR-mediated translational control. *Nature Reviews Molecular Cell Biology.* 2009;10:307-318.

92. Jacinto E, Loewith R, Schmidt A, Lin S, Ruegg MA, Hall A, Hall MN. Mammalian TOR complex 2 controls the actin cytoskeleton and is rapamycin insensitive. *Nature Cell Biology.* 2004;6:1122-1128.

93. Oh WJ, Jacinto E. mTOR complex 2 signaling and functions. *Cell Cycle.* 2011;10:2305-2316.

94. Copp J, Manning G, Hunter T. TORC-specific phosphorylation of mammalian target of rapamycin (mTOR): phospho-Ser2481 is a marker for intact mTOR signaling complex 2. *Cancer Research.* 2009;69:1821-1827.

95. Facchinetti V, Ouyang W, Wei H, Soto N, Lazorchak A, Gould C, Lowry C, Newton AC, Mao Y, Miao RQ, Sessa WC, Qin J, Zhang P, Su B, Jacinto E. The mammalian target of rapamycin complex 2 controls folding and stability of Akt and protein kinase C. *The EMBO Journal.* 2008;27:1932-1943.

96. Garcia-Martinez JM, Alessi DR. mTOR complex 2 (mTORC2) controls hydrophobic motif phosphorylation and activation of serum- and glucocorticoid-induced protein kinase 1 (SGK1). *Biochemical Journal.* 2008;416:375-385.

97. Laplante M, Sabatini DM. mTOR signaling in growth control and disease. *Cell.* 2012;149:274-293.

98. Maehama T, Dixon JE. The tumor suppressor, PTEN/MMAC1, dephosphorylates the lipid second messenger, phosphatidylinositol 3,4,5-trisphosphate. *The Journal of Biological Chemistry.* 1998;273:13375-13378.

99. Chalhoub N, Baker SJ. PTEN and the PI3-kinase pathway in cancer. *Annual Review of Pathology.* 2009;4:127-150.

100. Yu Y, Yoon SO, Poulogiannis G, Yang Q, Ma XM, Villen J, Kubica N, Hoffman GR, Cantley LC, Gygi SP, Blenis J. Phosphoproteomic analysis identifies Grb10 as an mTORC1 substrate that negatively regulates insulin signaling. *Science.* 2011;332:1322-1326.

101. Harrington LS, Findlay GM, Gray A, Tolkacheva T, Wigfield S, Rebholz H, Barnett J, Leslie NR, Cheng S, Shepherd PR, Gout I, Downes CP, Lamb RF. The TSC1-2 tumor suppressor controls insulin-PI3K signaling via regulation of IRS proteins. *The Journal of Cell Biology.* 2004;166:213-223.

102. Dibble CC, Asara JM, Manning BD. Characterization of Rictor phosphorylation sites reveals direct regulation of mTOR complex 2 by S6K1. *Molecular and Cellular Biology.* 2009;29:5657-5670.

103. Julien LA, Carriere A, Moreau J, Roux PP. mTORC1-activated S6K1 phosphorylates Rictor on threonine 1135 and regulates mTORC2 signaling. *Molecular and Cellular Biology.* 2010;30:908-921.

104. Lieberthal W, Levine JS. The role of the mammalian target of rapamycin (mTOR) in renal disease. *Journal of the American Society of Nephrology* 2009;20:2493-2502.

105. Hudson CC, Liu M, Chiang GG, Otterness DM, Loomis DC, Kaper F, Giaccia AJ, Abraham RT. Regulation of hypoxia-inducible factor 1alpha expression and function by the mammalian target of rapamycin. *Molecular and Cellular Biology.* 2002;22:7004-7014.

106. Zhong H, De Marzo AM, Laughner E, Lim M, Hilton DA, Zagzag D, Buechler P, Isaacs WB, Semenza GL, Simons JW. Overexpression of hypoxia-inducible factor 1alpha in common human cancers and their metastases. *Cancer Research.* 1999;59:5830-5835.

107. Toschi A, Lee E, Gadir N, Ohh M, Foster DA. Differential dependence of hypoxia-inducible factors 1 alpha and 2 alpha on mTORC1 and mTORC2. *The Journal of Biological Chemistry.* 2008;283:34495-34499.

108. Gordan JD, Bertout JA, Hu CJ, Diehl JA, Simon MC. HIF-2alpha promotes hypoxic cell proliferation by enhancing c-myc transcriptional activity. *Cancer Cell.* 2007;11:335-347.

109. Abou Youssif T, Fahmy MA, Koumakpayi IH, Ayala F, Al Marzooqi S, Chen G, Tamboli P, Squire J, Tanguay S, Sircar K. The mammalian target of rapamycin pathway is widely activated without PTEN deletion in renal cell carcinoma metastases. *Cancer.* 2011;117:290-300.

110. Holohan C, Van Schaeybroeck S, Longley DB, Johnston PG. Cancer drug resistance: an evolving paradigm. *Nature Reviews Cancer.* 2013;13:714-726.

111. Housman G, Byler S, Heerboth S, Lapinska K, Longacre M, Snyder N, Sarkar S. Drug resistance in cancer: an overview. *Cancers (Basel).* 2014;6:1769-1792.

112. Yamamoto Y, Koma H, Hiramatsu H, Abe M, Murakami K, Ohya A, Yagami T. Treatment of etoposide combined with 15-deoxy-Delta12,14-prostaglandin J2 exerted synergistic antitumor effects against renal cell carcinoma via peroxisome proliferator-activated receptor-gamma-independent pathways. *Molecular and Clinical Oncology* 2014;2:292-296.

113. Carew JS, Kelly KR, Nawrocki ST. Mechanisms of mTOR inhibitor resistance in cancer therapy. *Targeted Oncology.* 2011;6:17-27.

114. Delbaldo C, Albert S, Dreyer C, Sablin MP, Serova M, Raymond E, Faivre S. Predictive biomarkers for the activity of mammalian target of rapamycin (mTOR) inhibitors. *Targeted Oncology.* 2011;6:119-124.

115. Santoni M, Pantano F, Amantini C, Nabissi M, Conti A, Burattini L, Zoccoli A, Berardi R, Santoni G, Tonini G, Santini D, Cascinu S. Emerging strategies to overcome the resistance to current mTOR inhibitors in renal cell carcinoma. *Biochimica et Biophysica Acta.* 2014;1845:221-231.

116. Laviola L, Natalicchio A, Giorgino F. The IGF-I signaling pathway. *Current Pharmaceutical Design.* 2007;13:663-669.

117. Oldham S, Hafen E. Insulin/IGF and target of rapamycin signaling: a TOR de force in growth control. *Trends in Cell Biology.* 2003;13:79-85.

118. Sun XJ, Crimmins DL, Myers MG, Jr., Miralpeix M, White MF. Pleiotropic insulin signals are engaged by multisite phosphorylation of IRS-1. *Molecular and Cellular Biology.* 1993;13:7418-7428.

119. O'Reilly KE, Rojo F, She QB, Solit D, Mills GB, Smith D, Lane H, Hofmann F, Hicklin DJ, Ludwig DL, Baselga J, Rosen N. mTOR inhibition induces upstream receptor tyrosine kinase signaling and activates Akt. *Cancer Research.* 2006;66:1500-1508.

120. Tamburini J, Chapuis N, Bardet V, Park S, Sujobert P, Willems L, Ifrah N, Dreyfus F, Mayeux P, Lacombe C, Bouscary D. Mammalian target of rapamycin (mTOR) inhibition activates phosphatidylinositol 3-kinase/Akt by up-regulating insulin-like growth factor-1 receptor signaling in acute myeloid leukemia: rationale for therapeutic inhibition of both pathways. *Blood.* 2008;111:379-382.

121. Shi Y, Yan H, Frost P, Gera J, Lichtenstein A. Mammalian target of rapamycin inhibitors activate the AKT kinase in multiple myeloma cells by up-regulating the

insulin-like growth factor receptor/insulin receptor substrate-1/phosphatidylinositol 3-kinase cascade. *Molecular Cancer Therapeutics.* 2005;4:1533-1540.

122. Wan X, Harkavy B, Shen N, Grohar P, Helman LJ. Rapamycin induces feedback activation of Akt signaling through an IGF-1R-dependent mechanism. *Oncogene.* 2007;26:1932-1940.

123. Carracedo A, Ma L, Teruya-Feldstein J, Rojo F, Salmena L, Alimonti A, Egia A, Sasaki AT, Thomas G, Kozma SC, Papa A, Nardella C, Cantley LC, Baselga J, Pandolfi PP. Inhibition of mTORC1 leads to MAPK pathway activation through a PI3K-dependent feedback loop in human cancer. *The Journal of Clinical Investigation.* 2008;118:3065-3074.

124. Santarpia L, Lippman SM, El-Naggar AK. Targeting the MAPK-RAS-RAF signaling pathway in cancer therapy. *Expert Opinion on Therapeutic Targets.* 2012;16:103-119.

125. Sarbassov DD, Ali SM, Kim DH, Guertin DA, Latek RR, Erdjument-Bromage H, Tempst P, Sabatini DM. Rictor, a novel binding partner of mTOR, defines a rapamycin-insensitive and raptor-independent pathway that regulates the cytoskeleton. *Current Biology.* 2004;14:1296-1302.

126. Treins C, Warne PH, Magnuson MA, Pende M, Downward J. Rictor is a novel target of p70 S6 kinase-1. *Oncogene.* 2010;29:1003-1016.

127. Harada K, Miyake H, Kumano M, Fujisawa M. Acquired resistance to temsirolimus in human renal cell carcinoma cells is mediated by the constitutive activation of signal transduction pathways through mTORC2. *British Journal of Cancer.* 2013;109:2389-2395.

128. Brown RE, Buryanek J, Tammisetti VS, McGuire MF, Csencsits-Smith K. Morphoproteomics and biomedical analytics confirm the mTORC2/Akt pathway as a resistance signature and activated ERK and STAT3 as concomitant

prosurvival/antiapoptotic pathways in metastatic renal cell carcinoma (RCC) progressing on rapalogs: pathogenesis and therapeutic options. *Oncotarget.* 2016;7:41612-41621.

129. Gordan JD, Simon MC. Hypoxia-inducible factors: central regulators of the tumor phenotype. *Current Opinion in Genetics & Development.* 2007;17:71-77.

130. Wiesener MS, Jurgensen JS, Rosenberger C, Scholze CK, Horstrup JH, Warnecke C, Mandriota S, Bechmann I, Frei UA, Pugh CW, Ratcliffe PJ, Bachmann S, Maxwell PH, Eckardt KU. Widespread hypoxia-inducible expression of HIF-2alpha in distinct cell populations of different organs. *The FASEB Journal.* 2003;17:271-273.

131. Hu CJ, Wang LY, Chodosh LA, Keith B, Simon MC. Differential roles of hypoxia-inducible factor 1alpha (HIF-1alpha) and HIF-2alpha in hypoxic gene regulation. *Molecular and Cellular Biology.* 2003;23:9361-9374.

132. Kang CB, Hong Y, Dhe-Paganon S, Yoon HS. FKBP family proteins: immunophilins with versatile biological functions. *Neurosignals.* 2008;16:318-325.

133. Lam E, Martin M, Wiederrecht G. Isolation of a cDNA encoding a novel human FK506-binding protein homolog containing leucine zipper and tetratricopeptide repeat motifs. *Gene.* 1995;160:297-302.

134. Kang CB, Tai J, Chia J, Yoon HS. The flexible loop of Bcl-2 is required for molecular interaction with immunosuppressant FK-506 binding protein 38 (FKBP38). *FEBS Letters.* 2005;579:1469-1476.

135. Choi BH, Feng L, Yoon HS. FKBP38 protects Bcl-2 from caspase-dependent degradation. *The Journal of Biological Chemistry.* 2010;285:9770-9779.

136. Ma D, Bai X, Guo S, Jiang Y. The switch I region of Rheb is critical for its interaction with FKBP38. *The Journal of Biological Chemistry.* 2008;283:25963-25970.

137. Wang HQ, Nakaya Y, Du Z, Yamane T, Shirane M, Kudo T, Takeda M, Takebayashi K, Noda Y, Nakayama KI, Nishimura M. Interaction of presenilins with FKBP38 promotes apoptosis by reducing mitochondrial Bcl-2. *Human Molecular Genetics.* 2005;14:1889-1902.

138. Nakagawa T, Shirane M, Iemura S, Natsume T, Nakayama KI. Anchoring of the 26S proteasome to the organellar membrane by FKBP38. *Genes Cells.* 2007;12:709-719.

139. Bai X, Ma D, Liu A, Shen X, Wang QJ, Liu Y, Jiang Y. Rheb activates mTOR by antagonizing its endogenous inhibitor, FKBP38. *Science.* 2007;318:977-980.

140. Dunlop EA, Dodd KM, Seymour LA, Tee AR. Mammalian target of rapamycin complex 1-mediated phosphorylation of eukaryotic initiation factor 4E-binding protein 1 requires multiple protein-protein interactions for substrate recognition. *Cell Signal.* 2009;21:1073-1084.

141. Zheng X, Liang Y, He Q, Yao R, Bao W, Bao L, Wang Y, Wang Z. Current models of mammalian target of rapamycin complex 1 (mTORC1) activation by growth factors and amino acids. *International Journal of Molecular Sciences.* 2014;15:20753-20769.

142. Shirane M, Nakayama KI. Inherent calcineurin inhibitor FKBP38 targets Bcl-2 to mitochondria and inhibits apoptosis. *Nature Cell Biology.* 2003;5:28-37.

143. Bassik MC, Scorrano L, Oakes SA, Pozzan T, Korsmeyer SJ. Phosphorylation of BCL-2 regulates ER Ca2+ homeostasis and apoptosis. *The EMBO Journal.* 2004;23:1207-1216.

144. Cheng EH, Kirsch DG, Clem RJ, Ravi R, Kastan MB, Bedi A, Ueno K, Hardwick JM. Conversion of Bcl-2 to a Bax-like death effector by caspases. *Science.* 1997;278:1966-1968.

145. Kang CB, Feng L, Chia J, Yoon HS. Molecular characterization of FK-506 binding protein 38 and its potential regulatory role on the anti-apoptotic protein Bcl-2. *Biochemical and Biophysical Research Communications.* 2005;337:30-38.

146. Zou H, Lai Y, Zhao X, Yan G, Ma D, Cardenes N, Shiva S, Liu Y, Bai X, Jiang Y, Jiang Y. Regulation of mammalian target of rapamycin complex 1 by Bcl-2 and Bcl-XL proteins. *The Journal of Biological Chemistry.* 2013;288:28824-28830.

147. Cory S, Adams JM. The Bcl2 family: regulators of the cellular life-or-death switch. *Nature Reviews Cancer.* 2002;2:647-656.

148. Sayers TJ. Targeting the extrinsic apoptosis signaling pathway for cancer therapy. *Cancer Immunology, Immunotherapy.* 2011;60:1173-1180.

149. Takeda K, Naguro I, Nishitoh H, Matsuzawa A, Ichijo H. Apoptosis signaling kinases: from stress response to health outcomes. *Antioxidants & Redox Signaling.* 2011;15:719-761.

150. Vogler M, Dinsdale D, Dyer MJ, Cohen GM. Bcl-2 inhibitors: small molecules with a big impact on cancer therapy. *Cell Death & Differentiation.* 2009;16:360-367.

151. Tsujimoto Y, Finger LR, Yunis J, Nowell PC, Croce CM. Cloning of the chromosome breakpoint of neoplastic B cells with the t(14;18) chromosome translocation. *Science.* 1984;226:1097-1099.

152. Tsujimoto Y, Cossman J, Jaffe E, Croce CM. Involvement of the bcl-2 gene in human follicular lymphoma. *Science.* 1985;228:1440-1443.

153. Vaux DL, Cory S, Adams JM. Bcl-2 gene promotes haemopoietic cell survival and cooperates with c-myc to immortalize pre-B cells. *Nature.* 1988;335:440-442.

154. McDonnell TJ, Deane N, Platt FM, Nunez G, Jaeger U, McKearn JP, Korsmeyer SJ. Bcl-2-immunoglobulin transgenic mice demonstrate extended B cell survival and follicular lymphoproliferation. *Cell.* 1989;57:79-88.

155. Boise LH, Gonzalez-Garcia M, Postema CE, Ding L, Lindsten T, Turka LA, Mao X, Nunez G, Thompson CB. Bcl-x, a bcl-2-related gene that functions as a dominant regulator of apoptotic cell death. *Cell.* 1993;74:597-608.

156. Muchmore SW, Sattler M, Liang H, Meadows RP, Harlan JE, Yoon HS, Nettesheim D, Chang BS, Thompson CB, Wong SL, Ng SL, Fesik SW. X-ray and NMR structure of human Bcl-xL, an inhibitor of programmed cell death. *Nature.* 1996;381:335-341.

157. Czabotar PE, Lessene G, Strasser A, Adams JM. Control of apoptosis by the BCL-2 protein family: implications for physiology and therapy. *Nature Reviews Molecular Cell Biology.* 2014;15:49-63.

158. Huang DC, Strasser A. BH3-Only proteins-essential initiators of apoptotic cell death. *Cell.* 2000;103:839-842.

159. Kelekar A, Thompson CB. Bcl-2-family proteins: the role of the BH3 domain in apoptosis. *Trends in Cell Biology.* 1998;8:324-330.

160. Letai A, Bassik MC, Walensky LD, Sorcinelli MD, Weiler S, Korsmeyer SJ. Distinct BH3 domains either sensitize or activate mitochondrial apoptosis, serving as prototype cancer therapeutics. *Cancer Cell.* 2002;2:183-192.

161. Chen L, Willis SN, Wei A, Smith BJ, Fletcher JI, Hinds MG, Colman PM, Day CL, Adams JM, Huang DC. Differential targeting of prosurvival Bcl-2 proteins by their

BH3-only ligands allows complementary apoptotic function. *Molecular Cell* . 2005;17:393-403.

162. Sattler M, Liang H, Nettesheim D, Meadows RP, Harlan JE, Eberstadt M, Yoon HS, Shuker SB, Chang BS, Minn AJ, Thompson CB, Fesik SW. Structure of Bcl-xL-Bak peptide complex: recognition between regulators of apoptosis. *Science.* 1997;275:983-986.

163. Levine B, Sinha SC, Kroemer G. Bcl-2 family members: dual regulators of apoptosis and autophagy. *Autophagy.* 2008;4:600-606.

164. Wei MC, Zong WX, Cheng EH, Lindsten T, Panoutsakopoulou V, Ross AJ, Roth KA, MacGregor GR, Thompson CB, Korsmeyer SJ. Proapoptotic BAX and BAK: a requisite gateway to mitochondrial dysfunction and death. *Science.* 2001;292:727-730.

165. Suzuki M, Youle RJ, Tjandra N. Structure of Bax: coregulation of dimer formation and intracellular localization. *Cell.* 2000;103:645-654.

166. Moldoveanu T, Liu Q, Tocilj A, Watson M, Shore G, Gehring K. The X-ray structure of a BAK homodimer reveals an inhibitory zinc binding site. *Molecular Cell* . 2006;24:677-688.

167. Sedlak TW, Oltvai ZN, Yang E, Wang K, Boise LH, Thompson CB, Korsmeyer SJ. Multiple Bcl-2 family members demonstrate selective dimerizations with Bax. *Proceedings of the National Academy of Sciences of the United States of America.* 1995;92:7834-7838.

168. Danial NN. BCL-2 family proteins: critical checkpoints of apoptotic cell death. *Clinical Cancer Research.* 2007;13:7254-7263.

169. Youle RJ, Strasser A. The BCL-2 protein family: opposing activities that mediate cell death. *Nature Reviews Molecular Cell Biology.* 2008;9:47-59.

170. Bouillet P, Strasser A. BH3-only proteins - evolutionarily conserved proapoptotic Bcl-2 family members essential for initiating programmed cell death. *Journal of Cell Science.* 2002;115:1567-1574.

171. Sarosiek KA, Chi X, Bachman JA, Sims JJ, Montero J, Patel L, Flanagan A, Andrews DW, Sorger P, Letai A. BID preferentially activates BAK while BIM preferentially activates BAX, affecting chemotherapy response. *Molecular Cell* . 2013;51:751-765.

172. Annis MG, Soucie EL, Dlugosz PJ, Cruz-Aguado JA, Penn LZ, Leber B, Andrews DW. Bax forms multispanning monomers that oligomerize to permeabilize membranes during apoptosis. *The EMBO Journal.* 2005;24:2096-2103.

173. Westphal D, Dewson G, Czabotar PE, Kluck RM. Molecular biology of Bax and Bak activation and action. *Biochimica et Biophysica Acta.* 2011;1813:521-531.

174. Shamas-Din A, Kale J, Leber B, Andrews DW. Mechanisms of action of Bcl-2 family proteins. *Cold Spring Harb Perspect Biol.* 2013;5:a008714.

175. Schafer B, Quispe J, Choudhary V, Chipuk JE, Ajero TG, Du H, Schneiter R, Kuwana T. Mitochondrial outer membrane proteins assist Bid in Bax-mediated lipidic pore formation. *Molecular Biology of the Cell.* 2009;20:2276-2285.

176. Cain K, Bratton SB, Cohen GM. The Apaf-1 apoptosome: a large caspase-activating complex. *Biochimie.* 2002;84:203-214.

177. Bratton SB, Walker G, Srinivasula SM, Sun XM, Butterworth M, Alnemri ES, Cohen GM. Recruitment, activation and retention of caspases-9 and -3 by Apaf-1 apoptosome and associated XIAP complexes. *The EMBO Journal.* 2001;20:998-1009.

178. Bratton SB, Salvesen GS. Regulation of the Apaf-1-caspase-9 apoptosome. *Journal of Cell Science.* 2010;123:3209-3214.

179. Diamond E, Molina AM, Carbonaro M, Akhtar NH, Giannakakou P, Tagawa ST, Nanus DM. Cytotoxic chemotherapy in the treatment of advanced renal cell carcinoma in the era of targeted therapy. *Critical Reviews in Oncology/Hematologyl.* 2015;96:518-526.

180. Tsui KH, van Ophoven A, Shvarts O, Belldegrun A. Nephron-sparing surgery for renal cell carcinoma. *Reviews in Urology* 1999;1:216-225.

181. Ljungberg B, Hanbury DC, Kuczyk MA, Merseburger AS, Mulders PF, Patard JJ, Sinescu IC, European Association of Urology Guideline Group for renal cell c. Renal cell carcinoma guideline. *European Urology.* 2007;51:1502-1510.

182. Karakiewicz PI, Briganti A, Chun FK, Trinh QD, Perrotte P, Ficarra V, Cindolo L, De la Taille A, Tostain J, Mulders PF, Salomon L, Zigeuner R, Prayer-Galetti T, Chautard D, Valeri A, Lechevallier E, Descotes JL, Lang H, Mejean A, Patard JJ. Multi-institutional validation of a new renal cancer-specific survival nomogram. *Journal of Clinical Oncology.* 2007;25:1316-1322.

183. Yagoda A, Petrylak D, Thompson S. Cytotoxic chemotherapy for advanced renal cell carcinoma. *Urologic Clinics of North America.* 1993;20:303-321.

184. Motzer RJ, Russo P. Systemic therapy for renal cell carcinoma. *The Journal of Urology.* 2000;163:408-417.

185. Rosenberg SA, Lotze MT, Muul LM, Leitman S, Chang AE, Ettinghausen SE, Matory YL, Skibber JM, Shiloni E, Vetto JT, et al. Observations on the systemic administration of autologous lymphokine-activated killer cells and recombinant interleukin-2 to patients with metastatic cancer. *The New England Journal of Medicine.* 1985;313:1485-1492.

186. Rosenberg SA, Lotze MT, Muul LM, Chang AE, Avis FP, Leitman S, Linehan WM, Robertson CN, Lee RE, Rubin JT, et al. A progress report on the treatment of 157 patients with advanced cancer using lymphokine-activated killer cells and

interleukin-2 or high-dose interleukin-2 alone. *The New England Journal of Medicine*. 1987;316:889-897.

187. Fyfe G, Fisher RI, Rosenberg SA, Sznol M, Parkinson DR, Louie AC. Results of treatment of 255 patients with metastatic renal cell carcinoma who received high-dose recombinant interleukin-2 therapy. *Journal of Clinical Oncology*. 1995;13:688-696.

188. Lee-Ying R, Lester R, Heng D. Current management and future perspectives of metastatic renal cell carcinoma. *International Journal of Urology*. 2014;21:847-855.

189. Negrier S, Escudier B, Lasset C, Douillard JY, Savary J, Chevreau C, Ravaud A, Mercatello A, Peny J, Mousseau M, Philip T, Tursz T. Recombinant human interleukin-2, recombinant human interferon alfa-2a, or both in metastatic renal-cell carcinoma. Groupe Francais d'Immunotherapie. *The New England Journal of Medicine*. 1998;338:1272-1278.

190. Negrier S, Perol D, Ravaud A, Chevreau C, Bay JO, Delva R, Sevin E, Caty A, Escudier B, French Immunotherapy I. Medroxyprogesterone, interferon alfa-2a, interleukin 2, or combination of both cytokines in patients with metastatic renal carcinoma of intermediate prognosis: results of a randomized controlled trial. *Cancer*. 2007;110:2468-2477.

191. Najjar YG, Rini BI. Novel agents in renal carcinoma: a reality check. *Ther Adv Medical Oncology*. 2012;4:183-194.

192. Calvo E, Grunwald V, Bellmunt J. Controversies in renal cell carcinoma: treatment choice after progression on vascular endothelial growth factor-targeted therapy. *European Journal of Cancer*. 2014;50:1321-1329.

193. Lam JS, Shvarts O, Leppert JT, Figlin RA, Belldegrun AS. Renal cell carcinoma 2005: new frontiers in staging, prognostication and targeted molecular therapy. *The Journal of Urology.* 2005;173:1853-1862.

194. Di Lorenzo G, Buonerba C, Biglietto M, Scognamiglio F, Chiurazzi B, Riccardi F, Carteni G. The therapy of kidney cancer with biomolecular drugs. *Cancer Treatment Reviews.* 2010;36 Suppl 3:S16-20.

195. Randall JM, Millard F, Kurzrock R. Molecular aberrations, targeted therapy, and renal cell carcinoma: current state-of-the-art. *Cancer and Metastasis Reviews.* 2014;33:1109-1124.

196. Minguet J, Smith KH, Bramlage CP, Bramlage P. Targeted therapies for treatment of renal cell carcinoma: recent advances and future perspectives. *Cancer Chemotherapy and Pharmacology* . 2015;76:219-233.

197. Wilhelm SM, Carter C, Tang L, Wilkie D, McNabola A, Rong H, Chen C, Zhang X, Vincent P, McHugh M, Cao Y, Shujath J, Gawlak S, Eveleigh D, Rowley B, Liu L, Adnane L, Lynch M, Auclair D, Taylor I, Gedrich R, Voznesensky A, Riedl B, Post LE, Bollag G, Trail PA. BAY 43-9006 exhibits broad spectrum oral antitumor activity and targets the RAF/MEK/ERK pathway and receptor tyrosine kinases involved in tumor progression and angiogenesis. *Cancer Research.* 2004;64:7099-7109.

198. Escudier B, Eisen T, Stadler WM, Szczylik C, Oudard S, Siebels M, Negrier S, Chevreau C, Solska E, Desai AA, Rolland F, Demkow T, Hutson TE, Gore M, Freeman S, Schwartz B, Shan M, Simantov R, Bukowski RM, Group TS. Sorafenib in advanced clear-cell renal-cell carcinoma. *The New England Journal of Medicine.* 2007;356:125-134.

199. Santoni M, Conti A, De Giorgi U, Iacovelli R, Pantano F, Burattini L, Muzzonigro G, Berardi R, Santini D, Cascinu S. Risk of gastrointestinal events with sorafenib,

sunitinib and pazopanib in patients with solid tumors: a systematic review and meta-analysis of clinical trials. *International Journal of Cancer.* 2014;135:763-773.

200. Stein MN, Flaherty KT. CCR drug updates: sorafenib and sunitinib in renal cell carcinoma. *Clinical Cancer Research.* 2007;13:3765-3770.

201. Motzer RJ, Hutson TE, Tomczak P, Michaelson MD, Bukowski RM, Rixe O, Oudard S, Negrier S, Szczylik C, Kim ST, Chen I, Bycott PW, Baum CM, Figlin RA. Sunitinib versus interferon alfa in metastatic renal-cell carcinoma. *The New England Journal of Medicine.* 2007;356:115-124.

202. Motzer RJ, Hutson TE, Tomczak P, Michaelson MD, Bukowski RM, Oudard S, Negrier S, Szczylik C, Pili R, Bjarnason GA, Garcia-del-Muro X, Sosman JA, Solska E, Wilding G, Thompson JA, Kim ST, Chen I, Huang X, Figlin RA. Overall survival and updated results for sunitinib compared with interferon alfa in patients with metastatic renal cell carcinoma. *Journal of Clinical Oncology.* 2009;27:3584-3590.

203. Mizutani Y. Recent advances in molecular targeted therapy for metastatic renal cell carcinoma. *International Journal of Urology.* 2009;16:444-448.

204. Di Lorenzo G, Autorino R, Bruni G, Carteni G, Ricevuto E, Tudini M, Ficorella C, Romano C, Aieta M, Giordano A, Giuliano M, Gonnella A, De Nunzio C, Rizzo M, Montesarchio V, Ewer M, De Placido S. Cardiovascular toxicity following sunitinib therapy in metastatic renal cell carcinoma: a multicenter analysis. *Annals of Oncology.* 2009;20:1535-1542.

205. Sonpavde G, Hutson TE. Pazopanib: a novel multitargeted tyrosine kinase inhibitor. *Current Oncology Reports.* 2007;9:115-119.

206. Bukowski RM. Pazopanib: a multikinase inhibitor with activity in advanced renal cell carcinoma. *Expert Review of Anticancer Therapy.* 2010;10:635-645.

207. Sternberg CN, Davis ID, Mardiak J, Szczylik C, Lee E, Wagstaff J, Barrios CH, Salman P, Gladkov OA, Kavina A, Zarba JJ, Chen M, McCann L, Pandite L, Roychowdhury DF, Hawkins RE. Pazopanib in locally advanced or metastatic renal cell carcinoma: results of a randomized phase III trial. *Journal of Clinical Oncology.* 2010;28:1061-1068.

208. Motzer RJ, McCann L, Deen K. Pazopanib versus sunitinib in renal cancer. *The New England Journal of Medicine.* 2013;369:1970.

209. Rini BI, Escudier B, Tomczak P, Kaprin A, Szczylik C, Hutson TE, Michaelson MD, Gorbunova VA, Gore ME, Rusakov IG, Negrier S, Ou YC, Castellano D, Lim HY, Uemura H, Tarazi J, Cella D, Chen C, Rosbrook B, Kim S, Motzer RJ. Comparative effectiveness of axitinib versus sorafenib in advanced renal cell carcinoma (AXIS): a randomised phase 3 trial. *Lancet.* 2011;378:1931-1939.

210. van Geel RM, Beijnen JH, Schellens JH. Concise drug review: pazopanib and axitinib. *Oncologist.* 2012;17:1081-1089.

211. Rixe O, Bukowski RM, Michaelson MD, Wilding G, Hudes GR, Bolte O, Motzer RJ, Bycott P, Liau KF, Freddo J, Trask PC, Kim S, Rini BI. Axitinib treatment in patients with cytokine-refractory metastatic renal-cell cancer: a phase II study. *The Lancet Oncology.* 2007;8:975-984.

212. Qi WX, He AN, Shen Z, Yao Y. Incidence and risk of hypertension with a novel multi-targeted kinase inhibitor axitinib in cancer patients: a systematic review and meta-analysis. *British Journal of Clinical Pharmacology.* 2013;76:348-357.

213. Ferrara N, Hillan KJ, Gerber HP, Novotny W. Discovery and development of bevacizumab, an anti-VEGF antibody for treating cancer. *Nature Reviews Drug Discovery.* 2004;3:391-400.

214. Escudier B, Pluzanska A, Koralewski P, Ravaud A, Bracarda S, Szczylik C, Chevreau C, Filipek M, Melichar B, Bajetta E, Gorbunova V, Bay JO, Bodrogi I,

Jagiello-Gruszfeld A, Moore N, investigators AT. Bevacizumab plus interferon alfa-2a for treatment of metastatic renal cell carcinoma: a randomised, double-blind phase III trial. *Lancet.* 2007;370:2103-2111.

215. Rini BI, Halabi S, Rosenberg JE, Stadler WM, Vaena DA, Archer L, Atkins JN, Picus J, Czaykowski P, Dutcher J, Small EJ. Phase III trial of bevacizumab plus interferon alfa versus interferon alfa monotherapy in patients with metastatic renal cell carcinoma: final results of CALGB 90206. *Journal of Clinical Oncology.* 2010;28:2137-2143.

216. Chen J, Zheng XF, Brown EJ, Schreiber SL. Identification of an 11-kDa FKBP12-rapamycin-binding domain within the 289-kDa FKBP12-rapamycin-associated protein and characterization of a critical serine residue. *Proceedings of the National Academy of Sciences of the United States of America.* 1995;92:4947-4951.

217. Oshiro N, Yoshino K, Hidayat S, Tokunaga C, Hara K, Eguchi S, Avruch J, Yonezawa K. Dissociation of raptor from mTOR is a mechanism of rapamycin-induced inhibition of mTOR function. *Genes Cells.* 2004;9:359-366.

218. Sarbassov DD, Ali SM, Sengupta S, Sheen JH, Hsu PP, Bagley AF, Markhard AL, Sabatini DM. Prolonged rapamycin treatment inhibits mTORC2 assembly and Akt/PKB. *Molecular Cell* . 2006;22:159-168.

219. Pohanka E. New immunosuppressive drugs: an update. *Current Opinion in Urology.* 2001;11:143-151.

220. Kahan BD, Camardo JS. Rapamycin: clinical results and future opportunities. *Transplantation.* 2001;72:1181-1193.

221. Luan FL, Ding R, Sharma VK, Chon WJ, Lagman M, Suthanthiran M. Rapamycin is an effective inhibitor of human renal cancer metastasis. *Kidney International.* 2003;63:917-926.

222. Douros J, Suffness M. New antitumor substances of natural origin. *Cancer Treatment Reviews.* 1981;8:63-87.

223. Huang S, Bjornsti MA, Houghton PJ. Rapamycins: mechanism of action and cellular resistance. *Cancer Biology & Therapy.* 2003;2:222-232.

224. Luan FL, Hojo M, Maluccio M, Yamaji K, Suthanthiran M. Rapamycin blocks tumor progression: unlinking immunosuppression from antitumor efficacy. *Transplantation.* 2002;73:1565-1572.

225. Kwitkowski VE, Prowell TM, Ibrahim A, Farrell AT, Justice R, Mitchell SS, Sridhara R, Pazdur R. FDA approval summary: temsirolimus as treatment for advanced renal cell carcinoma. *Oncologist.* 2010;15:428-435.

226. Hudes G, Carducci M, Tomczak P, Dutcher J, Figlin R, Kapoor A, Staroslawska E, Sosman J, McDermott D, Bodrogi I, Kovacevic Z, Lesovoy V, Schmidt-Wolf IG, Barbarash O, Gokmen E, O'Toole T, Lustgarten S, Moore L, Motzer RJ, Global AT. Temsirolimus, interferon alfa, or both for advanced renal-cell carcinoma. *The New England Journal of Medicine.* 2007;356:2271-2281.

227. Dutcher JP, de Souza P, McDermott D, Figlin RA, Berkenblit A, Thiele A, Krygowski M, Strahs A, Feingold J, Hudes G. Effect of temsirolimus versus interferon-alpha on outcome of patients with advanced renal cell carcinoma of different tumor histologies. *Medical Oncology.* 2009;26:202-209.

228. Sun M, Lughezzani G, Perrotte P, Karakiewicz PI. Treatment of metastatic renal cell carcinoma. *Nature Reviews Urology.* 2010;7:327-338.

229. Anandappa G, Hollingdale A, Eisen T. Everolimus - a new approach in the treatment of renal cell carcinoma. *Cancer Management and Research.* 2010;2:61-70.

230. O'Donnell A, Faivre S, Burris HA, 3rd, Rea D, Papadimitrakopoulou V, Shand N, Lane HA, Hazell K, Zoellner U, Kovarik JM, Brock C, Jones S, Raymond E, Judson I. Phase I pharmacokinetic and pharmacodynamic study of the oral mammalian target of rapamycin inhibitor everolimus in patients with advanced solid tumors. *Journal of Clinical Oncology.* 2008;26:1588-1595.

231. Amato RJ, Jac J, Giessinger S, Saxena S, Willis JP. A phase 2 study with a daily regimen of the oral mTOR inhibitor RAD001 (everolimus) in patients with metastatic clear cell renal cell cancer. *Cancer.* 2009;115:2438-2446.

232. Motzer RJ, Escudier B, Oudard S, Hutson TE, Porta C, Bracarda S, Grunwald V, Thompson JA, Figlin RA, Hollaender N, Kay A, Ravaud A, Group R-S. Phase 3 trial of everolimus for metastatic renal cell carcinoma : final results and analysis of prognostic factors. *Cancer.* 2010;116:4256-4265.

233. Pal SK, Signorovitch JE, Reichmann WM, Li N, Koo V, Liu Z, Perez JR, Vogelzang NJ. Real-World effectiveness of everolimus subsequent to different first targeted therapies for the treatment of metastatic renal cell carcinoma: synthesis of retrospective chart reviews. *Clinical Genitourinary Cancer.* 2016;14:160-167 e163.

234. Faivre S, Kroemer G, Raymond E. Current development of mTOR inhibitors as anticancer agents. *Nature Reviews Drug Discovery.* 2006;5:671-688.

235. van der Mijn JC, Panka DJ, Geissler AK, Verheul HM, Mier JW. Novel drugs that target the metabolic reprogramming in renal cell cancer. *Cancer & Metabolism.* 2016;4:14.

236. Maira SM, Stauffer F, Brueggen J, Furet P, Schnell C, Fritsch C, Brachmann S, Chene P, De Pover A, Schoemaker K, Fabbro D, Gabriel D, Simonen M, Murphy L, Finan P, Sellers W, Garcia-Echeverria C. Identification and characterization of NVP-BEZ235, a new orally available dual phosphatidylinositol 3-kinase/mammalian target of rapamycin inhibitor with potent in vivo antitumor activity. *Molecular Cancer Therapeutics.* 2008;7:1851-1863.

237. Cho DC, Cohen MB, Panka DJ, Collins M, Ghebremichael M, Atkins MB, Signoretti S, Mier JW. The efficacy of the novel dual PI3-kinase/mTOR inhibitor NVP-BEZ235 compared with rapamycin in renal cell carcinoma. *Clinical Cancer Research.* 2010;16:3628-3638.

238. Zheng B, Mao JH, Qian L, Zhu H, Gu DH, Pan XD, Yi F, Ji DM. Pre-clinical evaluation of AZD-2014, a novel mTORC1/2 dual inhibitor, against renal cell carcinoma. *Cancer Letters.* 2015;357:468-475.

239. Basu B, Dean E, Puglisi M, Greystoke A, Ong M, Burke W, Cavallin M, Bigley G, Womack C, Harrington EA, Green S, Oelmann E, de Bono JS, Ranson M, Banerji U. First-in-human pharmacokinetic and pharmacodynamic study of the dual m-TORC 1/2 inhibitor AZD2014. *Clinical Cancer Research.* 2015;21:3412-3419.

240. Powles T, Wheater M, Din O, Geldart T, Boleti E, Stockdale A, Sundar S, Robinson A, Ahmed I, Wimalasingham A, Burke W, Sarker SJ, Hussain S, Ralph C. A Randomised phase 2 study of AZD2014 versus everolimus in patients with VEGF-refractory metastatic clear cell renal cancer. *European Urology.* 2016;69:450-456.

241. Cho HJ, Kim JK, Kim KD, Yoon HK, Cho MY, Park YP, Jeon JH, Lee ES, Byun SS, Lim HM, Song EY, Lim JS, Yoon DY, Lee HG, Choe YK. Upregulation of Bcl-2 is associated with cisplatin-resistance via inhibition of Bax translocation in human bladder cancer cells. *Cancer Letters.* 2006;237:56-66.

242. Takahashi M, Saito H, Atsukawa K, Ebinuma H, Okuyama T, Ishii H. Bcl-2 prevents doxorubicin-induced apoptosis of human liver cancer cells. *Hepatology Research.* 2003;25:192-201.

243. Huang A, Fone PD, Gandour-Edwards R, White RW, Low RK. Immunohistochemical analysis of BCL-2 protein expression in renal cell carcinoma. *The Journal of Urology.* 1999;162:610-613.

244. Reed JC, Meister L, Tanaka S, Cuddy M, Yum S, Geyer C, Pleasure D. Differential expression of bcl2 protooncogene in neuroblastoma and other human tumor cell lines of neural origin. *Cancer Research.* 1991;51:6529-6538.

245. McDonnell TJ, Troncoso P, Brisbay SM, Logothetis C, Chung LW, Hsieh JT, Tu SM, Campbell ML. Expression of the protooncogene bcl-2 in the prostate and its association with emergence of androgen-independent prostate cancer. *Cancer Research.* 1992;52:6940-6944.

246. Bauer JJ, Sesterhenn IA, Mostofi FK, McLeod DG, Srivastava S, Moul JW. Elevated levels of apoptosis regulator proteins p53 and bcl-2 are independent prognostic biomarkers in surgically treated clinically localized prostate cancer. *The Journal of Urology.* 1996;156:1511-1516.

247. Pezzella F, Turley H, Kuzu I, Tungekar MF, Dunnill MS, Pierce CB, Harris A, Gatter KC, Mason DY. Bcl-2 protein in non-small-cell lung carcinoma. *The New England Journal of Medicine.* 1993;329:690-694.

248. Ohmori T, Podack ER, Nishio K, Takahashi M, Miyahara Y, Takeda Y, Kubota N, Funayama Y, Ogasawara H, Ohira T, et al. Apoptosis of lung cancer cells caused by some anti-cancer agents (MMC, CPT-11, ADM) is inhibited by bcl-2. *Biochemical and Biophysical Research Communications.* 1993;192:30-36.

249. Gobe G, Rubin M, Williams G, Sawczuk I, Buttyan R. Apoptosis and expression of Bcl-2, Bcl-XL, and Bax in renal cell carcinomas. *Cancer Investigation.* 2002;20:324-332.

250. Lee CT, Genega EM, Hutchinson B, Fearn PA, Kattan MW, Russo P, Reuter VE. Conventional (clear cell) renal carcinoma metastases have greater bcl-2 expression than high-risk primary tumors. *Urologic Oncology.* 2003;21:179-184.

251. Kallio JP, Hirvikoski P, Helin H, Luukkaala T, Tammela TL, Kellokumpu-Lehtinen P, Martikainen PM. Renal cell carcinoma MIB-1, Bax and Bcl-2 expression and prognosis. *The Journal of Urology.* 2004;172:2158-2161.

252. Itoi T, Yamana K, Bilim V, Takahashi K, Tomita F. Impact of frequent Bcl-2 expression on better prognosis in renal cell carcinoma patients. *British Journal of Cancer.* 2004;90:200-205.

253. Yu W, Wang Y, Jiang Y, Zhang W, Li Y. Distinct immunophenotypes and prognostic factors in renal cell carcinoma with sarcomatoid differentiation: a systematic study of 19 immunohistochemical markers in 42 cases. *BMC Cancer.* 2017;17:293.

254. Ikegaki N, Katsumata M, Minna J, Tsujimoto Y. Expression of bcl-2 in small cell lung carcinoma cells. *Cancer Research.* 1994;54:6-8.

255. Robertson LE, Plunkett W, McConnell K, Keating MJ, McDonnell TJ. Bcl-2 expression in chronic lymphocytic leukemia and its correlation with the induction of apoptosis and clinical outcome. *Leukemia.* 1996;10:456-459.

256. Kitada S, Andersen J, Akar S, Zapata JM, Takayama S, Krajewski S, Wang HG, Zhang X, Bullrich F, Croce CM, Rai K, Hines J, Reed JC. Expression of apoptosis-regulating proteins in chronic lymphocytic leukemia: correlations with In vitro and In vivo chemoresponses. *Blood.* 1998;91:3379-3389.

257. Kaiser U, Schilli M, Haag U, Neumann K, Kreipe H, Kogan E, Havemann K. Expression of bcl-2--protein in small cell lung cancer. *Lung Cancer.* 1996;15:31-40.

258. Tu Y, Renner S, Xu F, Fleishman A, Taylor J, Weisz J, Vescio R, Rettig M, Berenson J, Krajewski S, Reed JC, Lichtenstein A. BCL-X expression in multiple myeloma: possible indicator of chemoresistance. *Cancer Research.* 1998;58:256-262.

259. Nguyen M, Marcellus RC, Roulston A, Watson M, Serfass L, Murthy Madiraju SR, Goulet D, Viallet J, Belec L, Billot X, Acoca S, Purisima E, Wiegmans A, Cluse L, Johnstone RW, Beauparlant P, Shore GC. Small molecule obatoclax (GX15-070) antagonizes MCL-1 and overcomes MCL-1-mediated resistance to apoptosis. *Proceedings of the National Academy of Sciences of the United States of America.* 2007;104:19512-19517.

260. Konopleva M, Watt J, Contractor R, Tsao T, Harris D, Estrov Z, Bornmann W, Kantarjian H, Viallet J, Samudio I, Andreeff M. Mechanisms of antileukemic activity of the novel Bcl-2 homology domain-3 mimetic GX15-070 (obatoclax). *Cancer Research.* 2008;68:3413-3420.

261. Oltersdorf T, Elmore SW, Shoemaker AR, Armstrong RC, Augeri DJ, Belli BA, Bruncko M, Deckwerth TL, Dinges J, Hajduk PJ, Joseph MK, Kitada S, Korsmeyer SJ, Kunzer AR, Letai A, Li C, Mitten MJ, Nettesheim DG, Ng S, Nimmer PM, O'Connor JM, Oleksijew A, Petros AM, Reed JC, Shen W, Tahir SK, Thompson CB, Tomaselli KJ, Wang B, Wendt MD, Zhang H, Fesik SW, Rosenberg SH. An inhibitor of Bcl-2 family proteins induces regression of solid tumours. *Nature.* 2005;435:677-681.

262. Del Gaizo Moore V, Brown JR, Certo M, Love TM, Novina CD, Letai A. Chronic lymphocytic leukemia requires BCL2 to sequester prodeath BIM, explaining sensitivity to BCL2 antagonist ABT-737. *The Journal of Clinical Investigation.* 2007;117:112-121.

263. Hann CL, Daniel VC, Sugar EA, Dobromilskaya I, Murphy SC, Cope L, Lin X, Hierman JS, Wilburn DL, Watkins DN, Rudin CM. Therapeutic efficacy of ABT-737, a selective inhibitor of BCL-2, in small cell lung cancer. *Cancer Research.* 2008;68:2321-2328.

264. van Delft MF, Wei AH, Mason KD, Vandenberg CJ, Chen L, Czabotar PE, Willis SN, Scott CL, Day CL, Cory S, Adams JM, Roberts AW, Huang DC. The BH3

mimetic ABT-737 targets selective Bcl-2 proteins and efficiently induces apoptosis via Bak/Bax if Mcl-1 is neutralized. *Cancer Cell.* 2006;10:389-399.

265. Tse C, Shoemaker AR, Adickes J, Anderson MG, Chen J, Jin S, Johnson EF, Marsh KC, Mitten MJ, Nimmer P, Roberts L, Tahir SK, Xiao Y, Yang X, Zhang H, Fesik S, Rosenberg SH, Elmore SW. ABT-263: a potent and orally bioavailable Bcl-2 family inhibitor. *Cancer Research.* 2008;68:3421-3428.

266. Roberts AW, Seymour JF, Brown JR, Wierda WG, Kipps TJ, Khaw SL, Carney DA, He SZ, Huang DC, Xiong H, Cui Y, Busman TA, McKeegan EM, Krivoshik AP, Enschede SH, Humerickhouse R. Substantial susceptibility of chronic lymphocytic leukemia to BCL2 inhibition: results of a phase I study of navitoclax in patients with relapsed or refractory disease. *Journal of Clinical Oncology.* 2012;30:488-496.

267. Gandhi L, Camidge DR, Ribeiro de Oliveira M, Bonomi P, Gandara D, Khaira D, Hann CL, McKeegan EM, Litvinovich E, Hemken PM, Dive C, Enschede SH, Nolan C, Chiu YL, Busman T, Xiong H, Krivoshik AP, Humerickhouse R, Shapiro GI, Rudin CM. Phase I study of Navitoclax (ABT-263), a novel Bcl-2 family inhibitor, in patients with small-cell lung cancer and other solid tumors. *Journal of Clinical Oncology.* 2011;29:909-916.

268. Rudin CM, Hann CL, Garon EB, Ribeiro de Oliveira M, Bonomi PD, Camidge DR, Chu Q, Giaccone G, Khaira D, Ramalingam SS, Ranson MR, Dive C, McKeegan EM, Chyla BJ, Dowell BL, Chakravartty A, Nolan CE, Rudersdorf N, Busman TA, Mabry MH, Krivoshik AP, Humerickhouse RA, Shapiro GI, Gandhi L. Phase II study of single-agent navitoclax (ABT-263) and biomarker correlates in patients with relapsed small cell lung cancer. *Clinical Cancer Research.* 2012;18:3163-3169.

269. Souers AJ, Leverson JD, Boghaert ER, Ackler SL, Catron ND, Chen J, Dayton BD, Ding H, Enschede SH, Fairbrother WJ, Huang DC, Hymowitz SG, Jin S, Khaw SL, Kovar PJ, Lam LT, Lee J, Maecker HL, Marsh KC, Mason KD, Mitten MJ,

Nimmer PM, Oleksijew A, Park CH, Park CM, Phillips DC, Roberts AW, Sampath D, Seymour JF, Smith ML, Sullivan GM, Tahir SK, Tse C, Wendt MD, Xiao Y, Xue JC, Zhang H, Humerickhouse RA, Rosenberg SH, Elmore SW. ABT-199, a potent and selective BCL-2 inhibitor, achieves antitumor activity while sparing platelets. *Nature Medicine.* 2013;19:202-208.

270. Cang S, Iragavarapu C, Savooji J, Song Y, Liu D. ABT-199 (venetoclax) and BCL-2 inhibitors in clinical development. *Journal of Hematology & Oncology.* 2015;8:129.

271. Motzer RJ, Escudier B, Oudard S, Hutson TE, Porta C, Bracarda S, Grunwald V, Thompson JA, Figlin RA, Hollaender N, Urbanowitz G, Berg WJ, Kay A, Lebwohl D, Ravaud A, Group R-S. Efficacy of everolimus in advanced renal cell carcinoma: a double-blind, randomised, placebo-controlled phase III trial. *Lancet.* 2008;372:449-456.

272. Markman B, Dienstmann R, Tabernero J. Targeting the PI3K/Akt/mTOR pathway--beyond rapalogs. *Oncotarget.* 2010;1:530-543.

273. Majumder PK, Febbo PG, Bikoff R, Berger R, Xue Q, McMahon LM, Manola J, Brugarolas J, McDonnell TJ, Golub TR, Loda M, Lane HA, Sellers WR. mTOR inhibition reverses Akt-dependent prostate intraepithelial neoplasia through regulation of apoptotic and HIF-1-dependent pathways. *Nature Medicine.* 2004;10:594-601.

274. Nitta A, Chung YS, Nakata B, Yashiro M, Onoda N, Maeda K, Sawada T, Sowa M. Establishment of a cisplatin-resistant gastric carcinoma cell line OCUM-2M/DDP. *Cancer Chemotherapy and Pharmacology* . 1997;40:94-97.

275. Yang J, Ikezoe T, Nishioka C, Ni L, Koeffler HP, Yokoyama A. Inhibition of mTORC1 by RAD001 (everolimus) potentiates the effects of 1,25-dihydroxyvitamin D(3) to induce growth arrest and differentiation of AML cells in vitro and in vivo. *Experimental Hematology.* 2010;38:666-676.

276. Demirci S, Dogan A, Basak N, Telci D, Dede B, Orhan C, Tuzcu M, Sahin K, Sahin N, Ozercan IH, Sahin F. A Schiff base derivative for effective treatment of diethylnitrosamine-induced liver cancer in vivo. *Anticancer Drugs.* 2015;26:555-564.

277. Chou TC, Talalay P. Quantitative analysis of dose-effect relationships: the combined effects of multiple drugs or enzyme inhibitors. *Advances in Enzyme Regulation.* 1984;22:27-55.

278. Huang L, Jiang Y, Chen Y. Predicting drug combination index and simulating the network-regulation dynamics by mathematical modeling of drug-targeted EGFR-ERK Signaling Pathway. *Scientific Reports.* 2017;7:40752.

279. Kuwana T, Bouchier-Hayes L, Chipuk JE, Bonzon C, Sullivan BA, Green DR, Newmeyer DD. BH3 domains of BH3-only proteins differentially regulate Bax-mediated mitochondrial membrane permeabilization both directly and indirectly. *Molecular Cell* . 2005;17:525-535.

280. Hsu SY, Lin P, Hsueh AJ. BOD (Bcl-2-related ovarian death gene) is an ovarian BH3 domain-containing proapoptotic Bcl-2 protein capable of dimerization with diverse antiapoptotic Bcl-2 members. *Molecular Endocrinology.* 1998;12:1432-1440.

281. Datta SR, Dudek H, Tao X, Masters S, Fu H, Gotoh Y, Greenberg ME. Akt phosphorylation of BAD couples survival signals to the cell-intrinsic death machinery. *Cell.* 1997;91:231-241.

282. Chipuk JE, Bouchier-Hayes L, Kuwana T, Newmeyer DD, Green DR. PUMA couples the nuclear and cytoplasmic proapoptotic function of p53. *Science.* 2005;309:1732-1735.

283. Green DR, Kroemer G. Cytoplasmic functions of the tumour suppressor p53. *Nature.* 2009;458:1127-1130.

284. Delahunt B, Cheville JC, Martignoni G, Humphrey PA, Magi-Galluzzi C, McKenney J, Egevad L, Algaba F, Moch H, Grignon DJ, Montironi R, Srigley JR, Members of the IRTP. The International society of urological pathology (ISUP) grading system for renal cell carcinoma and other prognostic parameters. *The American Journal of Surgical Pathology.* 2013;37:1490-1504.

285. Grunwald V, Karakiewicz PI, Bavbek SE, Miller K, Machiels JP, Lee SH, Larkin J, Bono P, Rha SY, Castellano D, Blank CU, Knox JJ, Hawkins R, Anak O, Rosamilia M, Booth J, Pirotta N, Bodrogi I, Group RS. An international expanded-access programme of everolimus: addressing safety and efficacy in patients with metastatic renal cell carcinoma who progress after initial vascular endothelial growth factor receptor-tyrosine kinase inhibitor therapy. *European Journal of Cancer.* 2012;48:324-332.

286. Kroeger N, Choueiri TK, Lee JL, Bjarnason GA, Knox JJ, MacKenzie MJ, Wood L, Srinivas S, Vaishamayan UN, Rha SY, Pal SK, Yuasa T, Donskov F, Agarwal N, Tan MH, Bamias A, Kollmannsberger CK, North SA, Rini BI, Heng DY. Survival outcome and treatment response of patients with late relapse from renal cell carcinoma in the era of targeted therapy. *European Urology.* 2014;65:1086-1092.

287. Broecker-Preuss M, Becher-Boveleth N, Muller S, Mann K. The BH3 mimetic drug ABT-737 induces apoptosis and acts synergistically with chemotherapeutic drugs in thyroid carcinoma cells. *Cancer Cell International.* 2016;16(27):1-12.

288. Juengel E, Maxeiner S, Rutz J, Justin S, Roos F, Khoder W, Tsaur I, Nelson K, Bechstein WO, Haferkamp A, Blaheta RA. Sulforaphane inhibits proliferation and invasive activity of everolimus-resistant kidney cancer cells in vitro. *Oncotarget.* 2016;7:85208-85219.

289. Yin P, Jia J, Li J, Song Y, Zhang Y, Chen F. ABT-737, a Bcl-2 selective inhibitor, and chloroquine synergistically kill renal cancer cells. *Oncology Research.* 2016;24:65-72.

290. Zhu S, Cohen MB, Bjorge JD, Mier JW, Cho DC. PI3K inhibition potentiates Bcl-2-dependent apoptosis in renal carcinoma cells. *Journal of Cellular and Molecular Medicine.* 2013;17:377-385.

291. Juengel E, Engler J, Natsheh I, Jones J, Mickuckyte A, Hudak L, Jonas D, Blaheta RA. Combining the receptor tyrosine kinase inhibitor AEE788 and the mammalian target of rapamycin (mTOR) inhibitor RAD001 strongly inhibits adhesion and growth of renal cell carcinoma cells. *BMC Cancer.* 2009;9:161.

292. Zou Y, Wang J, Leng X, Huang J, Xue W, Zhang J, Huang Y. The selective MEK1 inhibitor selumetinib enhances the antitumor activity of everolimus against renal cell carcinoma in vitro and in vivo. *Oncotarget.* 2017;8:20825-20833.

293. Lim S, Kaldis P. Cdks, cyclins and CKIs: roles beyond cell cycle regulation. *Development.* 2013;140:3079-3093.

294. Juengel E, Kim D, Makarevic J, Reiter M, Tsaur I, Bartsch G, Haferkamp A, Blaheta RA. Molecular analysis of sunitinib resistant renal cell carcinoma cells after sequential treatment with RAD001 (everolimus) or sorafenib. *Journal of Cellular and Molecular Medicine.* 2015;19:430-441.

295. Song JH, Kandasamy K, Zemskova M, Lin YW, Kraft AS. The BH3 mimetic ABT-737 induces cancer cell senescence. *Cancer Research.* 2011;71:506-515.

296. Jane EP, Premkumar DR, Cavaleri JM, Sutera PA, Rajasekar T, Pollack IF. Dinaciclib, a cyclin-dependent kinase inhibitor promotes proteasomal degradation of Mcl-1 and enhances ABT-737-mediated cell death in malignant human glioma cell lines. *Journal of Pharmacology and Experimental Therapeutics.* 2016;356:354-365.

297. Averous J, Fonseca BD, Proud CG. Regulation of cyclin D1 expression by mTORC1 signaling requires eukaryotic initiation factor 4E-binding protein 1. *Oncogene.* 2008;27:1106-1113.

298. Chen B, Tan Z, Gao J, Wu W, Liu L, Jin W, Cao Y, Zhao S, Zhang W, Qiu Z, Liu D, Mo X, Li W. Hyperphosphorylation of ribosomal protein S6 predicts unfavorable clinical survival in non-small cell lung cancer. *Journal of Experimental & Clinical Cancer Research.* 2015;34:126.

299. Kim SH, Jang YH, Chau GC, Pyo S, Um SH. Prognostic significance and function of phosphorylated ribosomal protein S6 in esophageal squamous cell carcinoma. *Modern Pathology.* 2013;26:327-335.

300. Hurvitz SA, Kalous O, Conklin D, Desai AJ, Dering J, Anderson L, O'Brien NA, Kolarova T, Finn RS, Linnartz R, Chen D, Slamon DJ. In vitro activity of the mTOR inhibitor everolimus, in a large panel of breast cancer cell lines and analysis for predictors of response. *Breast Cancer Research and Treatment.* 2015;149:669-680.

301. Humphrey SJ, Yang G, Yang P, Fazakerley DJ, Stockli J, Yang JY, James DE. Dynamic adipocyte phosphoproteome reveals that Akt directly regulates mTORC2. *Cell Metabolism* . 2013;17:1009-1020.

302. Yang G, Murashige DS, Humphrey SJ, James DE. A positive feedback loop between Akt and mTORC2 via SIN1 phosphorylation. *Cell Reports* . 2015;12:937-943.

303. Sionov RV, Vlahopoulos SA, Granot Z. Regulation of Bim in health and disease. *Oncotarget.* 2015;6:23058-23134.

304. Weber K, Harper N, Schwabe J, Cohen GM. BIM-mediated membrane insertion of the BAK pore domain is an essential requirement for apoptosis. *Cell Reports* . 2013;5:409-420.

305. Deng J, Shimamura T, Perera S, Carlson NE, Cai D, Shapiro GI, Wong KK, Letai A. Proapoptotic BH3-only BCL-2 family protein BIM connects death signaling

from epidermal growth factor receptor inhibition to the mitochondrion. *Cancer Research.* 2007;67:11867-11875.

306. Jebahi A, Villedieu M, Petigny-Lechartier C, Brotin E, Louis MH, Abeilard E, Giffard F, Guercio M, Briand M, Gauduchon P, Lheureux S, Poulain L. PI3K/mTOR dual inhibitor NVP-BEZ235 decreases Mcl-1 expression and sensitizes ovarian carcinoma cells to Bcl-xL-targeting strategies, provided that Bim expression is induced. *Cancer Letters.* 2014;348:38-49.

307. Rahmani M, Aust MM, Attkisson E, Williams DC, Jr., Ferreira-Gonzalez A, Grant S. Dual inhibition of Bcl-2 and Bcl-xL strikingly enhances PI3K inhibition-induced apoptosis in human myeloid leukemia cells through a GSK3- and Bim-dependent mechanism. *Cancer Research.* 2013;73:1340-1351.

308. Al-Harbi S, Hill BT, Mazumder S, Singh K, Devecchio J, Choudhary G, Rybicki LA, Kalaycio M, Maciejewski JP, Houghton JA, Almasan A. An antiapoptotic BCL-2 family expression index predicts the response of chronic lymphocytic leukemia to ABT-737. *Blood.* 2011;118:3579-3590.

309. Chipuk JE, Fisher JC, Dillon CP, Kriwacki RW, Kuwana T, Green DR. Mechanism of apoptosis induction by inhibition of the anti-apoptotic BCL-2 proteins. *Proceedings of the National Academy of Sciences of the United States of America.* 2008;105:20327-20332.

310. Masters SC, Yang H, Datta SR, Greenberg ME, Fu H. 14-3-3 inhibits Bad-induced cell death through interaction with serine-136. *Molecular Pharmacology.* 2001;60:1325-1331.

311. Danial NN. Bad: undertaker by night, candyman by day. *Oncogene.* 2008;27 Suppl 1:S53-70.

312. Liu Y, Sun SY, Owonikoko TK, Sica GL, Curran WJ, Khuri FR, Deng X. Rapamycin induces Bad phosphorylation in association with its resistance to human lung cancer cells. *Molecular Cancer Therapeutics.* 2012;11:45-56.

313. Stamelos VA, Redman CW, Richardson A. Understanding sensitivity to BH3 mimetics: ABT-737 as a case study to foresee the complexities of personalized medicine. *Journal of Molecular Signaling.* 2012;7:12.

314. Ezzoukhry Z, Louandre C, Francois C, Saidak Z, Godin C, Maziere JC, Galmiche A. The Bcl-2 homology domain 3 (BH3) mimetic ABT-737 reveals the dynamic regulation of bad, a proapoptotic protein of the Bcl-2 family, by Bcl-xL. *Molecular Pharmacology.* 2011;79:997-1004.

315. Galmiche A, Ezzoukhry Z, Francois C, Louandre C, Sabbagh C, Nguyen-Khac E, Descamps V, Trouillet N, Godin C, Regimbeau JM, Joly JP, Barbare JC, Duverlie G, Maziere JC, Chatelain D. BAD, a proapoptotic member of the BCL2 family, is a potential therapeutic target in hepatocellular carcinoma. *Molecular Cancer Research.* 2010;8:1116-1125.

316. Williams AB, Schumacher B. p53 in the DNA-damage-repair process. *Cold Spring Harbor Perspectives in Medicine.* 2016;6:1-15

317. Kao CL, Hsu HS, Chen HW, Cheng TH. Rapamycin increases the p53/MDM2 protein ratio and p53-dependent apoptosis by translational inhibition of mdm2 in cancer cells. *Cancer Letters.* 2009;286:250-259.

318. Loehberg CR, Strissel PL, Dittrich R, Strick R, Dittmer J, Dittmer A, Fabry B, Kalender WA, Koch T, Wachter DL, Groh N, Polier A, Brandt I, Lotz L, Hoffmann I, Koppitz F, Oeser S, Mueller A, Fasching PA, Lux MP, Beckmann MW, Schrauder MG. Akt and p53 are potential mediators of reduced mammary tumor growth by cloroquine and the mTOR inhibitor RAD001. *Biochemical Pharmacology.* 2012;83:480-488.

319. Yosef R, Pilpel N, Tokarsky-Amiel R, Biran A, Ovadya Y, Cohen S, Vadai E, Dassa L, Shahar E, Condiotti R, Ben-Porath I, Krizhanovsky V. Directed elimination of senescent cells by inhibition of BCL-W and BCL-XL. *Nature Communications.* 2016;7:11190.

320. Muller A, Zang C, Chumduri C, Dorken B, Daniel PT, Scholz CW. Concurrent inhibition of PI3K and mTORC1/mTORC2 overcomes resistance to rapamycin induced apoptosis by down-regulation of Mcl-1 in mantle cell lymphoma. *International Journal of Cancer.* 2013;133:1813-1824.

321. Garrison SP, Phillips DC, Jeffers JR, Chipuk JE, Parsons MJ, Rehg JE, Opferman JT, Green DR, Zambetti GP. Genetically defining the mechanism of Puma- and Bim-induced apoptosis. *Cell Death & Differentiation.* 2012;19:642-649.

322. Soderquist RS, Eastman A. BCL2 inhibitors as anticancer drugs: a plethora of misleading BH3 mimetics. *Molecular Cancer Therapeutics.* 2016;15:2011-2017.

323. Zall H, Weber A, Besch R, Zantl N, Hacker G. Chemotherapeutic drugs sensitize human renal cell carcinoma cells to ABT-737 by a mechanism involving the Noxa-dependent inactivation of Mcl-1 or A1. *Mol Cancer.* 2010;9:164.

324. Iacovelli S, Ricciardi MR, Allegretti M, Mirabilii S, Licchetta R, Bergamo P, Rinaldo C, Zeuner A, Foa R, Milella M, McCubrey JA, Martelli AM, Tafuri A. Co-targeting of Bcl-2 and mTOR pathway triggers synergistic apoptosis in BH3 mimetics resistant acute lymphoblastic leukemia. *Oncotarget.* 2015;6:32089-32103.

325. Olejniczak ET, Van Sant C, Anderson MG, Wang G, Tahir SK, Sauter G, Lesniewski R, Semizarov D. Integrative genomic analysis of small-cell lung carcinoma reveals correlates of sensitivity to bcl-2 antagonists and uncovers novel chromosomal gains. *Molecular Cancer Research.* 2007;5:331-339.

326. Nakajima W, Hicks MA, Tanaka N, Krystal GW, Harada H. Noxa determines localization and stability of MCL-1 and consequently ABT-737 sensitivity in small cell lung cancer. *Cell Death & Disease.* 2014;5:e1052.

327. Kim KW, Moretti L, Mitchell LR, Jung DK, Lu B. Combined bcl-2/mammalian target of rapamycin inhibition leads to enhanced radiosensitization via induction of apoptosis and autophagy in non-small cell lung tumor xenograft model. *Clinical Cancer Research.* 2009;15:6096-6105.

328. Gardner EE, Connis N, Poirier JT, Cope L, Dobromilskaya I, Gallia GL, Rudin CM, Hann CL. Rapamycin rescues ABT-737 efficacy in small cell lung cancer. *Cancer Research.* 2014;74:2846-2856.

APPENDIX A: APPROVAL OF ANIMAL STUDIES BY THE ANIMAL CARE AND WELFARE COMMITTEE

YEDİTEPE ÜNİVERSİTESİ

T.C. YEDİTEPE ÜNİVERSİTESİ, DENEY HAYVANLARI ETİK KURULU (YÜDHEK)

ETİK KURUL KARARI

Toplantı Tarihi	Karar No	İlgi	Proje Yürütücüsü
06.09.2013	355	03.09.2013 tarihli yazı	Doç.Dr.Dilek TELCİ

'ABT-737 ve RAD-001(Evarolimus) ilaç kombinasyonunun böbrek kanseri üzerinde kemoteropatik özelliğinin RenCA hücre modeli ile balb-c fareleri üzerinde incelenmesi' bilimsel araştırma Etik Kurulumuzda görüşülmüş olup, çalışmanın etik kurallara uygun olduğuna oybirliği ile karar verilmiştir.

Etik Onay Geçerlilik Süresi: 3Yıl

GÖREVİ	ADI SOYADI	İMZA
Başkan	Prof. Dr. M. Ece GENÇ	
Başkan Yardımcısı	Prof. Dr. Erdem YEŞİLADA	
Raportör	Prof. Dr. Işıl Aksan KURNAZ	
Üye	Prof. Dr. Bayram YILMAZ	
Üye	Prof. Dr. Başar ATALAY	KATILMADI
Üye	Yrd.Doç.Dr.Soner DOĞAN	
Üye	Yrd. Doç. Dr. Ediz DENİZ	
Üye	Doç. Dr. C. Narter YEŞİLDAĞLAR	KATILMADI
Üye	Sumru KİRAZCI	KATILMADI